



**HAL**  
open science

# Optimization of a tool to study the start-up of the gas phase olefin polymerization

Estevan Tioni

► **To cite this version:**

Estevan Tioni. Optimization of a tool to study the start-up of the gas phase olefin polymerization. Polymers. Université Claude Bernard - Lyon I, 2011. English. NNT : 2011LYO10338 . tel-01416887

**HAL Id: tel-01416887**

**<https://theses.hal.science/tel-01416887>**

Submitted on 15 Dec 2016

**HAL** is a multi-disciplinary open access archive for the deposit and dissemination of scientific research documents, whether they are published or not. The documents may come from teaching and research institutions in France or abroad, or from public or private research centers.

L'archive ouverte pluridisciplinaire **HAL**, est destinée au dépôt et à la diffusion de documents scientifiques de niveau recherche, publiés ou non, émanant des établissements d'enseignement et de recherche français ou étrangers, des laboratoires publics ou privés.

THESE DE L'UNIVERSITE DE LYON  
UNIVERSITE CLAUDE BERNARD LYON 1

ECOLE DOCTORALE

DIPLOME DE DOCTORAT  
Specialité CHMIE GENIE DES PROCEDES  
(arrêté du 7 août 2006)

par

M TIONI Estevan

---

**Optimization of a tool to study the start-up of the gas phase  
olefin polymerization**

---

soutenu le 14 Décembre 2011

Directeur de thèse : M. McKenna Timothy

JURY : M. B. MASCHKE (President)  
M. M. BARTKE (rapporteur)  
M. P. THÜNE (rapporteur)  
M. G. WEICKERT  
M.T. McKENNA  
M. V. MONTEIL  
M. R. SPITZ

# UNIVERSITE CLAUDE BERNARD - LYON 1

## Président de l'Université

**M. A. Bonmartin**

Vice-président du Conseil d'Administration

M. le Professeur G. Annat

Vice-président du Conseil des Etudes et de la Vie Universitaire

M. le Professeur D. Simon

Vice-président du Conseil Scientifique

M. le Professeur J-F. Mornex

Secrétaire Général

M. G. Gay

## ***COMPOSANTES SANTE***

Faculté de Médecine Lyon Est – Claude Bernard

Directeur : M. le Professeur J. Etienne

Faculté de Médecine et de Maïeutique Lyon Sud – Charles Mérieux

Directeur : M. le Professeur F-N. Gilly

UFR d'Odontologie

Directeur : M. le Professeur D. Bourgeois

Institut des Sciences Pharmaceutiques et Biologiques

Directeur : M. le Professeur F. Locher

Institut des Sciences et Techniques de la Réadaptation

Directeur : M. le Professeur Y. Matillon

Département de formation et Centre de Recherche en Biologie Humaine

Directeur : M. le Professeur P. Farge

## ***COMPOSANTES ET DEPARTEMENTS DE SCIENCES ET TECHNOLOGIE***

Faculté des Sciences et Technologies

Directeur : M. le Professeur F. Gieres

Département Biologie

Directeur : M. le Professeur F. Fleury

Département Chimie Biochimie

Directeur : Mme le Professeur H. Parrot

Département GEP

Directeur : M. N. Siauve

Département Informatique

Directeur : M. le Professeur S. Akkouche

Département Mathématiques

Directeur : M. le Professeur A. Goldman

Département Mécanique

Directeur : M. le Professeur H. Ben Hadid

Département Physique

Directeur : Mme S. Fleck

Département Sciences de la Terre

Directeur : Mme le Professeur I. Daniel

UFR Sciences et Techniques des Activités Physiques et Sportives

Directeur : M. C. Collignon

Observatoire de Lyon

Directeur : M. B. Guiderdoni

Ecole Polytechnique Universitaire de Lyon 1

Directeur : M. P. Fournier

Ecole Supérieure de Chimie Physique Electronique

Directeur : M. G. Pignault

Institut Universitaire de Technologie de Lyon 1

Directeur : M. le Professeur C. Coulet

Institut de Science Financière et d'Assurances

Directeur : M. le Professeur J-C. Augros

Institut Universitaire de Formation des Maîtres

Directeur : M. R. Bernard

This work is part of the Research program of the Dutch Polymer Institute, PO Box 902, 5600AX, Eindhoven, The Netherlands, projectnr. # 636.



# Remerciements

Ce travail n'aurait pas pu aboutir sans l'aide et le support que j'ai reçu par des nombreuses personnes.

En premier lieu je tiens à remercier mes encadrants de thèse, Tim et Vincent. Tim, bien que tu étais relégué à Kingston pendant mes deux premières années de thèse, tu as toujours pris le temps de me conseiller, de m'écouter et de diriger mon travail dans la bonne direction. J'ai beaucoup apprécié ton « American style » dans l'encadrement, les opportunités que tu m'as offert pour présenter mes travaux (que je n'ai pas toujours saisi...) et les soirées open bar du DPI....

Vincent, bien que tu n'ais pas apprécié l'open bar autant que moi et Tim, il faut que je te dédie un paragraphe entier. Je ne vais pas louer ici tes capacités en tant que scientifique qui sont déjà reconnues, mais je voudrais surtout te remercier pour l'engagement et l'humanité que tu mets dans l'encadrement des étudiants. Je n'ai jamais connu un « chef » qui se bats autant pour ses étudiants comme toi, qui est toujours prêt pour écouter et aider et qui n'hésite pas à s'exprimer sans chichis. Bien qu'au début j'ai eu un peu de mal à me faire à ton caractère, tes qualités sont un exemple pour moi maintenant. Ne change pas, ne deviens pas comme tout le monde !

Je ne peux pas oublier ici de remercier Jean Pierre. Tu m'as appris vraiment beaucoup de choses : la mécanique, la plomberie (pas l'électricité ; il faut dire que t'es un peu nul pour ça... ;), tu m'as fait découvrir de la bonne musique, des BDs et des blagues. Bref, tu m'as rendu la vie quotidienne au labo plus intéressante. Je ne pourrai jamais oublier ta gentillesse, ta sensibilité et ton altruisme. Tu as été, à mes yeux, la personne plus importante du laboratoire pendant mes années de thèse. Spécial dédicace.

Beaucoup d'autre permanents du labo ont été la pour m'aider, et je ne peux pas les oublier : Roger, pour vos idées géniales et vos blagues et anecdotes, Christophe pour les discussions sur les metallocenes, PY pour les repas à la cantine et pour avoir trouvé des Terabytes de stockage, Olivier pour le boulot sur les appareils d'analyse et Nathalie pour avoir toujours su m'aider en trouvant les bons papiers au milieu d'une marée des dossiers.

Je remercie aussi tous les étudiants du labo que j'ai pu croiser pendant ces 4 années. En particulier Elsa, sans qui le premier labo était un peu plus vide, Miloud, qui peut comprendre comme c'est galère d'utiliser le stop flow, Virginie, Miriam et Ariadna pour avoir pris plusieurs « bols d'air » avec moi, Ana pour les valse, Etienne pour les discussions plus ou moins scientifiques, et tous les autres aussi. La liste est trop longue pour ne pas oublier quelqu'un !

Un remerciement spécial a tous mes collègues de bureau et aux derniers en particulier, Cédric, Arash et Elena. Merci pour avoir partagé avec moi vos sucreries, vos histoires et pour avoir arrosé les plantes ;). Un grazie speciale a Elena per avermi permesso di non dimenticare il mio italiano, per le vacanze a Napoli, per aver organizzato il mio regalo e per aver reso la vita di tutti i giorni molto meno noiosa!

Je remercie aussi tous mes copains "pas scientifiques" avec qui j'ai passé de superbes moments pendant ces quatre ans et qui m'ont fait aimer ma vie à Lyon au point que je ne veux pas le quitter! Tous les copains « folkeux », en particulier Louis, Pedy, Hélène, Fanny, Claire D et Claire G et les copains grimpeurs, Yoann en primis. Merci aussi à la gendarmerie de Toulon pour le tour en helico !

Una pensiero anche per i miei genitori e per mia sorella, che purtroppo non vedo abbastanza spesso, ma che sono sempre al moi fianco e mi incoraggiano sempre nelle mie scelte, anche quando mi obbligano ad attraversare le Alpi. Vedete, non sono venuto fino a Lione per niente!

Je ne serai pas la ou je suis maintenant sans Karine, qui m'accompagne dans ma vie depuis maintenant 6 ans. Tu es mon épaule depuis longtemps, depuis que je suis parti d'Italie. Tu m'as toujours soutenu et tu m'as suivi ici à Lyon sans te poser trop des questions. Je ne peux que te remercier pour ça. Ton énergie et ta motivation ont été un vrai moteur pour surpasser les moments difficiles pendant ma thèse, et t'as toujours su tenir bon devant mes coups de gueule. Merci infiniment.







# Abstract

The early stages (from less than 1s to few minutes) of catalytic olefin polymerization are still fairly understood even if they are nowadays recognized to be the crucial phase for determination of the morphology of the polymer particle, the optimization of the whole catalyst performance and the thermal stability of the process.

In this work we will first of all present how we studied and optimized a specially conceived packed bed reactor which is capable to perform gas phase catalytic olefin polymerizations as short as 0.1s under industrially relevant conditions. The possibility to measure the reactor temperature and to recover the particles to characterize the morphology and the polymer properties allows to take a complete picture of the catalyst behavior at the reaction start-up. The study will be restrained to ethylene polymerization and special attention will be given to the relation between heat transfer from the growing particle and catalyst performance as gas phase reactions are usually highly unstable at the start-up. It will be seen how, choosing the right process conditions, particle temperature evolution can be followed indirectly by measuring the gas phase temperature evolution.

In the second part of this work different metallocene complexes supported on silica will be used to study the influence of process conditions, catalyst preparation method and support properties on the evolution of reaction rate, and polymer MWD during the first reaction seconds. Special attention will be given to the active site evolution during the transient phase and it will be shown that temperature excursions can not only provoke polymer melting but can be responsible for a local variation in active site behavior thus altering the properties of the formed polymer.

The last section will be dedicated to the study of the peculiar crystallization behavior of the polymer chains in an evolving inorganic support. It will be shown how the melting and crystallization temperatures of the polymers can be used as “sensors” to measure the degree of fragmentation of the support particle.

The results obtained in this work can not only spread some light in order to gain a deeper understanding of the key parameters for the polymerization start-up but can also be used as input for single particle models thus allowing to reduce the gap actually present between real catalyst behavior and model predictions.



# Table of contents

<b>Résumé.....</b>	<b>1</b>
<b>Introduction.....</b>	<b>11</b>
<b>Chapter 1: Literature review</b>	
<b>1. Introduction on polyolefins.....</b>	<b>20</b>
1.1. History and success .....	20
1.2. Reactors and processes .....	24
1.2.1. High pressure reactors.....	25
1.2.2. Solution reactors .....	25
1.2.3. Slurry reactors.....	26
1.2.4. Gas phase reactors.....	27
1.2.5. Process design.....	30
1.3. Catalysts .....	31
1.3.1. Ziegler-Natta catalyst.....	32
1.3.2. Phillips catalyst.....	33
1.3.3. Metallocene catalyst.....	34
<b>2. Heterogeneisation of single site catalysts .....</b>	<b>37</b>
2.1. Introduction .....	37
2.2. Silica as support .....	38
2.3. Methods of immobilization of metallocene catalysts.....	40
2.4. Influence of silica properties and preparation .....	42
2.4.1. Support preparation .....	43
2.4.2. Deshydroxilation temperature.....	45
2.4.3. Silica porosity.....	47
2.4.4. Silica particle size .....	51
<b>3. Single particle modeling.....</b>	<b>54</b>
3.1. Generalities.....	54
3.2. MGM and PFM based models .....	60
3.3. Morphology models .....	65
3.4. Conclusions .....	69
<b>4. Experimental studies on the early stages of polymerization .....</b>	<b>70</b>
4.1. Early porosimetry and adsorption studies.....	71
4.2. Offline microscopy at low reaction rates .....	74
4.3. Online videomicroscopy .....	78
4.4. Infrared measurements .....	80
4.5. Melt microscopy.....	82
4.6. Synchrotron X-Ray microtomography.....	83

4.7.	Laser scanning confocal fluorescence microscopy .....	85
4.8.	Stopped flow technology.....	86
<b>5.</b>	<b>Conclusion and introduction of experimental work .....</b>	<b>91</b>
<b>6.</b>	<b>References .....</b>	<b>94</b>

## **Chapter 2: Thermal study and optimization of the gas phase stopped flow reactor**

<b>1.</b>	<b>Reactor set up, materials and experimental procedure.....</b>	<b>108</b>
1.1.	Introduction .....	108
1.2.	Reactor description and procedure.....	109
1.3.	Materials.....	113
1.3.1.	<i>Catalyst preparation .....</i>	<i>113</i>
1.3.2.	<i>Support .....</i>	<i>115</i>
1.3.3.	<i>Inert seedbed .....</i>	<i>116</i>
1.4.	Preliminary tests.....	117
1.4.1.	<i>Flowmeter calibration.....</i>	<i>118</i>
1.4.2.	<i>Thermocouple check.....</i>	<i>120</i>
1.4.3.	<i>Repeatability.....</i>	<i>121</i>
1.4.4.	<i>Stopping the reaction .....</i>	<i>122</i>
1.4.5.	<i>On the addition of scavenger to the inert seedbed.....</i>	<i>124</i>
<b>2.</b>	<b>Heat transfer study and optimization.....</b>	<b>126</b>
2.1.	Introduction .....	126
2.2.	Optimization of heat transfer in the packed bed stopped flow reactor.....	131
2.2.1.	<i>Influence of gas thermal conductivity .....</i>	<i>131</i>
2.2.2.	<i>Influence of gas velocity.....</i>	<i>137</i>
2.2.3.	<i>Influence of inert seedbed properties .....</i>	<i>145</i>
2.2.4.	<i>Towards the optimum heat transfer conditions.....</i>	<i>147</i>
2.2.5.	<i>Influence of heat generation (catalyst amount).....</i>	<i>151</i>
<b>3.</b>	<b>Validation and modelling.....</b>	<b>152</b>
3.1.	Temperature inside the bed .....	152
3.2.	Concentration profiles .....	155
3.3.	Reactor homogeneity.....	156
<b>4.</b>	<b>Conclusions .....</b>	<b>157</b>
<b>5.</b>	<b>References .....</b>	<b>159</b>

# Chapter 3: Start-up behavior of supported metallocenes in gas phase reactions

<b>1. Introduction .....</b>	<b>166</b>
<b>2. Influence of reaction conditions .....</b>	<b>168</b>
2.1. Catalyst characterization .....	168
2.2. Start-up behavior under optimized conditions: homo- and co-polymerization.....	170
2.2.1. Activity and thermal profile.....	170
2.2.2. Evolution of the MWD.....	175
2.3. Start-up behavior under badly controlled regime: influence of gas velocity and catalyst amount.....	179
2.3.1. Activity and thermal profile.....	180
2.3.2. MWD evolution .....	182
2.3.3. Influence of the amount of heat generated (catalyst mass).....	183
2.4. Influence of reaction temperature .....	183
2.4.1. Activity and temperature profile .....	183
2.4.2. MWD evolution .....	184
<b>3. Influence of catalyst preparation .....</b>	<b>186</b>
3.1. Introduction .....	186
3.2. Different precatalyst .....	187
3.2.1. Introduction.....	187
3.2.2. Activity and temperature profile .....	188
3.2.3. MWD evolution .....	190
3.3. Influence of the nature and quantity of the Al .....	192
3.3.1. Influence of Aluminium content.....	192
3.3.1.1. Activity and temperature profile at start-up.....	194
3.3.1.2. MWD evolution.....	198
3.3.2. Cocatalyst impregnation time .....	199
3.3.3. Conclusions .....	203
3.4. Influence of Zr content .....	203
3.4.1. Activity and MWD profile .....	205
3.5. Conclusions .....	207
<b>4. Influence of support properties.....</b>	<b>209</b>
4.1. Introduction .....	209
4.2. Influence of support size .....	210
4.2.1. Activity and temperature profile at reaction start-up. ....	212
4.2.2. MWD evolution .....	214
4.3. Influence of support pore size .....	217
4.3.1. Activity and temperature evolution at reaction start-up.....	218
4.3.2. MWD evolution .....	219
<b>5. Conclusions .....</b>	<b>220</b>
<b>6. References .....</b>	<b>224</b>

# Chapter 4: Morphological interpretation of the thermal properties of polyethylene at reaction start-up

<b>1. Introduction .....</b>	<b>232</b>
<b>2. Overview of polymer crystallization at reaction start-up .....</b>	<b>236</b>
2.1. Ethylene (co)polymerization by EtInd <sub>2</sub> ZrCl <sub>2</sub> .....	236
2.2. Ethylene (co)polymerization by (nBuCp) <sub>2</sub> ZrCl <sub>2</sub> .....	239
2.3. Conclusions .....	242
<b>3. Morphological interpretation of the crystallization behavior.....</b>	<b>243</b>
3.1. Introduction .....	243
3.2. Fragmentation and crystallization in confined space .....	246
3.3. Morphological (re)interpretation of DSC results .....	249
3.3.1. <i>DSC study on homopolymers</i> .....	249
3.3.2. <i>X-ray microtomography study on homopolymer particles</i> .....	252
3.3.3. <i>Copolymerization</i> .....	260
3.3.4. <i>Influence of support size</i> .....	261
3.3.5. <i>Influence of support pore size</i> .....	264
3.3.6. <i>Influence of catalyst preparation</i> .....	268
<b>4. Conclusions .....</b>	<b>274</b>
<b>5. References .....</b>	<b>277</b>

## Conclusions and perspectives.....281

## Experimental part

<b>1. Synthesis of solid materials.....</b>	<b>293</b>
1.1. Supported metallocene catalysts .....	293
1.2. Silica/TEA .....	294
1.3. Fine NaCl .....	294
<b>2. Polymerization technique .....</b>	<b>295</b>
2.1. “Classic” gas phase reactor .....	296
<b>3. Analytical techniques .....</b>	<b>297</b>
3.1. Size Exclusion Chromatography (SEC).....	297
3.2. Differential Scanning Calorimetry (DSC).....	297

3.3.	Porosimetry .....	298
3.4.	[OH] measurement .....	298
3.5.	Synchrotron X-ray microtomography .....	299
3.6.	SEM.....	299
<b>4.</b>	<b>References .....</b>	<b>301</b>





# Résumé

Les polyoléfines sont une des premières familles de plastiques synthétisées par l'homme il y a plus de 80 ans. En dépit de leur ancienneté, l'intérêt pour ces polymères est loin de s'estomper et, au contraire, les polyoléfines sont en train de remplacer d'autres matériaux comme les métaux et les verres pour des applications de plus en plus évoluées. L'origine de leur succès réside principalement dans les innombrables possibilités de combiner des atomes de C et de H pour produire des matériaux avec tout un éventail de propriétés ainsi que dans leur faible coût de production. Une vraie révolution dans la science des polyoléfines s'est en effet produite dans les années 50 grâce à la découverte de la polymérisation catalytique qui permet de travailler dans des conditions douces (quelques dizaines de bars et moins de 100°C) et limiter ainsi la consommation d'énergie et de matière. Des matériaux avec des propriétés spécifiques peuvent être produits assez facilement après une sélection appropriée du système catalytique et/ou à partir d'une conception adéquate du procédé industriel. En conséquence le polyéthylène, qui est le polymère étudié dans cette thèse, est, avec le polypropylène, le polymère le plus utilisé dans le monde entier.

Dans une majorité des procédés industriels les oléfines sont polymérisées grâce à une espèce active (catalyseur) qui est supportée sur un support poreux. Ces supports sont principalement des particules inorganiques comme le  $MgCl_2$  ou la silice. L'industrie préfère les catalyseurs hétérogènes parce qu'ils sont capables de produire des particules de polymère bien définies et denses limitant ainsi l'encrassement des réacteurs. Toutefois l'hétérogénéisation des catalyseurs le plus souvent engendre la création de résistances au transport de la matière et de la chaleur qui ont un grand impact sur la performance globale du catalyseur. Les réactifs doivent en effet diffuser de la phase continue vers la surface des particules et dans leurs pores pour atteindre les sites actifs. La chaleur de réaction (la polymérisation des oléfines est très exothermique) suit le chemin opposé. La polymérisation catalytique des oléfines a, de plus, un degré de complexité plus élevé par rapport aux autres procédés catalytiques parce que le produit de réaction n'est pas évacué avec le flux sortant mais reste sous forme solide sur les particules de catalyseur. Une fois que le monomère a

atteint le site actif, le polymère commence à se déposer immédiatement sur les parois des pores qui se remplissent de polymère. Ceci crée localement des forces qui agissent sur la structure du support et, si tout se passe bien, le support fragmente tout en conservant l'intégrité de la particule. Des nouveaux espaces vides sont ainsi créés ce qui facilite l'accès des réactifs aux sites actifs. Une fois la fragmentation amorcée le polymère continue de grandir à l'intérieur et à la surface de la particule en causant son expansion. La morphologie de la particule est donc en évolution pendant les premiers instants de la polymérisation et ses variations influencent les propriétés de transport de la particule, qui montrent donc une dépendance spatiale et temporelle. L'évolution de la morphologie de la particule est elle-même influencée par les propriétés physiques et mécaniques du polymère et du support et par la vitesse d'accumulation du polymère qui, à son tour, est dépendante des profils de température et de concentration dans la particule.

Il est donc clair que les phénomènes qui déterminent les performances d'un catalyseur de polymérisation sont strictement dépendants les uns des autres. Le début de la polymérisation est donc la phase la plus délicate de la réaction. Les gradients de température et concentration le long du rayon de la particule sont en effet plus marqués. Au début de la réaction le transfert de chaleur est en effet critique à cause de la petite surface externe des particules et la production de chaleur est élevée à cause de la haute concentration des sites actifs. Les premiers instants de la polymérisation sont aussi la phase pendant laquelle la fragmentation du support a lieu et la particule subit les changements de morphologie les plus importants. C'est pendant cette période que la morphologie finale de la particule est fixée (réplication parfaite ou production de fines ou particules creuses etc.) et que les performances du catalyseur peuvent être compromises.

En dépit de l'importance industrielle des procédés de production des polyoléfines, le début de la réaction n'est pas encore complètement maîtrisé et compris et ceci peut entraîner des conséquences non désirées voir même dangereuses (arrêt du réacteur à cause de la production de fines ou même emballement thermique à cause d'un transfert de chaleur insuffisant). La raison principale est le manque d'outils expérimentaux fiables capables de fournir des données sur cette phase particulière de la réaction. L'intervalle de temps très court pendant lequel les phénomènes qui déterminent les propriétés du polymère et la morphologie des particules sont en jeu et la taille réduite des particules de catalyseur sont responsables des difficultés rencontrées dans la construction d'outils appropriés. Pour les mêmes raisons, même si de gros efforts ont été déployés pour modéliser la fragmentation de la particule et les

transferts de matière et de chaleur, la communauté scientifique manque encore d'un modèle complet et fiable capable de prédire le comportement de la particule au début de la réaction. Ceci est principalement dû au grand nombre de paramètres jouant un rôle dans ces modèles et aux hypothèses faites pour simplifier la situation et surmonter le manque de données expérimentales.

L'objectif principal de cette thèse est donc de réaliser une étude expérimentale complète pour combler les manques présentés ci-dessus et fournir des données pour la modélisation et, au delà, pour comprendre en détails les phénomènes clé du début de la polymérisation.

Les premiers instants de la polymérisation catalytique en phase gaz, ce qui correspond à la majorité des procédés industriels, seront en particulier étudiés. La faible conductivité thermique de la phase gaz augmente la possibilité d'emballement thermique au démarrage de la réaction. Une attention spéciale sera donc mise sur cet aspect. De plus, si quelques données expérimentales sont disponibles pour le début de la polymérisation catalytique hétérogène de l'éthylène en phase liquide, peu d'études ont traité les réactions en phase gaz. La première partie de ce travail sera dédiée à la présentation et au développement d'un nouveau outil adapté à ce projet et son comportement thermique sera analysé en détail.

Les catalyseurs choisis pour ce travail sont des métallocènes supportés sur silice traitée avec du MAO. Même si ils ne sont pas les catalyseurs les plus utilisés dans l'industrie, ils sont les meilleurs candidats pour démarrer une étude sur les premiers instants de la polymérisation catalytique de l'éthylène en phase gaz et ce pour plusieurs raisons. L'exposition de la particule de polymère/catalyseur à l'air ne devrait pas altérer excessivement sa morphologie au contraire des catalyseurs supportés sur  $MgCl_2$ , qui se dissout au contact de l'humidité ambiante. De plus il est connu que les catalyseurs de type métallocène, y compris supportés, sont censés produire des polymères avec une distribution de masses molaires étroite. Une perturbation du comportement des sites actifs par quelque phénomène que ce soit pendant le début de la réaction ou la présence de gradients excessifs de température ou de concentration dans la particule seront immédiatement détectées par un élargissement de la distribution des masses molaires. Ceci n'aurait pas été facilement observable si un catalyseur de type Ziegler-Natta, qui produit intrinsèquement un polymère avec une polydispersité élevée, avait été utilisé.

Dans la deuxième partie de ce travail l'influence de différents paramètres sera analysé comme les conditions de réaction, la préparation du catalyseur et les propriétés du support sur

le comportement du catalyseur au démarrage de la réaction en termes d'activité, évolution de la température des particules et des propriétés des polymères. Grâce aux caractéristiques du réacteur différents paramètres pourront facilement être corrélés entre eux (comme la vitesse de réaction, les propriétés des polymères, la morphologie et la température des particules). Leurs évolutions pourront être suivies et donner ainsi une représentation complète du comportement de la particule de catalyseur et de polymère au début de la réaction.

Plus précisément, la recherche bibliographique présentée dans le Chapitre 1, concernant les travaux expérimentaux et théoriques de la littérature sur l'étude des premiers instants de la polymérisation catalytique hétérogène, montrera qu'en effet il existe différents techniques pour étudier cet aspect de la polymérisation mais qu'aucune d'entre elles n'est capable de donner une description complète du comportement de la particule dans des conditions proches de celles utilisées industriellement. La plus prometteuse semble être la technique dite « stopped flow » qui sera utilisée dans ce travail. On verra aussi que même les résultats provenant des modèles les plus avancés sont en désaccord avec la réalité des faits expérimentaux concernant le début de la polymérisation. La raison pour cela est, comme déjà souligné par ailleurs, le manque de données expérimentales fiables qui oblige les auteurs à formuler un trop grand nombre d'hypothèses.

Le chapitre 2 sera dédié au développement et à l'optimisation d'un mini réacteur à lit fixe (3 mL) spécialement conçu pour des polymérisations très courtes (0.1 s minimum). Une attention spéciale sera portée sur le transfert de chaleur de la particule de catalyseur à la phase gaz, car c'est un paramètre crucial pour éviter la fonte du polymère et l'emballement thermique et d'autant plus que les polymérisations en phase gaz son particulièrement sujettes à ces risques. Une analyse systématique de l'équation de transfert de chaleur nous a permis de trouver les conditions de réaction optimales pour optimiser le transfert de chaleur et ainsi limiter la « surchauffe » du catalyseur. Celles-ci sont une augmentation de la conductivité de la phase fluide grâce à l'ajout de 33 % molaire d'hélium dans l'alimentation combiné avec une vitesse de gaz élevée (20 cm/s) et l'utilisation de particules de NaCl de tailles comparables à celles du catalyseur ainsi qu'une limitation de la masse de catalyseur à 30mg. Les meilleures conditions pour éviter une augmentation de température trop élevée tout en produisant assez de polymère pour effectuer toutes les analyses nécessaires sont ainsi définies. En particulier l'emballement thermique, mesuré en cas de mauvais transfert de chaleur et responsable d'une augmentation de température de 30°C en 75s entraînant la fonte du polymère, a été réduit pour donner un profil de température avec une augmentation de

seulement 10°C en 5s pour après retrouver les valeurs de départ. L'efficacité atteinte du transfert de chaleur permet aussi de suivre « en direct » l'évolution de la température de la surface des particules à travers la mesure de la température du gaz en sortie du réacteur. Ceci est une information très importante pour permettre la validation des modèles. Une première version d'un modèle calorimétrique de notre lit fixe a été aussi développée en collaboration avec le Laboratoire de Génies de Procédés Catalytiques (LGPC). Ce travail permet de confirmer les résultats expérimentaux, de fixer des conditions de réaction pour lesquelles l'augmentation de température est limitée, d'avoir les valeurs de température à chaque instant pour chaque position dans le lit catalytique et s'inscrit dans l'optique de construction d'un modèle prédictif qui permet de calculer le profil d'activité en continu à partir des mesures des profils des températures des gaz entrant et sortant.

Dans le Chapitre 3 les conditions de réaction retenues précédemment seront utilisées pour caractériser le comportement de différents catalyseurs métallocènes supportés au début de la réaction. En particulier on se focalisera sur l'évolution de l'activité du catalyseur, de la température des particules et de la distribution de masses molaire des polymères. L'influence des conditions de réaction, de la préparation du catalyseur et des propriétés du support sur ces variables sera aussi étudiée. Il a été en particulier mis en évidence qu'un transfert de chaleur peu efficace est problématique non seulement au niveau macroscopique (fonte du polymère) mais peut l'être aussi, plus finement, au niveau local et modifier le comportement des sites actifs qui forment ainsi des polymères ayant des propriétés altérées. Par exemple la simple utilisation d'une vitesse de gaz réduite (5.5 au lieu de 20 cm/s) n'est pas responsable de la fonte du polymère mais d'une augmentation de température assez élevée pour que les réactions de transfert deviennent hors contrôle et donnent des polymères avec des masses molaires décroissantes au cours de la réaction (de 35 à 5 Kg/mol) et des polydispersités croissantes (jusqu'à 10 après 10s de réaction). Les mêmes réactions conduites à vitesse de gaz élevée donnent des polymères avec distributions de masses molaires étroites et constantes ( $M_n = 35$  Kg/mol et  $IP = 4$ ). En revanche de faibles  $M_n$  et des MWD larges peuvent aussi être mesurés transitoirement au cours de la réaction même si les meilleures conditions sont utilisées. Ceci vient du fait que le réacteur opère dans tous les cas sous un gradient de température surtout dans les premières secondes de réaction, ce qui peut engendrer une hétérogénéité dans le comportement des sites actifs selon leurs positions dans le lit catalytique.

En général les catalyseurs testés montrent une très forte activité dans les premières 2-5 secondes de réaction. Les valeurs d'activités au démarrage peuvent être 20 fois plus élevées que celles à l'état stationnaire et ce indépendamment des conditions de réaction (présence du comonomère, température, type de métallocène). Cette chute spectaculaire suggère qu'il peut y avoir des sites actifs qui fonctionnent seulement pendant un temps très court et qui se désactivent tout de suite pour des raisons peu évidentes. L'étude de l'influence de la préparation du catalyseur montre qu'une augmentation de la quantité d'aluminium ou de zirconium fixé sur le support génère un catalyseur très actif dans la première seconde de réaction mais qui se désactive par la suite très vite. Ce comportement peut être expliqué par une probabilité accrue d'une désactivation des sites actifs par recombinaison de 2 atomes de zirconium. L'absence d'alkylaluminium rajouté dans le milieu réactionnel en guise d'agent nettoyant du milieu, exception faite pour le MAO supporté sur la silice, rend impossible la réactivation des sites désactivés, à l'inverse de ce qui peut se passer dans des réacteurs conventionnels. L'introduction d'alkylaluminium dans notre lit fixe s'est révélée en effet très problématique et le choix de ne pas en ajouter a été motivé aussi par le fait que notre méthode de synthèse produit un catalyseur monocomposant capable de polymériser par lui même les oléfines.

Dans la dernière partie du Chapitre 3 l'influence des propriétés du support sur le début de la polymérisation a été étudiée. La taille du support influence l'activité du catalyseur seulement à partir de 30 s de réaction avec une dépendance mesurable de la vitesse de réaction avec l'inverse du diamètre des particules. Pour des réactions plus courtes il n'y a pas de tendance nette. Le profil de désactivation est maintenu indépendamment de la taille du support. La taille des pores n'a pas d'influence majeure sur la vitesse de réaction sinon avec un léger retard dans l'évolution de l'activité provoqué par une augmentation du volume poreux. Ceci peut être dû au fait qu'un volume plus grand doit être rempli par le polymère pour avoir le même degré de fragmentation. La distribution de masses molaires ne dépend pas des propriétés du support.

Dans le Chapitre 4 l'évolution des propriétés thermiques des polymères (c'est à dire température de fusion, de cristallisation et cristallinité) a été étudiée et sa relation avec la morphologie de la particule évoluant à cause du processus de fragmentation sera explicitée. Pour la première fois le comportement inhabituel mesuré aussi par d'autres auteurs est rationalisé avec le phénomène de cristallisation en milieu confiné. En général dans les premiers instants de la polymérisation une augmentation de la température de fusion du

polymère avec le temps de réaction est mesurée. Pour des temps très courts (moins d'1s) des températures de fusion de 117°C peuvent être mesurées alors que le même catalyseur utilisé dans des réactions « classiques » produit un polymère qui fond à 131°C. La raison pour ce phénomène est la présence d'une quantité non négligeable de support dans la particule finale à cause des bas rendements atteints aux temps courts (max 2g/g). La particule de support/polymère se trouve alors tout au début du processus de fragmentation et une bonne partie du polymère est située dans des pores qui n'ont pas encore fragmentés. Ce confinement perturbe la cristallisation des chaînes et limite la croissance des cristaux de PE. Plus les cristaux sont petits et plus basse est leur température de fusion (moins d'énergie à fournir). Ces effets sont moins importants en cas de copolymérisation, car les ramifications réduisent elles-mêmes la taille des cristallites et donc leur croissance est moins perturbée par le confinement dans les pores. Ceci est confirmé expérimentalement par une température de fusion constante avec le temps de réaction si 4% molaire de butène est incorporé dans le polyéthylène. Avec l'avancement de la réaction la température de fusion mesurée augmente et approche des valeurs plus classiques. Des pics de fusion à 130°C ont été mesurés pour des réactions arrêtées à un rendement de 2-3 g/g. Plus la réaction avance et plus élevé est la quantité de pores qui ont disparu à cause de la fragmentation (et le confinement avec eux). Le rendement est donc le paramètre indépendant qui détermine le degré d'abaissement de la température de fusion. Plus il est élevé, majeure est la fraction de chaînes de polymère qui peuvent évoluer librement par rapport à celles qui se trouvent confinées dans des nanodomains.

La cristallisation du PE au démarrage de la réaction suit un chemin tout à fait similaire. Pour des rendements très faibles un pic de cristallisation à 75°C est visible, ce qui est typique de la cristallisation homogène du PE. Pour des rendements plus élevés un pic à 105°C est mesuré, ce qui est représentatif de la cristallisation hétérogène du PE en milieu confiné. La cristallisation hétérogène est plus probable dans les petits pores, à cause du ratio surface/volume plus élevé. Seulement pour des rendements supérieurs à 1 g/g le pic de cristallisation à 115°C, typique de la chaîne de PE linéaire cristallisant en masse, commence à devenir prédominant. Ce comportement peut être expliqué avec l'évolution de la morphologie de la particule de polymère en croissance: remplissage des pores les plus accessibles au début (typiquement les plus gros), des moins accessibles après (les plus petits, responsables de cristallisation hétérogène en milieu confiné) et démarrage de la fragmentation encore plus tard (avec de plus en plus de polymère qui n'est plus perturbé par les pores qui ont déjà « éclaté »).



Cette évolution a été en partie confirmée par une série de tomographies des rayons X effectué sur des particules à différent rendement.

Les températures de fusion et de cristallisation du PE au débute de la réaction de polymérisation peuvent donc être utilisées comme « capteurs » pour déterminer l'avancement de la fragmentation du support. Les conclusions obtenues dans ce chapitre montrent enfin que l'utilisation de donnés provenant de réactions « classiques » pour modéliser l'évolution de la particule de catalyseur/polymère au démarrage de la réaction n'est clairement pas fiable et peut être une des raisons qui explique les différences présentes entre prédiction provenant des modélisations et comportement des catalyseurs dans des procédés réels.





# Introduction

Polyolefins are one of the first families of plastics synthesized by man more than 80 years ago. Despite their age, the interest in such polymers is far from declining and, on the contrary, polyolefins are replacing other materials like glass, metals, polystyrene and polyester in intermediate and performance applications. The secret of their success lies in the infinite possibilities to combine C and H atoms to give materials with an extremely wide range of properties and in their low production cost. A real revolution in polyolefin science came in fact in the 50s with the discovery of the catalytic polymerization process which allows producers to work at mild conditions with low energy and material consumption. The production of materials with specific properties can be achieved by appropriate selection of the catalytic system and design of the industrial process. As a consequence polyethylene, which is the polymer of interest for this study, is, together with propylene, the most widely used polymer in the world.

In a majority of industrial processes the catalytic reaction of olefin polymerization is carried out by using active species supported on porous supports. These supports are mainly inorganic particles like  $MgCl_2$  or silica. Heterogeneous catalysts are preferred in industry because of their ability to produce well-defined, dense polymer particles, and to limit reactor fouling. However, as is the case in all the catalytic processes, the heterogeneization of active molecules leads to the creation of mass and heat transport resistances, which can have a great impact on the catalyst performance. Reactants must diffuse from the bulk phase to the support surface and into the support pores to reach the active sites. The heat of reaction (olefin polymerization is highly exothermic) follows the opposite path. In addition, catalytic olefin polymerization has a higher degree of complexity respect to other catalytic processes. In fact once the monomer has reached the active site, the polymer starts immediately to form onto the pore walls. After a short time the pores of the catalyst are filled with polymer. This creates localized forces acting on the support network and, if everything goes well, the support fragments while maintaining the particle integrity, thus creating new void space and facilitating the access of reactants to active site. Once the support fragments, polymer

continues to grow inside the particle causing its expansion. The particle morphology begins to evolve during the first instants of the reaction, and continues throughout almost the entire reaction. These changes will influence the transfer properties of the particle, which thus become space and time dependent. The evolution of particle morphology is itself influenced by the physical and mechanical properties of both support and polymer, and by the rate of polymer production which is, in turn, dependent on temperature and concentration profiles inside the particle.

It is then clear that the phenomena determining the performances of a polymerization catalyst are strongly interconnected. The most delicate phase of the polymerization reaction is arguable the start-up, when the highest concentration and temperature profiles inside the particle can arise. This is due to the fact that at the reaction start-up a low particle external surface is combined with a high volumetric density of active sites. Early reaction stages are also the phase when the fragmentation process is occurring and the particle undergoes the most extreme morphology changes. It is in this phase then that final particle morphology is fixed and that catalyst performance can be disrupted.

Despite the industrial relevance of polyolefin production, the phenomena happening during reaction start-up are still not completely mastered. So in order to avoid problems (i.e. reactor shut down because of production of fines or even thermal runaway because of insufficient heat removal), a prepolymerisation step is often used industrially to begin the reaction under mild, controlled conditions. A better mastery of what occurs at this stage would obviously be useful, but the lack of a reliable experimental apparatus to collect data related to this particular polymerization phase is a limiting problem. Similarly, the validation of models of particle fragmentation and mass and heat transport inside the particle also suffers from the need to make simplifying assumptions that have to be made in order to overcome the lack of experimental data. The extremely short time during which important phenomena fixing the polymer properties and the particle morphology are in play, the rapidity of the associated changes, and the small scale of the catalyst particles are, in large part, responsible for this situation.

The main scope of this PhD is thus to propose solutions to help fill the void presented above, and, more in generally, to gain a deep knowledge on the phenomena that take place at the reaction start-up.

Previous studies from this research group have concentrated mostly on developing tools and protocols for slurry phase reactors, and so there is a distinct need for tools for gas phase systems that we will attempt to fill with the work presented in the following manuscript. In the first part of the work a new tool to study this subject will be presented and developed and its thermal behavior will be deeply characterized. The poor conductivity of the gas phase is responsible for an increased probability of thermal runaway at the start-up so special attention will be given to this problem. In the following parts of the work it will be shown how this tool can be successfully used to characterize and understand the key phenomena for the olefin polymerization start-up.

Heterogeneous metallocenes supported on MAO/treated silica are the catalysts of choice for this work. Even if they might not be the most widely used catalysts in industry, they are the best choice to start the study of start-up of gas phase polymerizations for numerous reasons. First of all, since metallocenes are typically supported on silica particles, exposure of the polymer/catalyst particle to air will not damage the support as it does for  $\text{MgCl}_2$  supported catalysts, where the support is altered upon contact with the humidity in the air. In addition it is known that metallocene catalysts, even if supported, should give narrower molecular weight distribution than ZN or Phillips type catalysts. Perturbations in the catalyst behavior coming from temperature or concentration gradients or modification of the active sites will be immediately reflected on the polydispersity of the MWD of the produced polymer and detected. Finally, the slower fragmentation of silica supported catalysts will allow an easier detection of morphology evolution during the first reaction seconds.

The influence of various parameters related to reaction conditions, catalyst preparation and support properties on the reaction start-up in terms of catalyst activity, particle temperature and polymer properties will be analyzed in this work. Due to the particular features of the reactor set-up it will be easy to correlate different parameters like reaction rate, polymer properties, particle morphology and temperature and their evolution in the first reaction seconds and give a complete picture of the catalyst/polymer particle behavior at the reaction start-up.

The literature review presented in Chapter 1 on the previous investigations into the early stages of heterogeneous catalytic olefin polymerization will show that there exists different techniques to study this particular aspect of the polymerization, but none of them is capable of giving a completely reliable picture of the particle behavior under industrially relevant conditions. The most promising one in this sense seems to be the stopped flow technique,

which is the one used in this work. In a similar way we will see how even the results coming from the most advanced models are in discrepancy with the reality. The reason is to be found in the high number of assumptions that has to be made to represent the evolution of the particle structure and the transfer coefficients due to lack of experimental data.

Chapter 2 will be dedicated to the development and optimization of our specially conceived packed bed reactor which is capable to perform reactions as short as 100ms. Special attention will be given to the heat transfer from the particle to the fluid phase, as this is crucial to avoid polymer melting and thermal runaway at the start-up. It will be shown that thermal runaway is a highly possible scenario (at least locally) in such reactions and that selection of the right reaction conditions allows to have an indirect measurement of the surface particle temperature evolution from the values of the outlet gas phase temperature.

In Chapter 3 the most suitable reaction conditions found in Chapter 2 will be used to describe the evolution of the catalyst activity and the polymer properties in terms of MWD in the first reaction seconds. The influence of process conditions like gas composition, temperature and superficial gas velocity, support properties like particle and pore size and catalyst features like metal and cocatalyst loading and metallocene type will be shown. We will see in particular how the evolving behavior of the active sites at the start-up is responsible for unusual activity profiles. It will also be shown how the ratio between heat generated and heat removed from the particle is closely related to the evolution of the MWD of the produced polymers, and therefore how the evolution of the MWD can be used as an indication of the thermal history of the particle.

In Chapter 4 a similar analysis will be performed but focus will be put on the melting and crystallization properties of the polymer and their relation with the particle morphology evolving because of the fragmentation process. It will be shown in particular how the presence of polymer chains in nanometric pores is the reason for unusual melting and crystallization behaviors of the polyethylene during the early reaction stages. In addition the continually changing support pore network during the fragmentation phase is responsible for a continuous evolution of the polymer thermal properties until a situation similar to what is found in more classic long term reactions is reached. Synchrotron X-Ray tomography images will confirm that the unexpected crystallization and thermal behavior can be used as “sensors” to measure the degree of particle fragmentation and morphology evolution. Finally, the conclusions reached in this part will prove that using values coming from long term reactions to model the particle growth for short times, as it is usually the case, is a too rough

approximation and can partly be at the origin of the discrepancy between modeling results and real particle behavior.





# Chapter 1

*Literature review*



<b>1. Introduction on polyolefins.....</b>	<b>20</b>
1.1. History and success .....	20
1.2. Reactors and processes .....	24
1.2.1. High pressure reactors.....	25
1.2.2. Solution reactors .....	25
1.2.3. Slurry reactors.....	26
1.2.4. Gas phase reactors.....	27
1.2.5. Process design.....	30
1.3. Catalysts .....	31
1.3.1. Ziegler-Natta catalyst.....	32
1.3.2. Phillips catalyst.....	33
1.3.3. Metallocene catalyst.....	34
<b>2. Heterogeneisation of single site catalysts .....</b>	<b>37</b>
2.1. Introduction .....	37
2.2. Silica as support .....	38
2.3. Methods of immobilization of metallocene catalysts.....	40
2.4. Influence of silica properties and preparation .....	42
2.4.1. Support preparation .....	43
2.4.2. Deshydroxylation temperature.....	45
2.4.3. Silica porosity.....	47
2.4.4. Silica particle size .....	51
<b>3. Single particle modeling.....</b>	<b>54</b>
3.1. Generalities.....	54
3.2. MGM and PFM based models .....	60
3.3. Morphology models .....	65
3.4. Conclusions .....	69
<b>4. Experimental studies on the early stages of polymerization .....</b>	<b>70</b>
4.1. Early porosimetry and adsorption studies .....	71
4.2. Offline microscopy at low reaction rates .....	74
4.3. Online videomicroscopy .....	78
4.4. Infrared measurements .....	80
4.5. Melt microscopy.....	82
4.6. Synchrotron X-Ray microtomography.....	83
4.7. Laser scanning confocal fluorescence microscopy .....	85
4.8. Stopped flow technology.....	86
<b>5. Conclusion and introduction of experimental work .....</b>	<b>91</b>
<b>6. References .....</b>	<b>94</b>

# 1. Introduction on polyolefins

## 1.1. *History and success*

Polyolefins are 80 years old materials which are nowadays present in a number of aspects of everyday life (plastic bags, films, packaging, bottles, car bumpers) and are also used in more technical applications (medical devices, prosthesis, anticorrosion pipes, nonwoven textiles). Despite their age, the interest in such polymers is far from declining and, on the contrary, polyolefins are replacing other materials like glass, metals, PS and PET in intermediate and performance applications. As a consequence their production is still growing at an annual rate of more than 5% and the total capacity has overcome the barrier of the 100 million tons per year. The secret of their success as commodity plastics has to be found first of all in their cost. Raw materials like olefins have been for decades very cheap to produce with thermal cracking of fossil hydrocarbons and their price is nowadays as low as 1000 € / ton (bit less for ethylene and bit more for propylene) [1]. Researches ongoing on monomer production from renewable feedstocks are promising a bright future to these materials. In addition the discovery of the catalytic polymerization of olefins allowing to operate at low temperature and pressure (and thus with low energy consumption) contributed greatly to reduce the price of the finished materials. However the real driving force for the success of polyolefins as commodity products first, and intermediate and performance materials later, is the usefulness of their properties and the capability of tuning them over a wide range with a clever manipulation of the catalyst and the processes in play. The possibility to combine carbon and hydrogen atoms in many different ways allows for the production of an infinite number of chain microstructures comprising completely linear chains, long and short branches, random or blocks copolymers and mesophase materials. Different chain architectures are responsible for different properties of the end materials and widen enormously the application field of polyolefin. It is then easy to understand why a cheap, recyclable material which can have completely different properties according to the way it is produced has interested for such a long time the academia, the industry and the society.

More than a century ago in 1898 polyethylene was first made accidentally by Von Pechmann who generated a polymer after decomposition of diazomethane. The polymer produced had a low molecular weight and was called polymethylene but it was chemically identical to what is nowadays recognized as linear polyethylene. As frequently happens, this

discovery had no immediate commercial value. It was only from 1933 that industrial controlled production of polyethylene started. In this year Gibson and Fawcett were able to polymerize spontaneously ethylene working at high pressure (1700 bar) and temperature (170°C) [2]. This kind of polymer is nowadays recognized as low density polyethylene (LDPE) and is very different from the polymethylene synthesized by von Pechmann. Due to the polymerization mechanisms mediated by free radicals created by presence of traces of oxygen in the reactor, the product shows a high degree of random branching. An enormous breakthrough in the history of olefin polymerization came in the early 50's with the discovery that ethylene could also be polymerized catalytically using transition metals at lower temperatures and pressures. Within a few years and without being aware of each other's work Karl Ziegler at the Mülheim Max Planck Institute for Coal Research and Banks and Hogan at Phillips Petroleum Company discovered what is responsible today for the production of 100% of the polypropylene and of 70% of the polyethylene [3]: the Ziegler and Phillips catalysts. The polyethylenes produced via these catalysts showed high molecular weight with a linear backbone chain with a very few amount of branches and high density. This new family of original homopolymers was classified as high density polyethylenes (HDPE) and shows very different physical properties with respect to the LDPE. Since the development of the first catalyzed processes, the possibility of working at milder reaction conditions with lower energy consumption and simpler production units has been a driving force for the industrialization of these polymerizations. During the 2<sup>nd</sup> part of the 20<sup>th</sup> century a number of processes and catalysts have been developed allowing the production of copolymers of ethylene and  $\alpha$ -olefins (1-butene, 1-hexene, 1-octene) showing linear backbones with short branches only [4]. These materials have tunable properties and microstructures and are classified as linear low density polyethylenes (LLDPE). Isotactic Polypropylene was first synthesized in 1954 using a Ziegler type catalyst by Giulio Natta in Milan Polytechnic. Natta recognized immediately that polypropylene is composed of different stereoisomers having very different physical properties and found how to separate them. By X-ray diffraction he was able to identify isotactic, syndiotactic and atactic polypropylene. His new concept of polymer stereoregularity had a tremendous impact on the progress of polymer science [5].

A more recent breakthrough was the discovery of Sinn and Kaminsky in the late 70's that metallocene complexes (discovered in the 50's) can rapidly polymerize ethylene if activated by  $\text{AlMe}_3/\text{H}_2\text{O}$  activators or even better by methylaluminoxane (MAO) [6, 7]. The improvements brought by these discoveries reside in the fact that much larger comonomer

incorporation into the backbone can be reached and the formed polymers show narrow comonomer and molecular weight distribution while the previously discovered catalysts formed mixtures of a large variety of chains in terms of molar mass and chemical composition. This leads to new microstructures and improved physical properties such as impact, sealing and optical [4]. Nevertheless it has to be said this capacity to produce chains with narrow MWD is an advantage and a disadvantage at the same time. While it opens new fields of applications, polyolefins coming from metallocene catalysis are difficult to process. A quite broad MWD is in fact preferred during processing as it lowers the viscosity of the melt phase (small chains act as “lubricants” for the bigger chains). For the same reason a not too high molar mass and the presence of long chain branching is appreciated by the processing industry. Difficulties in processing are among the main reasons for the limited development of metallocene catalysts in industry.

The practical consequence of the brief history explained above is that nowadays polyolefins are the largest volume family of polymers in the plastics industry. According to ChemSystems, in 2005 the PE production was about 65 million tons and the PP one about 40 million tons with growth rate between 6 and 8 % (Figure 1) [4]. Even if the production capacity is nowadays shifted from mature markets (Europe, North America, Japan) to growing markets (China, Middle East, Brazil, Russia) research needs are not decreased because of the new applications that are continually developed.

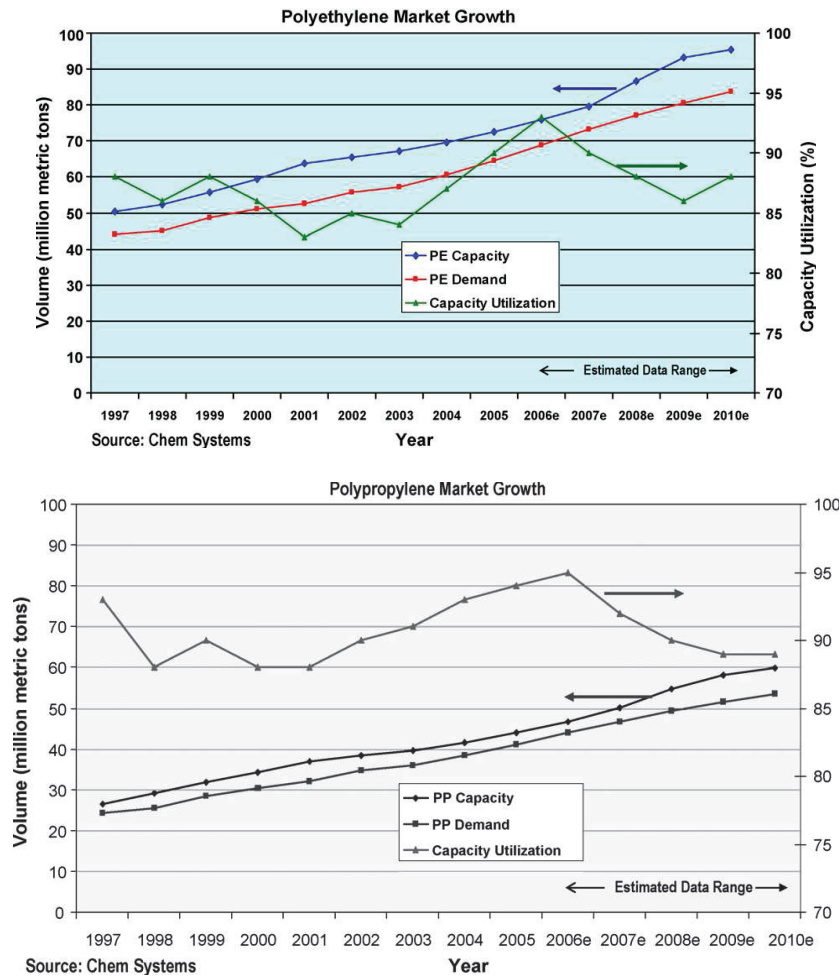


Figure 1: PE and PP market growth; reprinted with permission from [4].

It has been briefly said how using different polymerization mechanisms or different catalysts and different processes a wide range of chain microstructures can be produced and material properties obtained. The presence of branches pending from the backbone of the polymer chain has in fact a great influence on the density, the crystallinity and the rheological properties of the polymer.

The type and the frequency of the branches as long as the homogeneity of the branches distribution can be tuned by selecting the appropriate polymerization conditions, catalyst and comonomer. Varying one or more of these variables as well as the Mw and the MWD allows one to produce materials that have application in completely different fields. Figure 2 shows the chain microstructure for different PE families while Figure 3 shows the applications of polyolefins according to their physical properties.



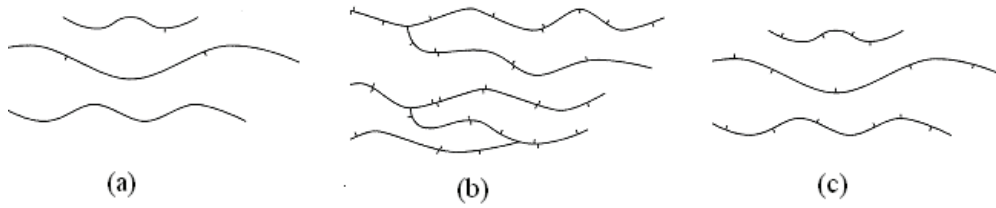


Figure 2: PE microstructures. HDPE (a), LDPE (b), LLDPE (c) ; reprinted with permission from [8].

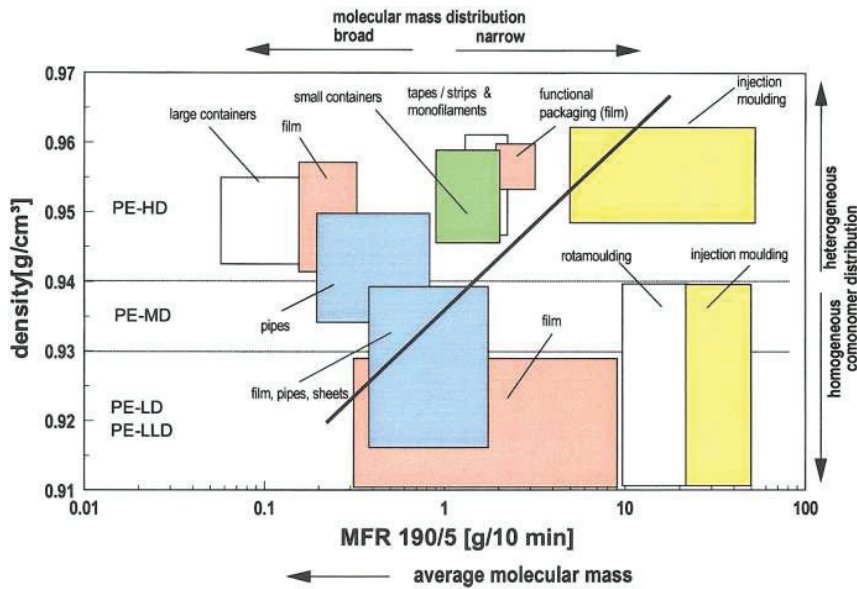


Figure 3: PE applications according to physical properties; reprinted with permission from [9].

## 1.2. Reactors and processes

The reactors used to produce all the broad range of polyolefins now available are divided in 4 main families:

- High pressure reactors
- Solution reactors
- Slurry reactors
- Gas phase reactors

The choice of the process depends mainly on economical factors which are in turn influenced by the type of product that is desired: different processes will be used if grade diversity is preferred rather than high production volume. Heat removal which, we will see, is an important problem in olefin polymerization, is also a criterion determining the choice of

the process and of the reactor. The main concern during olefin polymerization is in fact to remove the heat of reaction ( $\Delta H_r = -100$  kJ/mol [10]) from the growing polymer particles. If this is not done the control over the process will be lost. For instance in heterogeneous phase processes polymer particles can stick together and form agglomerates or chunks that can cause blockage of the unit or films sticking to the walls causing a drastic decrease in the heat transfer efficiency. Polymer fines are also undesired as they tend to deposit on heat exchange surface [11].

### 1.2.1. High pressure reactors

It is the oldest process used to polymerize ethylene to produce LDPE by a radical mechanism initiated by oxygen traces or peroxide. The process operates in solution in supercritical ethylene. The working conditions are very harsh with operating pressures up to 3000 bar and temperatures between 150 and 300°C. Even if the process has now almost 80 years it continues to be economically viable especially because there is no need for diluents and no catalyst residues or VOC are produced. One of its advantages is to be able to produce ethylene copolymer with polar monomers such as EVA [12]. This cannot be done in any other way as viable catalysts are poisoned by polar compounds. Propylene cannot be polymerized using this process.

### 1.2.2. Solution reactors

This was the first process used for catalytic polymerization of olefins. The requirement to keep polymer in solution obliges to work at temperature above 160°C in aliphatic hydrocarbon while operating pressures can be as high as 100 bars. The residence times are very short (1-10 min) to avoid excessive increase in viscosity of the reaction medium. As this process is much more responsive than slurry and gas phase processes allowing fast grade transitions and it can make different materials, the interest towards this technology is still high. Such processes in fact are operated in CSTR reactors and allow the copolymerization of ethylene with higher  $\alpha$ -olefin as 1-hexene, 1-octene, 1-decene and even 1-dodecene. Such process is well appreciated in the emerging countries like India since the possibility to change rapidly the grade allows to produce a lot of different products “in-house” reducing the costs of purchasing from third countries. Solution processes are limited to PE only and cannot produce too high molecular weight polymers due to viscosity problems.

### 1.2.3. Slurry reactors

Slurry processes were the first commercial processes for catalytic olefin polymerization using heterogeneous catalysts. The simplest process consists of one or more (usually more) CSTRs in series working up to 20 bar and between 70 and 90°C in aliphatic hydrocarbons. The presence of the solvent is responsible for swelling of the low molecular weight chains and limited solubility of hydrogen, the chain transfer agent, thus limiting the product range and requiring the solvent to be removed from the polymer. This problem can be partly circumvented if a light branched solvent (like isobutane) is used. Polymer swelling is less important and separation is then less energy demanding [12]. Heat removal can be simply performed by a cooling jacket and an external heat exchanger where a part of the slurry is cooled and recycled to the reactor. A more complex reactor configuration to perform slurry phase polymerization is the slurry loop reactor. This consists of one or more continuous loops of pipes where the slurry is circulated using an axial pump with a high recirculation ratio. The main advantage of this reactor is the high surface to volume ratio allowing efficient heat removal by external coils. The most important process of this type producing polyethylene is the Phillips process (Figure 4).

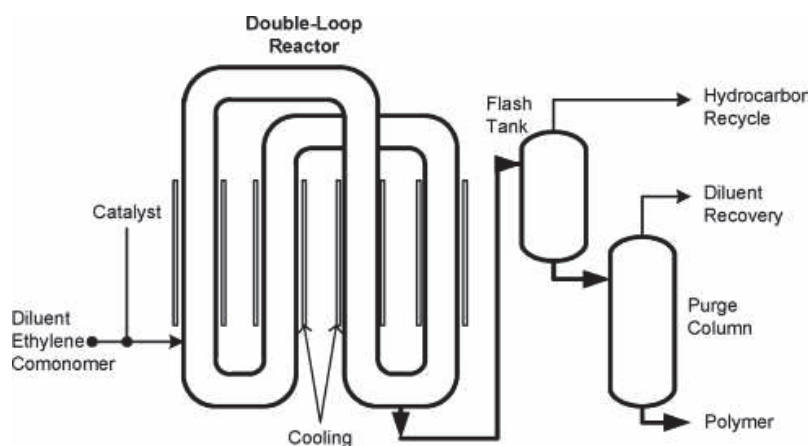


Figure 4: Representation of the Phillips process; reprinted with permission from [12]

In polypropylene production processes the aliphatic solvent and the problems related to its presence can be eliminated by performing the polymerization directly in the liquid monomer which is condensed by standard cooling water. This eliminates the need for extensive solvent recovery system and allows working at higher monomer concentrations. This way to operate is not suited for ethylene polymerization since in this case the condensation of ethylene would require a much more expensive process. This way of working is actually the most widely used to produce isotactic polypropylene in slurry reactors. The most known process of this type,

responsible for the production of one third of the world's polypropylene [11], is the Spheripol process licensed by LyondellBasell. In this process the polymerization is conducted in 2 loop reactors using liquid propylene and is preceded by a prepolymerization step at relatively low temperature. The presence of more than one loop allows the production of heterogeneous copolymers that can have interesting and innovative properties like bimodal molecular weight distribution. It has to be anticipated here that the synthesis of materials having properties spanning over a wide range can be reached by appropriately selecting the catalyst or a combination of them or by intelligently designing the process in order to make different products within the same unit. The possibility to produce new materials with previously unreachabele properties is one of the main driving forces that lead to the innovative process developments that will be reviewed in paragraph 1.2.5. As it has been discussed extensively in the literature [13-17], the very early stages of polymerization can be problematic in terms of heat removal and control of particle morphology. For this reason it is common practice in industry to use a prepolymerization step under mild conditions which gives a prepolymer particle capable to withstand mechanically and thermally the activity peak following introduction into the main reactor. In fact the mild conditions used during this step guarantee that polymer production rate is slow enough to have controlled and gradual support fragmentation. At the same time the presence of polymer onto the catalyst is responsible for a bigger particle area available for heat transfer with the reaction medium thus limiting the risks of thermal overshoots at the particle level and catalyst deactivation. These risks (onto which we will deeply come back later) are of course present in slurry reactions but are especially important in gas phase reactions and are one of the reasons for this work.

#### 1.2.4. Gas phase reactors

Gas phase olefin polymerization is now responsible for the majority of PO production worldwide. Its main advantage over the previously described processes is the absence of any liquid inert diluent leading to easy and inexpensive separation between the solid and the continuous phase. The absence of solubility limit allows using very high hydrogen and comonomer concentrations in the reacting gas thus extending enormously the product range (Figure 5).

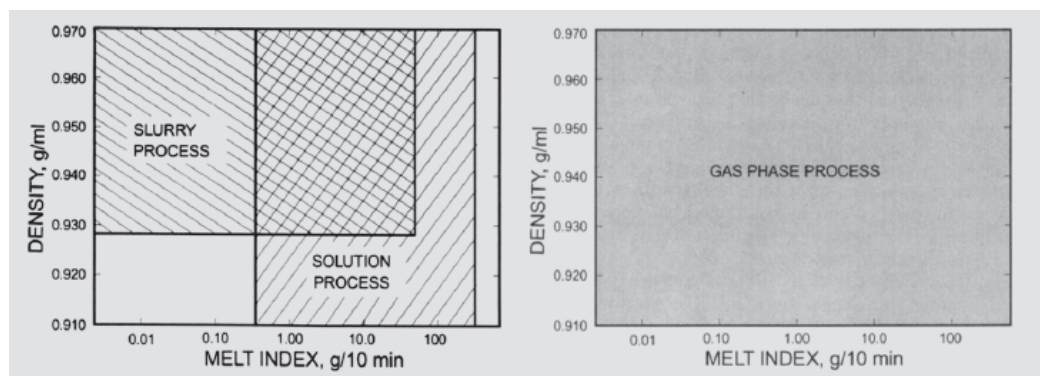


**Figure 5: Available product range with different production processes; reprinted with permission from [18]**

The main drawback of this technology respect to the ones involving a liquid phase is that heat removal from the reacting particle by a gas is much less efficient. Risks of hotspots and polymer agglomeration are then a real problem in gas phase technologies. That's why classically prepolymer particles rather than catalyst particles are fed to the reactor. Another solution to increase the heat removal is to introduce pulverulent inorganic particles (silica, alumina, NaCl) together with the prepolymer [18]. These solids act as diluents for the catalyst and the method is widely adopted at laboratory scale. The main solution adopted on industrial scale for heat removal is the condensed mode cooling which consists in using the latent heat of vaporization of the monomer to cool the reactor. The unreacted monomer is condensed in an overhead condenser and then the liquid monomer is recycled to the reactor where it evaporates again. In addition the super-condensed mode cooling can be adopted in which an inert (i.e. pentane) is introduced to the feed and used as the condensing phase to enhance heat transfer. Capacity of reactors operating in condensed mode can be more than doubled [11]. Another problem in gas phase operation is the presence of fines which, if electrostatic charges are present, can easily deposit on reactor and heat exchanger walls thus limiting heat removal capability.

The simplest reactors for gas phase polymerization are the stirred bed reactors (vertical or horizontal) where a complex stirring blade allows the bed to move along the reactor axis. Heat is removed by external heat exchangers or by side injections of liquid monomer in case of polypropylene (horizontal bed). The bed is moved from one zone to another by slow stirring. The RTD of such reactor can be approximated by few CSTR in series [18]. This feature is unique in gas phase polymerization and allows the production of polymer with uniform properties.

The most widely used gas phase reactor is the fluidized bed reactor first employed by Union Carbide in 1968 [18]. It consists of a vertical cylindrical reactor containing a distributor plate above which the bed of particles is fluidized by the gas feed (monomer + inert + hydrogen) introduced through the bottom. The gas velocity has to be high enough to fluidize the bed but low enough to prevent particle entrainment. For this reason the head of the reactor has a larger section (disengagement zone) where gas velocity is reduced and solid particles fall back to the reacting zone. Typical operating conditions are temperature between 70 and 110°C and pressure in the range 20-30 bar. The success of this reactor configuration comes from the fact that a much bigger heat removal respect to the stirred bed reactors can be achieved.

Recently LyondellBasell introduced a new technology called Spherizone (Figure 6). The reactor is similar to a loop reactor but it is operated in gas phase and divided in two parts each having different reaction conditions (hydrogen concentration for example). The first part (riser) is operated like an over-fluidized bed while in the second part the particles flow downward like in a moving packed bed and are recirculated to the riser. This allows the production of particles having layers of different composition corresponding to each pass. It is possible for example to obtain polymers with broad molecular weight distribution using “single-site” catalysts [12].

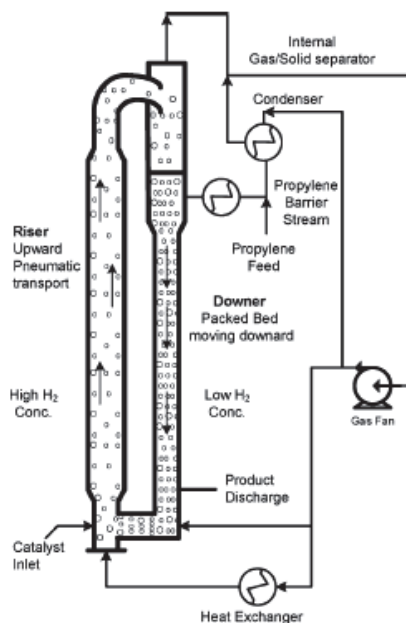


Figure 6: Schematic representation of the Spherizone reactor; reprinted with permission from [12].

### 1.2.5. Process design

On the basis of the different reactor technologies available to produce olefin based polymers, a lot of effort has been put, especially by industrial actors, to design process plants capable to producing competitive materials at a high production rate and reasonable cost. The possibility to produce completely different grades using similar catalyst only by intelligently selecting and combining different reactors is the main driving force responsible for the long lasting interest in polyolefins. The improvements reached in the reactor design allowing a high heat removal and increased production rates are further pushing the industry to invest in the polyolefin field. The few examples of successful process design presented in what follows testify the infinite possibilities that these simple materials can offer. As a general principle the control over the polymer properties can be displayed by varying the reaction conditions in the same production unit by operating with a reactor having different reaction zones or by using multiple reactors in series. The simplest configuration to obtain interesting materials in ethylene polymerization is the use of two CSTR slurry reactors in series as is done in the Mitsui process which allows the production of bimodal MWD polymers with increased processability. Another interesting process for slurry phase ethylene polymerization is the Borstar from Borealis consisting in a slurry loop reactor followed by a fluidized bed and preceded by a prepolymerization loop. The process is operated using supercritical propane as diluent. This is responsible for a low PE solubility in the diluent thus is possible to work at higher temperature and pressures and hydrogen concentration leading to polymers with very low molecular weights if compared with other slurry like processes. Interesting slurry phase processes for polypropylene production comprise the already cited Spheripol and Spherizone from LyondellBasell. The Spheripol process is the starting point for the production of impact copolymers which consists of high impact materials with polypropylene as the continuous phase and an elastomeric phase (usually an ethylene-propylene rubber) uniformly dispersed within the matrix. The rubbery phase must be homogeneously dispersed and its size controlled in order to achieve the best stiffness-impact balance. The polypropylene matrix is produced in a liquid slurry Spheripol reactor or in a fluidized bed (Unipol). The product is then sent to a second reactor into which ethylene-propylene copolymerization is performed. This process allows the production of heterophasic copolymers containing up to 40% of E/P rubber in the homopolymer matrix. For impact copolymer gas phase (fluidized or stirred bed) is the reactor of choice because of the stickiness of the copolymer and the solubility of the copolymer in the liquid propylene or in the solvent. Before the invention of this process the

heterophasic copolymers were essentially prepared by melt blending, in an extruder, the preformed polymers. This technology brought about significant limitations on the properties of the polymers to be blended. For instance, a strong difference of melt viscosities of the various components of the blend prevents from the formation of EPR domains of appropriate size. A last process worth mentioning is the Catalloy process developed by LyondellBasell. The Catalloy process consists of three gas phase reacting zones in series capable to produce random copolymers containing up to 15% of comonomer and alloys with up to 70% of multimonomer copolymers [19]. These results come from the use of a catalyst with controlled porosity and from the capability of controlling the porosity, the surface area, and the morphology of the growing polymer particle in the early stages. In this situation mechanical strength of the particle is optimized to resist to mechanical processing and allow fragmentation and the whole particle volume is easily accessible to different type of monomers throughout all the reaction steps.

From this last example it is clear how future developments in PO technology will not come only from chemical improvement of the catalyst but also from understanding of the relations between phenomena happening on multiscale levels (active site, polymer crystal, particle, reactor) during the reaction course. The most critical moment of the polymerization is undoubtedly the start-up, where significant gradients and fast transient phenomena are in play and far from being mastered. Nowadays part of the problem is shortcut by applying a prepolymerization step at soft conditions (that is reducing gradients and transients). A detailed knowledge of the behavior of the catalyst particle at the start-up could not only eliminate the need for prepolymerization but also open new possibilities to produce new materials (i.e. controlled production of EPR and PP alloys).

### 1.3. Catalysts

Due to the possibility to operate at low pressure (normally 10-30 bar) and temperature (80°C – 120°C) catalytic olefin polymerization has become the most used process to produce polyolefins. More than 80% of the total polyolefin production worldwide is carried on with catalytic processes. The capability to tune the polymer properties by selecting appropriate catalyst and process is another reason for the success of catalytic polymerization. Mainly three types of catalysis are used industrially. Catalysts history, properties and applications are briefly described in the following lines.



### 1.3.1. Ziegler-Natta catalyst

It is based on a transition metal salt of metals of groups IV to VIII and alkylmetals of group I to III. The most used formulation which derives directly from the studies of K. Ziegler in the 50's uses  $\text{TiCl}_4$  combined with alkylaluminiums (mainly triethylaluminium). The polymerization mechanism using this type of catalysis is of the coordination-insertion type (Figure 7) and has been firstly proposed by Cossee [20]. Ethylene coordinates to the metal center via the vacant site of the metal. This coordination activates the double bond and the monomer inserts into the Ti-C bond thus lengthening the polymer chain by one unit. The vacant site becomes free for the complexation of another monomer and the catalytic cycle is closed.

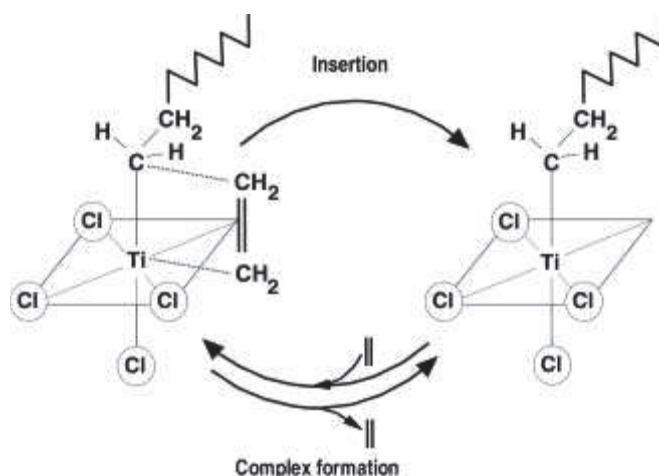


Figure 7: Cossee polymerization mechanism; reprinted with permission from [21].

The alkylmetal acts as co-catalyst or activator. It has the principal role to create the metal carbon bond where the monomer will insert by substitution of a chlorine with an alkyl group.

Ziegler-Natta catalysis is nowadays responsible for the production of a large part of the polyethylene (HDPE, LLDPE) and almost the totality of the polypropylene. This success has been achieved through a series of steep improvements driven by scientific discoveries that gave birth to new generations of ZN catalysts being capable of higher activity and higher stereospecificity. Currently the world is mostly using the 4<sup>th</sup> generation of catalysts to polymerize propylene which consists of titanium fixed on  $\text{MgCl}_2$  combined with an appropriate cocatalyst to activate the complex and internal and external electron donors. These donors are added during the preparation of the catalyst (internal Lewis base) and before the polymerization together with the alkylaluminium (external Lewis base). Their role is to selectively poison non-stereoselective sites while keeping a high activity. Ethylene

polymerization, not needing stereospecificity control, is performed mainly with the 3<sup>rd</sup> and 4<sup>th</sup> generation of catalyst without the additional electron donors.

The success of MgCl<sub>2</sub> as support is due to the high compatibility of the crystal structure of the MgCl<sub>2</sub> and Ti chlorides (TiCl<sub>4</sub>, TiCl<sub>3</sub>...) and in the high specific area of the inorganic solid leading to an increase in the number of active site species and propagation constant [22]. The metal active sites of a ZN catalyst can be influenced sterically and electronically by the environment surrounding them. The active site for monomer coordination will behave slightly differently (in terms of propagation and transfer constants) depending on the spatial coordination of the metal. A metal laying on a crystal surface is different than one supported on a crystal edge or corner. This leads to heterogeneity in the behavior of different active sites and polymer with broad molecular weight distribution (polydispersity indexes between 4 and 10) and comonomer incorporation. For these reasons ZN catalysts are also called “multi-site” catalysts.

### 1.3.2. Phillips catalyst

It is constituted mainly by chromium oxide supported on porous silica. It was discovered in 1951 by Banks and Hogan at Phillips Petroleum Company during their attempt to produce synthetic fuel from liquid hydrocarbon [5]. A chromium compound is normally reacted with silica and then calcined in an oxygen atmosphere to activate the catalyst [18]. The final catalyst is chromium in hexavalent state supported on silica. Classically CrO<sub>3</sub> has been used as initial precursor [23]. The mechanism of ethylene polymerization is still subject of debate. It is believed that ethylene can coordinate on the metal center and then reduce the Cr(VI) to Cr(II) (or other oxidation states). The active species bearing the carbon-metal bond is then formed directly by oxidative coupling upon contact of ethylene with the metal oxide and thus, differently from ZN or metallocene catalysts, no activator is needed. As is verified in ZN catalysis, the heterogeneity of the chromium active species, due to the electronic and steric influence of the environment surrounding the active sites, is responsible for a very broad molecular weight distribution of the polymers produced with Phillips catalysts (polydispersity indexes up to 20). The term “multi-site” catalyst is then usually employed also for these complexes. This catalyst is mainly used for production of HDPE and LLDPE [24] and it is very sensitive to impurities. Despite these drawbacks Phillips catalysis is still widely used in industry and is responsible for the production of one third of HDPE worldwide [25]. This is

mainly due to the facts that it exists only in the heterogeneous form (supported on silica) which is a basic requirements for large scale catalytic production processes and that no additional activator is needed. In addition the high polydispersity indexes of the produced polymers are responsible for a very easy processability of the material which is highly appreciated in industry. Because the catalyst activation can be too slow for industrial processes a solution is to pre-reduce the chromium complex with CO or other agents to eliminate the induction time [18].

### 1.3.3. Metallocene catalyst

Metallocenes are organometallic coordination complexes in which the central transition metal atom is bonded by a  $\pi$ -bond to one or two substituted or not cyclopentadienyl (Cp) rings (Figure 8). The metals used more frequently in olefin polymerization are Ti, Zr and Hf with Zr being the most popular. The possibility to vary the transition metal, the nature and the number of the substituents of the Cp rings and the rings themselves, the type of bridge between the rings (if present) and the cocatalyst opens an infinite number of ways to polymerize olefins (in terms of activity and chain microstructure).

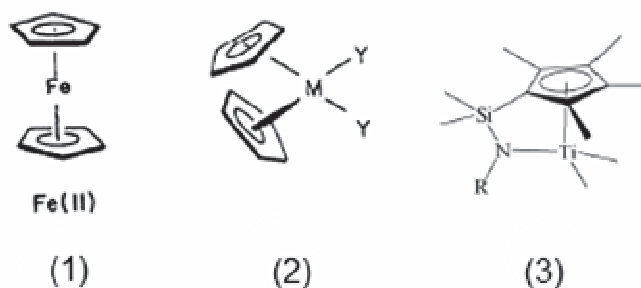


**Figure 8: Examples of metallocene types: (1) symmetric molecules with parallel Cp rings, (2) bent molecules with 2 Cp rings, (3) CGCT system.**

Metallocenes alone are not active in olefin polymerization and an activator is needed to create the active site consisting of an  $Al^- Met^+$  ion pair, a vacancy on which the monomer can coordinate and a metal carbon bond into which monomer can insert. The correct choice of the activator is in this case much more important than for the ZN catalyst and the history of the metallocene discovery and evolution clearly explains why. They have in fact been first used for olefin polymerization in the 50's by Natta to polymerize ethylene with very low activity [26]. During the 70's various research groups noted that addition of traces of water to the metallocene / trimethylaluminium (TMA) complex improved the activity in olefin

polymerization. Sinn and Kaminsky were the first to identify the potential of this discovery and came finally to the discovery of methylaluminoxane (produced by reaction of TMA with water) as a cocatalyst which increased consistently the activity of metallocenes [6, 7]. The exact structure of methylaluminoxane (MAO) is still not precisely known. Some hypothesis have been proposed by different research groups (Figure 9) ranging from one dimensional linear chain, cyclic rings, two and three dimensional structures [27].

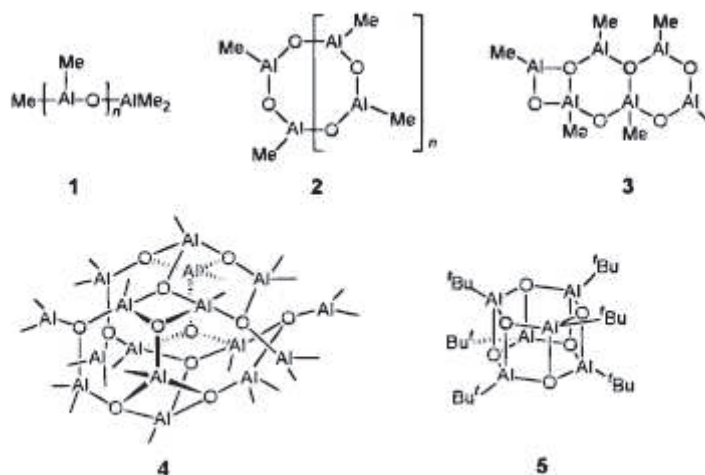


Figure 9: Different proposed metallocene structures; reprinted with permission from [27]

The structure 4 in figure 9 has been proposed by Sinn et al. [28] and up to now seems to be quite close to the reality. MAO forms a kind of cage in which unreacted TMA is present and very difficult to extract (associated TMA). The discovery of this compound opened the way for the synthesis of a high number of highly active metallocene complexes having well defined molecular architectures. Kaminsky reported activities up to  $4 \cdot 10^8$  g PE/mol Zr/h for  $\text{Cp}_2\text{ZrCl}_2/\text{MAO}$  system at  $95^\circ\text{C}$  and 8 bars of ethylene pressure [29] that is equal or even higher to classic activities for Ziegler Natta catalysts.

Catalytic activity is strongly related to the aluminium/transition metal ratio, normally increasing with increasing content of MAO. Very high contents of MAO are normally used to have interesting activities and Al / Metal ratios up to 50000 are commonly reported in literature [30]. This can be a drawback for commercial use of this catalytic system because of the high cost, the fouling properties and the high reactivity towards oxygen of MAO. One way to overcome this problem is to support the catalyst (and/or the cocatalyst) onto an inorganic support which leads to catalysts that are highly active without the need of too high Al quantities.

The polymerization mechanism is the same than for the ZN catalysts and they are sometimes called single site ZN catalysts. This is because all the active sites are surrounded by the same steric and electronic environment and behave in the same way giving polymer with a narrow molecular weight distribution (polydispersity index close to 2) and uniform comonomer incorporation. It has to be said anyway that heterogeneisation of these catalyst on inorganic supports leads to a broadening in the active sites distribution but still in a much less extent than ZN or Phillips catalyst. This phenomenon added to the fact that metallocenes are soluble in aliphatic and aromatic solvents, they can be completely characterized and the electronic and steric environment of the active center can be easily modified, has made them really interesting for industry and academia in the last 20 years.

The same type of metallocenes can be used effectively also for copolymerization. They have the ability to produce polymers with a very uniform comonomer incorporation that is essential to control copolymer composition and to produce materials that were not possible to have with Ziegler-Natta catalysts. For example Kaminsky used  $\text{Cp}_2\text{ZrCl}_2/\text{MAO}$  to copolymerize ethylene and 1-butene and obtained a copolymer with much lower melting point than the one produced with heterogeneous ZN catalysts for the same degree of 1-butene incorporation [31]. In 1992 Dow launched on the market its constrained geometry catalyst (CGC), also called half-sandwich metallocene, which consists in a cyclopentadienyl-amido complex with two very different ligands connected by a bridge. These complexes exhibit a much more opened structure in comparison to bis-Cp classical metallocenes. This unique feature allows the production of new products like polymers showing much higher incorporation of higher  $\alpha$ -olefins with narrow comonomer distribution and MWD and having an high degree of long chain branching. This causes an increased processability respect to polymers produced with classic metallocenes having narrow MWD without losing the physical properties typical of single site catalysis [4].

Propylene can also be successfully polymerized using these catalysts. In addition by selecting metallocenes with appropriate ligands it is possible to tune the chain microstructure of the polypropylene [32-35]. One of the main interests of metallocene complexes is in fact their ability to produce polymer that were not catalytically synthesizable before. We can remind here of syndiotactic polypropylene, which is a material having enhanced stability against UV and X-ray irradiation together with low density, low crystallinity, lower flexural modulus combined with high clarity [5] and which can be produced using bridged cyclopentadienyl-fluorenyl metallocenes. An outstanding example of the potential of the

metallocene-based catalysis is the production of syndiotactic polystyrene, which has been possible only from the mid 80's thanks to Ishihara who developed the CpTiX<sub>3</sub>/MAO system [5]. Syndiotactic polystyrene is a semi-crystalline material with melting temperature as high as 270°C (40°C more than isotactic polystyrene) with high heat and excellent chemical resistance [30] that can potentially replace denser polymers made by polycondensation.

In industrial processes the direct use of homogeneous metallocene complexes causes a high number of problems that will be listed in the following section. For this reason heterogeneous metallocenes, which consist of precatalysts and/or cocatalysts supported onto inorganic carriers are preferred.

Metallocene complexes supported on silica activated with MAO are the catalyst used in this study mainly because of their property to produce narrow MWD polymers. Unknown or unexpected phenomena raising during the start-up of the gas phase polymerization (which is the subject of this thesis) and leading to a modification in the active site behavior will then be easily detected. This would not have been possible in case of classical ZN catalyst that give intrinsically heterogeneous polymer properties.

## 2. Heterogeneisation of single site catalysts

### 2.1. Introduction

Despite the advantages that single site metallocene catalysts can bring, several technical problems have slowed down their industrialization. We have already said in the first pages of this chapter that polymers produced by metallocene catalysis, having a narrow MWD, can be more difficult to process respect to polyethylenes produced by other catalysts. In addition the direct use of homogeneous metallocenes in processes already existing for ZN catalysts is not possible mainly because of the difficulty in controlling polymer morphology thus causing extreme reactor fouling and because of the very large amount of MAO cocatalyst needed to have interesting activities. MAO is in fact an expensive and extremely reactive compound not suited for easy use in industry. Other cocatalysts free from those problems exist (i.e. borates) but they are even more expensive. One way to overcome these difficulties could be to design specific processes adapted for homogeneous metallocenes but this would not be economically viable. The other way is to use a heterogeneous form of metallocene in which the precatalyst,

the cocatalyst or both are supported on a solid carrier, allowing it to be directly usable in already existing slurry and gas phase processes.

Two main procedures are described in the literature for the synthesis of heterogeneous metallocene catalysts. The first consists in the construction of the metallocene precatalyst directly on the support starting with the metal atom or the Cp ligands followed by activation with the alkylaluminium. The second consist in generating the active site (constituted by an  $Al-Met^+$  ion pair) on the surface of the carrier from the ready-to-use precatalyst and cocatalyst species. The first method shows poorer catalyst performances respect to the second one as the activity and the special properties of metallocene complexes are highly compromised. The second method is the most commonly used and different orders of immobilization (precatalyst first, cocatalyst first or both together) can be employed. This method will be reviewed in section 2.3.

Different kinds of supports have been used for immobilization of metallocenes. Inorganic supports like silica, alumina, magnesium chloride or zeolites are the most studied and used. Organic supports like polysiloxanes or polkystyrenes have also been studied but, even if especially polystyrene gave promising results, more work has to be done before they can be industrialized.

## 2.2. *Silica as support*

Silica is the most widely used support for single site catalyst immobilization. Its success is due to the fact that it is a well-known solid available in an extreme variety of commercial grades. Properties like particles size, porosity, and pore size can be easily tuned during the synthesis and surface can be chemically modified without difficulty. These parameters allow to tune the precatalyst and cocatalyst distribution throughout the silica particles, the diffusion of the reactants to the active sites and the fragmentation behavior and morphology control of each specific support. In addition the mechanical properties of silica seem to be well suited for fragmentation caused by polymer growth allowing production of polymer particles with good morphology. For example Harrison et al [36] compared silica and alumina supports treated with MAO for ethylene homo and copolymerization. To prepare their catalyst they firstly performed an impregnation of the inorganic support with MAO followed by the reaction of the modified solid with different metallocene precatalysts. They found similar

activities for both supports but particles produced with alumina supports showed poor morphology properties with irregular shapes, broad size distribution and low density. It is then easy to understand how not only the physico-chemical properties of the support (porosity, surface area, [OH]) are important, but also mechanical properties should be adapted to ensure good morphology control during support fragmentation. It is possible that aluminium oxide could not offer adequate properties in this sense.

Silica exists in a number of phases including anhydrous crystalline phases (quartz, cristobalite etc.) but the phase used for catalyst support is normally the common amorphous silica [12]. Grades used for polymerization are usually fully hydroxylated amorphous silicas. These solids have the capability to adsorb a big amount of water due to the –OH groups present at the surface so that a thermal treatment to remove the water is compulsory before using in polymerization. During the same thermal treatment the concentration of silanol groups is also reduced. Three different types of hydroxyl groups (Figure 10) can be distinguished on silica surface: isolated, geminal and vicinal.

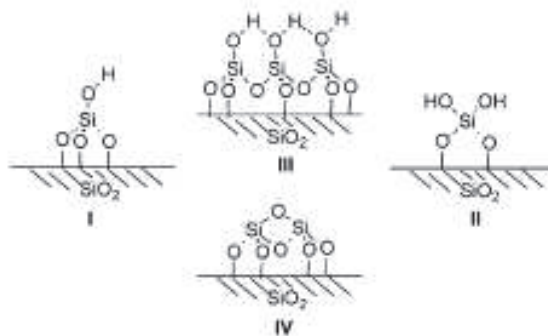


**Figure 10: Silica surface hydroxyl species: I isolated, II geminal, III vicinal, IV siloxane; reprinted with permission from [12]**

Adsorbed water starts to desorb between 25 and 105°C while hydrogen bonded water molecules need temperatures up to 180°C. At higher temperatures the adjacent vicinal silanol groups condense with each other to form a siloxane bridge. The final density of silanol groups is a physico chemical constant as found by Zhuravlev [37] and depends only on the calcination temperature. A fully hydroxylated silica has 4.6 +/- 0.5 OH/nm<sup>2</sup> and increasing calcinations temperature decreases this number in a way that is independent on silica properties (Figure 11) [38].



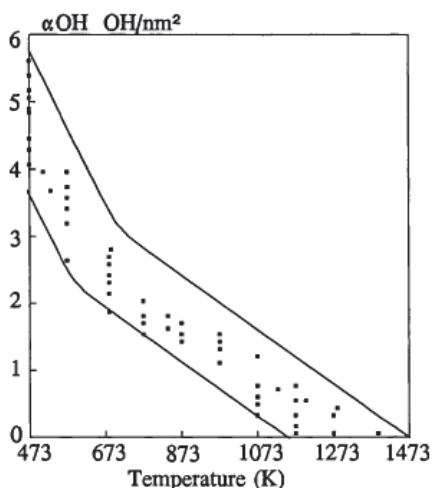


Figure 11: OH concentration dependence on calcination temperature; reprinted with permission from [38].

### 2.3. Methods of immobilization of metallocene catalysts

The main preparatory routes reported in the literature for the immobilization of the active species on silica supports are classified according to the impregnation order of the precatalyst and the cocatalyst:

1. Direct impregnation of the metallocene onto the silica and subsequent activation with MAO.
2. Immobilization of MAO on silica and subsequent reaction with the metallocene compound
3. Contacting the aluminoxane and the metallocene in solution before supporting and supporting of the precatalyst-MAO solution

Supporting aluminoxane on silica and then treating the modified support with metallocene is the earliest and most frequently used (also commercially) method to immobilize single site catalysts. This is also the technique that will be used in this study.

Welborn and Takahashi [39, 40] contacted silica with a toluene solution of MAO and treated the isolated solid with a metallocene obtaining a heterogeneous catalyst effective for homo and copolymerization of ethylene in gas-phase processes. Addition of alkylaluminium or aluminoxane during the reaction augments consistently the activity of these catalysts. MAO bonds chemically to the silica surface by reacting with the hydroxyl groups. In the

second stage metallocene reacts with the MAO fixed on the silica surface to form an ion pair (Figure 12). Several types of surface groups exist thus leading potentially to different type of active sites during the supporting. In this sense the supporting parameters and chemical and thermal treatments of the support play a tremendous role in defining the catalyst behavior. This can also explain why molecular weight distribution of supported single site catalysts is often broader than the one produced by the respective homogeneous version. Chen [41] proposed that metallocene ionic species are trapped and stabilized by multicoordinating “crown” of aluminoxane complexes that cover the surface of the support. In this case the metallocene species, being linked only by an ionic bond, is more or less free to float over the solid surface much like in solution and keeps the peculiar properties of stereospecificity of the respective non-supported version.

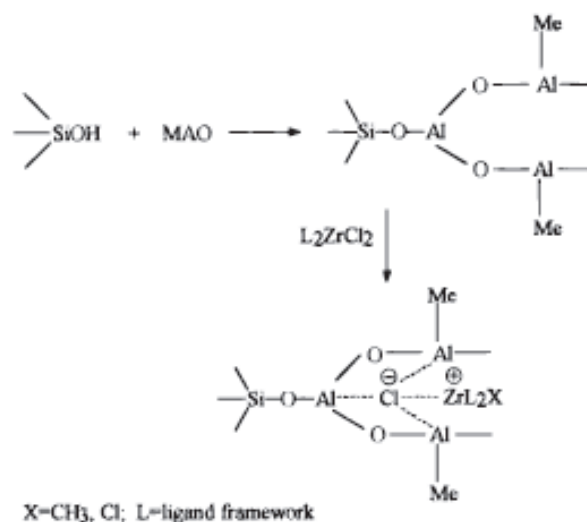


**Figure 12: Possible formation mechanism of zirconocene species in MAO modified silica; reprinted with permission from [42].**

Dos Santos [43], while studying the adsorption isotherms for TMA and MAO on silica showed that MAO plays a steric role during the surface reaction shielding the unreacted surface silanol from further reaction and from combination with the metallocene. This goes in the sense of what Chen proposed: MAO acts as a kind of protection for the metallocene complex avoiding decomposition of the coordination sphere upon reaction with surface silanol groups.

In general activities of heterogeneous catalysts produced with this method are around 1 order of magnitude lower than activities of homogeneous catalysts. Nevertheless stereospecificity is maintained supporting the idea that due to the shielding caused by MAO,

metallocene complex supported on silica/MAO behaves more or less like in solution with the advantage of being capable to work with low amounts of cocatalysts (Al/Zr ~ 300) [44].

Other numerous techniques to fix MAO on silica and successively react metallocene complexes are present in literature among which we can cite the generation of aluminoxane in situ by reaction of alkylaluminiums with water in presence of the support [45] and the in-situ immobilization of the precatalyst onto silica supported MAO within the polymerization reactor [46]. The interested reader will find an exhaustive literature review in [12, 42, 44, 47].

## 2.4. *Influence of silica properties and preparation*

We have seen in the previous paragraph how is possible to heterogenize a metallocene catalyst in different ways. The procedure used to support the catalyst is responsible for the creation of metal sites that are activated differently according to the preparation. This will give different catalyst activities and stabilities, and will influence polymer properties like molecular weight distribution, melting temperature and stereospecificity. Another important factor playing a role in defining catalyst behavior is the support itself. Physical and chemical properties of the support can be fundamental in determining the course of both the catalyst preparation and the polymerization reactions. For example particle size, porosity and pore size influence the diffusion of the cocatalyst and the precatalyst during the metallocene heterogeneization and the diffusion of the reactants together with the particle temperature profile during the polymerization. The support structure, which is defined by its specific surface, its pore size distribution and its pore volume, defines the way the particle fragments and how the morphology will evolve. Physicochemical properties as the density of surface hydroxyl groups have an influence mainly during the catalyst preparation by defining the amount of active sites that the inorganic particle can support and the electronic and steric environment that the active site experiences thus determining the intrinsic activity of the final catalyst. When using a commercial silica support intrinsic physical properties like pore size distribution and pore volume are fixed and cannot be altered. Controllable properties are the support size, which can be selected after appropriate sieving of the carrier or the end-catalyst and the hydroxyl groups concentration, which depends, as already said, on the degree of thermal treatment undergone by the silica particles. In this work controllable parameters will be varied to study their influence on the polymerization start-up while the effect of different intrinsic physical properties will be studied by selecting different commercial silica grades. A

brief review on the literature related to the influence of silica properties on olefin polymerization will be given below.

Before going on it is important to underline that properties like particle size, pore volume and pore size are usually characterized by an average value but are in reality distributed over a more or less wide range. The production method is responsible for a certain amount of heterogeneity in the properties of the silica particles [48]. This can be easily seen in Figure 13 where we can see that the silica carrier is formed of pseudospherical particles highly heterogeneous in terms of internal structure. Some of them are compact, other very porous, other show small fragments around a big central fragment with porosity only on the exterior of the particle

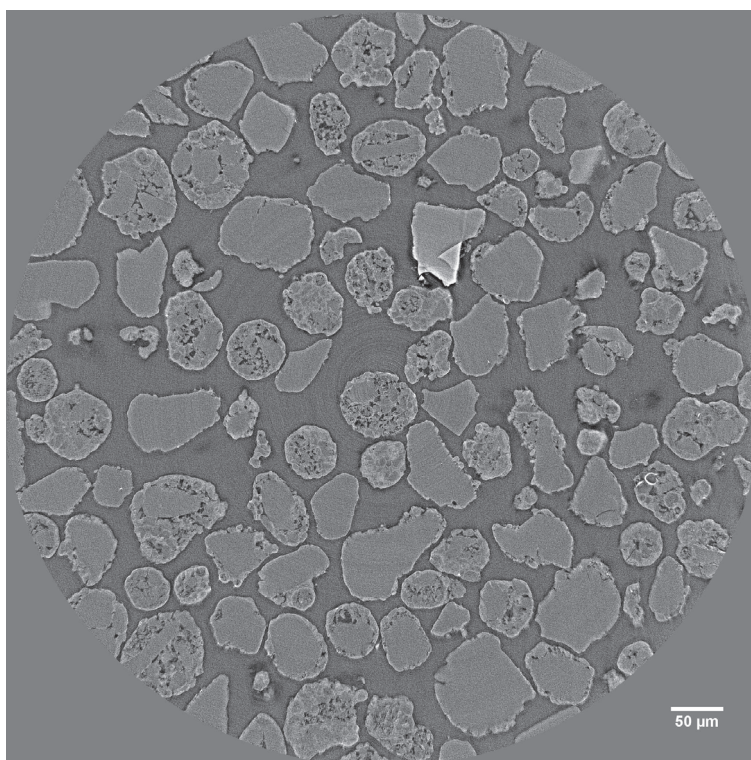


**Figure 13: Tomo -RX of a commercial silica sample (Grace 948)**

#### 2.4.1. Support preparation

We have seen that catalyst and cocatalyst impregnation on silica can be carried out using different methods. Dos Santos [43] prepared different catalysts using direct impregnation of a catalyst or a cocatalyst solution on silica Grace 948 and studied the effect of different initial Al concentration to determine the adsorption isotherm of cocatalyst on silica. The impregnation was conducted at room temperature using MAO (0.4-30 wt % Al/SiO<sub>2</sub>) or TMA (0.4-12 wt % Al/SiO<sub>2</sub>) as cocatalyst and Cp<sub>2</sub>ZrCl<sub>2</sub> (0.4-12 wt% Zr/SiO<sub>2</sub>) as precatalyst. It was

found that using MAO a saturation limit was attained at 12 wt % Al/SiO<sub>2</sub> in the initial solution that is 4 times higher than for TMA, thus confirming the MAO oligomeric structure. Upon reaction of the precatalyst with the alkylaluminium-modified silica an activity equal to the half of the one of the homogeneous reaction was observed, no matter the metal loading or the cocatalyst used. Later the same group [49] used MAO (0.5-20 wt % Al/SiO<sub>2</sub>) to modify the same support and reacted it with (nBuCp)<sub>2</sub>ZrCl<sub>2</sub> (1.5 wt % Zr/SiO<sub>2</sub>). Maximum fixed Zr was found for Al contents between 2 and 4 wt%. Increasing the Al/SiO<sub>2</sub> ratio led to a decrease in the fixed Zr content probably because of the plateau reached by the MAO adsorption isotherm around 10 wt% Al/SiO<sub>2</sub>. Excessive MAO is only physically deposited and washed away with part of the immobilized zirconocene species. Anyway the higher catalyst activities were found with MAO-modified silica having close to 2 wt% Al/SiO<sub>2</sub>. The authors explained this fact after spectroscopic analysis of the absorbed species saying that increased MAO (and related TMA) content is responsible for a larger consumption of silanol groups by the TMA leading to a less stable grafted MAO. It is also possible that an increased quantity of Al absorbed on the silica surface leads to a higher probability of formation of binuclear inactive species.

When contacting a support with a catalyst or a cocatalyst the two main reaction parameters are temperature and contact time. Dos Santos et al [50] studied the influence of these two parameters on the activity and polymer properties using (nBuCp)<sub>2</sub>ZrCl<sub>2</sub> directly grafted on the support and activated by MAO in ethylene homopolymerization. They found that, working at ambient temperature, maximum loading is achieved after 12h but the surface reaction is instantaneous (0.28 wt% Zr/SiO<sub>2</sub> after 0.1h). Higher reaction times bear reduced metal loadings. Activity, on the other side, was at maximum for grafting times between 1 and 6 h. For longer grafting times corresponding to higher metal loadings the catalyst seems to be deactivated. Molecular weight followed the same trend while polydispersity was not affected (except for the shortest grafting, showing broad molecular weight distribution). In the same study they varied the grafting temperature (298, 353, 383 K) while keeping constant the time (30 min). It was found that temperature of 353 K leads to higher activity than 298K even if the metal content is comparable. Too high grafting temperatures are responsible for a decrease in catalyst activity and diversity in nature of the catalytic sites as indicated by the broader molar mass distribution.

Chadwick et al [51, 52] studied the effect of grafting temperature and time using MAO modified silica reacted with *rac*-EtInd<sub>2</sub>ZrCl<sub>2</sub> in propylene polymerization. They prepared a silica/MAO using “soft” conditions (room T, 2h) and a second one using “harsh” conditions

(110°C, 4h). After EDX analysis they saw that using soft conditions it is frequent to have core-shell distribution of Al onto the support with MAO being unable to diffuse effectively towards the particle center probably because of its tendency to form gels that can be broken with higher temperature. This leads to the formation of undesired hollow polymer particles. Using a more rigorous impregnation procedure, the Al distribution into the particle was homogeneous. It was also found that increasing the initial quantity of MAO in the immobilization step resulted in increased activity, decreased molecular weight and some deterioration in particle morphology.

Finally Tisse [53] investigated the behavior of  $\text{EtInd}_2\text{ZrCl}_2$  supported on MAO-modified silica synthesized using different catalyst properties and reaction conditions. In her work she found that bigger catalyst particles showed lower activities. The activities were not so high to explain this only with monomer diffusion limitation so the hypothesis of MAO diffusion limitation was considered. The catalysts were prepared impregnating MAO on different supports at 85°C but using the same reaction time (1h), no matter the particle size. However, the characteristic time for diffusion is four times greater for the larger particles (80-100  $\mu\text{m}$ ) than in the smaller ones (36-45  $\mu\text{m}$ ). The impregnation time for larger particles was then multiplied by 4 and a visible increase in activity was observed (30%). However it was seen that increasing the impregnation time did not increase the observed activity to a level comparable to the smaller particles.

#### 2.4.2. Deshydroxilation temperature

It is known that the behavior of a silica support in the heterogeneization of metallocene systems is highly dependent on the surface chemical properties of the solid. These are mainly defined, in case of unmodified silica, by the nature and number of hydroxyl groups which, in turn, are fixed by the deshydroxilation (or calcination) temperature. The calcination temperature then affects deeply the ability of the support to anchor the different species. Van Grieken et al. [54] studied with IR techniques the variation of the nature of the surface hydroxyl groups on mesoporous silica calcined at different temperatures. They found that increasing dehydration temperature leads to higher concentration of isolated silanols. They performed a direct impregnation of  $\text{Cp}_2\text{ZrCl}_2$  at room temperature for 3 hours on silicas treated at different temperatures finding that the amount of immobilized Zr decreased with increasing calcination temperature in a way similar to the total number of hydroxyl groups.

They also prepared different MAO modified silicas by room temperature impregnation. They found a maximum in MAO adsorption for silicas treated at 450°C and a very quick adsorption degradation for higher calcinations temperature. This suggests a very different affinity of the silica surface towards precatalyst or cocatalyst. Al-O bond is more stable on geminal hydroxyls and higher calcinations temperature induce condensation thus decreasing the contribution of this hydroxyl group type.

Dos Santos et al. [55] studied the effect of silica dehydroxylation temperature on the activity of silica supported  $(n\text{BuCp})_2\text{ZrCl}_2$ . They found that higher metal loading was reached for silica treated at lower temperature (higher OH concentration) while calcinations temperature between 373 and 723 K led to similar immobilized metallocene contents. From IR measurements they saw that only 30% of the OH groups are consumed upon grafting. They advanced the hypothesis that the bulky nBuCp ligands of the grafted species can hinder the access to the residual OH groups to the incoming metallocene molecules. The catalyst activity progressively increased with calcination temperature. At low temperature the higher OH concentration could be responsible for the formation of inactive bimetallic species while higher temperature could lead to a better distribution of the surface active sites.

Chadwick [51] supported different metallocene catalysts for polypropylene polymerization on MAO modified silica calcined at 250 and 600°C. A decrease in the residual OH content was measured with increasing calcination temperature. The authors claimed that only isolated silanols should remain after treatment at 600°C. Higher activities were found for supports calcined at lower temperature while higher molecular weights and isotacticities were measured using support treated at higher temperatures. Complete disappearance of OH groups was found only in one support calcined at 600°C. The same support was the only one showing homogeneous Al distribution throughout the particle diameter. The higher activities for the support showing core-shell Al distribution (treated at lower temperatures) were attributed to a higher Al/Zr ratio at the particle shell and not to monomer diffusion limitations. The assumption is justified by the fact that higher molar masses were produced with less active supports. Performing the impregnation under more rigorous conditions (see previous paragraph) led to similar activities for supports calcined at different temperatures.

### 2.4.3. Silica porosity

The porosity of the inorganic support is the most important physical factor influencing the behavior of a supported metallocene catalyst. Porosity of a solid is described by the particle pore volume, the pore size distribution and the average pore size. Porosity influences mainly the diffusion of the catalytic species (cocatalyst, precatalyst) and of the reactants into the particle and the fragmentation behavior of the solid under the stresses produced on pore wall by the growing polymer. We will also see later that a polymer in a pore behaves differently than in bulk and properties like crystallinity, crystal size and melting temperature can be modified by the space constriction imposed by the pore walls (this is true especially prior to fragmentation). Pores can be classified mainly into three categories: micropores (less than 2 nm diameter), mesopores (diameter between 4 and 100 nm), macropores (bigger than 100 nm) [56]. Silica particles have mainly mesopores which are the ones playing a role in olefin polymerization. Macropores are present in the original support but can also form upon the carrier fragmentation.

Mc Daniel [57] was one of the firsts to study the effect of the silica morphology on activity and fragmentation of chromium and titanium based catalysts. He used particle sizes of 177-250  $\mu\text{m}$  and carefully burned the polymer produced at different reaction times to recover catalyst fragments and measure their particle size distribution. We have to point out here that particle size of modern catalysts is around 50 $\mu\text{m}$  for silica carriers and around 20  $\mu\text{m}$  for  $\text{MgCl}_2$  supports. The particles in Mc Daniel's work are much bigger, as it was common for Phillips catalysts in the early 80's. This difference could induce a completely different mass and heat transfer behavior respect to nowadays catalysts (included the ones we will use in this work). Nevertheless this was a pioneer work and has to be cited as it was the first to describe experimentally the fragmentation of silica carriers. For Ti based catalysts it was found that activity increased as pore volume increased. Non porous colloidal silica with very small particle sizes showed the same activity as the most porous micrometric silica. In addition the inactive silicas contained mainly pores smaller than 6nm even if the total pore volume could be high. Cr based catalysts produced lower molecular weight polymers if the support had higher pore diameter. By comparing  $\text{N}_2$  sorption of fragments and original support it was shown that most of the initial fracturing occurs in the bigger mesopores while smaller pores are involved later. Smallest pores (< 6 nm) are never involved in the fragmentation process. Fragmentation path was independent on particle size and no connection between reaction rate and fragment size was found. Ti and Cr based catalyst show different polymerization kinetics



profile even though their fragmentation pattern was comparable. Fracturing stopped when catalyst fragments reached 5 - 8  $\mu\text{m}$  (depending on the used silica). In summary pore volume and average pore size are both important parameters in controlling diffusion and fragmentation. If one thinks that modern catalysts can be as small as 10 $\mu\text{m}$  (which is a dimension comparable to the size of the smallest fragments observed by McDaniel) it is easy to notice that heterogeneous catalysts have greatly evolved in the last 30 years. It is then possible that the results obtained by McDaniel could not be entirely valid for modern particles. Nevertheless his work can be considered as a basis of the study of silica support fragmentation during ethylene polymerization.

Different studies agreed in finding that pores that are too narrow are deleterious for catalytic activity. The possible explanations given by the authors are nevertheless quite heterogeneous. Korach et al. [58] synthesised vanadium based catalysts supported on silica xerogels having different morphological features. They found that supports having average pore size lower than 5 nm were not active in ethylene polymerization neither in slurry nor in gas phase. They explained this with physical blocking of active sites located onto the internal surface by the growing polymer. This would mean that their support was not able to provide sufficient fragmentation. Unfortunately no morphological study was presented. The other tested supports were all active in ethylene polymerization with activity independent from pore size. Nevertheless the studied pore size range was quite narrow (10 to 18 nm).

In an earlier study Sano [59, 60] started from the assumption of MAO being constituted by a mixture of different oligomers and tried to separate them by adsorbing MAO on different siliceous porous materials (silica gels, MCM-41, silicalite) with average pore size ranging from 0.5 to 30 nm. The quantities of adsorbed and non adsorbed Al were measured and both fractions were used to perform ethylene and propylene polymerization with  $\text{Cp}_2\text{ZrCl}_2$ . It was found that the more active form of MAO is the one adsorbed onto 2.5 nm pore size. From NMR and mass spectrometry characterizations it seemed that the more active support is the one retaining the higher molecular weight MAO form.

Similar findings are available from the works of Kumkaev et al. [61, 62]. They used MAO modified microporous molecular sieves with pore sizes between 0.5 and 25 nm as support for  $(\text{nBuCp})_2\text{ZrCl}_2$  and they tested them in gas phase ethylene polymerization. All the catalysts showed the same amount of supported Zr. In case of homopolymerization, the maximum activity was found for pore sizes between 2.5 and 6 nm. Smaller or larger pores yielded lower catalyst activities. The differences were nevertheless reduced with increasing reaction

temperature. It was claimed that for smaller pores diffusion limitation of the cyclic cage structure of the MAO was the dominant factor. Adsorption of less active forms of MAO in larger pores (comparable to Sano et al.) was proposed as an explanation for the decreased activity with increasing pore size. Tisse [63] attributes this behavior to a lack of stabilization of the MAO cage by the pore walls in case of too large pores. The molar masses and polydispersities were not function of the support pore size. In case of gas phase ethylene-hexene copolymerization the activities were much more dependent on support pore size indicating that the comonomer participates in the activation processes. The pore size of the supports had a significant effect on the comonomer incorporation into the polymer backbone. TREF analysis indicate that multiple type of catalytic sites are present and that sites corresponding to homopolymerization are more present in supports having small pores (and higher activity) while comonomer insertion is favored with supports having larger pores. Logically the homopolymer content decreased with increasing pore size of the catalyst. It has to be added that for shorter reaction times (30min) significant amount of homopolymerization sites were present also for supports having large pores as confirmed by decrease in crystallinity with reaction time for this catalyst. Active site behavior can then change during the course of the reaction. Larger pores were also responsible for DSC endotherms with several maxima.

Tisse [53] studied quite in detail the effect of pore volume (1 to 3 mL/g ) and pore size (3.7 to 40 nm) on slurry ethylene polymerization using  $\text{EtInd}_2\text{ZrCl}_2$  supported on MAO modified silicas or on activated supports (silicas modified with Al and F so that no MAO is needed). For both supports, differently from what stated by McDaniel for Phillips catalysts, an increase in pore volume did not lead to a systematic increase in catalyst activity. In addition no clear relation was found between pore size and activity, except from the fact that too narrow pores led to inactive catalysts. Polymer properties like molar mass or polydispersity were not influenced by the pore size. The authors claimed pore blockage by polymer to be a possible explanation for this behavior. Another possible explanation can come from the concept of critical pore diameter introduced by Tian et al [64]. A pore diameter has to be sufficiently large to allow bounding of aluminoxane having size between 1 and 5 nm and diffusion of metallocene having size between 0.5 and 3 nm. Average sizes of aluminoxane and metallocene together could be around 2.5 nm so that too small pores could be completely blocked by active species only and not necessarily by the growing polymer.

Another work worth mentioning is the detailed study of Dos Santos et al. on the effect of silica texture on supported metallocene catalysts [65]. They supported a mixture of metallocenes on the supports and activated them with MAO to perform ethylene homopolymerizations in slurry phase. They found an increase in catalyst activity with increasing pore size with pore diameters ranging from 4 to 15 nm. This increase corresponded to a decrease in the Zr-C distance measured by EXAFS. It was stated that the grafted metallocenes are somehow interacting with the pore walls and that for small pores the proximity between silanol groups and the metallocene could provoke an increase in the Zr-C distance and a corresponding activity decrease. It is possible that in small pores residual silanols could be present because of hydrogen bonds between them caused by their proximity thus creating interactions with the metallocene complexes or even bimetallic inactive structures. It is interesting to notice that the authors came to the same conclusion as McDaniel: the increase in catalyst activity is accompanied by the reduction of the fraction of micropores. A decreased catalyst activity seems also to be caused by excessive roughness of the catalyst surface measured by AFM. Roughness can in fact be a source of obstacle for the diffusion of active species into the pores. Molecular weight variations of the produced polymers were explained with the Zr – O distance of the grafted metallocenes. It was seen that if the Zr- O distance increases the molar mass decreases. This could be explained with the known fact that the less the active site is sterically influenced by support, the more frequent will be the chain transfer reaction by  $\beta$ -H elimination.

Last but not least we cannot forget to mention the recent works of Denifl et al [66-69], dealing with the synthesis of novel ZN catalysts supported on  $MgCl_2$  or single site type heterogeneous catalysts (the nature of the support is unknown) based on an emulsion type process called Sirius and developed by Borealis. The peculiar preparation method allows the production of spherical homogeneous particles showing a very low surface area (less than 10  $m^2/g$ ) and, probably, predominance of micropores in the particle structure. The homogeneity of the formed objects is the major strength of this new type of heterogeneous catalyst and is responsible for a homogeneous behavior of different particles during the fragmentation step, thus overcoming one of the difficulties related to the use of silica supported catalysts ([48] and Figure 13). The emulsion type synthesis allows in addition to reach much higher levels of active metal in the final single site catalyst respect to more classical impregnation methods on inorganic carriers. In addition fragmentation of these particles seems to start instantaneously through all the particle section, thus not following the layer-by-layer behavior introduced by

Chiovetta. It seems however from the published work, that the use of severe polymerization conditions can easily lead to broken or open spherical morphologies and to the loss of the morphology replication behavior.

#### 2.4.4. Silica particle size

Support particle size should not have a strong direct influence on the evolution of particle morphology and fragmentation behavior. Nevertheless its impact on mass and heat transfer is clearly recognized in literature and can be a critical factor at the reaction start-up for the diffusion of monomers and during the catalyst preparation for the diffusion of the solution of the active species (bulky MAO especially). The characteristic diffusion times for mass and heat transport in a catalytic particle are both dependent on the square of the particle radius. The initial ratio of surface area to volume is the factor determining the heat transfer from the particle. Various modeling works [70-74] have come to the conclusion that particle size can play an important role in catalyst temperature overshoot and in monomer depletion at the start-up. Experimental works, on the other side, are quite rare in the literature and only in the last 5 to 10 years some consistent studies have been published.

The first work about the influence of the catalyst particle size on activity profile was published by Fink [48]. He studied the kinetic profile and fragmentation path of a metallocene catalyst supported on MAO modified silica in propene polymerization. It was found that activity showed an initial peak (prepolymerization period) followed by a sharp decrease to very low values. Low activity values were assigned to diffusion limitations caused by the PP layer formed during the prepolymerization period around the catalyst particle. This period lasted few minutes and was called induction period. With increasing reaction time an activity rise to a plateau was measured. This was attributed to exposure of new active sites to reactants due to beginning of support fragmentation because of polymer formation in the particle interior. This phase is called "polymer growth". The rise continues until a plateau in activity value is reached corresponding to completed fragmentation and particle growth. Varying the particle size changes the previously described activity profile. The larger the particle diameter is, the longer the induction period and the slower the activity rise. The researchers attributed this behavior to a smaller outer surface of the bigger particle and to a bigger volume that has to be fragmented for bigger particles. Nevertheless no indication of Al content and distribution on supports having different sizes has been given and thus the possibility of a

dependence of the Al content on the particle size can not be neglected. In addition the polymerizations were performed under very mild conditions (ambient pressure and temperature between 40 and 60°C) so that unusually low reaction rate was obtained.

Three years later the same group introduced the videomicroscopy technique to study in real time the particle growth during catalytic ethylene polymerization using a silica supported metallocene catalyst [75]. The activity was calculated by measuring the variation with time of the projection area of the catalyst/polymer particle. The particle volume was calculated supposing that the particle is a sphere having an equivalent projection area. The same activity profile as in the previous study was found, with an activity maximum around 15 minutes. It was found that small particles show lower activity respect to the larger ones. This was attributed to larger deactivation of catalyst surface by impurities and to less active centers per particle. The particle size range nevertheless was quite narrow (31 – 58  $\mu\text{m}$ ). In addition, if the same active site concentration is present on particles having different sizes, the reaction rate normalized to the particle weight or volume should not be dependent on particle diameter. Finally particle temperature, which can be responsible for partial catalyst deactivation at the start up, was not measured. Kumkaew [61] while testing catalysts with different porosities and sizes, advanced the hypothesis that activity profiles consisting of rapid activation followed by rapid deactivation (as he saw for one of his catalyst formed by chunky particles of 100-300 $\mu\text{m}$ ) can be due to temperature values inside the growing particles that can be much higher than measured in the gas phase.

Pater et al. [76] developed the videomicroscopy technique to study the behavior of ZN catalyst of the 4<sup>th</sup> generation in the gas phase polymerization of propylene. Their reactor, consisting of a 6 mL chamber, was equipped with an optical microscope and an infrared camera to measure single particle temperature evolution. The use of a stagnant gas could be nevertheless a reason for non optimal heat removal. The reaction rate was calculated with the projection method explained above which can be of course source of errors as the silica particles are far from being perfectly spherical. In spite of a quite poor reproducibility in the measured reaction rates (also because of spherical aberration and background blurring) the researchers could find interesting results. First of all they didn't see any influence of particle size on reaction rate (even if the studied particle size range was narrow, 25 to 45  $\mu\text{m}$ ). They saw that after only 10s the particle started already to grow. The reaction rates were 5 to 7 times lower than in liquid pool polymerization. This was explained with a difficult activation of the catalyst in such gas phase system. Infrared measurements showed a temperature

increase of 8°C in 7 minutes for reaction conducted at 66°C and 15 bar of propylene with the addition of 0.5 bar of hydrogen. In the case of ethylene and propylene copolymerization an increase of 8°C in 3 minutes was measured for particles of 10 µm while bigger particles (25 µm) showed a temperature overshoot of 15°C. As expected, larger particles show larger temperature rise. It has to be noticed how temperature maximum is reached much more lately than predicted by modeling. This can be due to the underlying surface that is in contact with the catalyst particles.

Hamilton et al. [77] used a similar setup to study the behavior of silica supported metallocene catalysts in gas phase ethylene polymerization. The main modification was the use of a nylon grid to support the active particles thus limiting the disturbing effect on heat transfer from the underlying surface. Maximum particle temperature increase lies in the range 2.5°C – 7.2°C for different reaction conditions (temperature, gas composition) for a support size of 50µm tested at a total pressure of 21 bar. The temperature peak was reached very quickly (after 3 to 12 s of reaction) as predicted by models. It is interesting to notice that the maximum temperature is reached far before the maximum in activity (1-10s for temperature, 50-100s for activity). The authors studied the effect of particle size in propylene polymerization at temperatures ranging from 80 to 90°C and total pressure of 7 bar (93 vol % propylene, 7 vol % hydrogen). The average particle peak temperature was 1.2, 2.3 and 3.7 °C for particles with a diameter of 25, 41 and 70 µm respectively. This trend agrees with model predictions and proves that the bigger the particle diameter, the lower the heat transfer from the particle.

The activity profile, measured as the temporal variation of the dimensionless particle volume, was independent of particle size, as found by Pater et al.

The same group showed also how particle clusters can potentially be the source of operational problems in fluidized bed reactors. The increase in temperature of a cluster of catalyst particles exposed to ethylene and butene was of 16.4°C while a single particle showed only 6 °C of temperature overshoot.

Tisse [53] studied the influence of the support particle size distribution on activity and polymer properties in slurry phase ethylene polymerization using metallocenes supported on MAO modified silica and on support activators. Batches of supports were sieved to obtain different cuts of particle sizes and each cut was used to synthesize a supported metallocene. For both supports they found that smaller particles show higher activities and faster

activation. It is interesting to notice also that the kinetic profile reconstituted from the weighted sum of the kinetic profile of each particle size is close to the one of the original support batch. No influence on molar masses was measured. The behavior was then attributed to possible different locations of active sites in particles having different diameters due to mass transfer resistances during the catalyst preparation step.

## 3. Single particle modeling

### 3.1. Generalities

Olefin polymerization using supported catalysts is a complex subject and various attempts of modeling have been published over the course of the past 4 decades (see [78] for a complete review). In spite of this effort a reliable model for calculation of polymer properties, particle fragmentation and morphology, temperature and concentration profile inside the particle is still unavailable. What is available are different models focusing on one or more of the properties just cited and applicable in some specific cases.

When a catalyst particle, typically on the order of 15-60 $\mu\text{m}$  in diameter, is exposed to a reactive environment (this could be in gas or liquid phase) the monomer and the other reactants (and the eventual inerts) diffuse from the bulk through the particle boundary layer to reach the particle surface. The monomers have then to diffuse into the particle pore space and eventually through the already formed polymer layer to reach the active sites, where the reaction happens. The reaction generates heat that is evacuated from the particle in the opposite way. Each of these steps can have an associated mass and heat transfer resistances that must be overcome (Figure 14).

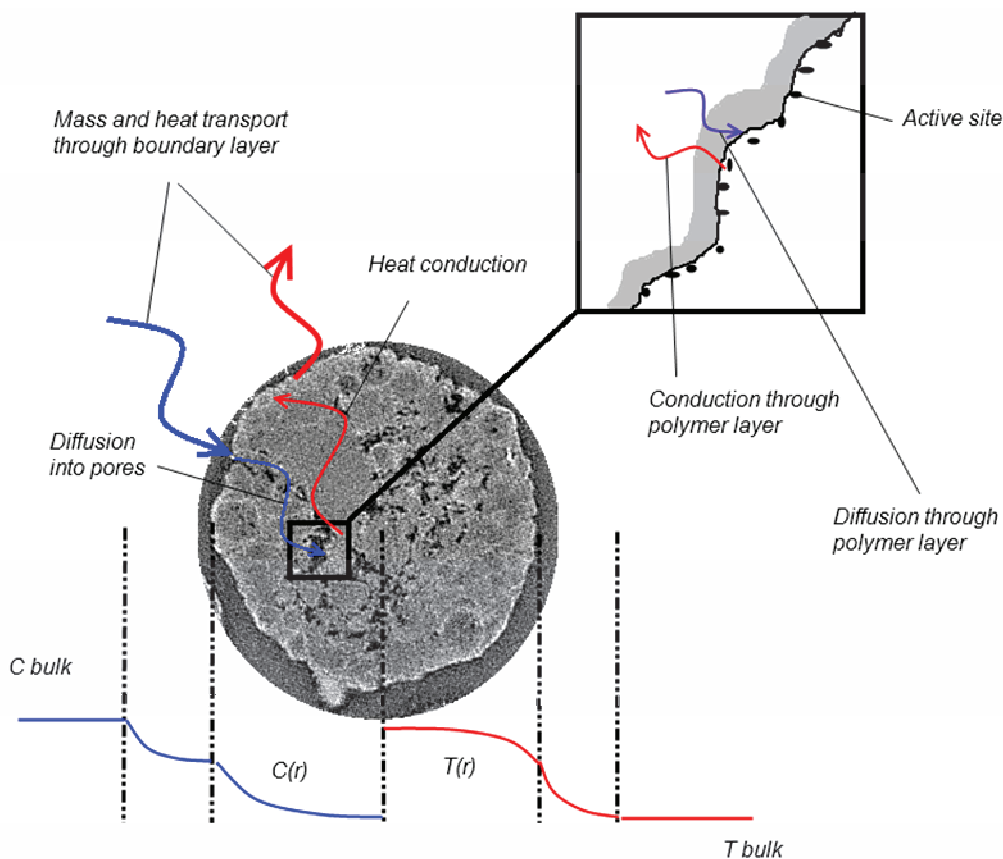


**Figure 14: Mass and heat transfer resistances in a polymerizing particle.**

Once the monomer has reached the active site the polymer starts immediately to form onto the pore walls. After a short time the pores (not all of them; which ones is still matter of debate) of the catalyst are filled with polymer. This creates localized forces acting on the support network. If the catalyst is too strong and does not break the pores become clogged with polymer thus creating an extremely high mass transfer resistance responsible for the gradual extinction of the polymerization. If everything goes well the support fragments thus creating new void space and facilitating the access of reactants to active site. Nevertheless fragmentation should not be too rapid or violent as the particle will break up into many pieces before enough polymer is made to maintain the integrity of the support. This will lead to fines generation and eventually to risk of reactor shutdown. In the ideal case one catalyst particle will generate one polymer particle. Due to the high productivities, the quantity of catalyst fragments in the final polymer particle will be negligible. Once the particle fragments, polymer continues to grow inside the particle causing its expansion. Temperature profile inside the particle must also be controlled during the reaction. An excessive temperature excursion will eventually lead to polymer softening or melting with subsequent particle clustering, pore clogging, diffusion limitation and reaction extinction. Temperature excursions



are more important at the reaction start-up, when the external particle surface is low and the volumetric heat generation rate is usually high. Concentration gradients are potentially significant at the beginning of the reaction for similar reasons. Fragmentation and changes in particle morphology will influence the transfer properties of the particle which are then space and time dependent. Particle morphology evolution is influenced by physical and mechanical properties of both support and polymer and by the rate of polymer production which is in turn dependent on temperature and concentration profiles inside the particle. Considering the small size of the catalytic particles, the high reaction rates and the small time scales in play for the critical phenomena, one can easily understand the difficulties in validating a comprehensive model.

A widely used model in the literature is the multigrain model (MGM), which takes into account the heterogeneous nature of the catalyst/polymer particle. This model takes into account two levels of mass and heat transfer, one at the macroparticle and one at the microparticle level. The mass balance for the macro-particle is shown together with boundary and initial conditions in Equations 1 to 4.

$$\frac{\partial M_l}{\partial t} = \frac{1}{r_l^2} \cdot \frac{\partial}{\partial r_l} \left( D_e \cdot r_l^2 \cdot \frac{\partial M_l}{\partial r_l} \right) - R_v \quad (1)$$

$$\frac{\partial M_l}{\partial r_l} (r_l = 0, t) = 0 \quad (2)$$

$$D_e \frac{\partial M_l}{\partial r_l} (r_l = R, t) = k_s (M_b - M_l) \quad (3)$$

$$M_l (r_l, t = 0) = M_{l0} \quad (4)$$

where  $D_e$  is the effective diffusivity of monomer in the macroparticle,  $k_s$  is the mass transfer coefficient in the external film,  $M_b$  is the bulk monomer concentration in the reactor,  $M_l$  and  $M_{l0}$  are the evolving and initial monomer concentrations in the macroparticle, respectively,  $R_v$  is the volumetric rate of polymerization in the macroparticle,  $r_l$  is the radial position in the macroparticle,  $R$  is the radius of macroparticle, and  $t$  is the polymerization time. In the multigrain model, it is supposed that the polymerization takes place only on the surface of the catalyst fragments in the primary particles (microparticles). It is then the  $R_v$  term that couples the models for the micro- and macroparticle.

The mass balance for the microparticle, together with the boundary and initial conditions are given in Equation 5 through 8.

$$\frac{\partial M}{\partial t} = \frac{1}{r^2} \cdot \frac{\partial}{\partial r} \left( D_p \cdot r^2 \cdot \frac{\partial M}{\partial r} \right) \quad (5)$$

$$4\pi \cdot r_c^2 \cdot D_p \frac{\partial M}{\partial t} (r = r_c, t) = \frac{4}{3} \pi \cdot r_c^3 \cdot R_p \quad (6)$$

$$M(r = R_s, t) = M_{eq} \leq M_l \quad (7)$$

$$M(r, t = 0) = M_0 \quad (8)$$

where  $D_p$  is the effective diffusivity of monomer in the microparticle,  $M_{eq}$  is the equilibrium concentration of monomer in the interface between micro- and macroparticles,  $M$  is the monomer concentration in the microparticle,  $M_0$  is the initial monomer concentration in the microparticle,  $R_p$  is the rate of polymerization on the surface of the catalyst fragments,  $r_c$  is the radius of catalyst fragments in the microparticle,  $r$  is the radial position in the microparticle, and  $R_s$  is the radius of the microparticle. The rate of polymerization on the microparticles is generally given by

$$R_p = k_p C^* M_{as} \quad (9)$$

where  $k_p$  is the propagation rate constant,  $C^*$  is the time-dependent concentration of active sites on the surface of the microparticle, and  $M_{as}$  the concentration of monomer on the active site.

The energy balance for the macroparticle with the boundary and initial conditions are given in equations (10) through (13).

$$\rho_p C_{p_p} \frac{\partial T_l}{\partial t} = \frac{1}{r_l^2} \cdot \frac{\partial}{\partial r_l} \left( k_e \cdot r_l^2 \cdot \frac{\partial T_l}{\partial r_l} \right) + (-\Delta H_p) \cdot R_v \quad (10)$$

$$\frac{\partial T_l}{\partial r_l} (r_l = 0, t) = 0 \quad (11)$$

$$k_e \frac{\partial T_l}{\partial r_l} (r_l = R, t) = h(T_b - T_l) \quad (12)$$

$$T_l(r_l, t = 0) = T_{l0} \quad (13)$$

where  $C_{p_p}$  is the heat capacity of the macroparticle,  $h$  is the film heat transfer coefficient,  $\Delta H_p$  is the heat of polymerization,  $k_e$  is the effective heat conductivity in the macroparticle,  $T_b$  is the temperature of the continuous phase in the reactor,  $T_l$  is the temperature in the macroparticle,  $T_{l0}$  is the initial temperature in the macroparticle, and  $\rho_p$  is the density of the macroparticle.

The energy balance for the microparticle together with the boundary and initial conditions are given in Equations (14) through (16)

$$\rho_p C p_p \frac{\partial T}{\partial t} = \frac{1}{r^2} \cdot \frac{\partial}{\partial r} \left( k_e \cdot r^2 \cdot \frac{\partial T}{\partial r} \right) \quad (14)$$

$$-4\pi \cdot r_c^2 \cdot k_e \frac{\partial T}{\partial t} (r = r_c, t) = \frac{4}{3} \pi \cdot r_c^3 \cdot R_p (-\Delta H_p) \quad (15)$$

$$T(r = R_s, t) = T_l \quad (16)$$

$$T(r, t = 0) = T_0 \quad (17)$$

where  $T_0$  is the initial temperature in the microparticle.

The existence of two levels of mass and heat transfer comes from the fact that the catalyst particle is represented as an aggregate of microparticles structured in spherical concentric layers (Figure 15). Polymer forms around the catalyst fragment so that each microparticle will be constituted of a catalyst fragment surrounded by a polymer layer. The newly formed polymer pushes the old polymer chains thus increasing the layer surrounding the fragments and the total macroparticle size. Monomer must diffuse through the macroparticle pores, absorb on the polymer layer and diffuse through it to reach the active site. The structured morphology of the polymer particle is confirmed by various microscopical analyses.

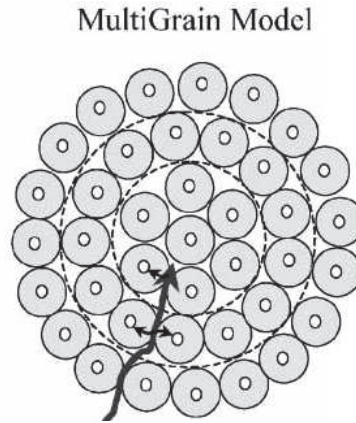


**Figure 15: Multigrain model representation, from [78]**

One of the most comprehensive modeling work using MGM model has been developed by Ray et al. [70, 71, 79-82]. A second series of works worth mentioning are the ones of Chiovetta et al. [16, 83-85]. The authors of these works considered also fragmentation and particle morphology together with heat and mass transfer in their model. For this reason these works will be reviewed in the following paragraph, where MGM and PFM based models taking into account the influence of morphology are presented.

An earlier version of the model (but probably more widely used in current studies because of its simplicity and its acceptable performances for many cases) is the polymeric flow model (PFM, Figure 16) which is a limiting case of the MGM. It was originally developed mainly by Schmeal and Street and by Galvan and Tirrell [86, 87] in the attempt to explain the high polydispersities found using ZN catalysts. It is nowadays widely accepted that the broad MWD of the polymers produced using ZN catalyst comes from the distribution of the active site behavior and is not due to mass diffusion limitations. Nevertheless the basis concepts of the PFM are still useful to calculate temperature and concentration profiles inside the particle.

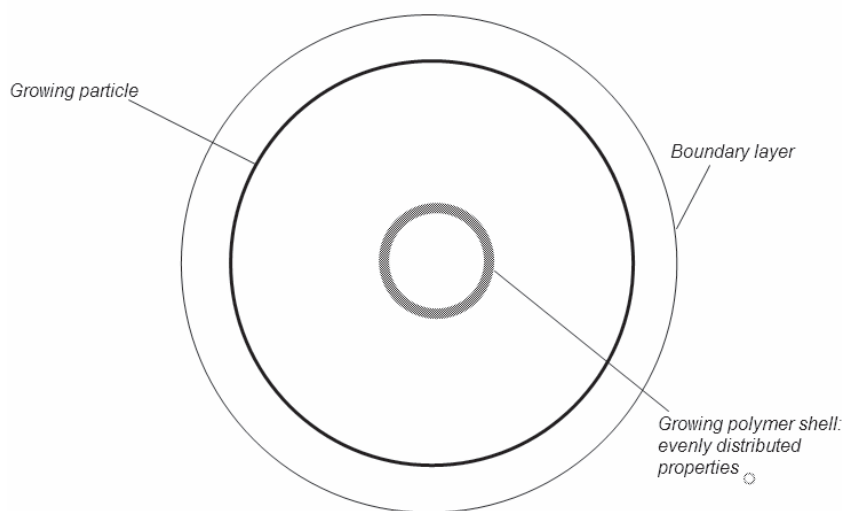


**Figure 16: Schematic representation of the PFM model.**

This model does not explicitly consider the presence of microparticles and represents the particle as a pseudohomogeneous solid with catalyst fragments dispersed in a polymeric matrix. Only one level of heat and mass transfer is then needed. Equations for intraparticle monomer concentration and temperature radial profiles for the polymer flow model are similar to the ones for the macroparticles of the multigrain model ((1) and (10)). It is either assumed that the mass transfer resistance at the level of the microparticles is negligible or that it can be accounted for indirectly in the effective diffusivity  $D_e$ , so that one can use equation (9) with a monomer concentration in equilibrium with the concentration of the macroparticle to calculate the radial variation of the polymerization rate.

The works cited in this section have focused on temperature and concentration profiles inside the particle and have been able to give general trends for specific cases. They have generally tried to model long lasting reactions without taking into account the effect of particle morphology or polymer properties on the reaction course. Only monomer concentration and temperature profiles have been calculated along the particle radius. For

example particle shape and morphology has rarely been considered as an important factor in early works.

A second observation that has to be made is that in early works phenomena happening at polymerization start-up were also neglected. This assumption was somehow justified invoking the fact that the relevant time scales for these phenomena are seconds or minutes while the entire polymerization lasts few hours. The most relevant example is the particle fragmentation. All the cited authors agreed in saying that this is an important step in polymerization reaction but most models started with a particle already fragmented. Apart from fragmentation other aspects as temperature overshoots and concentration profiles can be quite relevant at the reaction start-up.

It is nowadays known that the first reaction instants are fundamental in determining the behavior of the polymerization reaction in later stages especially in terms of morphology and catalyst deactivation profile. This reaction phase should then be included in modeling works in order to accurately predict the particle morphology evolution and eventual heat and mass transfer limitations. One of the main objective of this study is then to understand and characterize the phenomena happening during the polymerization start-up (i.e. evolution of polymer properties, particle temperature and morphology) in order to be able to give a useful basis of experimental results for future modeling work. In what follows we will present, as a starting point, a brief review on the firsts modeling works based on MGM and/or PFM which focus on the first reaction instants and which try to include a simple representation of the morphology evolution into the model equations.

It has to be anticipated that due to the simplified representations of the support structure made by these two models some aspects that are strictly depending on the support network and are particularly relevant at short reaction times (think about fragmentation and monomer diffusion) cannot be modeled with sufficient precision by these works. A new generation of models taking specifically into account the support structure and the polymer properties has been created for these reasons and it will be reviewed in section 3.3 of this chapter.

### **3.2. *MGM and PFM based models***

Modifications of MGM and PFM based models to take into account the evolution of the particle morphology especially for short reaction times involve mainly the definition of a

space-time dependent particle porosity and, as a consequence, a similar dependence for the effective monomer diffusion coefficient. In some works some attempts for a better description of the mass transfer have been made by including a convection term in the mass balance equations.

Hutchinson [72], for example, modified the MGM model developed by Ray's team [70, 71, 79] to take into account particle morphology evolution through porosity variation. To do this he froze the spatial arrangement of the microparticles within the growing particle so that a difference in polymer production rate at different particle radius will result in a porosity change. He focused on quite short reaction times (30 and 300s) and showed that in this time range significant monomer concentration gradients exist across the particle radius. These gradients affect the microparticle growth factor, defined as the ratio between the actual micrograin size and the original size. With this representation it was possible to simulate morphology variations with reaction time like separation of layers and increase in particle porosity if faster growth rate at the outer layers is verified. It was also shown that prepolymerization helps in keeping uniform porosity through the particle radius. This work, while being one of the firsts dealing with morphology and short time reactions, uses a very simplified particle representation, does not treat particle fragmentation (particles are assumed to be already fragmented at time 0) and describes morphology using porosity as the only parameter.

Kiparissides et al. [73, 88] modified the PFM with the aims to take into account convective mass transfer and the influence of morphology on the diffusion of monomers. This is done by defining a diffusion coefficient that evolves with particle morphology (porosity), polymer crystallinity and temperature. They did this by implementing the random pore model in the PFM which takes into account the increasing contribution of diffusion through polymer layer with reaction time. Nevertheless no morphology evolution except from porosity decrease was taken into account and particle was considered as already fragmented. They studied in particular the effect of catalyst particle size, diffusion coefficient, polymer crystallinity, particle porosity and gas relative velocity on temperature and concentration profile inside the particle for short reaction times (up to 100s). They found that, with a polymerization rate in the order of 10Kg PE / g cat / h, big catalyst particle (60 $\mu$ m) could show temperature overshoots of 60°C in the first reaction seconds together with severe mass transfer limitations lasting up to 100s. Insufficient gas velocities are also responsible for extreme temperature difference between the solid and the gas phase for reaction times lower than 1s. The authors

calculated, for a gas velocity of 20 cm/s and a particle size of 20 $\mu$ m, initial temperature difference of 70°C! These values are clearly too high and will certainly lead to polymer melting and reaction shutdown. In addition the authors did not include in their model a thermal deactivation of the catalyst. Modern catalysts can have activities higher than the ones used in this work without incurring in polymer melting or reactor shutdown. This shows one of the discrepancies between the PFM/MGM models and the experimental results that must be overcome. In addition they were able to represent rapid and uncontrollable polymer production by quick pore filling and porosity decrease. They imposed different porosity evolution with time and show that the faster the pores are filled with polymer the larger the particle overheating is, demonstrating that too high activity at reaction start-up can be deleterious.

In a similar work Kosek [89] studied particle overheating at the reaction start-up comparing Fickian and Dusty Gas Model taking convection in pores into account. While a big part of the work is dedicated to comparison of the two models (which is not of interest here), some results useful for this thesis should be cited. It has to be pointed out that mass transfer resistance in the polymer phase was neglected due to the low amount of polymer present at early stages of reaction and that porosity was considered to be independent on reaction time. These assumptions, together with the fact that the particle is considered already fragmented, limit the applicability of this model. The authors conclusions are in concordance with the ones of the works previously cited: extreme temperature overheating can happen during the first 10 s of reaction (they used a very high activity of 100 Kg PE / g cat / h) together with strong concentration profiles inside the particle. Due to the high catalyst concentration in the particle at the beginning, the growth is faster during the early stages, thus increasing the risks of overheating. Low catalyst activities allow more uniform particle growth because of lower mass transfer limitations. Simulations showed also that the smaller the particles are, the shortest is the time period during which the particles overheat, which is in agreement with the experimental results of Weickert [76] and Hamilton [77]. Study of the influence of the support properties showed that for lower porosities less overheating is calculated because of higher mass transport limitations (opposite to what found by Kiparissides, but activity values here are 10 times higher and mass transfer resistance more important). Finally, simulations of copolymerization showed that particle overheating is responsible for a composition profile of reactants inside the particle giving a broad copolymer chain structure. Broad molecular weight distribution in homopolymerizations could also be due to the same reasons.

All the works presented up to now consisted in modifications of classic MGM or PFM models aiming to have more reliable representation of mass transfer and some rough information on particle morphology evolution. All of them considered the particle as already fragmented while fragmentation and its influence on particle morphology evolution is a source of great “disturbance” for heat and mass transfer and catalyst activity.

The first model based on MGM/PFM taking explicitly into account the fragmentation step has been developed by Chiovetta et al. [16, 83-85]. This can be defined as the first version of the MGM as a particle morphology model [78]. The authors represented the catalyst particle as an agglomerate of concentric layers of microparticles and solved mass and energy balances for both levels in way very similar to the classic MGM. They assumed radial symmetry and defined a critical growth factor for the accumulation of polymer onto the micrograins that was such to create a rupture in the particle. When a certain micrograin layer reached the critical growth factor, continuity of the catalyst/support phase is broken. Critical growth factor is reached when the polymer layer deposited around the micrograin is about 1 nm. This separates the particle in two zones during the fragmentation stage: the external zone, already fragmented, and an inner core still unfragmented (Figure 17). The different properties of the two zones are represented by different transfer parameters for heat and mass.

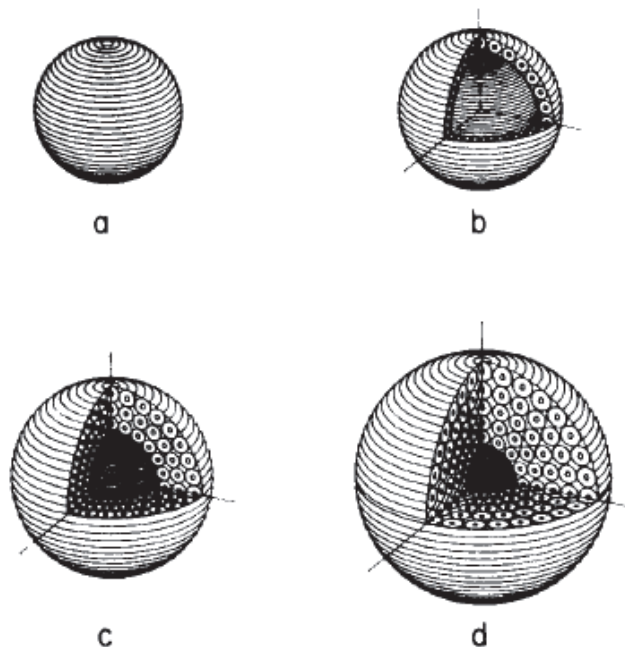


Figure 17: Fragmentation model layer-by-layer; reprinted with permission from [16]

The fragmented zone (fragmentation front) expands towards the center of the particle in a layer-by-layer manner until the center of the particle is reached. At this point fragmentation is completed and particle can only grow in size. It is easy to see that no particle deformation nor



changes in morphology (creation of macropores, porosity heterogeneity) were predicted with this model. Nevertheless this was a great advance respect to the state of the art at that time. For instance the authors were able to show that monomer availability at the active site increases immediately after fragmentation and the higher the fragmentation rate the higher the risks of particle overheating. After that, the growth of polymer layer around the microparticle increases the mass transfer limitation and the monomer concentration at the active site decreases. Chiovetta was also able to show how the fragmentation caused increased reaction rate due to better monomer diffusion and thus temperature maximums occurring during the fragmentation step. Calculated particle temperature increase varied from 20 to 60 K reaching the maximum largely before 1 s. These values were calculated by imposing an intrinsic activity profile with instantaneous activation and no deactivation. Of course a change of such profile will provoke a different evolution of the particle temperature and fragmentation.

Modifications of the structural representation of the original catalyst particle were introduced in following works to be able to schematically represent the support from experimental data of porosity and pore size distribution. The different representations have been specially conceived to represent  $\text{MgCl}_2$  based catalysts [17], Phillips catalysts on silica [13, 14] and metallocenes supported on silica [15]. It is interesting to notice how in case of catalysts supported on silica (which is also our case) [13, 14] the same group proposed another fragmentation behavior predicting that monomer will diffuse firstly into (and polymer will form onto) the most accessible (larger and external) pores. A filling factor is used in a way similar to the critical growth factor explained above and the particle is supposed to fragment when such filling factor in the pore is reached. Fragmentation passes through different steps before it is completed. It starts onto the larger pores and exposes progressively to monomer smaller and smaller pores. After each step the original piece (that is the whole particle for the first step) is divided into smaller pieces and this process continues until the fragments are not ruptured anymore (or they have too small pores) (Figure 18). This representation comes mainly from experimental observations made by Mc Daniel [57].

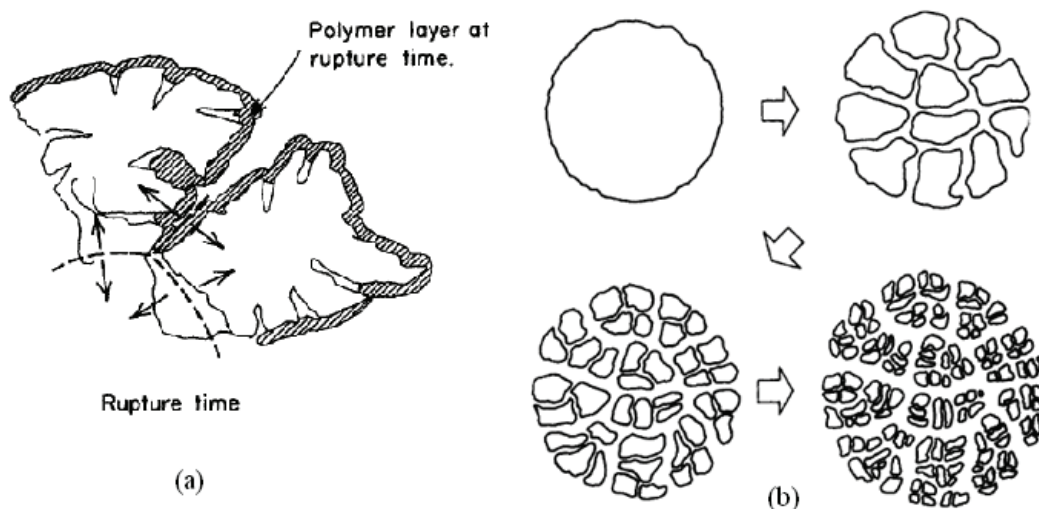


Figure 18: Detail on polymer layer in pores at rupture time (a) and fragmentation path (b); reprinted with permission from [13]

The limitations of all the modeling studies presented up to here are mainly two:

- 1) the schematic representation of the catalyst and support do not allow to calculate particle morphology changes during the reaction (both during the fragmentation step and the growth step). It is therefore not possible to link reaction rate and transport properties with morphology evolution.
- 2) Polymer properties are not explicitly considered in any of the previous models. They are nevertheless fundamental in determining the way the particle morphology evolves. It is immediate to understand that a particle forming a brittle polymer will behave differently than one forming a very soft material.

The need to include morphology and polymer properties in the modeling process has always been understood but it is only in the last ten years that modeling efforts have started in this sense. The following paragraph will review the main related works available in literature.

### 3.3. Morphology models

Kittilsen et al. [90, 91] were the first to propose a new modeling concept based on linking local reaction rate with buildup and relaxation of local tensions inside the catalyst particle. The viscoelastic properties of the polymer and the elastic properties of the supports are explicitly taken into account into the stress strain relationships. Fragmentation or breakage of the support material is defined to start when the stress exceeds a threshold value. This stress

depends also on the thickness of the pore wall and this is taken into consideration in the model. That's where the influence of porosity and pore size of the support is integrated into the model. The authors investigated the influence of reaction rate and support and polymer parameters on pore wall fragmentation.

It was shown that the important parameter is the ratio between pore filling (reaction rate) and stress relaxation (determined by the viscous properties of the polymer). Properties of the polymer phase play an important role as they define the way the stress is accumulated into the pore wall. For example less viscous polymer (softer, with branched architecture) will relax the stresses more quickly and particles with low porosity will be obtained. In the same way the support properties are fundamental in determining the particle morphology evolution. A friable support will be responsible for the generation of a highly porous particle, and supports with low porosity (having less pores and more solid) will be responsible of lower stresses into pore walls and low particle porosity. Pore size was also found to be crucial in determining the final particle morphology. Big pores having thinner walls (almost all the porosity of the particle is in fact caused by the macropores while the micropores contribute only to a small fraction of the specific surface) will fragment before the small ones. We are again in the situation experimentally described by McDaniel 20 years before.

The model presented here is an idealized model treating only isolated pores and only qualitative trends should be considered but nevertheless it has put under a clear light that one cannot model catalyst particle at start-up without referring to the support and polymer physico-mechanical properties to correctly describe the evolution of particle morphology. The same approach was used by the same group [90] and later extended by Di Martino et al. [92] and applied to the whole catalyst particle using a modified PFM. The aim of this study was to be able to reproduce irregular particle morphologies usually found in industry and academia (i.e. hollow particle).

The group of Kosek has deeply worked on modeling of fragmentation of catalyst during olefin polymerization and has produced a number of different models and modeling techniques that start from the catalyst morphology and link reaction rate and transport parameters to polymer and support properties and morphology evolution.

One of the directions of their work [93] was to develop an algorithm for reliable reconstruction of the porous medium from 2D images acquired by SEM, TEM or tomography. The need for this procedure is to be able to obtain reliable transport parameters

by solving locally the transport and balance equations in the pore space of a realistic representation of the particle morphology. This method is nevertheless dependent on the resolution of the original 2D images. A second aim of these techniques is to start from the catalyst reconstruction and create an algorithm capable to identify the loci of the weakest points of the support. The interested reader is referred to [93].

The most comprehensive model for particle structure development (including fragmentation) available in the literature has been developed by the same group [94-96] and is based on the use of the discrete element method. The polymer particle is supposed to be constituted by a large number of spherical microelements (not necessarily corresponding to the support microparticles of the MGM) with binary and ternary viscoelastic interactions that depend on polymer properties. The model starts with a particle already fragmented and is able to predict different particle morphologies thanks to the heterogeneous growth rate of each microelement depending on local catalyst activity, temperature and monomer availability, and to the viscoelastic interaction between the elements. The model can predict morphologies like fines generation, hollow particles, creation of macrocavities and perfect replication.

As found by Kittilsen, a decreased relaxation time of the polymer phase (indicating a more fluid and less elastic material) leads to delayed and reduced formation of ruptures with more compact particle formation. The important influence of polymer properties on evolution of particle morphology is represented by the fact that generation of fines has been simulated also in case of low activity or mass transfer limitations if brittle polymers are produced while flat concentration profile along the radius was generally associated in the literature to a perfect replication morphology.

The model also pointed out how the reaction start-up is the stage responsible for high stress generation because of the particle growth at high temperature. Once the initial stage is over, the stress relaxation becomes the dominant factor resulting in slow decrease of particle porosity during its growth.

The model was further improved in a following work [97] which considers also the early stage of particle evolution including catalyst fragmentation. In this work the catalyst carrier, the polymer phase and the void phase are discretized into microelements having different properties if belonging to different phases. The model is able to simulate catalyst fragmentation and exposure of new active sites to monomer and to predict different fragmentation paths depending on support and polymer mechanical properties. Simulation of

shrinking core and continuous fragmentation modes were both possible by simply varying the monomer transport resistance and the radial profile of the intrinsic activity of the catalytic microelements.

This work is a kind of state of the art of single particle modeling including fragmentation. The strengths of the model are multiple:

- The ability to mimic the real support morphology by introducing discontinuities and activity distribution. The next step will be to build a microelement based support configuration starting from experimental data.
- The ability to link polymer and support physico-mechanical properties to reaction-diffusion effects and vice versa and to take into account the influence of these parameters on particle morphology evolution.

A last type of model dealing with early stages of heterogeneous olefin polymerization and fragmentation of catalyst particle is the one developed by Pinto et al. [98] by implementing an energy balance in a dynamic PFM. The simulation of particle morphology is based on the analysis of the balance between the energy accumulated by polymer production rate and the energy released by polymer flow, chain relaxation or by rupture of the support. Different fragmentation scenarios arise depending on the ratio between pressure build-up due to polymer accumulation and local capacity of energy dissipation. With this work the authors were able to create working maps for prepolymerization step that were divided in different regions according to operating conditions and catalyst properties: uniform fragmentation, particle deformation, particle break-up into fines, polymer melting.

Later the authors proposed an improved version of this model [99] called the Two Phase Model (M2F) that takes into account the presence of solid and fluid phases into the support pores and allows for calculation of convective flux inside the particle during fragmentation step. The working maps presented in the previous work were recalculated using the new M2F and extremely different performances were found. Including convection allowed the simulation of regular polymer particles under conditions where the previous model predicted fines generation or melting. Calculation of high temperature values before the fragmentation showed that particle overheating should be carefully analyzed during prepolymerization step. Particle-bulk temperature differences up to 60K were calculated at reaction start-up for gas phase polymerizations with active catalysts.

### 3.4. Conclusions

From this brief review it is possible to see how the modeling efforts during the last years tried to link together the polymer and support properties with the fragmentation and particle morphology evolution. The way the particle fragments has also a great influence on the monomer availability at active site and on the development of temperature profiles thus it finally affects the total reaction rate. The attempt to link these two phenomena has also been matter of study in the latest models. Nevertheless all the models present in literature are obliged to make some assumptions regarding the support structure. Porosity and pore size uniformity are considered as it is impossible nowadays to run the models starting from real representation of the porous particles. The work of Kosek on 3D reconstruction goes in this way, but the simple image analysis and transport coefficient calculations were very machine-time demanding. In addition support particles are heterogeneous between them (see figure 13) so that more or less small deviation of modeling from reality will always be present. What is still missing in the most recent models is the use of real values concerning polymer and support properties and the evolution with time of such parameters. During polymerization start up in fact due to the quick and ample variations of temperature, reaction rate, transport properties and morphology, chemical, physical and mechanical properties of polymer are in transient state. Since they affect mass and heat transfer (think of polymer crystallinity effect on diffusivity) and fragmentation (think of molecular weight and chain architecture effect on mechanical modulus and relaxation time), taking constant values calculated from polymer samples produced at long reaction times, as is the case up to now, it's not reliable. One of the main objectives of this PhD work is then to collect and interpretate reliable experimental data on catalyst activity and particle temperature profile and on polymer properties at early reaction stages in order to reduce the gap between results coming from the modeling and the ones coming from the experiments.

## 4. Experimental studies on the early stages of polymerization

In the last 15 years there has been an increasing interest in investigating experimentally the early stages of olefin polymerization. The scientific community has in fact understood that this particular aspect of the polymerization is not a merely academic exercise but has important consequences on the performance and profitability of industrial processes. It is during this stage that the morphology of the final polymer particle is defined. The less porous and regular is the particle, the higher is its density and the bigger is the quantity that can be shipped or stored in a determined volume. It is also during this stage that temperature overshoots can cause partial catalyst deactivation and reduced volumetric production.

In this section we will see that many attempts to study the initial stages of olefin polymerization are presented in literature using different techniques. Each technique is particularly suited for a specific aspect of the subject (porosimetry is well adapted to study the pore filling and particle fragmentation mechanisms, microtomography gives a good representation of the spatial distribution of the different phases) but a number of difficulties are present independently on the used technique. The scale of the phenomena in play (support particles of some tenths of microns, pores of some tenths of nanometers and fragmentation times of some seconds) combined with the high activities in play at reaction start-up have been a big obstacle for the development of reliable methods capable to fully characterize the polymerization start-up. Just as an example reliable experimental data on the evolution of the particle temperature at the reaction start-up is not available in literature and only few pioneer works [100-102] have measured the build-up of the polymer properties during early stages of olefin polymerization. A review on the literature available about experimental data obtained for olefin polymerization start-up in terms of fragmentation, particle morphology, polymer properties and activity profile will be given in the following to conclude the bibliographic part of this work. This section will be divided in paragraphs regrouping works that used the same technique. Each technique will be critically analyzed highlighting advantages and drawbacks.

#### 4.1. *Early porosimetry and adsorption studies.*

This was the earliest technique used to study early stages of olefin polymerization and was mainly used in the late 80s and early 90s from research groups focused on Phillips catalysis. Nevertheless the similarity between the supports used in Phillips and in supported metallocene catalysis justifies a brief review on these results. Mc Daniel [57] polymerized ethylene in slurry phase and studied the fragmentation pattern of silica supported chromium catalysts. By stopping the reactions at various times, he collected particles with a polymer yield comprised between 20 and 20000 g PE / g cat. It has to be said that these are quite high yields to study fragmentation and that the support used in the study consisted of very big particles (177-250  $\mu\text{m}$ ) which could behave differently from the modern silica supported catalysts (20-60 $\mu\text{m}$ ). Nevertheless the findings are quite interesting. The authors compared two different catalysts showing different activity profiles and saw that fracturing pattern was similar in the two cases. They concluded that fragmentation is not controlling the reaction rate. Given the high yield values of this study this affirmation must be considered with precaution. The authors were able to separate the catalyst fragments from the polymer particle by burning the organic material. They then measured fragment and pore size distribution. They saw that active catalysts fragmented down to average size of 7-10  $\mu\text{m}$  while the inactive catalysts did not fragment. As already remarked, it has to be noticed that modern catalyst can be as small as 10 $\mu\text{m}$  which is a dimension comparable to the size of the smallest fragments observed by McDaniel. It is then possible that the results obtained by McDaniel could not be entirely valid for modern particles. However this result, together with the fact that inactive catalysts showed pores of less than 6nm in diameter, let the authors conclude that polymerization fractures the support along the largest pores. Mercury porosimetry and  $\text{N}_2$  adsorption on virgin catalyst and polymerized fragments confirmed this result. Pore volume of fragments corresponding to pore sizes higher than 60 nm was highly increased upon fragmentation. This is attributed to fragments pushed apart by the growing polymer. Fragmentation was found to be completed after few minutes. These results introduced the concept of a fragmentation starting in the biggest, easily accessible pores and then continuing in smaller and smaller pores. The behavior is different from the layer by layer fragmentation pattern introduced by Chiovetta in his model. We will see that both the patterns are actually realistic but the appearance of one rather than the other is determined by different factors like support properties and reaction conditions.



Later, Weist [103] performed the same kind of study on polymer particles produced in the gas phase polymerization of ethylene at 1 bar using a supported chromium catalyst. The researchers stopped the polymerization at low yields (0.1 to 20 g PE/ g cat) and removed the polymer by dissolution or oxygen plasma ashing. These methods damaged less the support fragments than the polymer removal by burning. The support had particle diameter between 63 and 125  $\mu\text{m}$  and the catalyst had a very low activity. Due to the high exothermicity of the reaction, ethylene was introduced in the fluidized bed in a very careful way: increasing its concentration in a nitrogen stream from 1% to 40% in 40 minutes or sending pulses of ethylene at 40% in nitrogen for 2s every 10s followed by pure nitrogen. The authors studied two deactivating catalysts and showed that activity stopped when the polymer production was corresponding to complete support pore filling (1 and 2.5 g PE/ g cat). SEM pictures showed no appreciable fragmentation for these supports. Pore clogging by the polymer was demonstrated by mercury porosimetry (Figure 19). With increasing polymer yield pore volume of the inactive supports was found to decrease consistently. In addition while pore throats size increased slightly indicating that the smaller throats were blocked, pore diameter decreased with yield, showing pore blocking caused by polymer growth. Porosimetry on an active support showed a much less important decrease in the pore volume and a constant pore diameter with increasing yield. This suggests that fragmentation of the support maintained a porous structure and particle expanded to accommodate the growing polymer. Porosimetry performed on separated fragments showed that up to a yield corresponding to complete pore filling (2 g PE/ g cat) there was little change in the pore structure of the fragments. At higher yields the pore volume accessible through throats larger than 100 nm was considerably increased while pore structure corresponding to smaller pores did not change. When fragments were compressed to obtain the original bulk density this difference disappeared. This clearly proves that fracture of the catalyst occurred through the largest pores at a time corresponding to complete filling of the support pores.

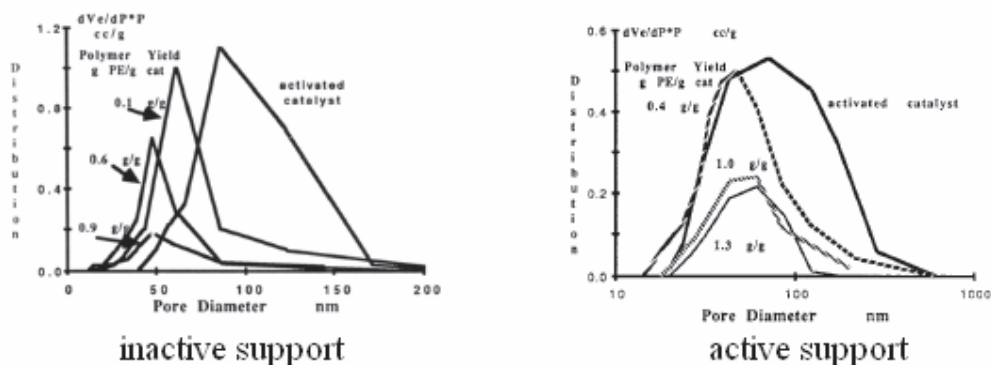


Figure 19: Pore size evolution with yield in active and inactive silica support; reprinted with permission from [104]

Similar results were found from the same research groups using different techniques like nitrogen adsorption [56] and solid gas chromatography [104]. Solid gas chromatography was used to study monomer diffusion and kinetics. Reactions had to be stopped at very low yield (less than 1 g/g) because higher degrees of polymerization led to excessive polymer formation on the catalyst particle surface and changes in the packing degree of the column. Nevertheless the authors found that at yield of 0.1 g/g internal void space and transport rate decreased because of the polymer accumulation in the macropores near the particle surface. One major disadvantage of this technique is the development of consistent temperature profiles in the column. Even pulse injections of ethylene resulted in interparticle fusion for yields higher than 0.1 g/g and measured temperature in a pellet raised from 100°C up to 140°C in less than one minute using a diluted stream of ethylene in nitrogen (9 mol %). Nitrogen adsorption using HRADS was also performed on particles at very low yield (up to 0.5 g/g) to study microporosity development. It was found that the first layer of polymer formed (up to 0.2 g/g) was responsible for a porosity peak at about 0.7 nm. For higher yield the porosity disappeared and the authors attributed this to the formation of amorphous polymer making the previous layer non-porous. It is nevertheless difficult to say if this ephemeral microporosity is really important for the reaction course and if it is due to the polymer or to the support initial fracture.

The studies presented here used a very low activity catalyst and were performed at very mild conditions. Polymerizations under industrial conditions are responsible for very different polymer and stress rate generation so that fragmentation behavior and dynamics could be completely different from what seen here. It is also reasonable to question the effects of the separation of polymer from the fragments in terms of modification of the fragments morphology. Nevertheless it has to be recognized that these pioneer works have been able to

investigate deeply the particle break-up at the early stages and provided experimental evidence to a precise fragmentation pattern.

## 4.2. *Offline microscopy at low reaction rates*

The simplest method to study early stages of the olefin polymerization reaction is to stop the reaction after a short time, recover the particles and analyze them with microscopy techniques (mainly SEM, TEM and EDX). If very active catalyst is used it could be difficult to recover particles with low enough yield so that most of the times a low active catalyst or very mild conditions are used to slow down the kinetics and be able to follow the start up and fragmentation phase. An active site submitted to these mild conditions can however behave differently to what is commonly seen in industrial processes so that results coming from these works have to be analyzed accurately. In addition the difficulty here is that slowing down the rate also changes fragmentation and morphology evolution. The exact reaction time could also be difficult to determine because the quenching or catalyst killing process is not immediate. In fact usually 1L or more reactors are used and quenching is done by addition of methanol or acidic methanol. Nothing assures us that the killing of all the active sites is not distributed over a range of time.

Different works on the subject aiming to link the evolution of the activity profile with particle morphology were published by the group of Weickert who studied particle produced at low yields using different catalysts and reaction conditions. In one of their first works [105] the authors studied propylene polymerization in the slurry phase at low yield (0.3 to 50 g PP/g cat) using a ZN catalyst under mild conditions. Their procedure consisted in injecting monomer pulses into the reactor and to follow the pressure decay to calculate the activity. Vapor pressure of the solvent, partial pressure of the inerts and the monomer dissolution into the solvent were taken into account. The authors found that during the initial stages (yield up to 4 g/g) the reaction rate decreased strongly with time, then remained constant for higher yields. This behavior was not dependent on monomer concentration or time but more on polymer yield. It was then assigned to physical causes (related to diffusion) and not to a catalyst deactivation. This trend was measured also in presence of hydrogen and the authors explained this with the 'phase transition' that the particle is undergoing at yields around 2-4 g/g: from a support continuous phase to a polymer matrix. This could influence the interaction between catalyst and cocatalyst and could change the equilibrium monomer concentration at

the active site. SEM analysis showed a high degree of replication and particle size increasing with yield. The support did not show an onion-like fragmentation but it seemed to break into large fragments first, which progressively increased in number and size. This reminds us of the fragmentation behavior described in the previous section. It is interesting to note that the authors found that the fragments seem to drift to the outside of the particle during the course of the reaction (Figure 20). Conner et al. [106] observed the same tendency of inert fragments to migrate to the exterior of the particle using synchrotron X-ray tomography. Tisse too observed the same behavior in her PhD work [63] for polymer produced using silica supported metallocene at low yields (3-5 g/g). The explanations offered by Weickert were two: phase separation due to polymer softening because of the high temperature reached into the particle or separation of the bigger, less active fragments from the smaller one producing more polymer and located homogeneously into the particle.

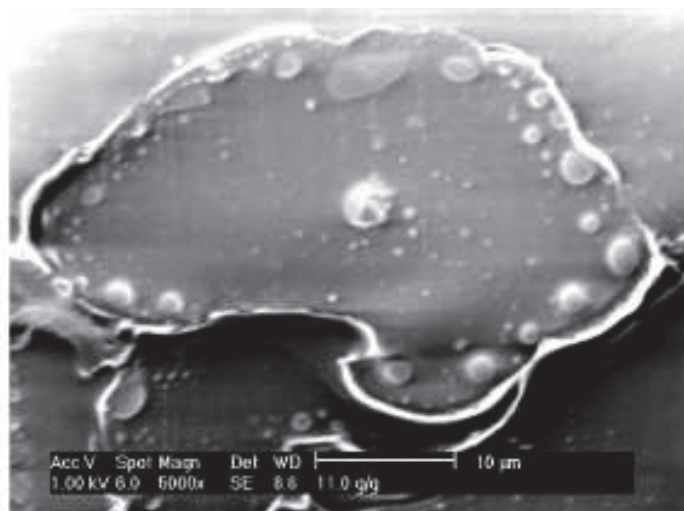


**Figure 20: Support fragments (brighter objects) distribution in PP particle with yield of 11 g/g; reprinted with permission from [105]**

It has to be kept in mind, and the authors themselves underlined it, that polymerization conditions applied here are far from the industrial ones and so it is possible that the observed fragmentation behavior is very different from what is observed under different conditions. For example experiments with very low yield were performed at very low monomer concentration thus giving formation of waxes that are hopefully not present in industrial prepolymerizations. Similar conclusions were presented in a successive work from the same group [107] where it was mainly shown that calculation of the true initial reaction rate is quite complicated if classic setup is used (mass flowmeter, calorimetry) due to the dynamic non-equilibrium change in temperature and pressure during the first tens of seconds. The authors proposed to

use the adiabatic temperature rise directly after catalyst injection to estimate the initial reaction rates. Doubled values of activity were found when using this method.

Zheng et al. [108, 109] studied the morphology evolution in propylene homopolymerization and ethylene-propylene copolymerization using different ZN catalysts supported on magnesium chlorides having different porosities. The reactions were performed in slurry phase under mild conditions and stopped at low yield. Briefly it was shown that, according to the support properties, different fragmentation patterns could be seen. For more porous supports a rapid fragmentation of the catalyst into a large number of sub particles like in [105] was seen, while for less porous supports a layer-by-layer fragmentation was present. This difference was attributed to a more homogeneous polymer growth through the particle for the more porous support. In case of copolymerization the same behaviors are observed but somewhat delayed to higher yields. That's where polymer properties came to play: copolymers have low crystallinity and are less rigid. They can then absorb more stress and deform more before releasing the tension to the support and break it.

The same group studied also fragmentation of a silica supported metallocene in ethylene and propylene polymerization [52]. The general observation for silica supports under these low activity conditions is that they undergo a layer-by-layer fragmentation. Catalyst rupture starts at the very beginning of the reaction with support surface broken into irregular subparticles. Cauliflower morphologies can then appear on the surface while the core remains unfragmented up to yields in the order of 30 g/g. Instantaneous fragmentation was seen for supports having cocatalyst distributed only on the outer surface of the particle. This led to the formation of a thick polymer layer at the surface. Due to the stress build-up inside the particle because of uneven growth, the core separated from the shell and fragmented coarsely.

The group of Fink was one of the firsts to focus its attention on evolution of the morphology of polyolefin particles. More in detail, they studied the growth of polypropylene on silica supported metallocene catalysts in slurry [48, 110, 111] and bulk phase [110, 112]. They used very mild conditions and catalyst of low activity to be able to control and follow particle fragmentation. Catalyst activity was measured by weighing the recovered polymer. This could be source of errors especially when few tens of milligrams are recovered from a 1.8L vessel and after several washes [112]. As said before, extremely low reaction rates can also lead to behaviors that are different from the ones found in industry. Nevertheless the authors have the merit to have deeply studied the influence of different parameters (especially catalyst preparation and support properties) on initial reaction rate and fragmentation. Slurry

polymerizations gave a similar trend in kinetic profile no matter the reaction conditions: activity reached a maximum at the very beginning and then decreased to very low values. This induction period lasted several minutes after which activity started to increase again to reach a steady state value (Figure 21). The dynamics of this evolution was dependent upon reaction conditions and support properties (i.e. higher temperature and smaller particle sizes reduced the induction period) but the different zones of the activity profile were always visible. The authors performed a number of SEM and EDX analysis on the recovered samples and were able to show that regardless of the reaction medium used (slurry or bulk) the fragmentation progressed in a layer-by layer manner from the outside to the inside. At the initial time a homogeneous polymer layer started to grow on the external particle surface producing splitting of small fragments from the external particle shell. With increasing time the polymer growth continued to the interior of the particle until complete fragmentation was attained. The link between activity and morphology evolution is then easy to find. Initial induction period is due to the formation of the high crystalline polymer layer at the particle surface (measured crystallinities varied from 80 to 40% with increasing reaction time [110]) which limits monomer arrival to the active sites. During the successive phase of polymer growth, fragmentation exposes more active sites to the monomer and thus activity increases reaching a maximum when fragmentation is complete.

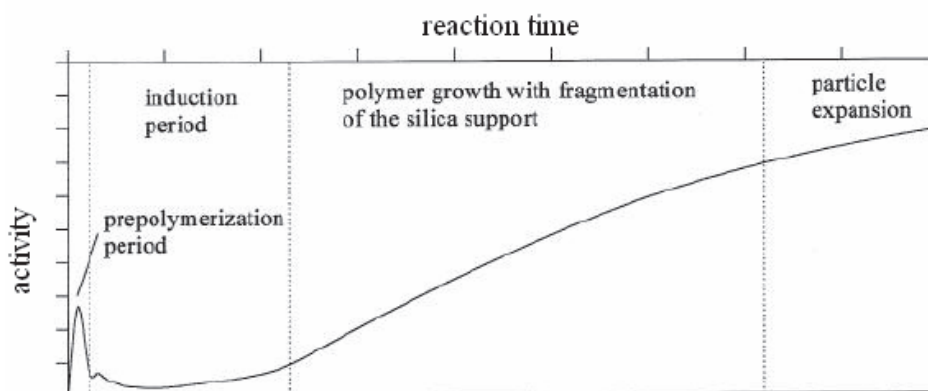


**Figure 21: Activity profile for silica supported metallocenes in propylene slurry polymerization; reprinted with permission from [48]**

Special attention was given to the influence of catalyst preparation on particle morphology. A high heterogeneity in particle activity and morphology was found in the same samples with morphologies corresponding to different fragmentation stages present at the same time in the reactor. This behavior was assigned, after EDX analysis, to an inhomogeneous repartition of the MAO cocatalyst between different particles.

The studies presented in this section showed how it is possible to link activity profile with evolution of particle morphology. In addition they were able to point out the importance of the polymer and support properties and the catalyst preparation in the fragmentation step. They finally showed how different fragmentation paths are possible. Nevertheless the distance from industrial conditions and some uncertainties in the measurement of kinetic profiles raised the need to create new or adapt existing methods to analyze the early stages of olefin polymerization.

### 4.3. *Online videomicroscopy*

This technique was firstly applied in the polyolefin field by Reichert et al. [113] to study polymerization of butadiene at low pressure. It consists of a combination of a small reactor equipped with a transparent window and an optical microscope allowing observation of growing particles in real time. The advantages of this technique are numerous since it can be used to analyze many particles at the same time (ideal for catalyst screening or study of the influence of particle properties); to measure with some precision the activity of individual catalyst particles without manipulating them and, it is very flexible, allowing fast changes in temperature and gas composition. The early studies, nevertheless, dealt with reactions conducted at mild conditions. The first group to adapt the system to industrially relevant conditions was the one of Weickert [76, 114]. They studied ethylene and propylene homo and copolymerization on ZN catalysts in gas phase. Their reactor consisted in a 6 mL thermostated polymerization cell with a support disk onto which the catalyst particles are placed. The transparent lid allows particle observation but care has to be taken into choosing its material and thickness to avoid excessive image aberration. TEA treated polymer powder placed around the support disk acts as scavenger. Reactions were conducted at temperatures up to 70°C and pressures up to 15 bars for 20 minutes maximum. Individual particle reaction rate is measured by recording the increase in the particle size with time. The authors found good homogeneity in particle behavior during a specific experiment while reproducibility between different experiments was rather unsatisfying. Activity of the catalyst in this setup was 5-7 times smaller than expected from liquid pool polymerization. It is possible, due to the different reaction procedure, that activation in this case is poorer because of the distance between scavenger containing particles and catalyst. Particle size, cocatalyst concentration and activation time did not seem to influence the activity profile at the start-up while reaction

temperature and prepolymerization in presence of comonomer did (Arrhenius and comonomer effect). Reaction rate profile was found to be constant for the first 20 minutes, differently from what showed by Fink. In spite of the fact that different catalysts at different reaction conditions are tested in the two studies, it can be that this work did not investigate the earliest stages of the reaction. The lowest yield presented in the publications is in fact around 5 g/g. Another point to be improved is the fact that the gas is stagnant during the reaction. This, apart from being very far from the realistic conditions, limits the heat transfer from the particle to the gas and can result in particle overheating and deactivation.

The group of Fink was also quite active in studying early stages of gas phase olefin polymerization using videomicroscopy technique. They focused most of their efforts on supported metallocene catalysts [75, 115]. Their reactor was similar to the previous described one and the kinetic profile was calculated by looking at the variation of the projection area of the growing particles (more precisely, the variation with time of the volume of a sphere having an equivalent projection area was calculated). It has to be pointed out that this calculation method is quite inaccurate (as is the one used by the other groups) as the support particles are far from being spherical and initial pore filling not accompanied by particle growth is not detected. Ethylene homopolymerization conducted at 60°C and 10 bars confirmed the behavior previously found by the same group, that is an activity profile showing an induction period due to formation of crystalline polymer film on the particle surface. It was also confirmed that different particles showed different initial behaviors in a same experiment and this was attributed to inhomogeneous cocatalyst distribution. TEM analysis on particles with high polymer yields showed that the 30-60  $\mu\text{m}$  large support was fragmented in 10-20 nm primary particles distributed through the polymer phase. Copolymerization of ethylene with higher  $\alpha$ -olefins was also studied. The authors found that increasing the comonomer concentration in the gas phase led to a longer induction period but also to higher overall activities and bigger particle sizes. The same effect was found for different comonomers (propylene and butene) and was explained with a bigger diffusion limitation for comonomer through the crystalline polymer film followed by increased comonomer effect because of the increased comonomer concentration. At the beginning of the reaction in fact ethylene is consumed faster than the comonomer provoking a gas phase composition drift. This was confirmed by NMR studies on polymers produced at different reaction times. The results showed that the amount of comonomer incorporated augmented with time. Composition drift in the feed is an undesired consequence of using a stagnant gas



phase. The same research groups investigated also the behavior of  $\text{MgCl}_2$  supported ZN catalysts [116]. Differently from the silica supported catalysts this support shows immediate acceleration of reaction rate without induction period. It is possible that an immediate fragmentation of this support is the reason for this behavior.

Hamilton et al. improved the reactor setup presented by Weickert especially in terms of heat transfer from the particles (see next paragraph) [77]. They studied the behavior of active silica supported metallocenes in ethylene and propylene polymerization at high temperature (80–100°C) and pressure (21 bar) for reactions lasting 5 to 10 minutes. Images of the growing particles were recorded every second. They found that increasing reaction temperature or adding hydrogen to the feed increase the reaction rate at the start-up but this was not dependent on the original catalyst particle size as found by Weickert. All the experiments conducted in their study showed a reaction rate that increase steadily at the reaction start-up to reach a maximum around 50 to 100s depending on reaction conditions. The activity then decreased but passed through a shallow maximum at higher reaction times (200 to 300s). The profile is then similar to what found in the previous studies except the presence of the second maximum that the authors assigned to fragmentation of the growing particles temporarily exposing new active sites to the monomer. A catalyst activity of 5000 g/g/h was claimed by the authors. This would mean that at reaction times of 200 to 300s the yield is around 300–400g/g. We have seen that a number of studies have measured fragmentation start very soon (at yields even below 1g/g) and end of fragmentation at yields of around 50 g/g. It seems then that the reason for the shallow maximum in reaction rate found by the authors should be looked elsewhere.

#### 4.4. *Infrared measurements*

Infrared technique is widely used in chemical engineering and allows to have temperature measurements without perturbing the measured zone. Using it in combination with other techniques to study early stages of olefin polymerization can give quite interesting results. In the literature the main application of this technique can be found in the works of Weickert and Hamilton [76, 77] coupled to videomicroscopy applied to gas phase small reactors. In this way temperature evolution of the growing particle can be measured and linked with reaction rate profile. Weickert found that temperature increase of growing particles exposed to monomers can reach values of 7 to 20 K depending on reaction conditions (temperature, gas

composition). Of course the higher the reaction rate the higher the temperature increase. Interesting to notice, and in concordance with modeling studies, larger particles having a larger volume to surface ratio and less capability of heat removal show larger temperature rise than the smaller ones. Nevertheless it has to be said that the measured temperature reached its maximum after few minutes of reaction while the modeling studies predicted immediate (few seconds) temperature rise. This is due to the surface under the particles which perturbs the catalyst heat balance. In addition gas phase temperature is changing with time and is neither measured nor controlled. Finally the resolution of the IR camera being of  $6\mu\text{m}$  (with a catalyst particle size spanning from  $20$  to  $40\mu\text{m}$ ), some errors in temperature measurement coming from the background emission can be present.

Hamilton focused extensively on temperature evolution of catalyst particles at reaction start-up. He improved the system of Weickert by replacing the surface onto which the particles were laying by a nylon grid with  $25\ \mu\text{m}$  mesh. The low thermal conductivity and heat capacity of such support minimizes the perturbations in particle heat balance. The temperature of the single particles increased of  $3$  to  $10\ \text{K}$  depending on reaction temperature and presence of hydrogen, and was proportional to reaction rate. The maximum was in this case reached very soon, in accordance with models. Around  $10\ \text{s}$  were needed in case when only ethylene were present in the gas phase while addition of hydrogen reduced this time to  $4\ \text{s}$ . Results obtained during the study of the effect of particle size were similar to the ones found by Weickert: the bigger is the particle, the higher its temperature increase and this independently on the reaction conditions. An interesting phenomena pointed out by this study is the effect of particle clusters on the reaction start-up. Particle clustering can happen in industrial reactors mainly due to electrostatic forces. A situation close to clustering can arise in a very concentrated fluidized bed (tending to the fixed bed limit) if more active particles are close each other. The heat generated by a particle can be responsible for excessive temperature increase of the neighbor particles and vice versa leading to hot spot formation. The authors demonstrated this by co-polymerizing ethylene and butene at  $93^\circ\text{C}$ . In the case when a cluster of particles was placed in the reactor the temperature increased by  $16\text{K}$  while only  $6\text{K}$  were measure in case of single particle. The cluster simply acts as a single particle with much bigger diameter.

The utility of this technique coupled with videomicroscopy is clear here. Nevertheless some aspects like the stagnant gas or the presence of a surface perturbing the particle heat balance place this works still not so close to realistic conditions. It has to be said anyway that these are

the most refined measurements of temperature of catalyst particles during olefin polymerization present in the literature.

#### 4.5. *Melt microscopy*

Up to now we have reviewed different microscopic techniques allowing to follow the evolution of particle size and temperature with reaction time. Nevertheless the internal aspect of the particles in terms of fragment size distribution and location and element distribution could be analyzed only with EDX and SEM measurements on sections of particles. Particle cutting suffers sometimes of technical and optical problems like deformation of particle upon cutting or difficult detection of fragments.

Abboud et al [117] used melt microscopy technique to study the evolution of fragment size distribution and location with time. Polymer particles produced at different low yields were melted under a light microscope thus revealing the fragments location. Different catalyst like  $\text{MgCl}_2$  supported ZN or silica supported ZN or silica supported metallocene were used to polymerize propylene at mild conditions ( $50^\circ\text{C}$ , 5 bar) in slurry phase. It has to be pointed out that a prepolymerization step took place in the system while the reactor was heated up to the working temperature. For  $\text{MgCl}_2$  supported catalyst, fragments into the particle were found to be homogeneous in size and equally distributed through the particle volume (Figure 22A). In addition the different analyzed particles showed similar degrees of support disintegration. This confirms that  $\text{MgCl}_2$  fragments easily and rapidly thus facilitating monomer diffusion to a high number of exposed active sites. In case of silica supported catalyst the behavior is different (Figure 22B). Strong heterogeneities between different particles have been found indicating a broad distribution in activity of each particle as previously found in Fink's studies. In addition, due to the heterogeneity in support strength and structure, fragments of different sizes were found inside a single particle. Finally even after 1h of reaction at these conditions 20% of the particle remained unfragmented.

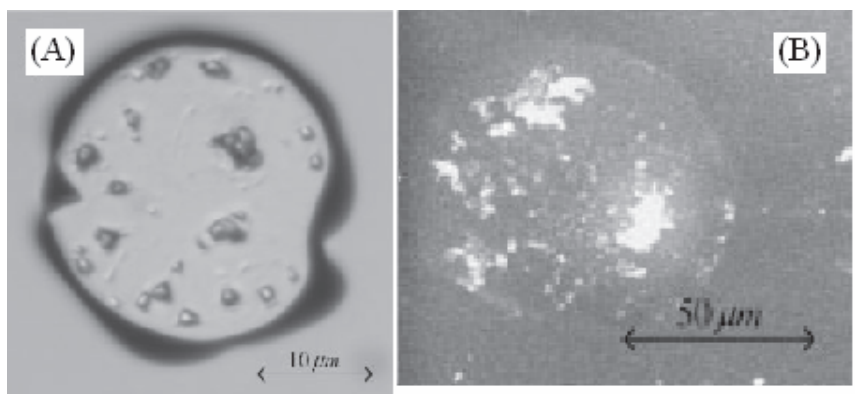


**Figure 22: Picture of (A)  $\text{MgCl}_2$  supported catalyst and (B) silica supported catalyst; reprinted with permission from [117]**

For this support, fractures are observed to develop from the particle surface at various points and break the particle into smaller fragment at later stages. A continuous increase in fragments number and surface area was measured. More in detail, the rate of increase of surface area, which is an indication of the rate of fragmentation, was seen to increase fast at the beginning and slower at later reaction stages. Interestingly, the same profile was observed under videomicroscopy for the reaction rate [66]. The authors then concluded that fragmentation could be the limiting reaction step and that for this catalyst larger pores are much easily filled at early stages. Their fracturing creates a large surface area for some time, and then smaller pores are gradually filled with slower formation of newly exposed surface.

The results presented here are difficult to interpret due to the lack of kinetic data. In addition nothing assures us that the support fragments are not moving in the polymer melt. Nevertheless this work confirmed clearly that the fragmentation behaviors of silica and  $\text{MgCl}_2$  based heterogeneous catalysts differ greatly. To conclude it has to be said that this technique implying destruction of the original particle structure, internal distribution of phases like polymer, support and void and their evolution cannot be observed. Non destructive techniques like tomography are more adapted to study particle morphology at early polymerization stages.

#### 4.6. *Synchrotron X-Ray microtomography*

Tomography is a non invasive technique that allows 3D observation of the interior of a solid by sending an X-ray beam through the sample and measuring the amount of photons that crossed it. The different attenuation coefficients of the solid and the void phases are

responsible for an X-ray absorption that is depending on the material crossed by the beam. Even different solid phases can be recognized inside a sample if their attenuation coefficients are not too close. Usually the sample is rotating around one of its axes while exposed to the X-rays. The beam is imaging a sample slice of a thickness depending on the system resolution during a complete sample rotation. The operation is repeated for different slices along the z-axis and the data collected at different heights are compiled and reconstructed to have 2D images of the sample slices. The raw data are in reality spatial representations of the attenuation coefficient calculated for each image pixel from the amount of transmitted energy measured by the detector. By means of numerical algorithm is possible to combine the different slices and to have 3D reconstruction of sampled area. Pixels that correspond to material with a high absorption coefficient will be represented in lighter grey tones (white being the limit) while darker areas correspond to less absorbing materials. X-ray absorption depends mainly on material atomic number and density with more dense material giving lighter pixels. Synchrotron sources allow the use of a high energy X-ray beam with small source size giving high spatial resolution. This is desirable when studying small objects like olefin polymerization catalytic particles (tens of microns). In addition, due to the distance between the source and the sample, synchrotron X-rays beam has a parallel geometry (Figure 23), thus the sample is not magnified on the detector and quantitative reconstruction free of artifacts is possible [118].

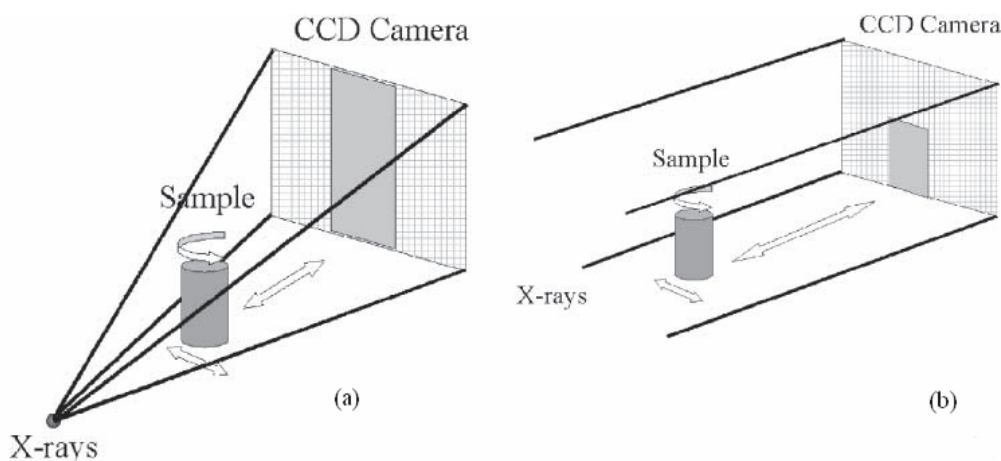


**Figure 23: Difference between cone (a) and parallel (b) beam geometry; reprinted with permission from [118]**

Conner [106] was the first to apply this technique to study fragmentation of silica supported chromium catalyst in gas phase ethylene polymerization. He was especially interested in determining fragments size and location inside the growing particle together with internal particle porosity in order to gain knowledge on the effective monomer transport length to

reach the active sites. His group analyzed particles with yield varying from 11 to 200 g PE / g cat with a “high-resolution” synchrotron tomography. The term high resolution was corrected for the early nineties, but not for the actual setups. The researchers could have a maximum of 5 $\mu$ m resolution thus their analysis was limited to pores and fragments of few tens of microns. Nowadays the resolution attainable with the same technique is of 0.2  $\mu$ m. Nevertheless interesting results that have been reproduced only some years later by other groups were found. It was confirmed that fragments and void distribution within the particle were not uniform, with larger fragments concentrating at the exterior of the particles having yields of 200 g PE / g cat. For lower polymer yields (50 g PE / g cat) an unfragmented support core was still visible and it was noticed that fragments size decreased with yield. In addition it was possible to see that polymer particles were composed at least for 20-30% of volume by cavities bigger than 50 $\mu$ m. Particles with lower yield were too small to be easily mounted and imaged. The authors concluded that active site uniformity through the polymer phase is clearly not verified in the reality and that the transport length is much smaller than the particle diameter. In fact the fragments located at the exterior of the particle could be responsible for a reduced monomer diffusion limitation. In another work [119] the same conclusion confirmed later by many other research groups was found: MgCl<sub>2</sub> based catalysts fragments more uniformly and quickly

#### 4.7. *Laser scanning confocal fluorescence microscopy*

A technique with similar principles is the laser scanning confocal fluorescence microscopy, which consists of imaging a solid treated with a fluorescent dye. A laser exciting the fluorescent material scans the sample sequentially point by point and optical slices of the solid can be produced. Moving the focus plane allows production of multiple slices that can be combined for 3D reconstruction. Jang applied the technique to study fragmentation of catalyst during olefin polymerization [120]. By staining the catalyst support with an appropriate molecule, fragmentation at different yields can be observed through localization of the fluorescent fragments inside the polymer matrix. The authors used different supports (silica or polystyrene beads) for a metallocene complex and tested it in slurry phase polymerization of ethylene at 70°C and 40 bar. Different fragmentation paths were observed depending on the support: non fragmenting support giving low activity catalyst, extensive fragmentation

throughout the entire catalyst particle or layer by layer fragmentation completed in 30 minutes. The last behavior was typical for a silica support (Figure 24).

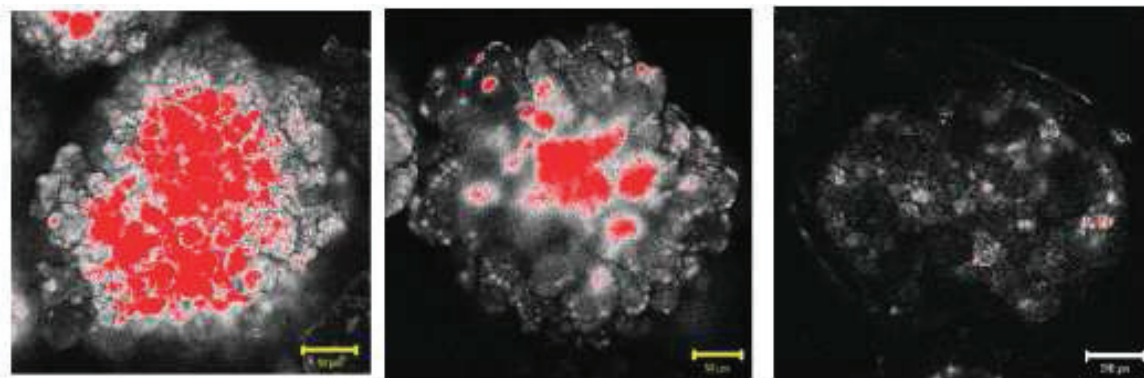


**Figure 24: Distribution of silica fragments in a PE particle after reaction time of 5 min (left), 15 min (center) and 30 min (right); reprinted with permission from [120]**

The authors proved that this technique can be used to follow particle fragmentation. Nevertheless some remarks have to be given. No kinetic profile was available in their publications and, as we have seen, the fragmentation path depends not only on support properties but also on reaction rate. In addition staining of the sample or the support can be delicate in terms of finding the right molecule and there is no certainty up to now that the used dye does not interfere with the catalyst complex. Last but not least the resolution of this method is limited to the laser wavelength, which is around 50 times lower than electron microscopy.

#### 4.8. *Stopped flow technology*

This technology consists in the rapid mixing of two or more reagents and instantaneous stopping of the reaction after a predetermined time by changing the reaction environment. The main advantage of the technique is its capability of perform very short reactions, with minimum times much lower than a second. The typical times for fragmentation of olefin polymerization catalysts under industrial conditions are in the order of seconds so that online characterization of the relevant phenomena is very difficult to perform. As we have seen, this can be circumvented by using reaction conditions or catalysts giving very slow fragmentation or by offline measurements. Even in this case the classic laboratory setups used to polymerize olefins do not allow the recovery of very low yield particles. The potential advantages of the application of stopped flow technology to olefin polymerization are easily understandable. In

addition, if properly conceived, a stopped flow reactor will allow recovering the particle without altering the morphology so that following of fragmentation and build up of polymer properties will be possible. Stopped flow technology was first developed by Chance to study enzymatic reactions [121] but the first group to apply it to catalytic olefin polymerization was the one of Soga [122, 123]. The authors studied, among other subjects, the early stages of supported ZN catalysts in slurry phase propylene and ethylene polymerization and investigated many aspects related to the nature of the active sites, the determination of true kinetic parameters, the effect of hydrogen, the effect of catalyst preparation and much more. They were also able to define the basic requirements of the method. The reader is referred to the previously cited references for more details. Their setup (Figure 25) basically consisted in two flasks filled of solvent containing the catalyst and eventually the cocatalyst in one of them and the monomer and eventually the cocatalyst in the other. The two mixtures are driven together by the monomer pressure through tubes until they came into contact in a common tube. Upon rapid mixing they react for a time determined by the length of the reaction tube and the flow rate (residence time). Finally they flow into a flask containing a strong quenching agent that stops the reaction immediately.

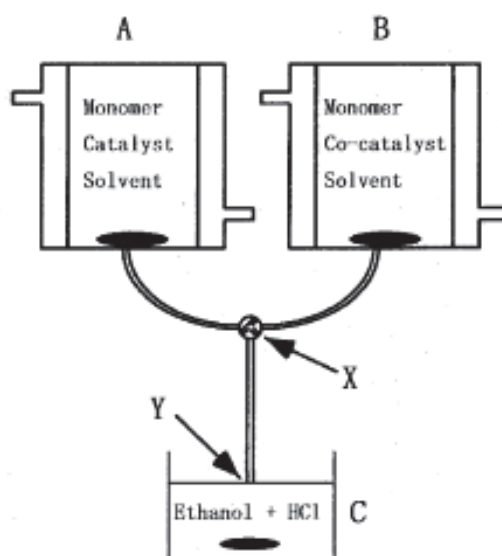


**Figure 25: Schematic view of the original stopped flow apparatus used by Terano : A,B reagent containing flask ; C quenching flask ; X mixing point; Y end of reaction point; reprinted with permission from [122]**

The simplicity and effectiveness of this technique drove the attention of many research groups in the following years but almost all the efforts were concentrated on determination on kinetic parameters using homogeneous or, to a lesser extent, heterogeneous catalysts in



solution or slurry phase reactions [124-126]. In addition experiments were carried under mild conditions.

Di Martino et al. [100, 127, 128] were able to build a modification of the original reactor setup of Terano allowing to work at temperatures up to 90°C and pressures up to 20 bar. They worked with MgCl<sub>2</sub> supported ZN catalyst in ethylene polymerization in slurry phase for reaction times varying from 0.04 to 1.6 s (corresponding to yields varying from 0 to 5 g PE / g cat according to the reaction conditions). Their detailed study focused on evolution of particle morphology of the growing polymer and fragmentation of the catalyst particle but they gave at the same time the kinetic profile of the catalyst and, for the first time in literature, the evolution of the polymer properties in terms of molecular weight distribution, crystallinity and melting point with reaction time. The authors were able to modulate the reaction time by varying both the length of the reaction tube and the pressure difference between the upstream and the downstream (which in facts varies the slurry flow rate). Regardless of the reaction conditions the authors measured an unusual kinetic profile in the first polymerization instant with very high activity values at the beginning decreasing rapidly after 1 s to classical values. Such kinetic behavior was attributed mainly to the complex nature of the catalyst and the possibility to have “one-off” active sites working for only a fraction of second created by TEA pretreatment before the polymerization. Temperature gradients inside the particle were not considered as responsible for the high activity because the consequent overheating would have melted the polymer. The hypothesis that monomer diffusion limitation is responsible for the decay rate profile is discredited by the fact that the molecular weight is not decreasing in the studied time range, quite the opposite.

The authors studied the effect of TEA pretreatment on kinetic profile and morphology and were able to demonstrate that without pretreatment, TEA diffusion limitations are present due to the polymer layer formed around the active sites. This leads to uneven reaction rate through the particle radius and shell expanding more than the core. In fact, in case of preactivation, the recovered particles have a full morphology while in case of no pretreatment the particles have a “raisin-like” aspect, with an expanded shell that has collapsed on a compact core. It is also interesting to notice that in case of precontact with TEA the number average molecular weight reaches constant values immediately, while the weight average molecular weight increases with reaction time. This means that at very short reaction times a big number of small chains are produced, while longer chains are produced later and need more time to undergo their first transfer reaction. This is a clear indication of the active site evolution with reaction time. In

case of no pretreatment with TEA the situation is different: the number average molecular weight is much higher and the polydispersity index is lower than for the previous case. This clearly indicates that a large number of small chains is not produced when the catalyst is not precontacted with the alkylaluminium.

Another new aspect studied by the authors is the evolution of the polymer melting temperature and crystallinity with reaction time. It was found that for very short reaction times the polymer showed unusually low crystallinity (less than 20%). The authors said (without further validation) that this behavior can be attributed to polymerization rate higher than crystallization rate. The chains at the beginning have not the time to organize themselves in regular crystals. In addition the thermogram of the polymer produced after 40ms showed two melting peaks which were attributed to two types of crystals (two different polymers).

Even if some explanations for the observed phenomena are still missing (i.e. low melting temperature for short reaction times) it is clear from these results that this technique has an enormous potential and allows to collect realistic data to use as input for studies modeling the fragmentation and particle morphology evolution. For example evolution of polymer properties and their influence on the diffusion coefficient and the stress relaxation parameters can be included in the morphology models of Kittilsen, Pinto or Kosek.

In addition this system allowed to recover the particles without exposure to air that could have damaged the support. A complete morphological study has been carried on, which clearly depicts the way the particle morphology evolves. As a general conclusion the authors found that long term morphology is the same found in the early stages of the polymerization thus confirming the importance of reaction start-up in controlling the particle structure. More in detail, the particles show nodular morphology with inhomogeneous nodule growth at the very beginning. Upon sufficient growth, more nodules merge together giving rise to the “cauliflower” morphology. In some cases strong local variation of the growth conditions of a cluster of active sites can be responsible for rapid axial extensions and formation of “wormlike” structures. On the particle level the authors showed that the support cleaves very early during the fragmentation process and that the cracks can be progressively filled by growing polymer fibrils oriented along the direction of the deformation. In case of very high stress generation the shell can dissociate completely from the whole particle. A number of morphologies like cobweb structures and “spotty-like” particles was imaged by the authors according to the reaction conditions.

In a following study the group of Terano [129] used the stopped flow method combined with classical reactors to study the pore filling and fragmentation path and time scale of a  $\text{Mg}(\text{OEt})_2$  based ZN catalyst in propylene polymerization under mild conditions (1 atm,  $30^\circ\text{C}$ ). By combining SEM analysis, mercury porosimetry and BET they showed that the macropores play the dominant role in the initial volume filling while the micropores are much less relevant at the initial stages. Macropore filling accompanied by decrease in pore diameter and constant pore size distribution lasted up to a yield of 0.7 g/g. After that, fragmentation begun and pores become larger and larger. Fragmentation occurred first in the most porous parts and propagated progressively to the more compact one until it was completed at a yield of 19 g/g. These results are consistent with the ones of many studies presented above. From the most recent works it seems that, as it is logical, first the most accessible pores are filled (mainly macropores located on the outer part of the particle). Fragmentation front propagates from the wall of the filled pores and exposes new pores to the monomer.

The group of Pinto and McKenna [101, 102] developed a special reactor setup to study early stages of olefin polymerization in the gas phase. Their reactor puts together the advantages of using a microreactor in terms of heat and mass transfer and the ones of using a stopped flow method to study very short reaction times. It consists in fact in a packed bed having a volume of 1mL where the feed stream flows through the catalyst bed. The catalyst is diluted using inert glass beads to avoid bed overheating. The reaction time is controlled through manipulation of the feed composition: after a predetermined time the monomer feed is replaced by a quenching gas stream. The use of computer controlled solenoid valves allow to perform reaction as short as 100 ms. This method is also called “short stop method”. The used setup can perform reactions up to  $90^\circ\text{C}$  and 10 bar thus approaching industrial conditions. The authors studied propylene polymerization using classical ZN catalyst and ethylene polymerization using classical or silica supported ZN catalyst or silica supported metallocene catalyst. As found by Di Martino the authors measured an high activity at the very early reaction instants and a rapid decay in the first second followed by a slower decay to steady state values. Reaction rate at the start-up can be almost 10 times higher than at the steady state. Polydispersity indexes were found to increase with reaction time meaning that the growth of chains takes place under non-steady state conditions. Molecular weights evolved in a way that depends on reaction conditions, in particular on monomer concentration. Evolution of molecular weight distribution during the course of the reaction indicates that the kinetic constants of propagation and transfer are changing, probably because

of the variation of the active site together with the development of temperature and concentration gradients inside the particle. Similar to what found in slurry phase, the authors measured increasing crystallinity and melting temperature with reaction time.

In a second version of the reactor setup [130] thermocouples were introduced to measure the inlet and outlet temperature of the feed stream. The high PDI values (4 to 13 depending on the used catalyst) and the deactivation measured with highly active catalyst if too high temperature or too much catalyst is used, suggested the presence of important temperature gradients inside the particle. Unluckily no information on feed temperature evolution is given in the publication.

One of the advantages of this method is to be able to recover undamaged polymer particles. SEM studies showed that, depending on the carrier features, different morphologies can be obtained.  $\text{MgCl}_2$  supported catalysts showed large cracks on the surface, induced by the reduced capacity of the particles to dissipate the stresses produced at their inside. When the deformation front propagates through the particle, this can be deformed upon release of the accumulated energy. Large cracks are present from the very beginning of the reaction showing that particle fragmentation can be initiated from the particle inside. This is confirmed by the observation of polymer fibrils at the interior of the surface fractures. The morphological feature described here have been observed on particles having yields of less than 1 g polymer / g catalyst confirming that the final structure of the polymer particle is defined in the early stages of the polymerization.

## 5. Conclusion and introduction of experimental work

As seen through this literature review, initial stages of olefin polymerization using a supported catalyst are fundamental in determining the quality of the final polymer and the productivity of the catalyst. Strong effort has been put into modeling particle fragmentation and mass and heat transport inside the particle with newest modeling concepts considering also mechanical properties of the polymer and of the support starting to be quite close to the reality. Nevertheless, due to the number of parameters playing a role in this type of modeling, assumptions have to be made. The quality of the model depends on the goodness of such

assumptions. Experimental data can be used to limit the number of the assumptions of a model but, in our specific case, these are still quite rare in literature. The reasons for this are the extremely short time during which important phenomena fixing the polymer properties and the particle morphology are in play and the small scale of the catalyst particles. It is only during the last 5-7 years that some of the experimental difficulties have been solved and that experimental setups capable of performing very short reactions under industrial conditions are available. Let us cite here the works of Di Martino [100, 127, 128] and Machado [101, 102] which are the first ones that used specially conceived stopped flow apparatus capable to work under conditions of pressure and temperature close to the ones used in industry. The use of this technique allows to measure the activity profile together with the polymer properties evolution and to recover the particles to study their morphology. In other words it allows a complete characterization of the polymerization start-up under realistic conditions. It is for these reasons that stopped flow technique was chosen to perform the PhD study presented in this thesis. Di Martino, with her PhD, was able to give a complete picture of the phenomena at play in slurry phase reactions. The works of Machado and Silva are, on the other side, only the first attempts to obtain perform the same type of study for gas phase reactions.

In the PhD work presented here we will further develop and optimize the gas phase stopped flow technique and used it under industrially relevant conditions in order to be able to give for the first time a complete characterization of the early stages of gas phase olefin polymerization with special focus on the relations between activity, temperature profiles, polymer properties and particle morphology.

The scope of this study is to explore a number of parameters related to reaction conditions, catalyst preparation and support properties and to identify their influence on early stages of gas phase ethylene polymerization. A number of reliable experimental data will then be collected and interpreted with the scope, among others, to be able to use them to improve single particle models.

Our attention will focus on MAO treated silica supported metallocene catalysts for a number of reasons. First of all exposure of the polymer/catalyst particle to air will not damage the support as is the case for  $MgCl_2$  based catalysts, where the support is damaged upon contact with the air humidity. In addition it is known that metallocene catalysts, even if supported, should give narrow molecular weight distribution. Perturbations in the catalyst behavior coming from temperature or concentration gradients or modification of the active sites will be immediately reflected on the polydispersity of the produced polymer and

detected. This would not have been possible if using classic ZN catalysts that show intrinsically broad MWD. Last but not least the slower fragmentation of silica supported catalysts will allow an easier detection of morphology evolution during the first reaction seconds.

To conclude, with this work we aim to give a better understanding of the phenomena happening at the reaction start-up from an experimental point of view and we hope to be able to provide to the modeling works a number of realistic input data especially in terms of particle temperature evolution, relation between activity and temperature rise at the start-up of gas phase polymerization and evolution of polymer properties in the early reaction seconds.

## 6. References

1. Available from: <http://www.yarnsandfibers.com>.
2. Nooijen, G.A.H., *Ziegler/Natta catalysts in particle form ethylene polymerization: The effect of polymerization start-up on catalyst activity and morphology of the produced polymer*. *Catalysis Today*, 1991. **11**(1): p. 35-46.
3. Kashiwa, N., *The discovery and progress of MgCl<sub>2</sub>-supported TiCl<sub>4</sub> catalysts*. *Journal of Polymer Science Part A: Polymer Chemistry*, 2004. **42**(1): p. 1-8.
4. Chum, P.S. and K.W. Swogger, *Olefin polymer technologies--History and recent progress at The Dow Chemical Company*. *Progress in Polymer Science*, 2008. **33**(8): p. 797-819.
5. Mülhaupt, R., *Catalytic Polymerization and Post Polymerization Catalysis Fifty Years After the Discovery of Ziegler's Catalysts*. *Macromolecular Chemistry and Physics*, 2003. **204**(2): p. 289-327.
6. Sinn, H., et al., *Ziegler-Natta Catalysis*, in *Advances in Organometallic Chemistry*. 1980, Academic Press. p. 99-149.
7. Sinn, H., et al., "Living Polymers" on Polymerization with Extremely Productive Ziegler Catalysts. *Angewandte Chemie International Edition in English*, 1980. **19**(5): p. 390-392.
8. Peacock, A.J., *Handbook of Polyethylene: Structures, Properties and Applications*. 2000, New York: Marcel Dekker.
9. Galli, P. and G. Vecellio, *Polyolefins: The most promising large-volume materials for the 21st century*. *Journal of Polymer Science Part A: Polymer Chemistry*, 2004. **42**(3): p. 396-415.
10. Jessup, R., *The heat and free energy of polymerization of ethylene*. *J. Chem. Phys.* , 1948. **16**(7.): p. 661-664.
11. Soares, J.B.P., T. McKenna, and C.P. Cheng, *Coordination Polymerization*. *Polymer Reaction Engineering*. 2008: Blackwell Publishing Ltd. 29-117.
12. Severn, J.R., et al., "Bound but Not Gagged" - Immobilizing Single-Site  $\alpha$ -Olefin Polymerization Catalysts. *Chemical Reviews*, 2005. **105**(11): p. 4073-4147.
13. Estenoz, D.A. and M.G. Chiovetta, *A structural model for the catalytic polymerization of ethylene using chromium catalysts. Part I: Description and solution*. *Polymer Engineering & Science*, 1996. **36**(17): p. 2208-2228.

14. Estenoz, D.A. and M.G. Chiovetta, *A structural model for the catalytic polymerization of ethylene using chromium catalysts. Part II: Thermal effects*. Polymer Engineering & Science, 1996. **36**(17): p. 2229-2240.
15. Estenoz, D.A. and M.G. Chiovetta, *Olefin polymerization using supported metallocene catalysts: Process representation scheme and mathematical model*. Journal of Applied Polymer Science, 2001. **81**(2): p. 285-311.
16. Ferrero, M.A. and M.G. Chiovetta, *Catalyst fragmentation during propylene polymerization: Part I. The effects of grain size and structure*. Polymer Engineering & Science, 1987. **27**(19): p. 1436-1447.
17. Ferrero, M.A., et al., *Characterization of the changes in the initial morphology for MgCl<sub>2</sub>-supported Ziegler-Natta polymerization catalysts*. Journal of Polymer Science Part A: Polymer Chemistry, 1992. **30**(10): p. 2131-2141.
18. Xie, T., et al., *Gas Phase Ethylene Polymerization: Production Processes, Polymer Properties, and Reactor Modeling*. Industrial & Engineering Chemistry Research, 1994. **33**(3): p. 449-479.
19. Albizzati, E. and M. Galimberti, *Catalysts for olefins polymerization*. Catalysis Today, 1998. **41**(1-3): p. 159-168.
20. Cossee, P., *Ziegler-Natta catalysis I. Mechanism of polymerization of [alpha]-olefins with Ziegler-Natta catalysts*. Journal of Catalysis, 1964. **3**(1): p. 80-88.
21. Böhm, L.L., *The Ethylene Polymerization with Ziegler Catalysts: Fifty Years after the Discovery*. Angewandte Chemie International Edition, 2003. **42**(41): p. 5010-5030.
22. Soga, K. and T. Shiono, *Ziegler-Natta catalysts for olefin polymerizations*. Progress in Polymer Science, 1997. **22**(7): p. 1503-1546.
23. McDaniel, M.P., H.P. D.D. Eley, and B.W. Paul, *Supported Chromium Catalysts for Ethylene Polymerization*, in *Advances in Catalysis*. 1985, Academic Press. p. 47-98.
24. Thüne, P.C., et al., *The CrOx/SiO<sub>2</sub>/Si(100) catalyst – a surface science approach to supported olefin polymerization catalysis*. Macromolecular Symposia, 2001. **173**(1): p. 37-52.
25. Thüne, P.C., et al., *Bonding of Supported Chromium during Thermal Activation of the CrOx/SiO<sub>2</sub> (Phillips) Ethylene Polymerization Catalyst*. The Journal of Physical Chemistry B, 2001. **105**(15): p. 3073-3078.
26. Natta, G., et al., *A CRYSTALLIZABLE ORGANOMETALLIC COMPLEX CONTAINING TITANIUM AND ALUMINUM*. Journal of the American Chemical Society, 1957. **79**(11): p. 2975-2976.
27. Chen, E.Y.-X. and T.J. Marks, *Cocatalysts for Metal-Catalyzed Olefin Polymerization: Activators, Activation Processes, and Structure-Activity Relationships*. Chemical Reviews, 2000. **100**(4): p. 1391-1434.



28. Sinn, H., *Proposals for structure and effect of methylalumoxane based on mass balances and phase separation experiments*. Macromolecular Symposia, 1995. **97**(1): p. 27-52.
29. Kaminsky, W., Catal. Soc. Jpn., 1991. **33**: p. 36.
30. Hamielec, A.E. and J.B.P. Soares, *Polymerization reaction engineering -- Metallocene catalysts*. Progress in Polymer Science, 1996. **21**(4): p. 651-706.
31. Kaminsky, W. and M. Schlobohm, *Elastomers by atactic linkage of  $\alpha$ -olefins using soluble Ziegler catalysts*. Makromolekulare Chemie. Macromolecular Symposia, 1986. **4**(1): p. 103-118.
32. Kaminsky, W., et al., *Polymerisation von Propen und Buten mit einem chiralen Zirconocen und Methylaluminoxan als Cokatalysator*. Angewandte Chemie, 1985. **97**(6): p. 507-508.
33. Tsutsui, T., et al., *Propylene homo- and copolymerization with ethylene using an ethylenebis(1-indenyl) zirconium dichloride and methylaluminoxane catalyst system*. Polymer, 1989. **30**(7): p. 1350-1356.
34. Jüngling, S., et al., *Propene polymerization using homogeneous MAO-activated metallocene catalysts:  $Me_2Si(Benz[e]Indenyl)_2ZrCl_2/MAO$  vs.  $Me_2Si(2-Me-Benz[e]Indenyl)_2ZrCl_2/MAO$* . Journal of Polymer Science Part A: Polymer Chemistry, 1995. **33**(8): p. 1305-1317.
35. Spaleck, W., et al., *The Influence of Aromatic Substituents on the Polymerization Behavior of Bridged Zirconocene Catalysts*. Organometallics, 1994. **13**(3): p. 954-963.
36. Harrison, D., et al., *Olefin polymerization using supported metallocene catalysts: development of high activity catalysts for use in slurry and gas phase ethylene polymerizations*. Journal of Molecular Catalysis A: Chemical, 1998. **128**(1-3): p. 65-77.
37. Zhuravlev, L.T., *Concentration of hydroxyl groups on the surface of amorphous silicas*. Langmuir, 1987. **3**(3): p. 316-318.
38. E.F. Vansant, P.V.D.V. and K.C. Vrancken, *Characterization and Chemical Modification of the Silica Surface*. Studies in Surface Science and Catalysis. Vol. Volume 93. 1995: Elsevier.
39. Takahashi, T., US 5 026 797, Mitsubishi Petrochemical Co., Ltd., 1991.
40. Welborn, J. and C. Howard, US 4 808 561, Exxon Chemical Patents Inc., 1989.
41. Chen, Y.-X., M.D. Rausch, and J.C.W. Chien, *Heptane-soluble homogeneous zirconocene catalyst: Synthesis of a single diastereomer, polymerization catalysis, and effect of silica supports*. Journal of Polymer Science Part A: Polymer Chemistry, 1995. **33**(13): p. 2093-2108.

42. Ribeiro, M.R., A. Deffieux, and M.F. Portela, *Supported Metallocene Complexes for Ethylene and Propylene Polymerizations: Preparation and Activity*. Industrial & Engineering Chemistry Research, 1997. **36**(4): p. 1224-1237.
43. dos Santos, J.H.Z., et al., *Silica supported zirconocenes and Al-based cocatalysts: surface metal loading and catalytic activity*. Macromolecular Chemistry and Physics, 1997. **198**(11): p. 3529-3537.
44. Chien, J., *Supported metallocene polymerization catalysis*. Topics in Catalysis, 1999. **7**(1): p. 23-36.
45. Goretzki, R., et al., *Unusual ethylene polymerization results with metallocene catalysts supported on silica*. Journal of Polymer Science Part A: Polymer Chemistry, 1999. **37**(5): p. 677-682.
46. Chu, K.-J., et al., *Copolymerization of ethylene and 1-hexene with in-situ supported Et[Ind]2ZrCl2*. Macromolecular Chemistry and Physics, 1999. **200**(10): p. 2372-2376.
47. Hlatky, G.G., *Heterogeneous Single-Site Catalysts for Olefin Polymerization*. Chemical Reviews, 2000. **100**(4): p. 1347-1376.
48. Fink, G., et al., *Propene Polymerization with Silica-Supported Metallocene/MAO Catalysts*. Chemical Reviews, 2000. **100**(4): p. 1377-1390.
49. Bianchini, D., F.C. Stedile, and J.H.Z. dos Santos, *Effect of MAO silica surface loading on (nBuCp)2ZrCl2 anchoring, on catalyst activity and on polymer properties*. Applied Catalysis A: General, 2004. **261**(1): p. 57-67.
50. dos Santos, J.H.Z., et al., *Optimization of a silica supported bis(butylcyclopentadienyl)-zirconium dichloride catalyst for ethylene polymerization*. Macromolecular Chemistry and Physics, 1999. **200**(4): p. 751-757.
51. Smit, M., et al., *Effects of methylaluminoxane immobilization on silica on the performance of zirconocene catalysts in propylene polymerization*. Journal of Polymer Science Part A: Polymer Chemistry, 2005. **43**(13): p. 2734-2748.
52. Zheng, X., et al., *Fragmentation Behavior of Silica-Supported Metallocene/MAO Catalyst in the Early Stages of Olefin Polymerization*. Macromolecules, 2005. **38**(11): p. 4673-4678.
53. Tisse, V.F., R.M. Briquel, and T.F.L. McKenna, *Influence of Silica Support Size on the Polymerisation of Ethylene Using a Supported Metallocene Catalyst*. Macromolecular Symposia, 2009. **285**(1): p. 45-51.
54. van Grieken, R., et al., *The Role of the Hydroxyl Groups on the Silica Surface When Supporting Metallocene/MAO Catalysts*. Polymer Reaction Engineering, 2003. **11**(1): p. 17 - 32.
55. dos Santos, J.H.Z., et al., *The effect of silica dehydroxylation temperature on the activity of SiO2-supported zirconocene catalysts*. Journal of Molecular Catalysis A: Chemical, 1999. **139**(2-3): p. 199-207.

56. Webb, S.W., et al., *Morphological influences in the gas phase polymerization of ethylene by silica supported chromium oxide catalysts*. The Canadian Journal of Chemical Engineering, 1991. **69**(3): p. 665-681.
57. McDaniel, M.P., *Fracturing silica-based catalysts during ethylene polymerization*. Journal of Polymer Science: Polymer Chemistry Edition, 1981. **19**(8): p. 1967-1976.
58. Korach, L., et al., *Effect of silica-type sol-gel carrier's structure and morphology on a supported Ziegler-Natta catalyst for ethylene polymerization*. European Polymer Journal, 2006. **42**(11): p. 3085-3092.
59. Sano, T., et al., *Adsorptive separation of methylalumoxane by mesoporous molecular sieve MCM-41*. Chemical Communications, 1999(8): p. 733-734.
60. Sano, T., et al., *Application of porous inorganic materials to adsorptive separation of methylalumoxane used as co-catalyst in olefin polymerization*. Microporous and Mesoporous Materials, 2001. **44-45**: p. 557-564.
61. Kumkaew, P., et al., *Gas-phase ethylene polymerization using zirconocene supported on mesoporous molecular sieves*. Journal of Applied Polymer Science, 2003. **87**(7): p. 1161-1177.
62. Kumkaew, P., et al., *Rates and product properties of polyethylene produced by copolymerization of 1-hexene and ethylene in the gas phase with (n-BuCp)<sub>2</sub>ZrCl<sub>2</sub> on supports with different pore sizes*. Polymer, 2003. **44**(17): p. 4791-4803.
63. Tisse, V.F., *Kinetics and morphology of metallocene catalysts used in ethylene polymerization*, 2006, PhD Thesis, Université Claude Bernard Lyon 1.
64. Tian, J., et al., US 20030236365, FINA Technology, Inc. (Houston, TX) 2003.
65. Silveira, F., et al., *Effect of the silica texture on the structure of supported metallocene catalysts*. Journal of Molecular Catalysis A: Chemical, 2009. **298**(1-2): p. 40-50.
66. Abboud, M., P. Denifl, and K.-H. Reichert, *Study of the morphology and kinetics of novel Ziegler-Natta catalysts for propylene polymerization*. Journal of Applied Polymer Science, 2005. **98**(5): p. 2191-2200.
67. Abboud, M., P. Denifl, and K.-H. Reichert, *Advantages of an Emulsion-Produced Ziegler-Natta Catalyst Over a Conventional Ziegler-Natta Catalyst*. Macromolecular Materials and Engineering, 2005. **290**(12): p. 1220-1226.
68. Bartke, M., et al., *A New Heterogenization Technique for Single-Site Polymerization Catalysts*. Macromolecular Materials and Engineering, 2005. **290**(4): p. 250-255.
69. Linonen, T. and P. Denifl, EP 1,273,595 A1, Borealis Technology Oy, 2003.
70. Floyd, S., et al., *Polymerization of olefins through heterogeneous catalysis. III. Polymer particle modelling with an analysis of intraparticle heat and mass transfer effects*. Journal of Applied Polymer Science, 1986. **32**(1): p. 2935-2960.

71. Floyd, S., et al., *Polymerization of olefines through heterogeneous catalysis IV. Modeling of heat and mass transfer resistance in the polymer particle boundary layer*. Journal of Applied Polymer Science, 1986. **31**(7): p. 2231-2265.
72. Hutchinson, R.A., C.M. Chen, and W.H. Ray, *Polymerization of olefins through heterogeneous catalysis X: Modeling of particle growth and morphology*. Journal of Applied Polymer Science, 1992. **44**(8): p. 1389-1414.
73. Kanellopoulos, V., et al., *Comprehensive Analysis of Single-Particle Growth in Heterogeneous Olefin Polymerization: The Random-Pore Polymeric Flow Model*. Industrial & Engineering Chemistry Research, 2004. **43**(17): p. 5166-5180.
74. Zacca, J.J. and J.A. Debling, *Particle population overheating phenomena in olefin polymerization reactors*. Chemical Engineering Science, 2001. **56**(13): p. 4029-4042.
75. Knoke, S., et al., *Microkinetic Videomicroscopic Analysis of Olefin Polymerization with a Supported Metallocene Catalyst*. Angewandte Chemie International Edition, 2003. **42**(41): p. 5090-5093.
76. Pater, J.T.M., G. Weickert, and v.W.P.M. Swaaij, *Optical and infrared imaging of growing polyolefin particles*. AIChE Journal, 2003. **49**: p. 450 - 464.
77. Hamilton, P., D.R. Hill, and D. Luss, *Optical and infrared study of individual reacting metallocene catalyst particles*. AIChE Journal, 2008. **54**(4): p. 1054-1063.
78. McKenna, T.F. and J.B.P. Soares, *Single particle modelling for olefin polymerization on supported catalysts: A review and proposals for future developments*. Chemical Engineering Science, 2001. **56**(13): p. 3931-3949.
79. Floyd, S., et al., *Polymerization of olefins through heterogeneous catalysis. VI. Effect of particle heat and mass transfer on polymerization behavior and polymer properties*. Journal of Applied Polymer Science, 1987. **33**(4): p. 1021-1065.
80. Floyd, S., R.A. Hutchinson, and W.H. Ray, *Polymerization of olefins through heterogeneous catalysis—V. Gas-liquid mass transfer limitations in liquid slurry reactors*. Journal of Applied Polymer Science, 1986. **32**(6): p. 5451-5479.
81. Hutchinson, R.A. and W.H. Ray, *Polymerization of olefins through heterogeneous catalysis. VII. Particle ignition and extinction phenomena*. Journal of Applied Polymer Science, 1987. **34**(2): p. 657-676.
82. Hutchinson, R.A. and W.H. Ray, *Polymerization of olefins through heterogeneous catalysis. VIII. Monomer sorption effects*. Journal of Applied Polymer Science, 1990. **41**(1-2): p. 51-81.
83. Ferrero, M.A. and M.G. Chiovetta, *Catalyst fragmentation during propylene polymerization: Part II. Microparticle diffusion and reaction effects*. Polymer Engineering & Science, 1987. **27**(19): p. 1448-1460.

84. Ferrero, M.A. and M.G. Chiovetta, *Catalyst fragmentation during propylene polymerization. III: Bulk polymerization process simulation*. Polymer Engineering & Science, 1991. **31**(12): p. 886-903.
85. Ferrero, M.A. and M.G. Chiovetta, *Effects of catalyst fragmentation during propylene polymerization. IV: Comparison between gas phase and bulk polymerization processes*. Polymer Engineering & Science, 1991. **31**(12): p. 904-911.
86. Galvan, R. and M. Tirrell, *Molecular weight distribution predictions for heterogeneous Ziegler-Natta polymerization using a two-site model*. Chemical Engineering Science, 1986. **41**(9): p. 2385-2393.
87. Schmeal, W.R. and J.R. Street, *Polymerization in expanding catalyst particles*. AIChE Journal, 1971. **17**(5): p. 1188-1197.
88. Yiagopoulos, A., et al., *Heat and mass transfer phenomena during the early growth of a catalyst particle in gas-phase olefin polymerization : the effect of prepolymers temperature and time*. Chemical Engineering Science, 2001. **56**(13): p. 3979-3995.
89. Kosek, J., et al., *Dynamics of particle growth and overheating in gas-phase polymerization reactors*. Chemical Engineering Science, 2001. **56**(13): p. 3951-3977.
90. Kittilsen, P., et al., *The interaction between mass transfer effects and morphology in heterogeneous olefin polymerization*. Chemical Engineering Science, 2001. **56**(13): p. 4015-4028.
91. Kittilsen, P., H.F. Svendsen, and T.F. McKenna, *Viscoelastic model for particle fragmentation in olefin polymerization*. AIChE Journal, 2003. **49**(6): p. 1495-1507.
92. Di Martino, A., et al., *Modelling Induced Tension in a Growing Catalyst/Polyolefin Particle: A Multi-Scale Approach for Simplified Morphology Modelling*. Macromolecular Reaction Engineering, 2007. **1**(3): p. 338-352.
93. Grof, Z., et al., *Modeling of morphogenesis of polyolefin particles: Catalyst fragmentation*. AIChE Journal, 2003. **49**(4): p. 1002-1013.
94. Grof, Z., J. Kosek, and M. Marek, *Modeling of morphogenesis of growing polyolefin particles*. AIChE Journal, 2005. **51**(7): p. 2048-2067.
95. Grof, Z.k., J. Kosek, and M. Marek, *Principles of the Morphogenesis of Polyolefin Particles*. Industrial & Engineering Chemistry Research, 2005. **44**(8): p. 2389-2404.
96. Horackova, B., et al., *Morphogenesis of polyolefin particles in polymerization reactors*, in *Computer Aided Chemical Engineering*. 2006, Elsevier. p. 1137-1142.
97. Horácková, B., Z. Grof, and J. Kosek, *Dynamics of fragmentation of catalyst carriers in catalytic polymerization of olefins*. Chemical Engineering Science. **62**(18-20): p. 5264-5270.

98. Merquior, D.M., E.L. Lima, and J.C. Pinto, *Modeling of Particle Fragmentation in Heterogeneous Olefin Polymerization Reactions*. Polymer Reaction Engineering, 2003. **11**(2): p. 133-154.
99. Merquior, D.M., E.L. Lima, and J.C. Pinto, *Modeling of Particle Fragmentation in Heterogeneous Olefin Polymerization Reactions, 2*. Macromolecular Materials and Engineering, 2005. **290**(6): p. 511-524.
100. Di Martino, A., G. Weickert, and T.F.L. McKenna, *Contributions to the Experimental Investigation of the Nascent Polymerisation of Ethylene on Supported Catalysts, 2*. Macromolecular Reaction Engineering, 2007. **1**(2): p. 229-242.
101. Machado, F., et al., *Evaluation of the Initial Stages of Gas-Phase Ethylene Polymerizations with a SiO<sub>2</sub>-Supported Ziegler–Natta Catalyst*. Macromolecular Reaction Engineering, 2009. **3**(1): p. 47-57.
102. Silva, F.M., et al., *Investigation of Catalyst Fragmentation in Gas-Phase Olefin Polymerisation: A Novel Short Stop Reactor*. Macromolecular Rapid Communications, 2005. **26**(23): p. 1846-1853.
103. Weist, E.L., et al., *Morphological study of supported chromium polymerization catalysts. 2. Initial stages of polymerization*. Macromolecules, 1989. **22**(8): p. 3244-3250.
104. Webb, S.W., W.C. Conner, and R.L. Laurence, *Monomer transport influences in the nascent polymerization of ethylene by silica-supported chromium oxide catalyst*. Macromolecules, 1989. **22**(7): p. 2885-2894.
105. Pater, J.T.M., et al., *High precision prepolymerization of propylene at extremely low reaction rates--kinetics and morphology*. Chemical Engineering Science, 2001. **56**(13): p. 4107-4120.
106. Conner, W.C., et al., *Use of x-ray microscopy and synchrotron microtomography to characterize polyethylene polymerization particles*. Macromolecules, 1990. **23**(22): p. 4742-4747.
107. Pimplapure, M.S., et al., *Low-Rate Propylene Slurry Polymerization: Morphology and Kinetics*. Macromolecular Rapid Communications, 2005. **26**(14): p. 1155-1158.
108. Zheng, X. and J. Loos, *Morphology Evolution in the Early Stages of Olefin Polymerization*. Macromolecular Symposia, 2006. **236**(1): p. 249-258.
109. Zheng, X., et al., *Influence of Copolymerization on Fragmentation Behavior Using Ziegler-Natta Catalysts*. Macromolecular Rapid Communications, 2006. **27**(1): p. 15-20.
110. Fink, G., et al., *The particle-forming process of SiO<sub>2</sub>-supported metallocene catalysts*. Macromolecular Symposia, 2001. **173**(1): p. 77-88.


111. Steinmetz, B., et al., *Polypropylene growth on silica-supported metallocene catalysts: A microscopic study to explain kinetic behavior especially in early polymerization stages*. *Acta Polymerica*, 1997. **48**(9): p. 392-399.
112. Knoke, S., et al., *Early Stages of Propylene Bulk Phase Polymerization with Supported Metallocene Catalysts*. *Macromolecular Chemistry and Physics*, 2003. **204**(4): p. 607-617.
113. Eberstein, C., et al., *Gasphasenpolymerisation von Butadien*. *Chemie Ingenieur Technik*, 1996. **68**(7): p. 820-823.
114. Pater, J.T.M., G. Weickert, and W.P.M. van Swaaij, *New Method for Online Observation of Growing Polyolefin Particles*. *CHIMIA International Journal for Chemistry*, 2001. **55**: p. 231-233.
115. Ferrari, D. and G. Fink, *Video Microscopy for the Investigation of Gas Phase Copolymerization*. *Macromolecular Materials and Engineering*, 2005. **290**(11): p. 1125-1136.
116. Ferrari, D., et al., *Microkinetic Videomicroscopic Analysis of the Olefin-Copolymerization with Heterogeneous Catalysts*. *Macromolecular Symposia*, 2006. **236**(1): p. 78-87.
117. Abboud, M., P. Denifl, and K.-H. Reichert, *Fragmentation of Ziegler-Natta Catalyst Particles During Propylene Polymerization*. *Macromolecular Materials and Engineering*, 2005. **290**(6): p. 558-564.
118. Salvo, L., et al., *X-ray micro-tomography an attractive characterisation technique in materials science*. *Nuclear Instruments and Methods in Physics Research Section B: Beam Interactions with Materials and Atoms*, 2003. **200**: p. 273-286.
119. Jones, K.W., et al., *Determination of polymerization particle morphology using synchrotron computed microtomography*. *Nuclear Instruments and Methods in Physics Research Section B: Beam Interactions with Materials and Atoms*, 1992. **68**(1-4): p. 105-110.
120. Jang, Y.-J., et al., *Study of the Fragmentation Process of Different Supports for Metallocenes by Laser Scanning Confocal Fluorescence Microscopy (LSCFM)*. *Macromolecular Chemistry and Physics*, 2005. **206**(20): p. 2027-2037.
121. Gomez-Hens, A. and D. Perez-Bendito, *The stopped-flow technique in analytical chemistry*. *Analytica Chimica Acta*, 1991. **242**: p. 147-177.
122. Liu, B., H. Matsuoka, and M. Terano, *Stopped-Flow Techniques in Ziegler Catalysis*. *Macromolecular Rapid Communications*, 2001. **22**(1): p. 1-24.
123. Mori, et al., *Stopped-flow techniques in olefin polymerization*. Vol. 5. 1997, Cambridge, ROYAUME-UNI: Elsevier.

124. Busico, V., R. Cipullo, and V. Esposito, *Stopped-flow polymerizations of ethene and propene in the presence of the catalyst system rac-Me<sub>2</sub>Si(2-methyl-4-phenyl-1-indenyl)<sub>2</sub>ZrCl<sub>2</sub>/methylaluminoxane*. *Macromolecular Rapid Communications*, 1999. **20**(3): p. 116-121.
125. Soga, K., M.-a. Ohgizawa, and T. Shiono, *Copolymerization of ethylene and propene with a TiCl<sub>4</sub>/MgCl<sub>2</sub>-Al(C<sub>2</sub>H<sub>5</sub>)<sub>3</sub> catalyst system using a stopped-flow method*. *Die Makromolekulare Chemie*, 1993. **194**(8): p. 2173-2181.
126. Song, F., R.D. Cannon, and M. Bochmann, *Zirconocene-Catalyzed Propene Polymerization: A Quenched-Flow Kinetic Study*. *Journal of the American Chemical Society*, 2003. **125**(25): p. 7641-7653.
127. Di Martino, A., et al., *Design and Implementation of a Novel Quench Flow Reactor for the Study of Nascent Olefin Polymerisation*. *Macromolecular Reaction Engineering*, 2007. **1**(2): p. 284-294.
128. Di Martino, A., G. Weickert, and T.F.L. McKenna, *Contributions to the Experimental Investigation of the Nascent Polymerisation of Ethylene on Supported Catalysts, 1*. *Macromolecular Reaction Engineering*, 2007. **1**(1): p. 165-184.
129. Taniike, T., et al., *Initial Particle Morphology Development in Ziegler-Natta Propylene Polymerization Tracked with Stopped-Flow Technique*. *Macromolecular Chemistry and Physics*. **212**(7): p. 723-729.
130. Machado, F., et al., *An experimental study on the early stages of gas-phase olefin polymerizations using supported Ziegler-Natta and metallocene catalysts*. *Polymer Engineering & Science*. **51**(2): p. 302-310.






# Chapter 2



*Thermal study and  
optimization of the  
gas phase stopped  
flow reactor*





<b>1. Reactor set up, materials and experimental procedure.....</b>	<b>108</b>
1.1. Introduction .....	108
1.2. Reactor description and procedure .....	109
1.3. Materials .....	113
1.3.1. Catalyst preparation .....	113
1.3.2. Support .....	115
1.3.3. Inert seedbed .....	116
1.4. Preliminary tests .....	117
1.4.1. Flowmeter calibration.....	118
1.4.2. Thermocouple check.....	120
1.4.3. Repetability.....	121
1.4.4. Stopping the reaction .....	122
1.4.5. On the addition of scavenger to the inert seedbed .....	124
<b>2. Heat transfer study and optimization.....</b>	<b>126</b>
2.1. Introduction .....	126
2.2. Optimization of heat transfer in the packed bed stopped flow reactor.....	131
2.2.1. Influence of gas thermal conductivity .....	131
2.2.2. Influence of gas velocity.....	137
2.2.3. Influence of inert seedbed properties .....	145
2.2.4. Towards the optimum heat transfer conditions.....	147
2.2.5. Influence of heat generation (catalyst amount).....	151
<b>3. Validation and modelling.....</b>	<b>152</b>
3.1. Temperature inside the bed .....	152
3.2. Concentration profiles .....	155
3.3. Reactor homogeneity.....	156
<b>4. Conclusions .....</b>	<b>157</b>
<b>5. References .....</b>	<b>159</b>

# 1. Reactor set up, materials and experimental procedure

## 1.1. Introduction

As mentioned in the previous chapter, the aim of this PhD work is to study the influence of different reaction parameters on the start-up of gas phase reactions of ethylene polymerization. This work should be able to describe the evolution of activity, polymer properties, particle morphology and temperature with reaction time. In order to capture the time range in which important transient phenomena are at play, low and very low yield reactions should be performed. At the same time realistic reaction conditions should be studied. In fact it has been said in the previous chapter that morphology and temperature and concentration profiles, which in turn influence activity and polymer properties, depend not only on the quantity of polymer present on the support particle but also on the rate of polymer production. One of the objectives of this work being to give reliable experimental data for single particle modeling, it is clear that it is not recommended to work under conditions that differ greatly from the industrial ones (i.e. very mild conditions responsible for “slow” polymerization). Finally it is also suitable to have the possibility to explore a wide range of experimental conditions like temperature, pressure and gas phase composition.

It is quite clear that the success of this study will depend on an accurate design of the appropriate reactor.

Reactors classically used to study gas phase olefin polymerization do not assure the performances needed to perform this kind of study. They normally consist in big autoclaves (more than 500mL volume) equipped with vigorous stirring, a circulating fluid (water or oil) for temperature control and injection system for the solid catalyst (simple valve or injection chamber). Mass flow controller is typically used to measure the catalyst activity by controlling the monomer flow rate needed to keep the reactor pressure constant [1]. The autoclaves can be quite close to the industrial reactors in terms of shape [2] and consist of a more or less dense stirred bed or fluidized bed reactors. Usually reactor temperature is measured at a single position thus giving information only on the temperature of the fluid phase. Although more sophisticated measurements at different positions are presented in literature [3] the registered values can be quite far from the real particle temperature. In

addition, due to the large reactor volume, a big inertia in heat transfer is present in this type of reactors. Because of the nature of the reactor contents, the hydrodynamics inside a fluidized bed reactor or stirred powder bed reactors (the major types of polyolefin reactors used in commercial processes) can be very complex, making the early stages of the reaction difficult to study in a bench scale device. In addition, the rapid reactions and sensitive nature of the catalyst make it difficult to study this aspect even at the laboratory scale using standard reactors. It is then clear that in a classic gas phase reactor very short reactions requiring immediate contact between the reactants, precise control over the time (in the order of fractions of seconds) and immediate stop of the reaction (by catalyst poisoning or monomer removal) are impossible to perform. Another disadvantage of these reactors is that they normally operate in batch mode, while industrial reactors operate in continuous mode. In continuous reactors the relative gas-particle velocity has a tremendous impact on heat transfer and can be modulated to vary the temperature profiles.

Reactors suitable to study the early stages of gas phase olefin polymerization must fulfill the following requirements. It has to be noticed that some of them are quite close to the ones presented by Terano in its review [4].

- Contact between reagents and catalyst must be immediate
- Reaction end must be effective and immediate
- Reaction time should be precisely controlled
- No excessive temperature or concentration gradients should form inside the reactor
- Reaction conditions (pressure, temperature, gas composition, gas velocity) should stay constant during the reaction.
- Particle should be recovered without morphology alteration
- Enough polymer has to be produced to perform the necessary analysis

## *1.2. Reactor description and procedure*

The reactor used in this work is a modified version of the one used by Pinto et al. in their works [5]. This modification has been firstly introduced in the literature by Olalla et al. [6] and further developed later during this PhD.

The reactor is practically a fixed packed bed which is crossed by a pulse of reactants of a predetermined duration (Figure 1). It consists of a circular metal cartridge with a diameter of 20 mm and a depth of 10 mm which is located into a chamber. The filled chamber is closed with a frittered metal filter. Due to the particular aspect ratio of the packed bed, the reactor can be assimilated to a thin section of a classic packed bed or, in other words, to a differential reactor in which, by definition, the conversion of the reactants in the bed is extremely small, as is the change in the reactants concentration through the bed. Gas enters through the hole in the bottom of the external chamber and leaves through a similar hole at the back of the metal lid (Figure 2). Filters 3-mm thick with 13  $\mu\text{m}$  pores are present at the inlet and at the outlet to assure the bed stability under the flow of gas and to prevent solids loss during the reaction.

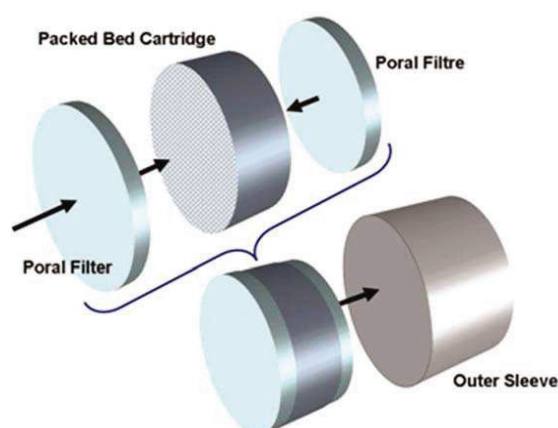


Figure 1: Schematic view of the packed bed

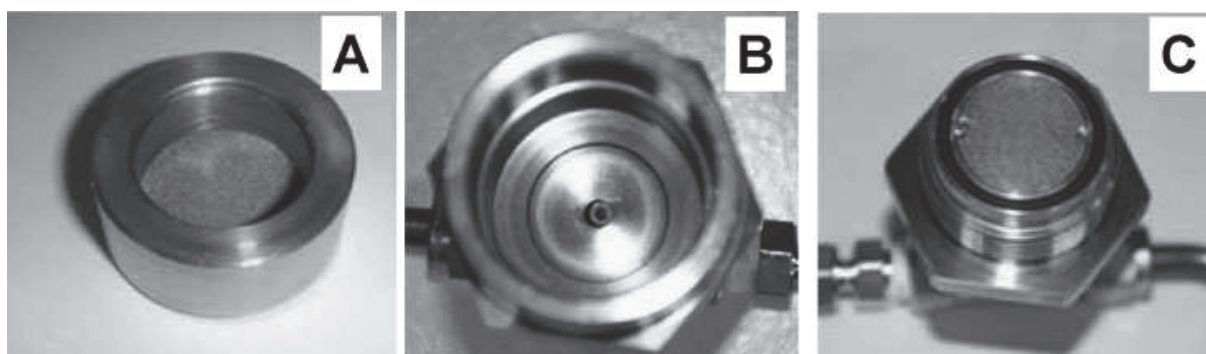


Figure 2: Interior view of the fixed bed reactor: (A) reactor cartridge, (B) external chamber, (C) sealing metal filter

Reaction temperature is controlled by plunging the reactor assembly into a heated water bath. Inlet gas stream is preheated at the reaction temperature by passing through a coil immersed in the water bath and by an electrical heat tape. It has to be said that the water bath does not act as a temperature controller. The water temperature is fixed at the desired level and does not change during the reaction to compensate reactor temperature variations. Due to

the low duration of the performed reactions and to the rapid temperature evolution in the early stages, temperature control by an external fluid is difficult to attain. The temperature will be controlled, as explained later, by selecting appropriate gas and solid properties. Due to the short reaction times and thick steel walls (10mm total), the reactor can be said to work in adiabatic mode. Thermocouples placed just before the inlet frit and just after the outlet frit allow us to record the temperature rise of the gas phase as it flows through the bed. This is one of the major strengths of the reactor. If the right conditions are chosen, it is possible to calculate the evolution of the temperature inside the reactor by measuring the temperature of the inlet and outlet stream and get an idea of the evolution of the catalyst particle temperature with time at the reaction start-up. Reaction gases are stored in a ballast and reaction pressure is set by a pressure relief valve. It is the pressure difference between the ballast and the reactor that allows the gas to flow. The outlet of the systems is at ambient pressure and is equipped with a ball float flowmeter for flow rate reading. Gas velocity is set by a metering valve placed just before the flowmeter and allowing a wide operational range. A schematic view of the reactor system is presented in Figure 3.

The reactor is equipped with three miniature solenoid valves (ASCO Joucomatic, France) controlled by a Programmable Logic Controller equipped with software (Crouzet, Millennium II, France): one for the feed, one for the quenching gas (CO<sub>2</sub>) and one for degassing. The minimum time between subsequent actions of the solenoid is 0.1 s. The automatic control of the solenoid valves allows a very fine control of the reaction time and to perform reactions as short as 100ms. In addition an infinite number of programs can be edited by varying the pulse time, number and sequence.

The polymerization procedure is described in what follows. The cartridge is filled with a mixture of seedbed (inert solid) and catalyst (1–15% catalyst w/w depending on seedbed and reaction time) in a glove box to avoid contamination of the contents, inserted into the external chamber, and then closed with the frittered metal lid. The catalyst particles have to be highly diluted with inert solids in this type of reactor to ensure good control of the reaction temperature by reducing the quantity of heat produced per unit volume of bed. The reactor is then connected to the feed line, plunged into the water bath, and swept with argon during the heating step.



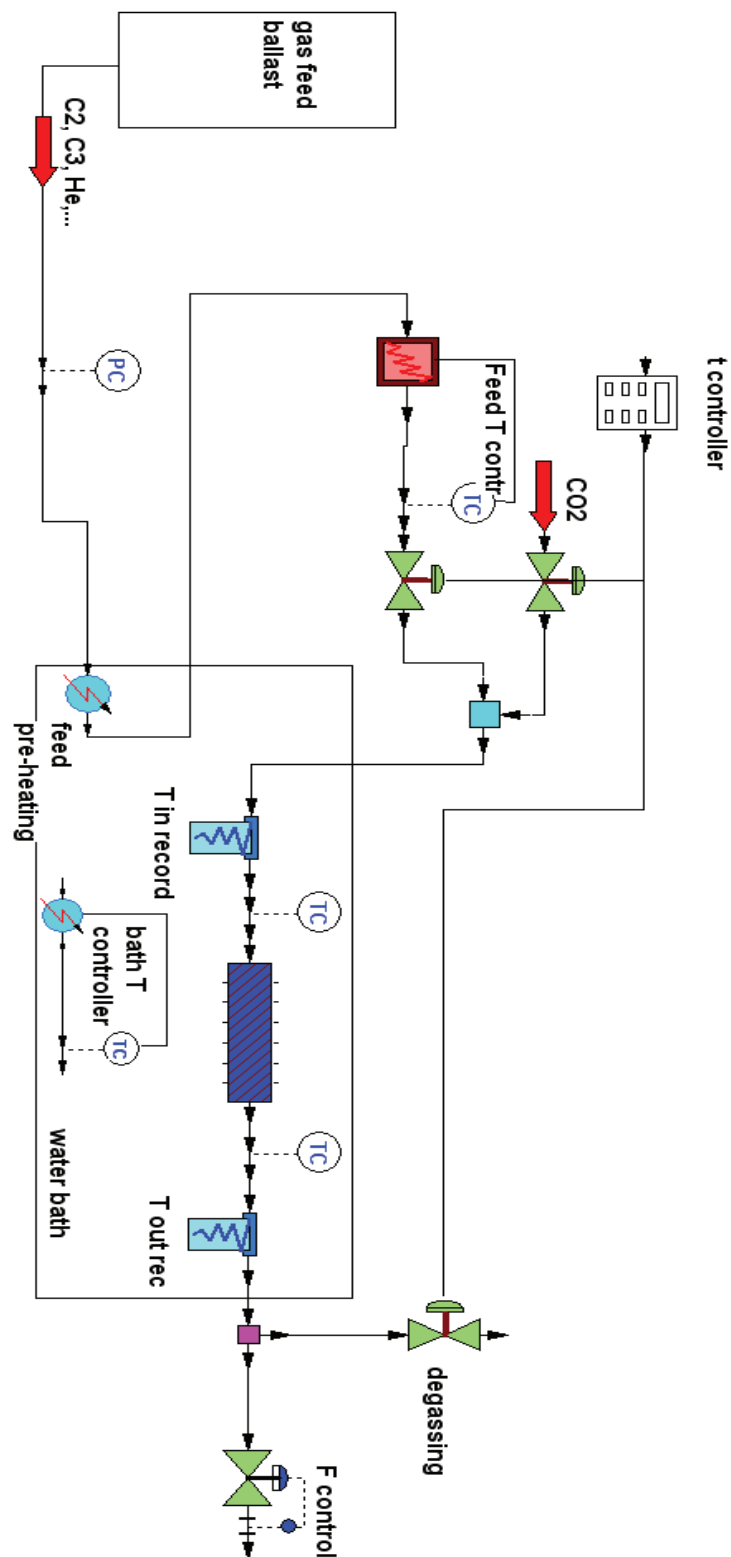


Figure 3: Reactor system scheme

Once the working temperature is reached, the argon flow is stopped and then the feed solenoid is opened to allow the feed mixture to flow through the catalytic bed. After a predetermined time the reaction has to be stopped immediately. This is an important step and

the best conditions for it have to be found. Productivities are measured by weighing the reactor before and after the polymerization step in a glove box (after a drying period to ensure that there is no residual water on the reactor assembly). The polymer is recovered from the fixed bed after separation of the solid inert by washing with demineralized water. The polymer recovered is then dried under vacuum at 80°C for at least 1 h to eliminate the last traces of water.

It has to be said that the olefin monomers used in this work are of high purity as they are passed over three purification columns before use: : a first one filled with reduced BASF R3-16 catalyst (CuO on alumina), a second one filled with molecular sieves (13X, 3A, Sigma-Aldrich) and a last one filled with Selexsorb® COS (Alcoa).

Using a fixed bed for olefin catalytic polymerization might seem quite exotic. As already said, stirred or fluidized bed are preferred because of their capacity to remove the heat generated by the reaction. Nevertheless the need to perform very short reactions drove our choice to packed beds. It is easy to figure out the difficulties that one may have when trying to fluidize or stir a solid bed for few seconds or even fractions of seconds. Manipulation of gas pulses of short duration is much easier. Of course the performances of our reactor in terms of heat transfer are lower than the ones of more classic configurations. One of the reasons for this is that, opposite to what happens in classic packed bed catalytic reactors, the reaction product stay in the bed and thus the contribution of heat removal by the flowing products is missing.

Nevertheless by operating with the right procedures and conditions the gas phase stopped flow reactor reveals to be a very powerful tool which allows to have a complete picture of the situation. Activity can be measured together with temperature profile, polymer properties and particle morphology. It is then possible to link all these variables each other and to understand the relations between them.

## **1.3. *Materials***

### **1.3.1. Catalyst preparation**

In this work metallocenes supported on MAO treated silica are investigated. Different reasons led to the choice of this type of catalyst. First of all exposure of the polymer/catalyst particle to air will not damage the support as is the case for MgCl<sub>2</sub> based catalysts, where the

support is altered upon contact with the air humidity. In addition it is known that metallocene catalysts, even if supported, should give narrow molecular weight distribution. Perturbations in the catalyst behavior coming from temperature or concentration gradients or modification of the active sites will be immediately reflected on the polydispersity of the produced polymer and detected. This would not have been possible if using classic ZN catalysts that show intrinsically broad MWD. Last but not least the slower fragmentation of silica supported catalysts will allow an easier detection of morphology evolution during the first reaction seconds.

Two precatalysts were studied and used as received:  $\text{EtInd}_2\text{ZrCl}_2$  and  $(\text{nBuCp})_2\text{ZrCl}_2$ . The synthesis of the supported catalyst was slightly varied along this study in order to study the influence of the catalyst preparation on the reaction start-up. The reference synthesis procedure consists in two steps, first impregnation of MAO on silica at  $85^\circ\text{C}$  for 1 h in toluene, and secondly the tethering of the metallocene complex at  $30^\circ\text{C}$  for 1 h in toluene. The preparation of this type of catalyst is largely discussed on the literature and we followed the synthesis developed by Welborn [7] and Takahashi [8]. In order to prepare silica treated MAO (SMAO) bearing different Al content we used two types of MAO solutions (10 or 30 wt% in toluene) leading to an Al content in the final solid varying from 8 to 15 wt%. The catalyst used as reference in this work was synthesized by adding to the SMAO an amount of metallocene complex in order to tether 2 wt. % on the silica. Due to the similar molecular weight of the two metallocene complexes used in this work, the final solid contained a Zr quantity around 0.4 wt%. Higher amounts have been added when an increase of the Zr content in the final catalyst was desired. Impregnation time and Al and Zr quantities in the final catalyst will be varied during this study. Exact values measured from inductive coupled plasma (ICP) will be given in the appropriate sections. The catalyst synthesized in this way is directly active in olefin polymerization as the ion pair between Al and Zr as the metal carbon bond and the electron vacancy on the metal are formed during the synthesis (Figure 4). Additional activator or scavenger is then theoretically not needed.

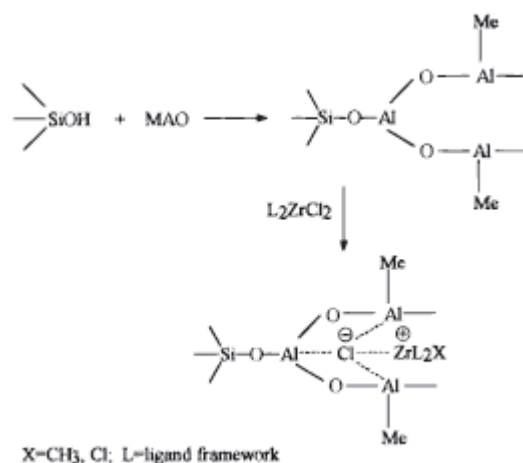


Figure 4: Schematic representation of possible catalyst active site formation.; reprinted with permission from [9].

### 1.3.2. Support

Different silicas were used to support the precatalysts during this work. The reference support is composed by silica Grace 948 (from Grace Davidson). All of them were treated at 200 °C for 4 h under vacuum ( $10^{-5}$  mbar) before use. Before reaching the 200°C plateau the solid was heated under vacuum at 130°C for 30 minutes to remove the water adsorbed on the surface. After the treatment the concentration of hydroxyl groups on the surface is around 5 OH/nm<sup>2</sup> (determined using titration with triethylaluminium as described in the thesis of V. Gachard-Pasquet [10]). Nitrogen porosimetry studies were performed to determine the pore volume and pore diameter as well as the specific surface area of the support used. The physical properties of Grace 948 are presented in the following table. Properties of the other used supports will be presented in the relative section.

Table 1: Physical properties of Grace 948

<i>Silica</i>	<i>Average particle size (μm)</i>	<i>Pore volume (mL/g)</i>	<i>Mean pore diameter (Å)</i>	<i>Surface area (m<sup>2</sup>/g)</i>
Grace 948	58	1.6	24	271

The following figures show SEM (Figure 5) and X ray tomography (Figure 6) images of the silica Grace 948. It has to be noticed how the particles are quite heterogeneous in size and porosity.

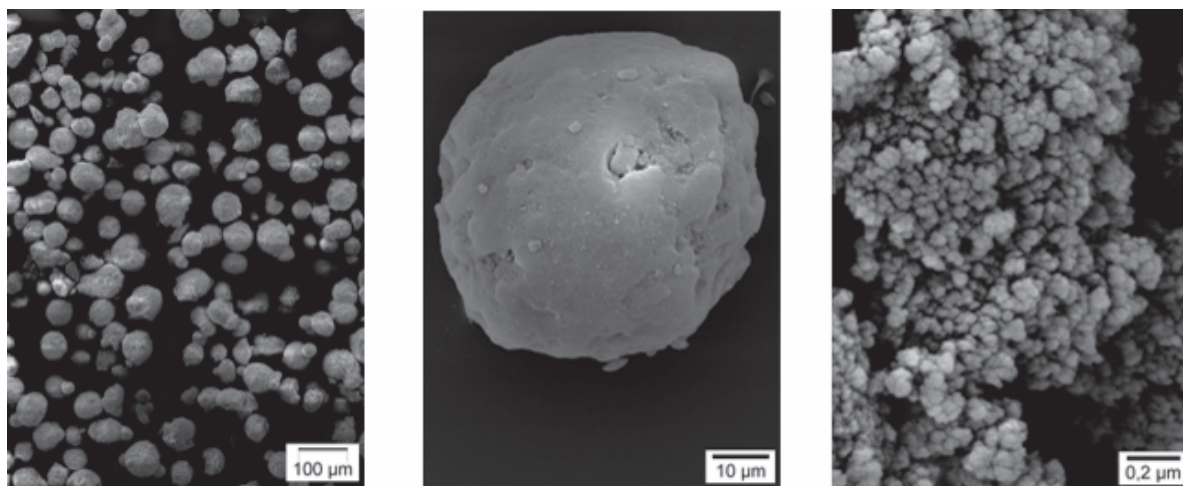


Figure 5: SEM images of Grace 948 particles.

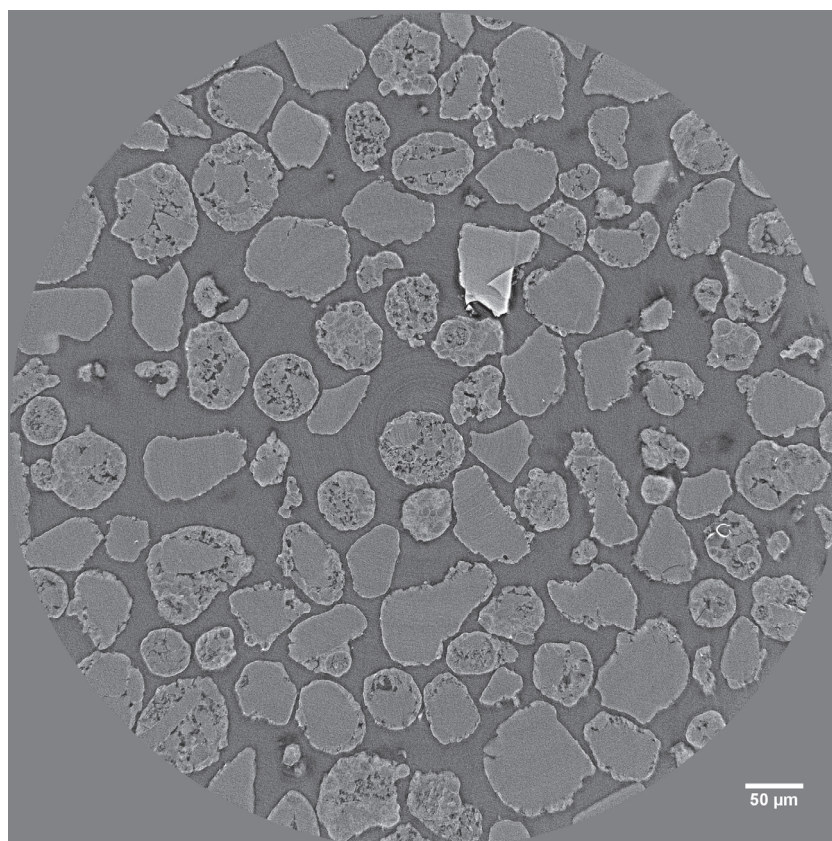


Figure 6: Synchrotron X-ray tomography image of internal structure of Grace 948 particles

### 1.3.3. Inert seedbed

The catalyst particles have to be highly diluted with inert solids in this type of reactor to ensure good control of the reaction temperature by reducing the quantity of heat produced per unit volume of bed [5, 6, 11, 12]. In the studies of Pinto, triethylaluminium (TEA)-treated silica was used as the inert diluent. In this work we focused also on a second type of seedbed

which is mainly prepared from commercially available NaCl particles. The main advantages respect to a silica seedbed are that the cubic form of NaCl crystals makes them easily recognizable in microscopy and a simple and elegant operating way to recover the catalyst/polymer particles for analysis is to wash the bed with demineralized water.

NaCl (Laurylab, France) was treated in different ways according to the desired application and used as seedbed. Large particle seed beds with a relatively narrow distribution were prepared by sieving the original salt to obtain a cut between 250  $\mu\text{m}$  and 500  $\mu\text{m}$ . Seedbeds with smaller particle diameter were also synthesized according to the method presented in the experimental part. The final solid consists of single cubes of 5–10  $\mu\text{m}$  slightly agglomerated to give a final single object of around 30  $\mu\text{m}$  (Figure 7).

All the inert seedbeds were dried under vacuum at 200°C for 4 h to remove the adsorbed water molecules before mixing with active catalyst.

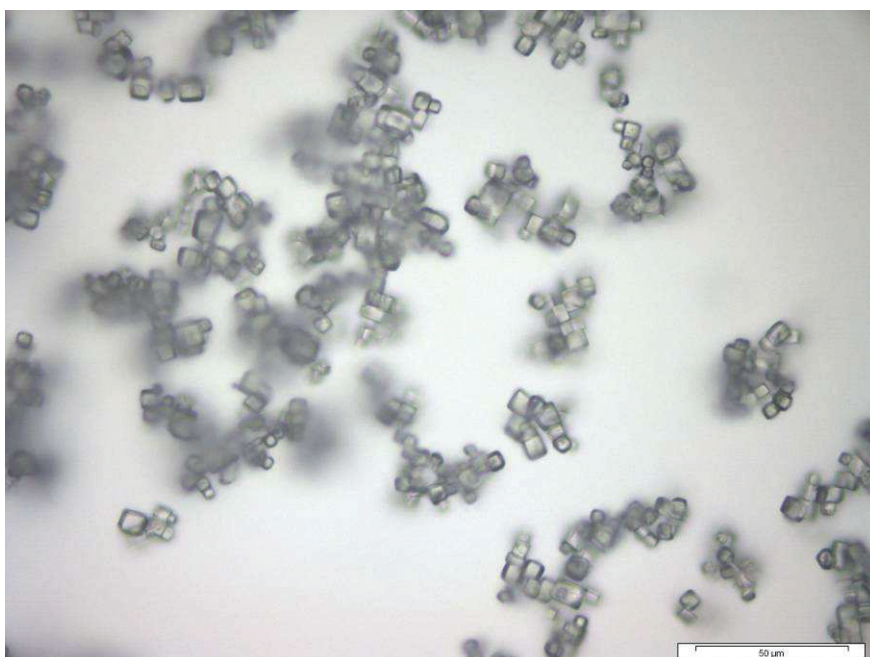


**Figure 7: Optical microscopy image of small synthesized NaCl crystals**

#### **1.4. Preliminary tests**

Before starting the study of the influence of the reaction conditions on early stages of gas phase ethylene polymerization, some preliminary tests have to be carried on in order to check the reliability of the reactor equipment and of the experimental procedure and to calibrate the different reactor parts.

### 1.4.1. Flowmeter calibration

Two different ball float flowmeters have been used for this study. One has a diameter of 4 mm and is equipped with a sapphire sphere to measure low flow rates (up to 100 mL/s) and the other has a diameter of 6 mm and is equipped with a heavier glass sphere allowing to measure flow rates up to 600 mL/s. Both the instruments have been calibrated by comparing the ball height in the tube with the value in mL/s given visually by a soap bubble flowmeter under the same reaction conditions. The metering valve has been opened at different degrees and for each position the flow rate has been measured. The results show that the instruments are highly accurate and reproducible (Figures 8 and 9). With this information an immediate conversion from ball height to mL/s is possible for a wide range of reaction conditions.

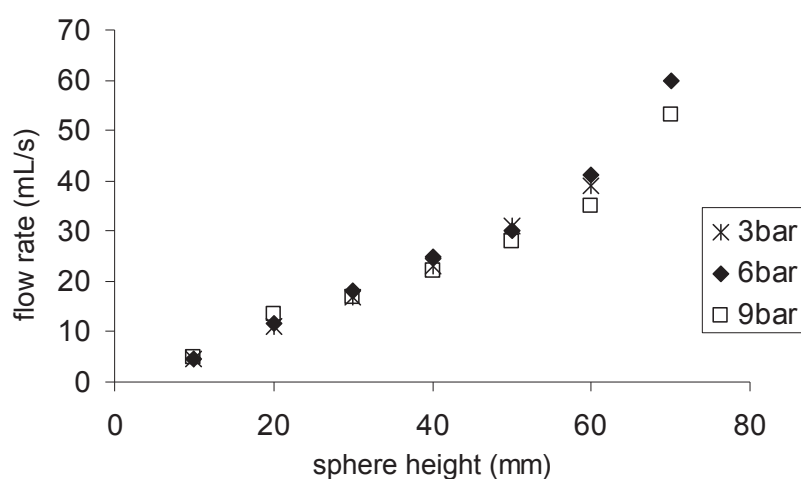


Figure 8: Calibration of sapphire flowmeter at different pressures

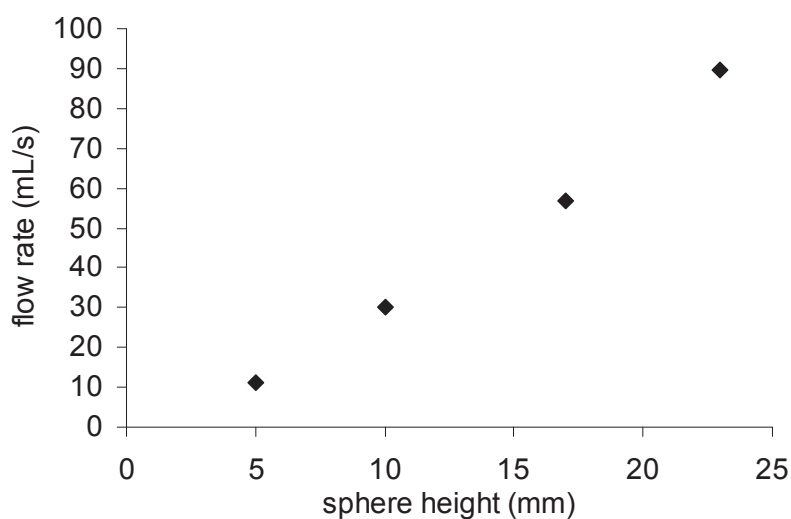


Figure 9: Calibration of the glass flowmeter at 9 bar

Filling the reactor with inert solid does not have a consistent effect on the pressure drop and the gas flow rate as shown in Figure 10. In this case the bed was filled with NaCl crystals having diameter between 250 and 500 $\mu$ m. The results are in accordance with Ergun equation (1), that is:

$$\frac{dP}{dz} = -\frac{G}{\rho D_p} \left( \frac{1-\varepsilon}{\varepsilon^3} \right) \left[ \frac{150(1-\varepsilon)\mu}{D_p} + 1.75G \right] \quad (1)$$

where P is the pressure, z the bed length, G the superficial mass velocity ( $\rho u$ ),  $\rho$  is the gas density, u is the superficial velocity,  $D_p$  the particle size,  $\varepsilon$  the bed porosity and  $\mu$  the gas viscosity.

This relation is normally used to calculate pressure drop of a fluid through a fixed bed of solid particles. We can anticipate that the maximum pressure drop calculated at the most unfavorable conditions of this work is of 30mbar.

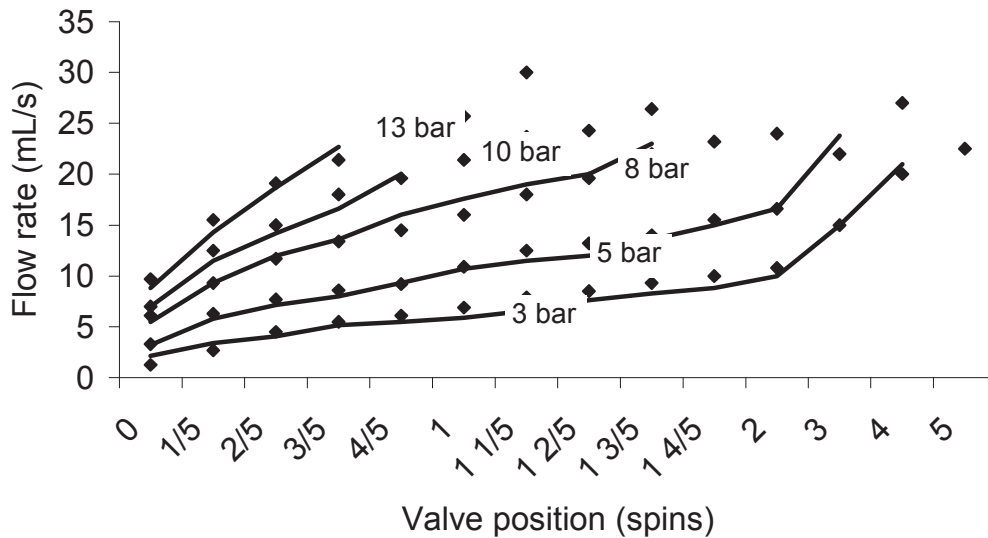


Figure 10: Gas flow rate dependence on valve position and pressure for empty (line) and NaCl filled (dots) bed

The value of the linear gas velocity inside the reactor is more interesting than the volumetric gas flow rate at the reactor outlet. To convert one value to the other we used the simple equation of state for ideal gases supposing mass conservation between the reactor bed and the flowmeter (which is true due to the low monomer conversion, as we will see later). The linear gas velocity ( $u$ ) is expressed as a function of the volumetric flow rate as follows:

$$u = \frac{P_{room} T_r}{P_r T_{room}} Q_{room} \frac{1}{\pi \left( \frac{D_t}{2} \right)^2 \varepsilon} \quad (2)$$



where  $P_{\text{room}}$  and  $T_{\text{room}}$  are the pressure and temperature of the flowmeter, namely 1 atm and 25°C,  $P_r$  and  $T_r$  are the reaction conditions,  $Q_{\text{room}}$  is the volumetric flowrate measured by the flowmeter,  $D_t$  is the reactor diameter and  $\varepsilon$  is the bed porosity. Using this expression means that the system is supposed to work in plug flow conditions.

#### 1.4.2. Thermocouple check

Four distinct stopped flow reactors equal each other are available for this work. One of the first parameters to check is the correct behavior and reproducibility of the thermocouples of each reactor. In order to do this, two type of analysis have been performed. In the first one we have measured the evolution of the inlet and outlet gas temperatures for three different flow rates using each reactor at 50°C. The flow rates have been varied by setting three different operating pressures and by keeping the same position of the metering valve. The results are highly reproducible and all the four reactors show the same temperature profiles. In figure 11 the results for a particular reactor is presented. In addition the effect of the different flow rates can be seen in the temperature measurements. The inlet and outlet temperatures are lower if higher flow rate is used because of the higher gas velocity responsible for gas stream cooling. The fluctuations in the curves corresponding to 15 bars are due to the pressure variation during the filling of the ballast that was necessary in order to maintain a positive pressure drop between the ballast and the reactor all along the experiment. The beginning and end of the gas flow can be seen by abrupt change in the temperature profile. It is interesting to notice that there are always some degrees of difference between the inlet and the outlet temperature value. This is due to the particular reactor configuration. The set up is in fact not symmetrical (Figure 12) so that the heat exchange between each thermocouple and the external ambient is not the same and a different equilibrium for the inlet and the outlet is reached.

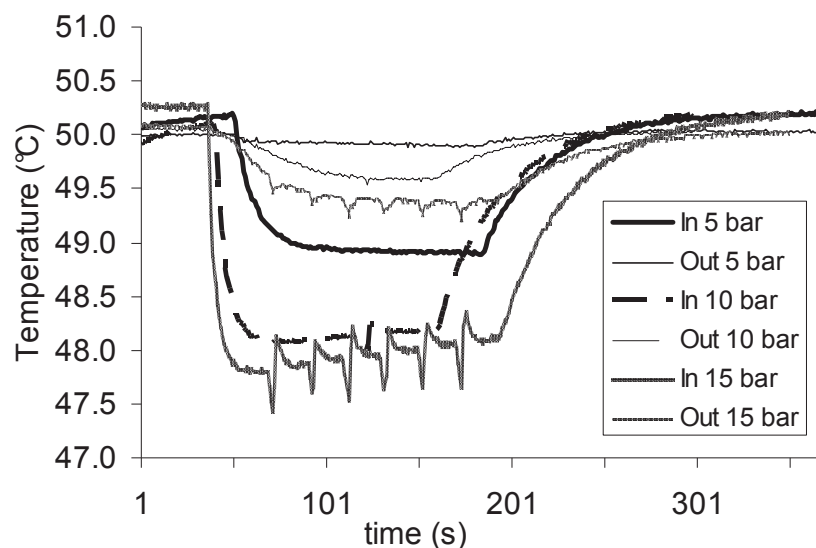


Figure 11: Inlet and outlet T for different flow rates at 50°C and empty reactor

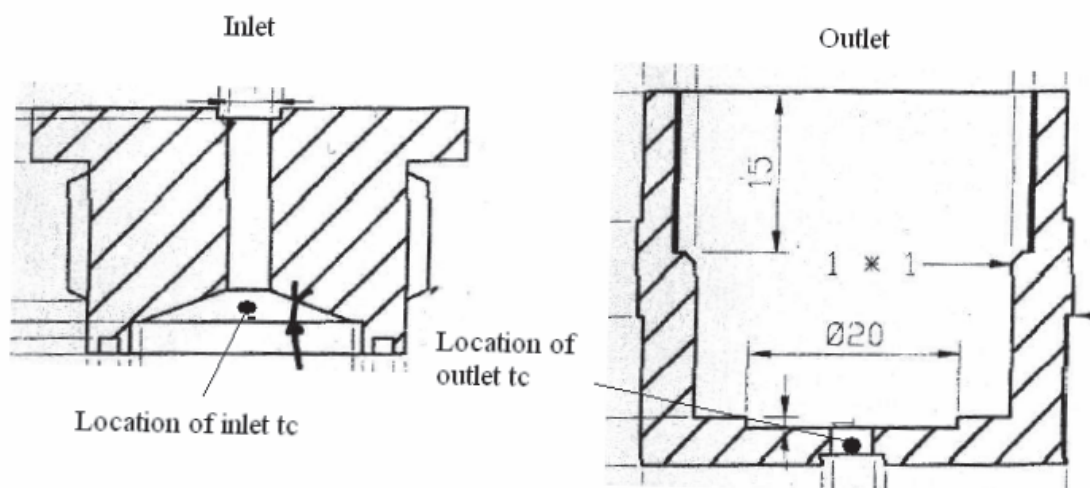


Figure 12: Cut view of the frittered lid (left) and external chamber (right) with thermocouple location

It has to be said that due to the rapid reaction rates that are typical during the start up of olefin polymerization, sudden temperature variations could occur. In order to capture them with a good precision fast responding thermocouples have been chosen. These consist of insulated type T thermocouples (nickel/copper) having a diameter of 1 mm. The insulation imparts the desired robustness to the device. The response time of the instrument is 150 ms (to reach 67% of the final value).

### 1.4.3. Repetability

In order to check if the four different reactors behave in the same way repeatability studies have been performed in which the same reaction has been conducted in each reactor and

repeated several times. In detail we performed reactions lasting 75s at 80°C and 6 bars of flowing ethylene, with a gas flow rate of about 20 mL/s and a catalyst mass of 45 +/- 5 mg. The catalyst is diluted using NaCl with crystal size between 250 and 500 μm.

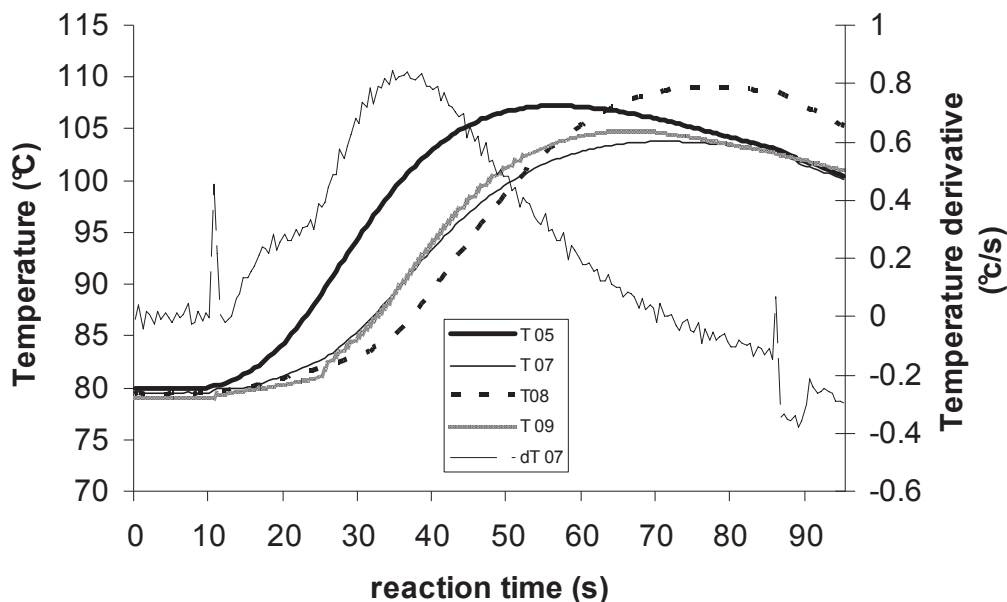


**Figure 13: Outlet T profile for the same reaction conducted in the 4 different reactors. Dashed thin line represents the derivative of the thin line**

In figure 13 the outlet temperature profile of the four different reactors have been plotted against the reaction time. A good reproducibility is visible among different reactors with maximum reached temperatures varying between 104°C and 109°C. These values are very high, sign of the extreme catalyst activity at the reaction start-up. A deep discussion on it will be given in the following paragraphs. Yield of the four reactions were also reproducible with values varying between 4.7 and 5.2 g PE / g catalyst.

In figure 13 we also plotted the derivative of the outlet temperature for one of the reactions. This helps in identifying the exact instants of the reaction beginning and end which are marked by a peak in the temperature derivative.

#### 1.4.4. Stopping the reaction

As said previously the reaction must be stopped effectively and immediately to have a precise control over the reaction time. In the setup used in this work various possibilities are available:

- Monomer removal by rapid degassing
- Chemical poisoning of the catalyst by replacing the reactants with a CO<sub>2</sub> flow
- Both the solutions together

The same reaction has been conducted using the three different methods and results are compared. We performed a very short reaction (0.1s) as it is for very short times that ending has to be the most immediate and effective. The reactions have been conducted using 150 mg of catalyst at 80°C and 6 bars of ethylene and 3 bars of helium. The gas velocity was around 5.5 cm/s. The reasons for the use of helium and of the particular gas velocity will be given later. What matters here is to compare the performances of the three stopping methods. From Table 2 it is possible to see that the best way to operate seems to be the simple system degassing or the simultaneous use of CO<sub>2</sub> and degassing as they give the lower yields. Replacing CO<sub>2</sub> with inert gases (using 50 mg catalyst in a 4s reaction) does not change the results, meaning that what it is more important is to rapidly remove the monomer from the reactor. The chemical effect of CO<sub>2</sub> on the catalyst seems to be negligible.

**Table 2: influence of reaction stopping method on yield**

<i>Exp</i>	<i>Reaction time (s)</i>	<i>Stopping method</i>	<i>Yield (g/g)</i>
SFG 115	0.1	CO <sub>2</sub>	0.125
SFG 113	0.1	Degassing	0.08
SFG 114	0.1	Degassing + CO <sub>2</sub>	0.08
SFG 122	4	Degassing + CO <sub>2</sub>	0.91
SFG 131	4	Degassing + N <sub>2</sub>	0.90
SFG 133	4	Degassing + He	0.92

Nevertheless we adopted the simultaneous use of degassing and CO<sub>2</sub> to stop our reaction. This is because the introduction of another gas after the ethylene is believed to facilitate the evacuation of the monomer from the particle pores. We could have used nitrogen instead of CO<sub>2</sub> but the system was already equipped with the carbon dioxide bottle. Helium is too expensive to be used in this way. In addition, as it can be seen from figure 14, the use of a second gas allows to remove the heat remaining inside the reactor (visible from the outlet gas temperature peak appearing after the reaction end). This is useful for quantification of the heat produced during the reaction and can be used in modeling studies.

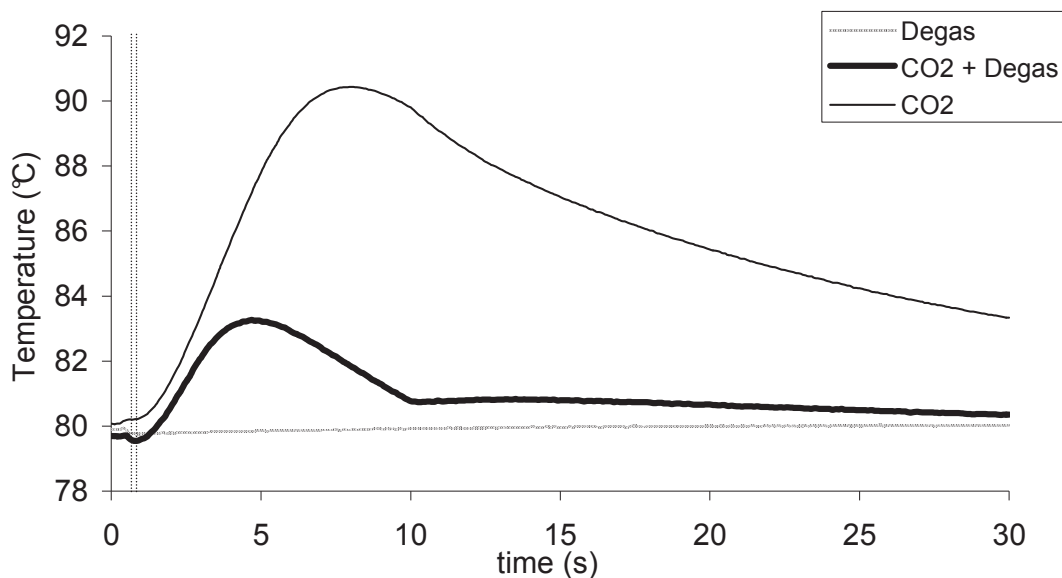


Figure 14: Evolution of the outlet gas temperature after reaction end. Reaction time is delimited by the vertical dotted lines

#### 1.4.5. On the addition of scavenger to the inert seedbed

In a classical gas (or slurry) phase reactor the addition of an excess of alkylaluminium (in addition of the MAO supported on silica particles) is necessary for the reaction to work for long times. Normally the supported metallocene complex is already preactivated by the MAO bonded on silica's hydroxyl groups and does not need extra activator to work. Nevertheless the alkylaluminium acts as scavenger for impurities present in the reactor volume or the feed and so its presence is fundamental in classic reactions.

In our stop flow system, being the volume of the reactor and the quantity of feed very small there is theoretically no need for a scavenger. Nevertheless comparing the advantages and disadvantages of the addition of scavenger to the reacting bed can help in selecting the best working procedure.

A classical scavenger used in olefin polymerization is triethylaluminium (TEA). TEA can easily react with the hydroxyl groups of the silica surface and thus give a seedbed containing a chemically bonded scavenger. A series of experiments comparing two different seedbeds, namely small NaCl and TEA treated silica, was conducted with the catalyst  $\text{EtInd}_2\text{ZrCl}_2$  to quantify the influence of an addition of scavenger to the bed. The reactions were performed at 80°C and 6 bars of ethylene and 3 bars of helium with a gas velocity of 5.5 cm/s. The results shown in figure 15 confirm that addition of scavenger to the bed is responsible for an activity that is 40 to 60% higher. Nevertheless activity improvement seems to be effective only for

reaction times higher than 10s. The longer the reaction time, the higher the quantity of moles of gas and of transported impurities that have passed through the catalyst. For low reaction times no scavenger is really needed. It is also possible that TEA acts more as an activator than a scavenger by reconstituting the metal carbon bond necessary for polymerization that can have been broken for different reasons (reaction with impurities, thermal deactivation...). We will see in the following Chapter how this is particularly true when using catalysts with a high Al or Zr content, for which the active site deactivation is more important. For the reference catalyst used in this part these problems are limited, and the role of TEA is less important in this sense.

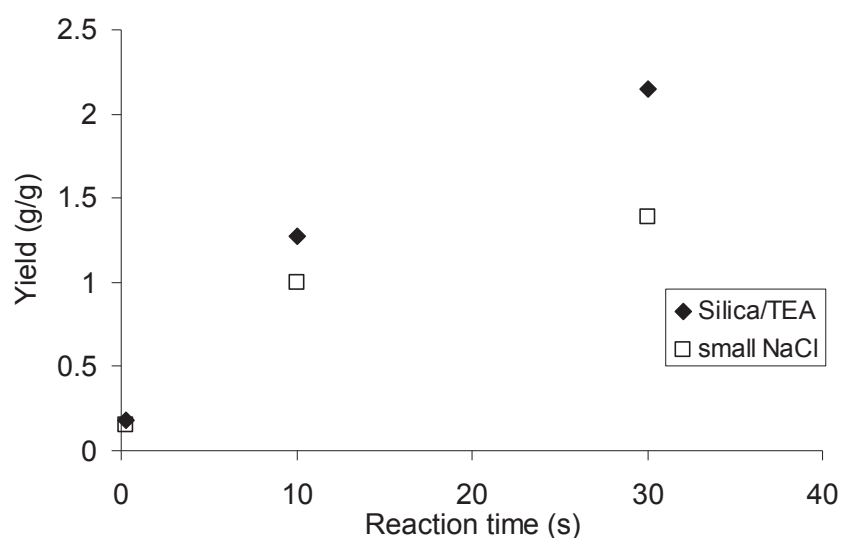


Figure 15: Effect of scavenger addition to the reaction yield

In addition the advantages in using a TEA treated silica as seedbed are less than the disadvantages: with this inert a solid liquid extraction is necessary to recover the polymer for analysis. The task can be particularly hard and tedious when dealing with very short reaction times, where the weight ratio of polymer/silica can be as low as 0.01. In addition, if one would like to observe the particles under Scanning Electron Microscopy (SEM) or other microscopy techniques, it will be difficult, especially for reactions where the catalyst has not fragmented yet, to distinguish catalyst particles (supported on silica) from inert bed particles.

The ideal situation would be to have a NaCl seedbed (easily separable from the polymer) impregnated with the scavenger. Unluckily no chemical bond is possible between TEA and NaCl. Some scavenger can nevertheless be deposited by physical adsorption on small size NaCl having a high specific surface. In a second series of experiments we compared three salt based seedbeds: simple NaCl, NaCl washed with TEA (to remove eventual impurities present

in the crystals) but with no Al remaining in the final solid and NaCl treated with TEA in order to have 2.8 wt % of Al in the final solid. Reaction conditions were the same as described above.

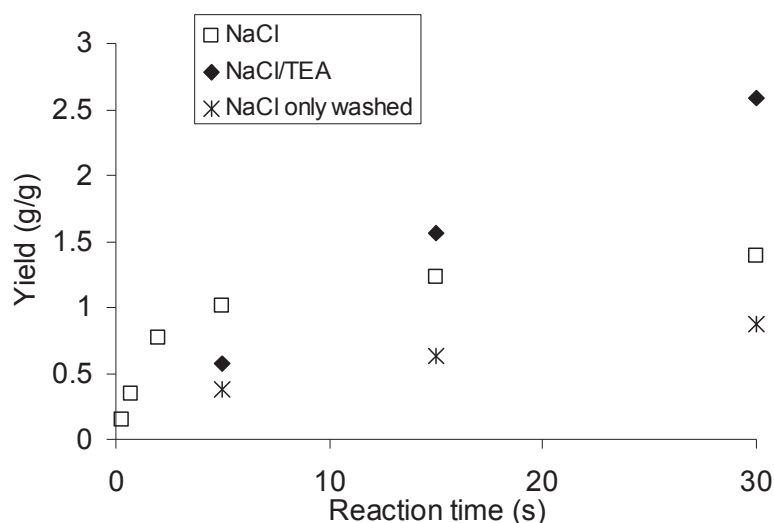


Figure 16: Comparison of NaCl seedbed treated in different ways: effect on Yield

From figure 16 it is easy to see that the results found with a silica/TEA seedbed are confirmed using NaCl/TEA: productivity is almost doubled for reactions of 30s but this difference decreases with decreasing reaction times. No activity improvement was measured using the seedbed only washed with TEA. It has to be said that due to the fact that only adsorption is responsible for the fixing of the scavenger on NaCl, the final solid is somewhat wet resulting in some difficulties in manipulation and in perturbations of the flow and flow pattern inside the reacting bed. For these reasons and because only for longer reaction times a consistent improvement is seen in the presence of a scavenger, we have chosen to not add any alkylaluminium to our seedbed during this work.

## 2. Heat transfer study and optimization

### 2.1. Introduction

The early stages of olefin polymerization can be crucial in ensuring adequate polymer properties, obtaining or maintaining stable reactor operation, preventing fines generation, and avoiding temperature excursions and catalyst deactivation. The risks of overheating of particles are highest during the early instants of the reaction given the highly exothermic

nature of these polymerizations and the high active site volumetric concentration and the low external surface area of fresh catalyst. Heat of reaction is in the order of 100 kJ/mol [13] and rates of reaction on the order of 5–35 kg of polymer per gram of catalyst per hour are normally found in industrial processes. This problem is even more pronounced in gas phase reactions due to the poor thermal properties of the fluid phase. Simulations presented in the bibliographic chapter have shown that particle overheating is likely during the initial instants of reaction in gas phase reactions for highly active catalysts, and especially for catalysts that are quickly activated. The extent of the temperature excursions is of course dependent on a number of parameters (catalyst activity and size, gas velocity and properties). One of the roles of the prepolymerization step used in industry is to limit this problem.

It is clear how extreme precautions have to be taken when studying early stages of olefin polymerization especially in terms of heat removal in order to avoid collateral phenomena like thermal reaction autoacceleration or even polymer melting. The particular configuration of our stopped flow reactor allows to accurately measure the temperature evolution of the gas phase during the reaction course and to vary a bunch of parameters related to heat transfer from the polymerizing particles to the gas (i.e. gas velocity and composition). The same particular configuration is also source of some disadvantages, as a high volumetric production of heat due to the bed being fixed and less heat removal due to the reaction product remaining in the bed. Supposing a constant reaction rate of 1 Kg PE/g cat/h (measured activities for the used catalyst in this reactor vary from 2.3 Kg PE/g cat/h to 0.1 Kg PE/g cat/h) gives an average volumetric heat rate production in the bed of 20 MW/m<sup>3</sup> that has to be transferred to the flowing gas and the inert seedbed by conduction and convection in the most efficient possible way. This simple quantification of the heat generation explains that is highly possible for the aforementioned risks (hotspots, polymer melting) to happen. A simple solution would have been to reduce at minimum level the quantity of catalyst used for each reaction without caring too much about the other reaction conditions. It has to be said nevertheless that, a part from being an imprecise way of working, this solution cannot be easily put into practice because a sufficient amount of recovered polymer is needed for each reaction time in order to be able to perform all the wanted analysis (SEC, DSC, microscopy).

The objective of this chapter is then to find the best experimental conditions that allow, for a wide range of reaction times, to produce enough polymer for analysis without incurring in excessive bed overheating due to too high heat production (or too low heat removal). In addition the particular reactor configuration is the reason why a deep heat transfer study to



optimize the working conditions is needed. Using a packed bed to perform catalytic polymerizations means that the heat of reaction must, as usually, be transferred from the active sites by conduction through the particle surface and from the catalyst particle to the gas phase. In addition in our reactor the heat can also be transferred from the catalyst to the inert seedbed and successively to the gas phase. All this amount of heat must be removed some way from the reactor. This can be achieved by conduction through the walls (not predominant for short reaction times) or by the flowing gas phase (more important). If this is not done properly, reaction runaway can incur because of the Arrhenius dependence of the activation energy on temperature. A work aiming to optimize the heat removal from the catalyst particles by the flowing phase is also justified by the fact that only gas phase temperatures can be measured in a cheap, rapid and reliable way due to the very small size of the catalyst particles. The better is the heat transfer, the closer will be the solid and fluid phase temperatures and thus it will be possible to follow the evolution of the catalyst surface temperature by measuring the outlet gas phase temperature.

We have chosen to work with the time interval 0.1–75 s as it is thought that this will be indicative of the critical period for particle breakup and potential loss of control of bed temperature in gas phase reactions. More in general we aim to investigate the relationship between heat transfer and operating conditions for relatively short times in order to get some fundamental knowledge about the thermal behavior of the reaction in the most critical phase (the start-up).

Packed beds are extensively used in chemical and process industries not only as reactors but also as separators and heat exchangers. Heat transfer plays a crucial role in determining the performance of these devices and has been studied for a number of decades. Different heat transfer mechanisms are at play in a packed bed: heat exchange with the environment, heat transfer from the solid and the fluid to the reactor wall, radial and axial conduction through the solid and the fluid, forced convection by the flowing fluid and heat transfer from the solid to the fluid. Each one of these mechanisms is characterized by a parameter which is obtained using macroscopic models. As said by Dixon in one of his numerous publications on fixed bed modeling [14], “there must surely by now be almost as many fixed bed reactor models in the vast literature of this subject as there are fixed bed reactors actually in operation around the world”. Such models, in fact, can be uni- or bi-dimensional, assume plug flow or consider dispersion, be pseudohomogenous or consider two phases and for each of them, depending on reaction conditions, a large number of correlations for the transfer parameters are available. A

complete modeling of the fixed bed is not in the aim of this PhD thesis. This subject is being treated in a parallel work in collaboration with LGPC (Laboratoire de Génie des Procédés Catalytiques) at CPE Lyon. The results of this modeling are nevertheless useful for the experimental study described here and part of them will be presented as support of experimental results when needed. What can be said here is that our fixed bed presents a high  $D_t / D_p$  and a low  $L_t/D_t$  (with  $D_t$  being the reactor diameter and  $L_t$  the reactor length). This allows to consider plug flow inside the bed and thus to neglect axial dispersion [15]. In addition the presence of a frittered lid at the reactor entrance helps in obtaining a homogeneous distribution of the gas flow. The high number of particles contained in a reactor diameter allows assuming uniform porosity distribution and neglecting radial flow distribution [16 15].

In our case the most important phenomenon to study and control in order to avoid particle overheating and minimize the difference between solid and fluid phase temperatures, is the heat transfer from solid to gas. This has been discussed in a number of publications but, for obvious reasons, not for the specific case of olefin polymerization [16-22]. The complexity of the subject is such that the choice of the most suitable equations to apply for the calculation of the particle-gas heat-transfer coefficient in a packed bed is still an open question, particularly for low particle Reynolds number ( $<10$ ). The result is a number of different equations whose validity depends on packing characteristics and flow field (Table 3).

**Table 3 : Different equations for Nu number in packed beds**

<i>Equation</i>	<i>Validity</i>	<i>Author</i>
$Nu = 2 + 1.8 Re^{0.5} Pr^{0.33}$		Kunii, Levenspiel
$Nu = 2 + 1.1 Re^{0.6} Pr^{0.33}$	$3 < Re < 3000$	Wakao
$Nu = \frac{0.255}{\varepsilon} Re^{0.665} Pr^{0.33}$	$Re > 100$ $D_t/D_p > 8$	Handley, Heggs
$Nu = 0.664 \left(\frac{Re}{\varepsilon}\right)^{0.5} Pr^{0.33}$	$Re > 500$	Gnielinski
$F = 0.664 \sqrt{1 + \left[\frac{0.0557 Re^{0.3} Pr^{0.67}}{1 + 2.44(Pr^{0.67} - 1) Re^{-0.1}}\right]^2}$		
$Nu^* = 2 + \frac{F}{\sqrt{\varepsilon}} Re^{0.5} Pr^{0.67}$		Martin
$Nu = Nu^* [1 + 1.5(1 - \varepsilon)]$		

A large number of these equations can be expressed in the following general form:

$$Nu = C + Re^a Pr^b \quad (3)$$

with ‘‘a’’ and ‘‘b’’ assuming positive values between 0 and 1. Nusselt, Reynolds, and Prandtl numbers are defined as follows:

$$Nu = \frac{hD_p}{k_f} \quad (4)$$

$$Re = \frac{\rho_f V D_p}{\mu_f (1 - \varepsilon)} \quad (5)$$

$$Pr = \frac{Cp_f \mu_f}{k_f} \quad (6)$$

where  $h$  is the heat-transfer coefficient between a particle and the surrounding medium,  $D_p$  is the particle (catalyst) diameter,  $k_f$  is the fluid thermal conductivity,  $\rho_f$  is the fluid density,  $V_s$  is the fluid superficial velocity (volumetric flow rate/cross sectional area of the bed),  $\mu_f$  is the fluid viscosity,  $\varepsilon$  is the bed porosity, and  $Cp_f$  is the fluid specific heat. Expressing the adimensional numbers in terms of the physical variables allows us to rewrite (3) in the following way:

$$h \propto Cp_f^b \mu_f^{(b-a)} V_s^a D_p^{a-1} k_f^{1-b} \rho_f^a \quad (7)$$

Equation (7) shows the influence of physical and operating parameters on the particle/gas heat-transfer coefficient. The parameters easily controllable in our system on a wide range are the thermal conductivity of the gas phase ( $k_f$ ) and its specific heat ( $Cp_f$ ) that depend on the gas composition, the gas velocity ( $V_s$ ), and the particle diameter ( $D_p$ ).

Also important in determining the bed temperature is the quantity of heat evacuated from the solid phase by convection, which is also dependent on physical and operating parameters as is expressed in the following equation:

$$Q_{gas} = Q \rho_f Cp_f \int_0^{tr} (Tg_{out} - Tg_{in}) dt = Q_{out} - Q_{in} \quad (8)$$

where  $Q_{\text{gas}}$  is the heat transferred to the gas phase,  $Q$  is the gas volumetric flow rate,  $\tau$  is the reaction time and  $T_{\text{gout}}$  and  $T_{\text{gin}}$  the measured inlet and outlet gas temperatures respectively.

A heat balance on the whole reactor is presented in Equation 9, where  $Q_{\text{gen}}$  is the heat generated by the reaction,  $Q_{\text{loss}}$  is the heat transferred through the reactor walls and  $Q_{\text{acc}}$  is the heat accumulated inside the reactor. Evaluation of  $Q_{\text{acc}}$  allows to approximatively calculate the temperature evolution of the reacting bed.

$$Q_{\text{acc}} = Q_{\text{gen}} - Q_{\text{gas}} - Q_{\text{loss}} \quad (9)$$

The heat produced by the reaction can be easily calculated from values of activity or yield according to

$$Q_{\text{gen}} = Y m_{\text{cat}} (-\Delta H_r) \quad (10)$$

Where  $Y$  is the yield of polymer (g polymer / g catalyst),  $m_{\text{cat}}$  the catalyst mass inside the reactor and  $\Delta H_r$  the reaction enthalpy.

Equation 7 allows to select the most significant variables that could be varied to improve heat transfer from solid to gas while equation 8 permit to quantify the quality of the heat transfer and check whether catalyst particles have undergone excessive overheating. Experimental results are presented in what follows.

## 2.2. Optimization of heat transfer in the packed bed stopped flow reactor

### 2.2.1. Influence of gas thermal conductivity

As can be seen from equation (7) a change in the gas thermal conductivity can have an impact on the gas solid heat transfer coefficient. An increase in thermal conductivity of the feed can be easily obtained by changing the feed composition, i.e. adding a very conducting gas to the ethylene feed. From Table 4 we can see that gases commonly used in laboratories have similar values of thermal conductivity, with the exception of hydrogen and helium that have conductivity values 10 times higher than the other gases. It is known that hydrogen is not inert in catalytic olefin polymerization and can be responsible of hydrogenolysis of the metal-carbon bond as is seen in ZN catalysis. This can have an impact on the activity and on the molecular weight distribution of the produced polymers. Our study being aimed to look

only at heat transfer, we decided then to use helium, available with high purity, because of its high conductivity and inertness. A series of reactions were conducted for 75 seconds with 30 mg of supported EtInd<sub>2</sub>ZrCl<sub>2</sub> catalyst diluted in coarse NaCl at 80 °C, 3.0 cm/s gas velocity, 6 bars of ethylene partial pressure and variable helium partial pressure.

**Table 4: Thermal conductivity of some gases at 300K, 1 atm, from [23]**

<i>gas</i>	<i>k<sub>f</sub> (W/(m*K))</i>
Ethylene	0.0236
Nitrogen	0.0226
Argon	0.0177
Propane	0.0183
Helium	0.172
Hydrogen	0.180

Table 5 shows that addition of as little as 33% of He to the process gas without changing the flow rate leads to much lower outlet gas temperatures than in case of pure ethylene. The increase in outlet gas temperature drops from 21 °C to 3–4 °C.

**Table 5: Influence of He addition on Yield and temperature increase**

<i>Exp</i>	<i>P<sub>C2</sub> (bar)</i>	<i>P<sub>He</sub> (bar)</i>	<i>ΔT (K)</i>	<i>Yield (g/g)</i>
SFG 11	6	0	21.2	6.60
SFG 12	6	3	3.0	1.50
SFG 13	6	6	4.0	2.06
SFG 14	6	12	3.7	1.91

When helium is added to the reacting mixture the measured productivity (and the catalyst activity as a consequence) also decreases. There are two possible reasons for this phenomenon. The increased capacity of the system to transfer the heat generated during the reaction from the solid to the gas results in a much lower average reactor temperature as manifested by the lower outlet gas temperature. Thus the exothermic polymerization reaction is inherently slower than when the local temperature decreases. Note that there is no visible deactivation in the curves with He whereas there is in absence of He (Figure 17).

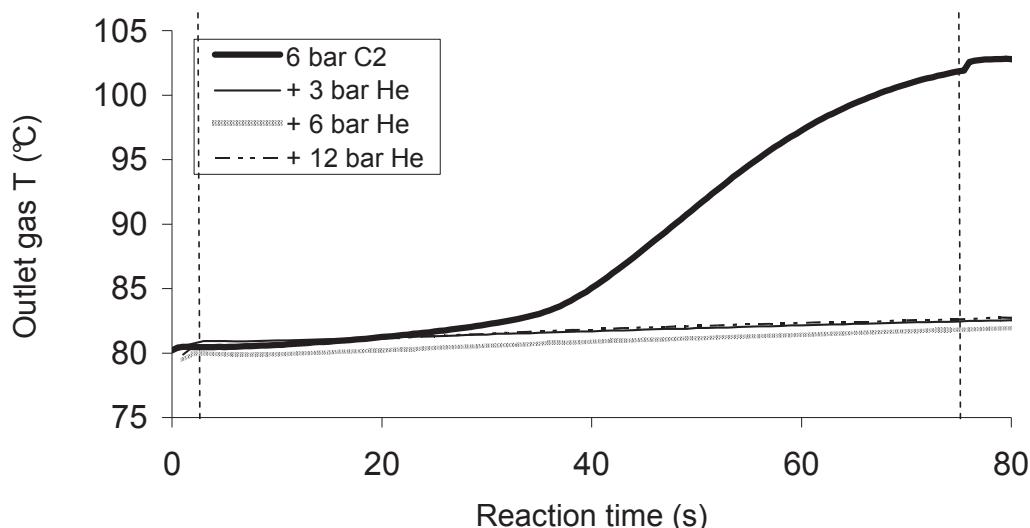


Figure 17: Outlet gas temperature evolution for different He content in the feed

It is also true that diluting the reacting gas with an inert could lower the ethylene concentration at the active site. Strong convection effects are possible especially at the beginning of the reaction if the monomer consumption is very high and for big and/or active catalytic particles. In this case the monomer concentration will not be constant in the particle pores along the radial dimension with accumulation of inerts at the active site [24]. This seems not to be the case because the measured productivity does not change greatly increasing the helium partial pressure. Nevertheless we decided to replace helium with nitrogen as it has the advantages of retaining the inert characteristic of the diluent and, at the same time, deleting the positive effect of the increased heat transfer coefficient (see Table 4). A series of experiences similar to that realized with helium has been carried out using nitrogen.

Table 6: Influence of N<sub>2</sub> addition on Yield and temperature increase

<i>Exp</i>	$P_{C_2}$ (bar)	$P_{N_2}$ (bar)	$\Delta T$ (K)	<i>Yield</i> (g/g)
SFG 19	6	0	14	6.7
SFG 20	6	3	11	5.7
SFG 21	6	6	10	5.8

As can be seen from Table 6, in this case the maximum  $\Delta T$  decrease from 14 °C if no nitrogen is present to 10 °C if 6 bars of nitrogen are added. The productivity drops respectively from 6.7 gPE/gcat to 5.8 gPE/gcat. Recall that in the case of He, the productivities dropped from 6.6 g/g with no He, to 1.8 +/- 0.3 g/g with He. This shows very clearly that dilution by inerts does not play a significant role in the decrease of the measured productivity since higher temperatures and yields are seen for the case of nitrogen as a carrier.

Rather it appears that thermal conductivity increase when He is used as opposed to ethylene alone or ethylene plus N<sub>2</sub> leads to a better evacuation of the heat of reaction in the first case, and therefore a lower particle temperature than in the other two cases. A comparison of the effects of two inert gases on the outlet gas temperature evolution and productivity is presented respectively in Figure 18 and Figure 19.

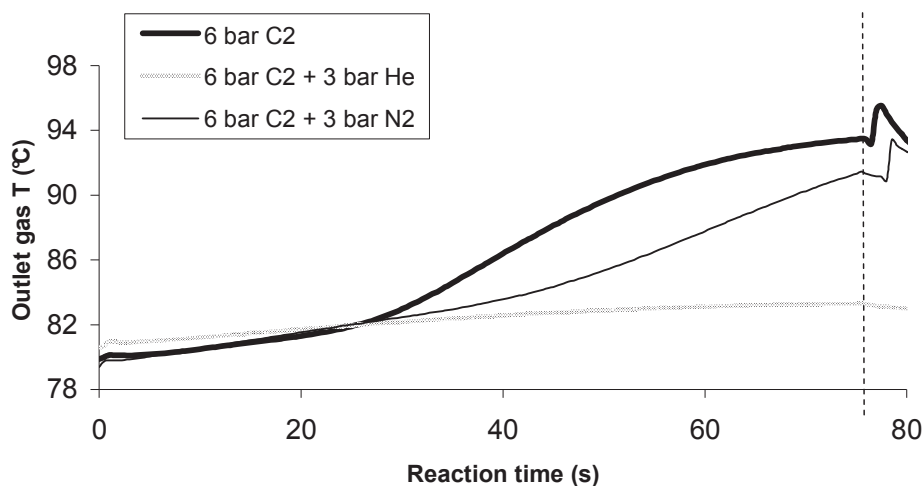


Figure 18: Influence of addition of 3 bar of inert on temperature evolution

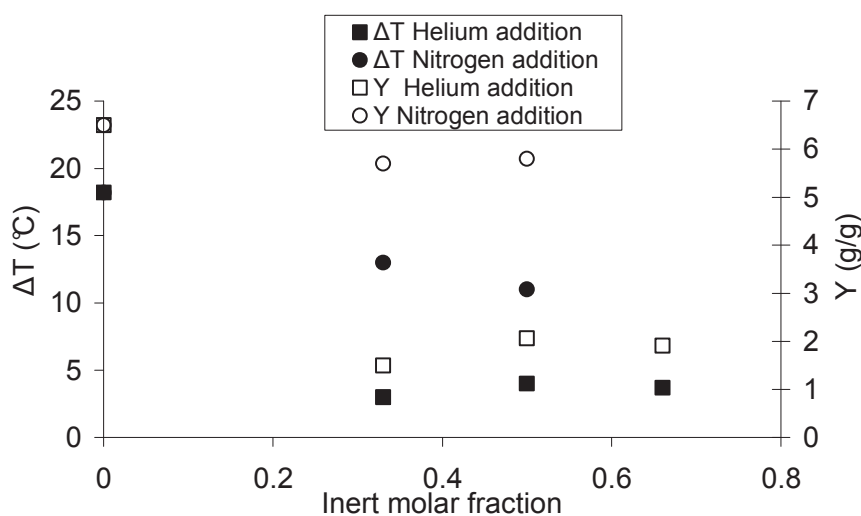
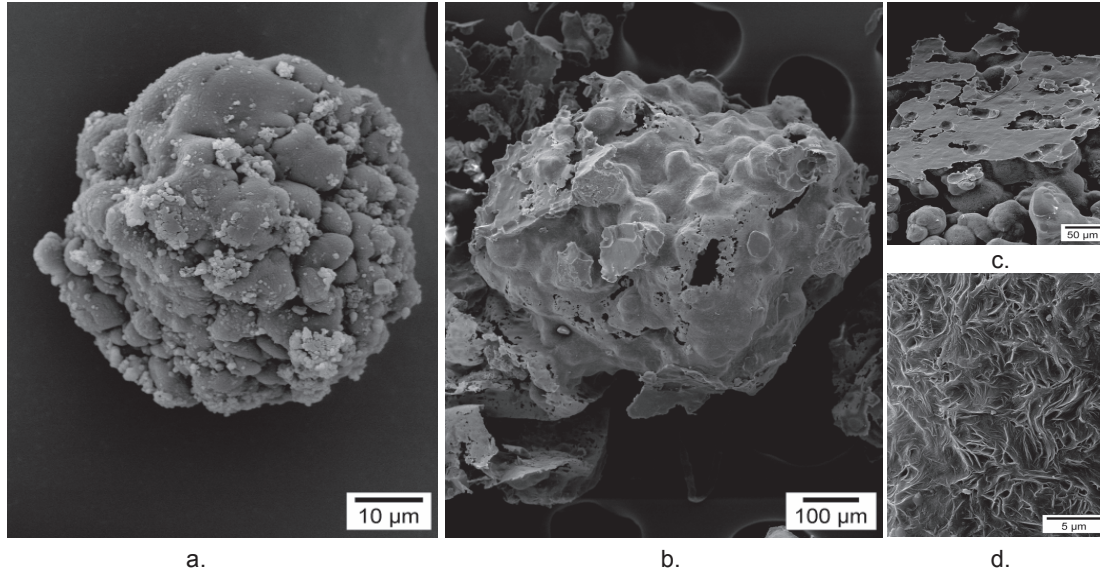


Figure 19: Summary of influence of addition of inert gas to the feed

Confirmation of the benefits coming from the addition of helium to the ethylene feed comes from the observation that in this case a free flowing bed is recovered after the reaction. If no helium was mixed to the feed at least the central part of the bed was a solid block and only a small external annular section was a free flowing powder. This is caused by an excessive temperature in the bed provoking PE melting ( $T_m$  around 130°C) and bed sintering. In figure 20, SEM pictures of polymer particles produced with (a) or without (b–d) addition of helium to the feed are represented. It is clear how the particles are spherical in the case when helium

is used, whereas agglomerated and irregular particles showing signs of polymer melting and cubic NaCl crystals footprint are visible when no helium is used in the gas stream.



**Figure 20: (a) Particle produced with addition of 0.67 helium molar fraction in the feed, (b) particle produced without addition of helium, (c) zoom on melted particle produced without helium addition: the flat surface is the footprint of a side of a NaCl grain, and (d) zoom of (b).**

High gas conductivity has then the merit of improving the heat transfer from solid to gas and avoids particle overheating and thermal runaway of the reaction. Heat-transfer coefficient is in fact proportional to the fluid thermal conductivity and specific heat. Adding helium to the ethylene feed increases both values of these properties.

By using the Wassiljewa-Mason–Saxena method, it is possible to calculate the thermal conductivity of a gas mixture according to the following equation [25]:

$$k_{mix} = \sum_i \frac{k_i y_i}{\sum_j A_{ij} y_j} \quad (11)$$

where  $y_i$  is the molar fraction of the  $i$ -th component of the mixture,  $k_i$  is the thermal conductivity of the pure  $i$ -th component, and  $A_{ij}$  are mixing parameters accounting enthalpic and entropic effects due to intermolecular interactions defined as follows:

$$A_{ij} = \frac{\left[ 1 + \left[ \frac{\eta_i}{\eta_j} \right]^{0.5} \left( \frac{M_j}{M_i} \right)^{0.25} \right]^2}{\left[ 8 \left( 1 + \frac{M_i}{M_j} \right) \right]^{0.5}} \quad (12)$$



where  $\eta_i$  is the viscosity of the pure i-th component and  $M_i$  its molecular weight. The viscosity and thermal conductivity of the pure components are calculated according to the Stiel–Thodos equations [23].

$$k_f = k'_f + \frac{A * 10^{-4} (e^{B\rho_r} + C)}{\left(\frac{Tc^{1/6} M^{1/2}}{Pc^{2/3}}\right) Zc^5} \quad (13)$$

$$A = 2.702 \quad B = 0.535 \quad C = -1$$

where  $\rho_r$  is the reduced density,  $T_c$  the critical temperature,  $P_c$  the critical pressure and  $Z_c$  the critical compressibility factor.  $k'_f$  is the conductivity at room conditions defined as

$$k'_f = 10^{-7} (14.52Tr - 5.14)^{2/3} \left(\frac{Cp}{\lambda}\right) \quad (14)$$

$$\lambda = Tc^{1/6} M^{1/2} \left(\frac{101.325}{Pc}\right)^{2/3}$$

for ethylene and

$$k'_f = 2.5 \frac{\mu C_v}{M} \quad (15)$$

for helium with  $C_v$  being the specific heat at constant volume.

Viscosity is given by

$$\mu_f = 4.6 * 10^{-4} \frac{NM^{1/2} Pc^{2/3}}{Tc^{1/6}} \quad (16)$$

$$N = 0.0001778(4.58Tr - 1.67)^{0.625} \quad \text{for } Tr > 1.5$$

To evaluate if the improvement in heat transfer is really due to a fluid thermal conductivity increase caused by helium, we used the simple Ranz-Marshall equation to calculate an approximate value of  $h$ , the gas solid heat-transfer coefficient, for different gas compositions. We used an average value of 50  $\mu\text{m}$  for the catalyst particle diameter and a gas velocity of 3.0 cm/s. Table 7 shows how the gas properties and the adimensional Nusselt number vary with varying helium mole fraction in the mixture.

**Table 7: Physical properties of the gaseous mixtures (T= 80°C, P<sub>C2</sub>= 6bar)**

$y_{He}$ (molar fraction)	$k_{mix}$ (W/(m*K))	$C_{p_{mix}}$ (J/(Kg*K))	$\eta_{mix}$ (cP)	$Nu$	$h$ (W/(m <sup>2</sup> *K))
0	0.0078	2087	0.0118	2.75	429
0.33	0.026	2294	0.0129	2.42	1262
0.5	0.041	2476	0.0136	2.34	1874
0.66	0.059	2778	0.0145	2.29	2754

Specific heats of pure compounds are calculated using the formulas proposed in [23]. For ethylene the equation is

$$C_p = 0.3338 * 10^5 + 0.9479 * 10^5 \left( \frac{1.596 * 10^3 / T}{\sinh(1.596 * 10^3 / T)} \right) + 0.551 * 10^5 \left( \frac{740.8 / T}{\cosh(740.8 / T)} \right) \quad (17)$$

while for helium is

$$C_p = \frac{0.2079 * 10^5}{M} \quad (18)$$

Density and specific heat of the mixture are calculated using the ideal gas mixing rule. Viscosity of gaseous mixture is calculated with the same mixing rule used for thermal conductivity.

It is clear that helium addition to the feed increases mainly the thermal conductivity of the mixture and the heat transfer coefficient. For example, adding 3 bars of helium to the ethylene feed increases by a factor of 3 the heat-transfer coefficient. In addition, the increase of the specific heat of the gaseous mixture and of the mass flow rate of the gas phase provoked by an addition of helium in the feed (increased total pressure) leads to an augmentation of the quantity of heat evacuated from the solid phase by convection as is expressed in Equation 8.

### 2.2.2. Influence of gas velocity

It is known that one of the most influent parameters determining heat transfer in a packed bed is the relative velocity between the solid particles and the flowing fluid. Our setup has the possibility to work under a wide range of linear velocities that can be controlled and measured. This is one of the biggest improvements respect to previous works related to the

study of the growth of polymer particles in gas phase reactions (think of the videomicroscopy works by Weickert [26], Fink [27] and Hamilton [28]). In an earlier work Olalla et al [6] used this reactor to show how the heat transfer rate depends on the gas flow rate and affects the productivity of the catalyst. The authors measured an increase in the outlet gas temperature and a decrease in the reaction yield if the gas flow rate was increased. They came to the conclusion that a higher flow rate was responsible for a higher heat transfer coefficient and a better indication of the average particle temperature. Although this conclusion is of course acceptable, their work dealt with very low gas velocities. They used flow rates of 5, 8 and 16 mL/s at room conditions corresponding to linear gas velocity values between 0.4 and 1.3 cm/s in the reactor. It is more interesting to characterize the heat transfer in a much wide range of velocities, especially values that are closer to industrial conditions. In this sense we performed a number of experiments varying the flow rate of the gas on a bed of coarse NaCl particles (250–500  $\mu\text{m}$ ). The reactions were conducted for 75 s at a monomer relative partial pressure of 6 bars with eventual addition of 3 bars of helium and at 80°C.

Two series of experiments with varying gas velocity are presented in this section: one series (A) corresponding to poor heat transfer conditions (low gas thermal conductivity) and one (B) corresponding to improved heat transfer conditions (higher gas conductivity by helium addition). It is interesting to study the effect of the relative solid gas velocity for both experimental conditions on the thermal behavior of our packed bed.

The results of the runs in series A show that increasing the gas velocity through the bed up to about 6 cm/s leads to a higher outlet gas temperature (Figure 21) and to slightly lower yields (Figure 22). Beyond 6 cm/s, the maximum temperature (still at 75 s) of the outlet gas decreases then levels off. This implies that, at least in the range of velocity considered here, at low velocities the particles overheat and the gas–solid heat-transfer coefficient is too low to remove all the heat. As the velocity increases, the heat-transfer coefficient obviously increases as well. It appears that as  $h$  increases, the particles overheat less and this leads to a drop in the temperature of the polymerizing particles and thus the gas temperature.

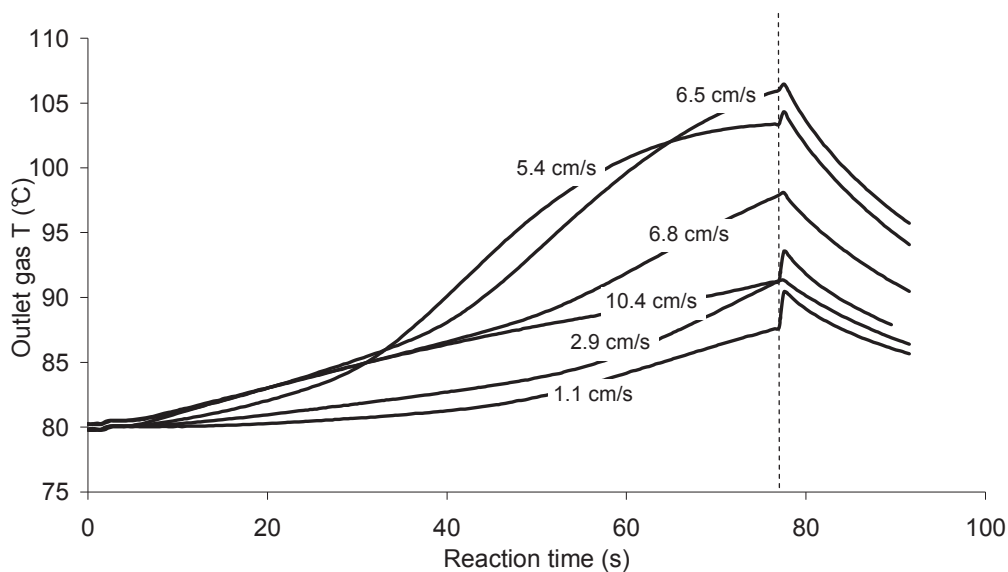


**Figure 21: Outlet gas temperature profiles for different velocities; pure ethylene.**

As these reactions are exothermic, lower temperature means slower rate. The lower rate gives lower yields and less heat being generated. This further suggests that the gas temperature at the outlet begins to approach that of the surface of the particles in the bed at a sufficiently high flow rate through the bed. In other words by maintaining an appropriately high flow rate, we can get an estimate of the actual surface temperature of the particles and therefore begin to quantify the relationship between the reaction rate and the temperature of the nascent particles.

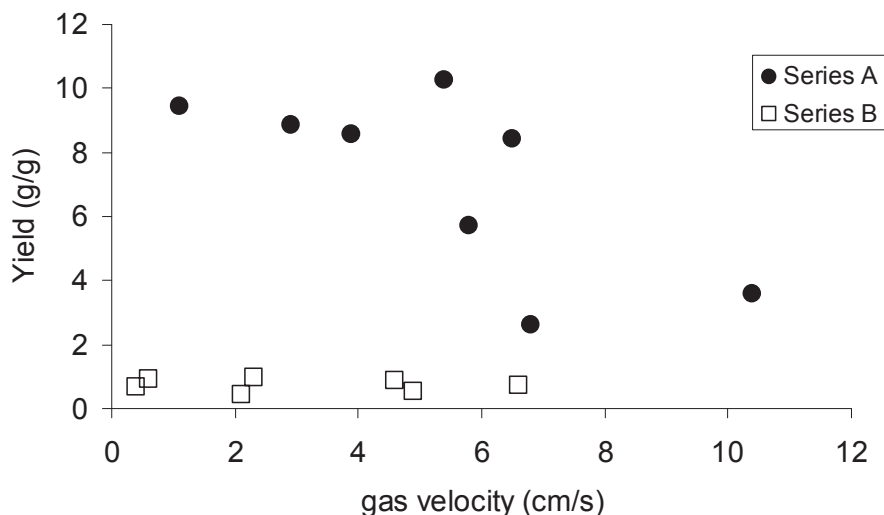


**Figure 22: Influence of gas velocity on yield; pure ethylene (series A) or with 33 mol % helium (series B).**

Before starting to discuss the results obtained with helium, it should be noticed from Figure 22 how the yield corresponding to a gas velocity of 3 cm/s is around 9 g/g. If one compares the values presented in figure 18 he can see that the yield there, obtained under the same gas velocity, is of 6.7 g/g. The difference between the two experiments is the catalyst mass: 15

mg have been used in reactions presented in Figure 22 (series A) while 30 mg have been used previously. As we will see later, the good functioning of our reactor depends not only on the amount of heat removed (controllable by varying the operating parameters) but also on the amount of heat generated which is determined by the quantity of catalyst present in the bed. From Figure 23, where yields of reaction conducted at 80°C, 6 bars of ethylene and a gas velocity of 3 cm/s are presented, one can see that yield decreases as the catalyst mass increases (at least up to 40 mg of catalyst). The phenomena can be explained by the fact that if too much heat is generated, the average particle temperature (at least in hottest reactor zone) can reach values high enough to melt the formed polymer and then cause catalyst deactivation. Reactions conducted for 75s with a catalyst quantity higher than 30 mg resulted in a partial or total agglomeration of the fixed bed and negligible dependence of the yield on the catalyst mass. The NaCl crystals were sticking each other due to the softened (or melted) polymer layer between them. It is possible that using more than 30 mg of catalyst causes the deactivation of the hottest part of the packed bed by thermal reasons and thus levels off the productivity of the reactor.

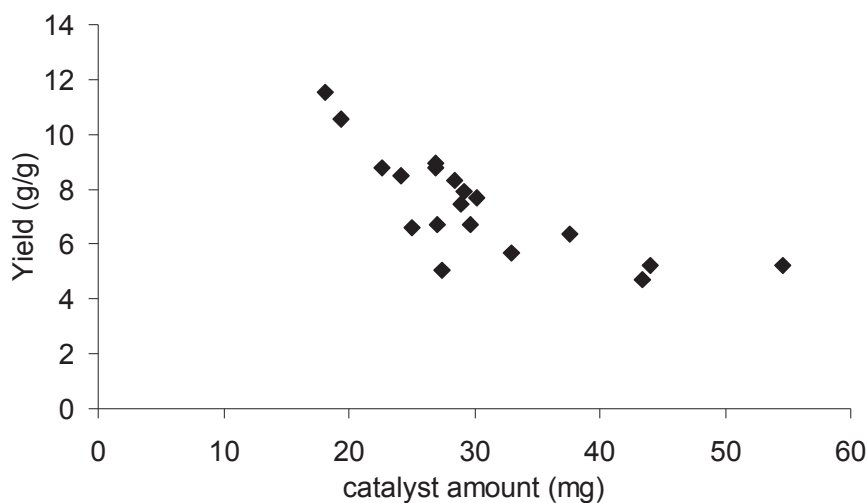


Figure 23: Influence of catalyst loading on yield

It would then be logical, from a first sight, to work with the lowest possible amount of catalyst. Nevertheless it should be kept in mind that we want to recover enough polymer to perform all the analysis that are needed. That's where the interest of a deep heat transfer study comes out: if the heat removal is optimized, then the catalyst amount can be increased to get a satisfying quantity of polymer without too many consequences. As we will see in the following chapter, the quantity of heat generated has an influence also on the properties of the produced polymer.

Going back to the analysis of the effect of the gas flow rate on heat transfer we see that changing the relative gas–particle velocities in the presence of He (series B) leads to slightly different conclusions from what has been explained for series A. As we saw above, using a carrier gas with a high thermal conductivity can itself help to avoid hotspots and thermal runaway. The combination of this with an increased flow rate has the effect of reducing the overheating of the particles and lowering the difference between the gas and the solid surface temperatures. Increasing the gas velocity provokes an increased outlet gas temperature (Figure 24), whereas yield stays constant (Figure 22) at very low values. This is clearly an indication that higher quantities of heat are transferred to the gas flowing with an increased velocity.

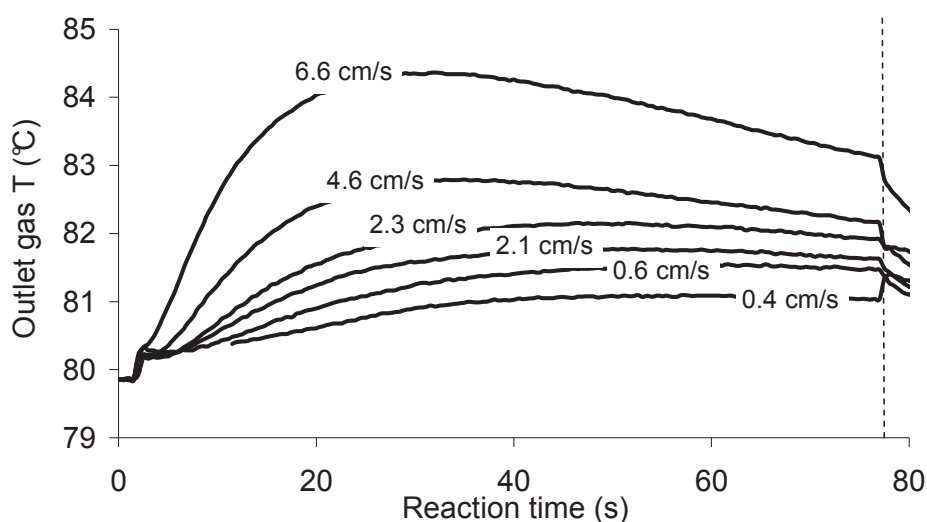


Figure 24: Outlet gas temperature profiles for different velocities; 33 mol % He.

Comparing the shapes of the temperature profiles of Figures 21 and 24 it can also be seen that when no helium is added to the feed the maximum temperature is reached at the end of the reaction (75s). In case of high gas conductivity as the gas flow rate increases the maximum temperature at the outlet is observed earlier and earlier in the experiment. An increase in the linear gas velocity is then responsible for a faster heat transfer to the outlet thermocouple.

The effects of gas velocity and conductivity on heat removal can be easily quantified by defining a heat removal “efficiency” as the ratio between the heat removed from the gas and the heat generated during an experiment. The heat generated is calculated according to equation 10 where the yield and the catalyst mass are measured and the reaction enthalpy is known from literature. The heat transferred to the gas is calculated with equation 8 where  $Q$ ,  $T_{g,out}$  and  $T_{g,in}$  are measured and  $\rho_f$  and  $C_{p_f}$  calculated. From Figure 25 it can be seen how

working with bad conditions leads to a very poor heat removal. When using gas velocities up to 4 cm/s (no matter the gas composition), less than 10% of the heat produced is removed by the fluid. It is also clear that helium increases the quantity of heat transferred to the gas as does an increase in the gas velocity.

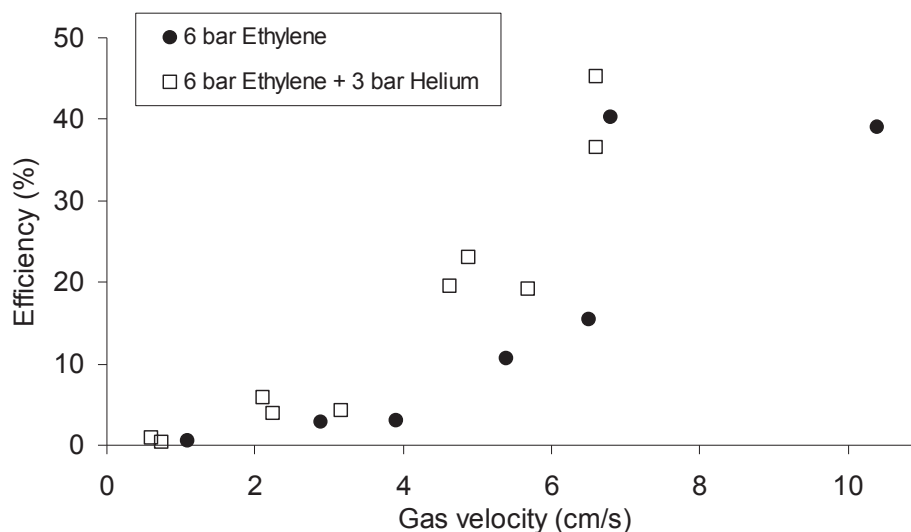


Figure 25: Heat removal efficiency as a function of gas velocity and conductivity

It is important to underline that the gas conductivity is an influent term for heat transfer only if conduction is responsible for a relevant contribution. At high flow rates (that is when convection is the dominant mechanism for heat transfer) addition of helium to the flowing feed of monomers does not improve drastically the situation. These considerations are confirmed from the following graph, where the ratios between the efficiency in absence and in presence of helium are calculated for increasing gas velocities. These values come from a fit of the two sets of data presented in Figure 25.

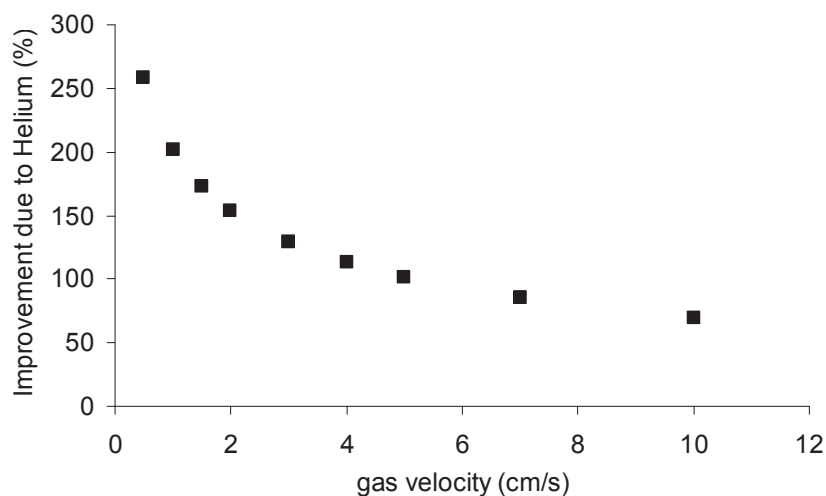


Figure 26: Influence of gas conductivity on heat removal as function of gas velocity

Simulations using a simple model for the reactor allow us to estimate qualitatively the influence of the gas velocity and composition on heat removal from the solid particles and supporting the experimental observations shown above. The quantity of heat accumulated into the solid phase ( $Q_{acc}$ ) is calculated according to Equation 9. The solid phase is composed by the catalyst, the produced polymer, the inert seedbed, and the outlet steel frit (which has an estimated mass of 5 g) and is expressed by

$$Q_{acc} = \sum_i (m_i C_{p_i}) \Delta T \quad (19)$$

The outlet frit has to be put into the heat balance because the point at which the outlet gas temperature is measured is located beyond the frit itself. All the solids cited above are assumed to be under thermal equilibrium among each other. Calculation of  $Q_{acc}$  for different reaction conditions allows estimating the solid temperature increase and its dependence on gas velocity and composition. Remind that Equation 19 is not differential so that only an “integral” increase in the solid temperature can be calculated and not its time dependent profile. In addition we assumed the reactor to be adiabatic thus the term  $Q_{loss}$  reduces to 0. The assumptions of the reactor being adiabatic and the solids being under thermal equilibrium are clearly not fully true but justified. They allow in fact a tremendous simplification of the calculations without affecting the trends of the results. The goal of these calculations being to obtain order of magnitude estimates of temperature changes supporting experimental observations shows that these assumptions are fully acceptable at this point.

The series of experiments A and B presented previously were “simulated”. Constant catalyst activity has been supposed to perform the calculations. This is not so far from reality for these reaction conditions as can be seen from the measured linearity between yield and reaction time presented in Figure 27.



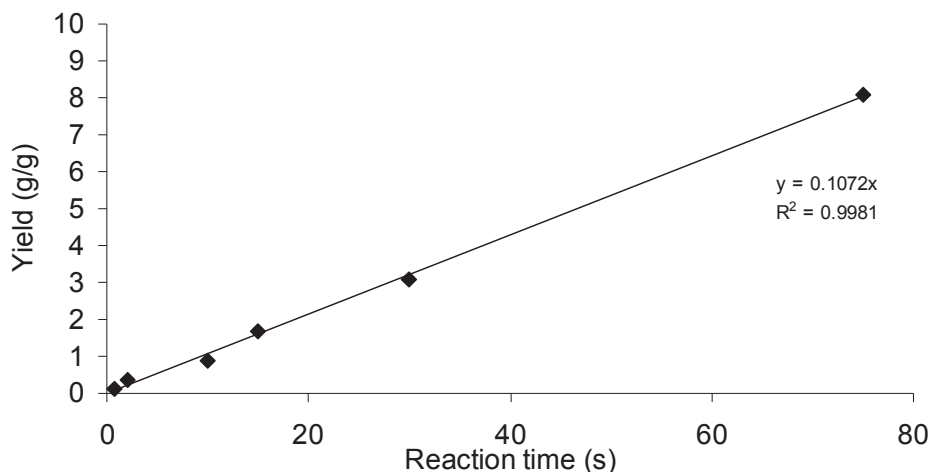


**Figure 27: Yield evolution with reaction time for reactions conducted at 80°C, 6 bar of ethylene, 3 cm/s gas velocity and using NaCl coarse as seedbed**

Figure 28 shows the calculated temperature differences between the solid and the gas phase for different gas velocities. It can be seen how the increase of solid temperature can reach very high values leading to polymer melting (as seen in experiments) if no helium is added to the feed.

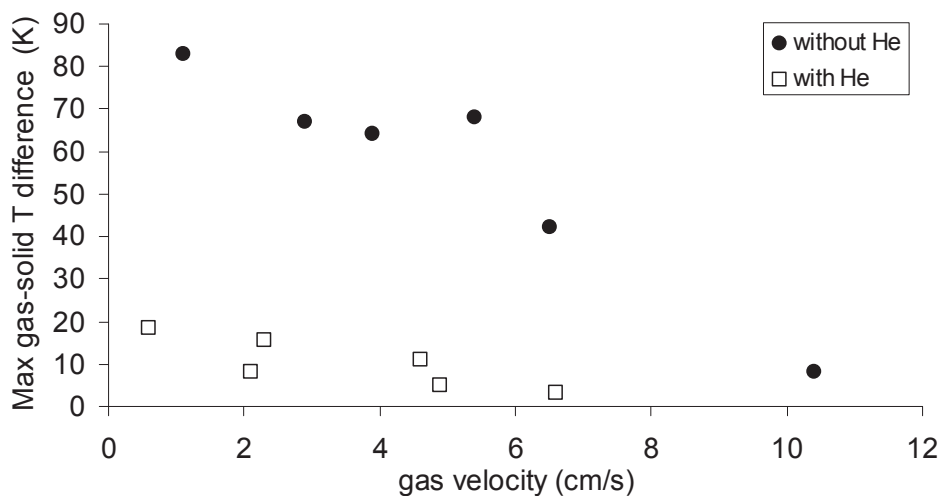


**Figure 28: Solid bed temperature increase as function of gas velocity and composition.**

Taken into account that gas temperatures can reach easily 100°C, values of 180°C has been estimated for the solid phase at low gas velocity. Only with gas velocities higher than 10 cm/s the solid heating is limited and melting is reduced. When helium is present in the gas feed (series B), the calculated solid temperature increase shows much lower values so that melting and thermal runaway are avoided as confirmed by experimental observations. It is clear that increasing the gas velocity (no matter if helium is present or not in the feed) leads to an

improvement in the heat transfer from the solid to the gas. The particle temperature is closer and closer to the measured outlet gas temperature.

### 2.2.3. Influence of inert seedbed properties

In this section, we will investigate the role of the bed packing on the evolution of the outlet gas phase temperature.

The influence of the solid phase properties on the heat transfer in a packed bed is a well known topic that has been studied for longtime. Implementation of these parameters in the mass and energy balance of the reacting bed can be easily found in literature [15, 22, 29-31]. From these studies, we can learn that decreasing the particle size improves the heat transfer from solid to gas because of the increase of the heat-transfer coefficient, whereas the solid thermal conductivity has a limited role in the overall rate of heat transfer in the bed.

Our case is slightly different from what is discussed in literature because the concentration of reacting particles is relatively low here with respect to what one might encounter in a typical industrial process. Defining the volumetric dilution as volume of catalyst over the total volume of the solids into the bed, we can calculate values of dilution varying from 0.04 to 0.11 according to the inert used. We can also neglect the impact of polymer production here as the expansion of the bed for the most productive run shown above is 11%. This means that we can approximately represent our bed as a fixed bed heat exchanger with a heat source distributed homogeneously through the bed. Different works are presented in literature dealing with the effect of catalyst dilution on the performances of a fixed bed. They all agree in saying that dilution of catalyst is a great method to improve the heat-transfer characteristics of the bed and to reduce the amount of the catalyst needed in the process. Nevertheless the conclusions reached by different authors on the influence of dilution on reactor performance are quite different: some say dilution is responsible for a lower conversion [32, 33], other say that dilution is responsible for a more effective use of the catalyst bed [34, 35]. A strong impact of heat transfer limitation into the packed bed can be the reason for these discrepancies [34]. The importance of the optimization of the catalyst dilution is nevertheless confirmed by the opacity of these results.

Varying the inert seedbed particle size will lead to differences in the flow field around the catalyst particles. Channeling or even by pass of the reacting particle by the gas is known to be deleterious for the bed performance (this is true also for fluidized beds [36]) because of the

incomplete utilization of the reacting volume. This can happen in particular if an inert solid with too high particle diameter is used when some catalyst particles might be placed “behind” (from the flowing gas point of view) an inert one. In this case, the reacting particle is shielded by the bigger one and its productivity is decreased.

To study the effect of the particle seedbed properties on heat transfer in start up of olefin polymerization in a packed bed, different reactions have been performed using coarse NaCl, small NaCl or silica as inert diluent. Small NaCl has been used because of the advantages of the separation of the formed polymer from the inert diluent by simply washing with water. Experiments using silica as seedbed have been done only to reproduce the conditions used in the previously published works [5, 6] as using this type of inert diluent will result in difficult and tedious separation of the polymer particles from the inert ones and impossible identification of catalyst particles from seedbed particles in SEM pictures. Results and reaction conditions are shown in Table 8. As usual these reactions have been conducted at 80°C, with 6 bars of ethylene and 30 mg of catalyst. It should be noted that the gas velocities are slightly different if small NaCl is used as inert. All the experiments have been performed at the same gas volumetric flow rate (controllable parameter). The difference in gas velocity comes from the fact that the porosity of a bed of fine NaCl is much higher than that of coarse NaCl or silica (0.40) because of the irregular and slightly agglomerated structure of the synthesized crystals.

Table 8: Influence of inert diluent on reaction performance

<i>Exp</i>	<i>Bed type</i>	<i>Bed size</i> ( $\mu\text{m}$ )	<i>Yield</i> (g/g)	<i>Gas velocity</i> (cm/s)	<i>Gas max</i> $\Delta T$ (K)	<i>Time of gas max</i> $\Delta T$ (s)	<i>Efficiency</i> (%)
SFG100	NaCl coarse	250-500	8.1	3.0	25	75	6
SFG99	NaCl small	10-30	3.6	2.0	23	35	10
SFG105	Silica	60	2.9	3.0	15	35	12

Decreasing the seedbed particle size leads to an improved heat transfer in the bed: the gas peak temperature does not decrease considerably with seedbed particle diameter while the yield is reduced by a factor of 2 (Table 8). Smaller particles have a higher specific surface and more contact points so that convection to the fluid and especially conduction from catalyst to

seedbed is improved. The last column of Table 8 tells us that the improvement in the heat transferred to the gas is not significant, but appears to be real. Varying the seedbed particle diameter has in fact only a minor effect on the gas phase. Increasing the mean conduction of the solid phase has as consequence to accelerate the system dynamic response for heat transfer to the gas (as confirmed by temperature profiles of Figure 29).

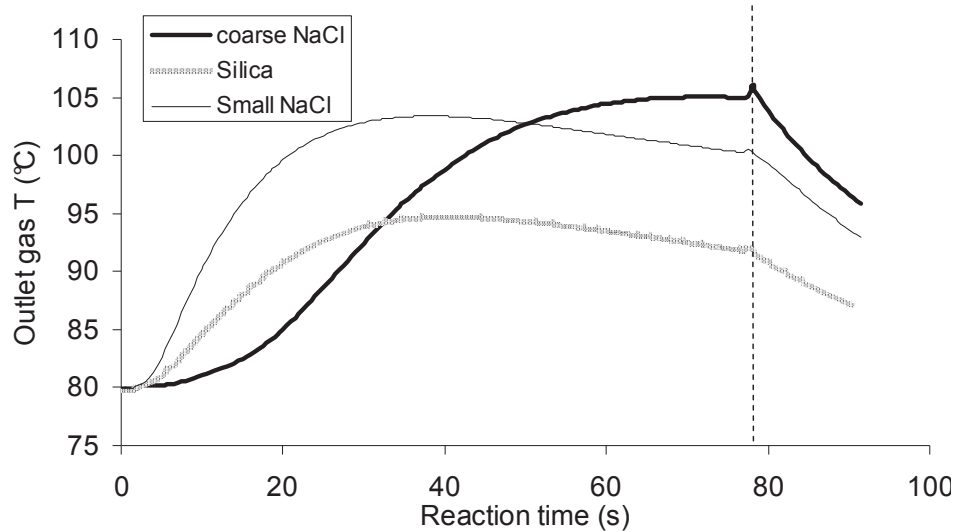


Figure 29: Outlet gas T profile for different inert diluents.

#### 2.2.4. Towards the optimum heat transfer conditions

The three parameters discussed in the previous paragraphs can be varied together to find the optimum conditions to have a tool capable of performing highly exothermic transient reactions without affecting the real kinetics or the particle morphology by maximization of heat removal by the gas phase. To summarize, we have seen what are the independent effects of each one of the three variables:

- Gas conductivity ( $k_f$ ): if increased, it improves heat transfer to the gas at low gas velocities avoiding catalyst overheating and thermal runaway.
- Gas velocity ( $u$ ): if increased, it increases consistently the heat transfer to the gas and the dynamic response of the system.
- Seedbed particle size ( $D_p$ ): if decreased, it increases mainly the bed average conductivity and the system dynamic response.

A judicious choice of the three parameters listed above leads to a significant improvement in the system performance as can be seen in Table 9.

Table 9: Optimization of heat transfer (80°C, 30mg catalyst, 6 bar ethylene, 75s)

<i>Exp</i>	<i>NaCl</i> ( $\mu\text{m}$ )	<i>Helium</i> ( <i>bar</i> )	<i>Gas</i> <i>velocity</i> ( <i>cm/s</i> )	<i>Gas max</i> $\Delta T$ (K)	<i>Time of</i> <i>gas max</i> $\Delta T$ (s)	<i>Efficiency</i> (%)	<i>Yield</i> (g/g)
SFG100	250-500	0	3.0	25	75	6	8.1
SFG99	10-30	0	2.0	23	35	10	3.6
SFG93	250-500	3	2.3	2.3	45	8	1.0
SFG107	10-30	3	2.8	17	15	33	1.3

A gas velocity of 2.8 cm/s coupled with the presence of 33% molar helium in the feed and a small bed particle diameter (exp SFG107) is sufficient to avoid thermal runaway (see yield column in Table 9) for our catalyst at 6 bars of ethylene and 80°C. By analyzing figure 30 we can see two main important things: addition of helium avoids thermal runaway, as confirmed by the final temperature reached by the gas, and using small seedbed particle size is responsible for an early apparition of temperature overshoot that was not visible when coarse NaCl was used. This confirms that the reactor is now operating in a controlled way. It has to be said in fact (anticipating the following results) that catalyst activity in gas phase ethylene polymerization is 10 times higher at the very beginning of the reaction (first 2–5 s) than later. The rate of heat production follows this trend (Figure 31) so that a high gas temperature in the first seconds is to be expected with satisfactory heat transfer conditions. Operating with a gas velocity of 5.5 cm/s, addition of 33 molar percent of helium and fine NaCl as seedbed allows to remove 90% of the produced heat after a reaction of 75 s. Heat removal operating with the initial non-optimized conditions (SFG100) was of only 6%. Note that after the maximum, the outlet gas temperature falls back to the same values reached when coarse NaCl is used as seedbed.

In addition it can be seen that an increase in the gas velocity leads to a faster heat transfer dynamics and an earlier apparition of the maximum, while yield remains constant. This corresponds to an increased quantity of heat transferred to the gas even in the first reaction seconds.

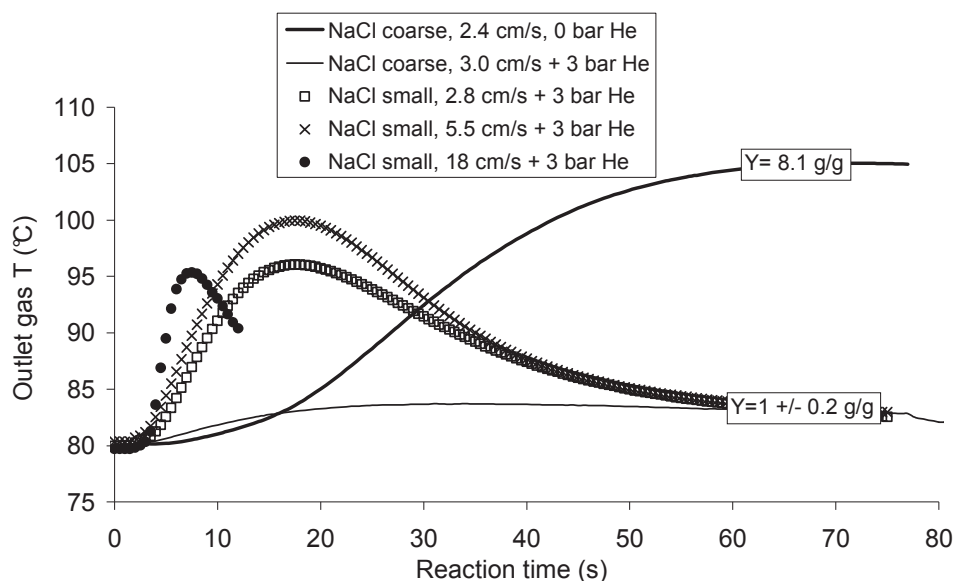


Figure 30: Outlet gas temperature and yield for different reaction conditions (80°C, 30 mg catalyst, 75s)

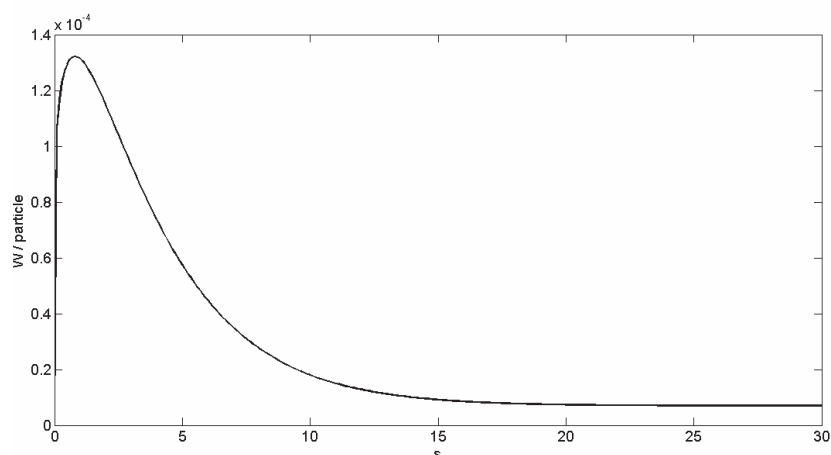
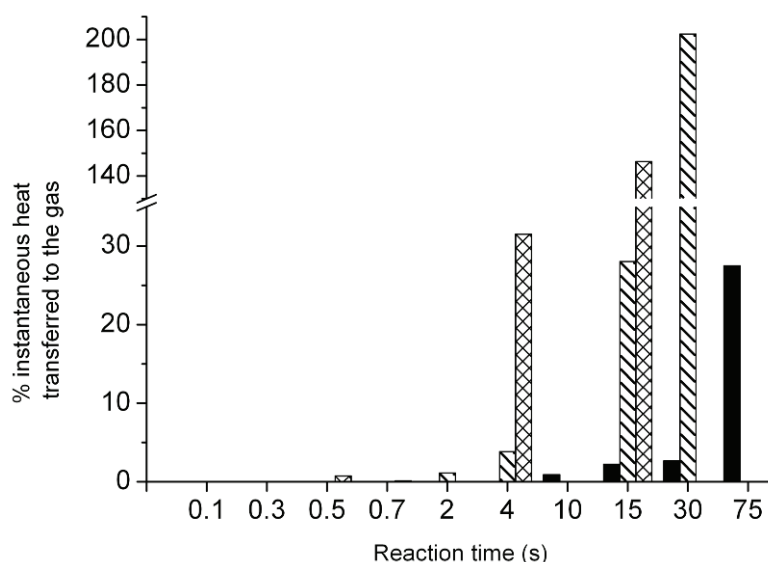


Figure 31: Heat generation as function of reaction time calculated from experimental results

In any case it is not possible to observe an instantaneous appearance of the temperature peak of the outlet gas stream in this kind of reactor. This is because the heat produced at the active sites must diffuse through the catalytic particle to reach the surface (this is very rapid) and then it is evacuated either by leading to a local increase in the temperature of the neighboring bed particles or by being convected out of the reactor in the gas phase. It is likely that there is going to be a small but unavoidable time lag (determined mainly by the outlet frit) in establishing a high outlet gas temperature associated with heating of the bed material.

In Figure 32, the ratio of the instantaneous heat (power) removed by the gas to the power generated is plotted for experiments conducted at different reaction times. Each bar on the graph corresponds then to an experiment. Three series of experiments are shown: coarse NaCl as seedbed, no helium addition, 3 cm/s gas velocity (black bars); fine NaCl as seedbed, addition of 33 molar percent of helium to the feed, 5.5 cm/s gas velocity (stripy bar); and fine

NaCl as seedbed, addition of 33 molar percent of helium to the feed, 18 cm/s gas velocity (crossed bars). It is noticeable from this figure how for very short times ( $< 2$  s), no matter the reaction conditions, very little heat is absorbed by the gas phase. This supports the conclusions explained above.



**Figure 32: Relative power transferred to the gas at different reaction times for different working conditions**

In addition it is easy to see how an improvement in heat transfer conditions increases not only the quantity of heat removed by the gas at “long” reaction times (30–75 s) but also allows a quicker removal thus lowering the probability for thermal runaway or for hotspots formation in the early instants of the polymerization. An instantaneous heat removal higher than 100% means that the flowing gas is capable both of evacuating all the heat produced and of cooling down the reacting bed. The sooner the instantaneous heat removal reaches these values, the sooner the bed starts to cool down and the less the probability to have bed overheating or melting and hotspots. Working with the original conditions (black bars) leads to an instantaneous heat removal of only 28% after 75 s of reaction: the bed is still heating up and is probably completely melted down. Working with the best conditions for heat transfer (crossed bars) leads to a heat removal of 150% after only 15 s: the bed heats up because of the produced heat reaching a maximum temperature between 4 and 15 s and then rapidly cools down. The shortness of the period during which the bed is heating up decreases the probability to have reached too high temperatures. These two opposite situations explain the sensitivity of this reacting system (catalyst and reactor) to heat transfer and its influence on catalyst activity. Finally, a percentage of heat transferred to the gas reaching high values very soon can be translated into a fast increase of gas temperature and an early apparition of the

maximum. The outlet gas temperature profile is then closer to the heat rate production profile (Figure 31) and, as a consequence, particle surface and gas temperatures are close each other all along the duration of the reaction.

All the work presented here allows to choose the reaction conditions capable of satisfying the objectives presented above. These are:

- Use fine NaCl as seedbed
- Work with gas velocities of 15-20 cm/s
- Add Helium to the monomer feed

The importance to have a correct heat removal and its impact on the activity of the catalyst even for very short times is easily understood by looking at the following graph, where activity profile of the same catalyst used under the best and the worst reaction conditions (in terms of heat transfer) is plotted as a function of time. Each point on the graph represents an experiment stopped at a predetermined reaction time. It is easy to notice how the activity profile can vary just by changing the reaction conditions

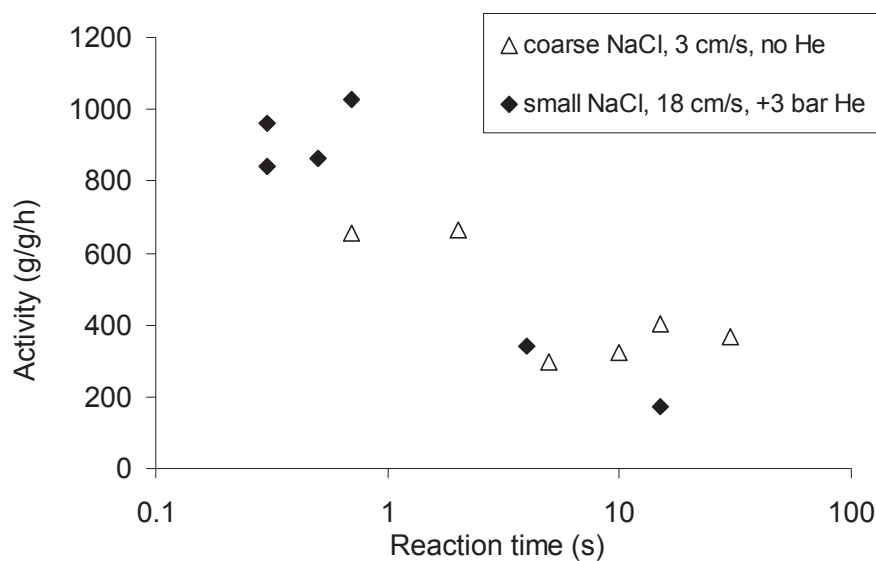


Figure 33: Activity profile for different heat transfer regimes

### 2.2.5. Influence of heat generation (catalyst amount).

The catalyst mass is a last important parameter influencing heat transfer. Its role has been exposed in Figure 23 for bad heat transfer conditions. A simple sensitivity study has been conducted using the optimum reaction conditions selected here with the aim to determine which is the catalyst quantity that allows to minimize heat generation without affecting the



reaction rate. Reactions of 30s have been performed at 80°C. All the reactions showed outlet gas phase temperature profiles similar to the dotted curve of figure 30 but the values of the maximum reached temperature and of the yield were dependent on the catalyst mass as shown by the following table.

**Table 10: Influence of the mass of catalyst on yield and gas heating**

<i>Exp</i>	<i>m cat (mg)</i>	<i>Max T (°C)</i>	<i>Yield (g/g)</i>
SFG327	47	93	1.12
SFG328	25.2	90	1.11
SFG329	14.2	82	0.8
SFG330	4.5	80.7	0.0

The activity is not dependent on the catalyst mass for values down to 25mg. With lower catalyst quantities the activity decreases probably because the quantity of catalyst deactivated by impurities becomes important and no additional scavenger or activator is present in the packed bed. If only 5 mg are used no activity at all is measured. Catalyst mass between 25 and 35 mg will then be used in the following. For reaction times lower than 2s the problem of having enough polymer will strike back if these amounts will be used. The solution is to increase the mass of catalyst as the reaction time decreases. Amounts in the order of 70-80mg will then be used for the shortest reactions (0.1 to 0.7 s).

### 3. Validation and modelling

#### 3.1. *Temperature inside the bed*

We have seen by a simple calculation how the balance between the quantity of heat removed from the bed and the amount of heat generated by the reaction depends on the working conditions. It would be nice to have some more precise indication on the temperature evolution inside the reacting bed. Let us remind that the outlet gas phase temperature is measured after the outlet frit, and not directly at the bed end. The presence of the frit can induce some differences between the measured and the actual bed temperature. This is confirmed by the fact that, as already exposed in Figure 14, the CO<sub>2</sub>, flowing after the reaction has ended, heats up a bit more than the ethylene stream during the reaction. This

happens because the flow of a non-reacting gas allows to remove the heat remaining inside the reactor. In Figure 34 one can see that, working under bad heat transfer conditions, the difference between the temperature of ethylene at the reaction end and the maximum temperature reached by the CO<sub>2</sub> can be as high as 30°C!

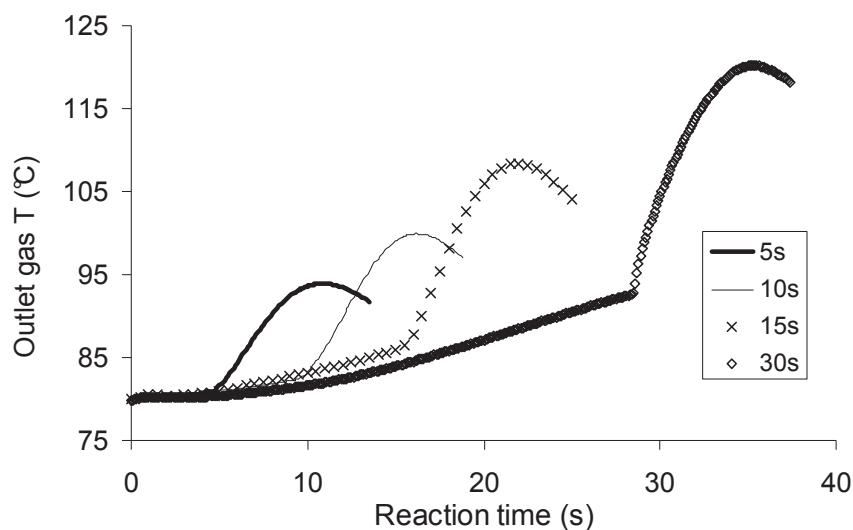


**Figure 34: Outlet gas temperature profile for reaction conducted at 80°C, 6 bar C<sub>2</sub> and different time; reaction starts at 0s and ends at the curve discontinuity. The second part of the curve corresponds to CO<sub>2</sub> flowing**

It is interesting to notice that there is a coherence between what observed during the flowing of the CO<sub>2</sub> and Figure 32: the non reacting gas heats up only for reaction times lower than the time needed to reach values of instantaneous heat removal higher than 100%. This means that for these short times there is still a certain amount of heat that has not been transferred to the ethylene (and has not been measured) and that has increased the bed temperature. Such amount of heat can be evacuated only during the stopping phase. This could be source of some differences between the actual bed temperature and the value measured in the outlet gas stream.

To measure more precisely the temperature of the bed we modified one of the four available reactors by introducing a thermocouple from the outlet inside the reactor. Measurements on reactions performed using conditions responsible for bad heat transfer showed that the actual bed temperature is not only quite far from the measured outlet gas phase temperature, but is in fact reaching values responsible for polymer melting! This confirms fully the finding exposed in the previous paragraphs. In Figure 35 it is possible to see the evolution of the bed temperature at depths of 1mm and 5mm. At 5mm (the middle of the bed) the temperature seems to reach a steady value of 120°C. This value will be even higher for bigger depths.

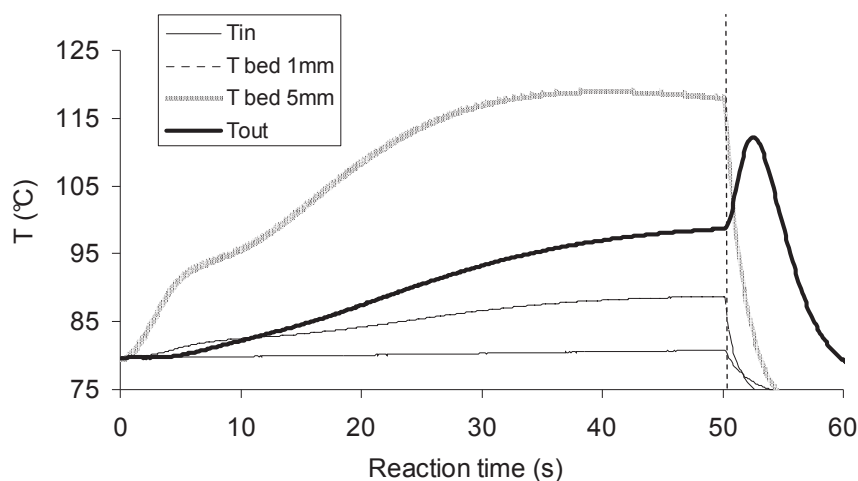


**Figure 35: Temperature profile at inlet, outlet and inside the bed (1 and 5 mm) during reaction conducted under bad heat transfer regime**

The same experiments performed using optimum reaction conditions gives the following results.

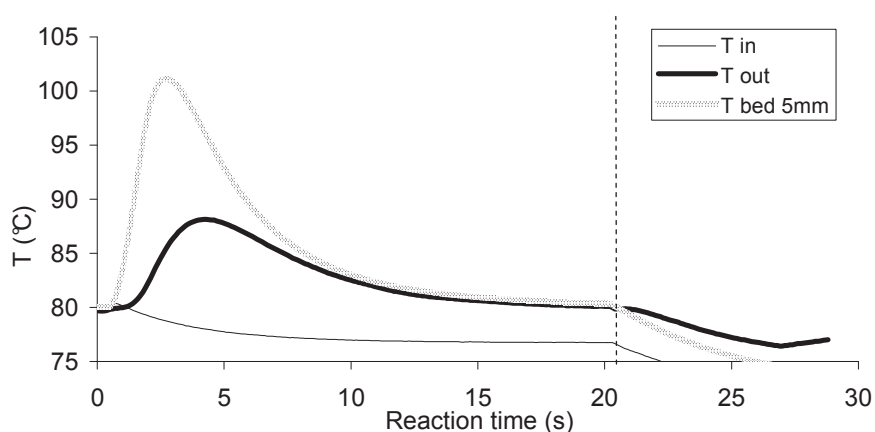


**Figure 36: Temperature profile at inlet, outlet and inside the bed (5 mm) during reaction conducted with optimum conditions**

In this case one can see that temperature overshoot inside the bed lasts only for 2-3 seconds and after that the heat removal is enough to cool down the bed. The critical time when overheating can happen is then greatly reduced. Nevertheless the magnitude of the temperature excursions can be high enough to be responsible for a temporary deviation of the active sites behavior from controlled conditions (variation of  $k_p/k_t$ ) that can result in some perturbation of the MWD of the produced polymers (as it will be seen in the following Chapter). These measurements have been used by a parallel project conducted at the LGPC (Laboratoire de Génie des Procédés Catalytiques) at CPE Lyon aimed to build a calorimetric model of our packed bed reactor. Results coming from extensive simulations and allowing to calculate the temperature profile inside the reactor along the axis and the radius are presented in the following figure.

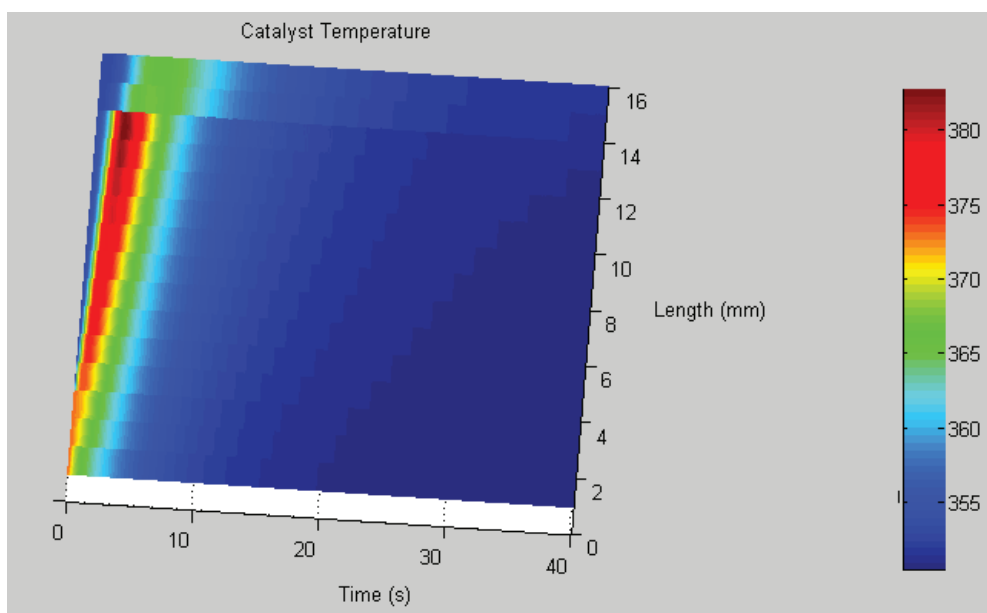


**Figure 37: Evolution of bed temperature with time and position along the reactor axis. The reacting bed is between 3 and 13mm, the rest being the inlet and outlet frits.**

Temperatures higher than 100°C are represented by red and brown colors. As supposed, one can see that the dangerous temperature zone is reached especially near the reactor exit but it lasts 2s at maximum.

### 3.2. Concentration profiles

It is then clear that optimization of heat removal from the gas phase allows to work under controlled conditions. Activity in this case is not falsified by extreme temperature variations that can alter the kinetic constant of the propagation reaction by an Arrhenius effect. At the same time risks of polymer melting or softening are avoided. Once it has been verified that temperature remains below the desired values (this is true except for the very beginning of the reaction, when an overshoot is unavoidable. The point here is to make the temperature decrease as quick as possible) we have to be sure that there are no concentration profiles along the reacting bed. In paragraph 1.1 we reported the requirements that we need to satisfy to work in stopped flow conditions. One of them (introduced by Terano) is that the conversion of the monomer should be always lower than 10%. This allows more or less uniform concentration profile and catalyst activity along the bed.

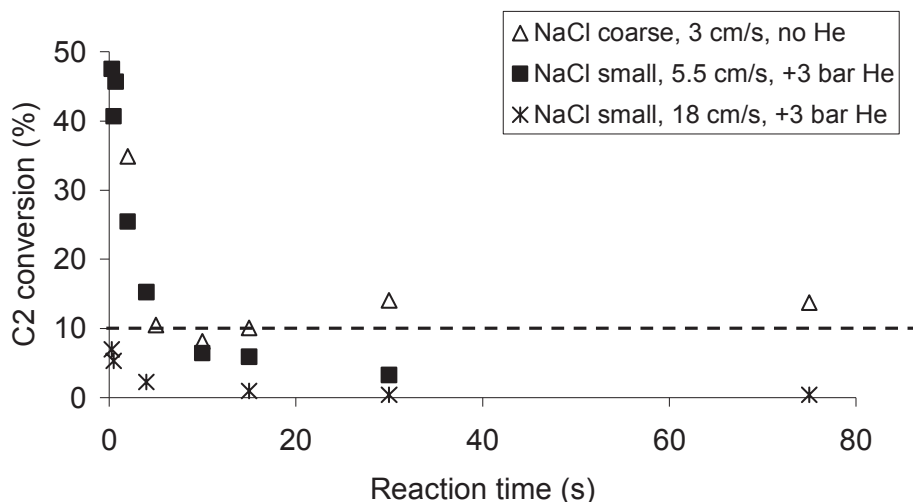


**Figure 38: Conversion of ethylene as function of reaction time**

From the previous figure one can see that this criterion is satisfied for every reaction time only working at the highest gas velocity. With lower gas velocities concentration profiles are expected to be present inside the reactor for the first 2 seconds of reaction. Using the worst possible conditions for heat transfer gives, for every reaction time, conversions that are very close to the limiting value. Nevertheless the heat transfer limitations arising in this case are the main reason for which these conditions should not be used. One solution to reduce conversion would be to reduce the catalyst mass but if this was done, not enough polymer would be available for analysis.

### 3.3. Reactor homogeneity

In order to check if the conclusions explained above lead to homogeneous reaction conditions into the bed we performed a reaction of 30s at 80°C using the conditions responsible for optimum heat removal and we analyzed by thermo gravimetric analysis (TGA) samples taken at different positions in the reactor as shown in figure 39. In this way we will know the polymer mass fraction in each section and compare it to the average in the whole reactor.

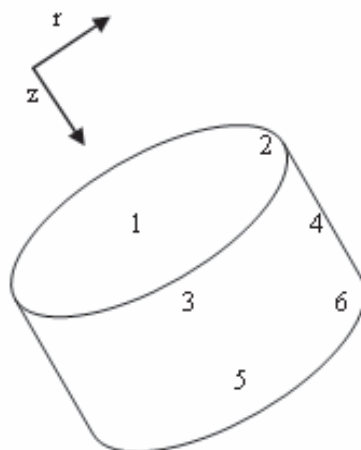


**Figure 39: Sampling zones in the reactor**

The composition of the whole reactor bed and of each zone is presented in the Table 11. These results shows that the PE concentration in the bed increases along the reactor axis and decreases from the center to the wall. This follows the temperature distribution inside the reactor that will be inevitably present at some extent. A maximum difference of 25% in PE content (and activity) can be seen between the zone with the lower PE concentration and the one with higher PE concentration. This value is low enough that we can assume constant activity along  $r$  and  $z$  dimensions.

**Table 11: PE weight fraction in different reactor zones**

<i>Zone</i>	<i>PE (wt %)</i>
Whole	6.5
1	6.74
2	6.44
3	7.26
4	6.81
5	8.08
6	7.52

## 4. Conclusions

In this chapter we have seen how a deep study on the heat transfer of our packed bed stopped flow reactor was needed to gain a complete understanding of the thermal phenomena happening inside the reacting bed and to find the best working conditions in order to avoid the

most important problems that one could find at the gas phase polymerization start-up (polymer melting, hot spots and falsified kinetics).

The optimization has been conducted through a systematic analysis of the equation representing the heat transfer between the reacting particles and the gas phase. This has led us to find the best values of the physical parameters that is possible to vary over a wide range in our setup. These are

- The gas composition
- The gas velocity
- The inert diluent
- The mass of catalyst.

Experimental results have been confirmed by simple calculations and a preliminary version of an accurate model capable of giving the temperature distribution along the two reactor dimensions is available thanks to the collaboration between LCPP and LGPC.

One of the most important objectives reached by this work is to have measurable outlet gas phase temperature as close as possible to the actual particle temperature, or at least to know the relation between them. Direct measurement of the catalyst temperature is very hard to accomplish and knowledge of its value by means of experimental work is still missing in the literature. Nevertheless this is an important information for validation of single particle models.

In the following chapters we will work with the optimum conditions determined here in order to have reliable results on the influence of reaction conditions and catalyst properties on the start-up of the gas phase polymerization in terms of activity and polymer properties.

## 5. References

1. Samson, J.J.C., et al., *Gas-phase polymerization of propylene with a highly active ziegler-natta catalyst*. *AIChE Journal*, 1999. **45**(7): p. 1548-1558.
2. Han-Adebekun, G.C., J.A. Debling, and W.H. Ray, *Polymerization of olefins through heterogeneous catalysis. XVI. Design and control of a laboratory stirred bed copolymerization reactor*. *Journal of Applied Polymer Science*, 1997. **64**(2): p. 373-382.
3. Kumkaew, P., et al., *Gas-phase ethylene polymerization using zirconocene supported on mesoporous molecular sieves*. *Journal of Applied Polymer Science*, 2003. **87**(7): p. 1161-1177.
4. Mori, et al., *Stopped-flow techniques in olefin polymerization*. Vol. 5. 1997, Cambridge, ROYAUME-UNI: Elsevier.
5. Machado, F., et al., *An experimental study on the early stages of gas-phase olefin polymerizations using supported Ziegler–Natta and metallocene catalysts*. *Polymer Engineering & Science*. **51**(2): p. 302-310.
6. Olalla, B., J.-P. Broyer, and T.F.L. McKenna, *Heat Transfer and Nascent Polymerisation of Olefins on Supported Catalysts*. *Macromolecular Symposia*, 2008. **271**(1): p. 1-7.
7. Welborn Jr., H.C., US 4,808,561, Exxon Chemical Patents Inc. , 1989.
8. Takahashi, T., US 5,026,797, Mitsubishi Petrochemical Co., Ltd., 1988.
9. Ribeiro, M.R., A. Deffieux, and M.F. Portela, *Supported Metallocene Complexes for Ethylene and Propylene Polymerizations: Preparation and Activity*. *Industrial & Engineering Chemistry Research*, 1997. **36**(4): p. 1224-1237.
10. Gaschard-Pasquet, V., 1985, PhD Thesis, Universite Claude-Bernard-LYON 1.
11. Tioni, E., et al., *Heat Transfer in Gas Phase Olefin Polymerisation*. *Macromolecular Symposia*, 2009. **285**(1): p. 58-63.
12. Tioni, E., et al. *Packed-bed reactor for short time gas phase olefin polymerization: Heat transfer study and reactor optimization*. *AIChE Journal*, 10.1002/aic.12576.
13. Jessup, R., *The heat and free energy of polymerization of ethylene*. *J. Chem. Phys.* , 1948. **16**(7.): p. 661-664.
14. Dixon, A.G., *An improved equation for the overall heat transfer coefficient in packed beds*. *Chemical Engineering and Processing: Process Intensification*, 1996. **35**(5): p. 323-331.



15. Duarte, S.I.P., O.A. Ferretti, and N.O. Lemcoff, *A heterogeneous one-dimensional model for non-adiabatic fixed bed catalytic reactors*. Chemical Engineering Science, 1984. **39**(6): p. 1025-1031.
16. Wen, D. and Y. Ding, *Heat transfer of gas flow through a packed bed*. Chemical Engineering Science, 2006. **61**(11): p. 3532-3542.
17. Dhingra, S.C., D.J. Gunn, and P.V. Narayanan, *The analysis of heat transfer in fixed beds of particles at low and intermediate Reynolds numbers*. International Journal of Heat and Mass Transfer, 1984. **27**(12): p. 2377-2385.
18. Dixon, A.G. and D.L. Cresswell, *Theoretical prediction of effective heat transfer parameters in packed beds*. AIChE Journal, 1979. **25**(4): p. 663-676.
19. Gunn, D.J. and P.V. Narayanan, *Particle-fluid heat transfer and dispersion in fluidised beds*. Chemical Engineering Science, 1981. **36**(12): p. 1985-1995.
20. Mears, D.E., *Diagnostic criteria for heat transport limitations in fixed bed reactors*. Journal of Catalysis, 1971. **20**(2): p. 127-131.
21. Shent, J., S. Kaguei, and N. Wakao, *Measurements of particle-to-gas heat transfer coefficients from one-shot thermal responses in packed beds*. Chemical Engineering Science, 1981. **36**(8): p. 1283-1286.
22. Wakao, N., *Particle-to-fluid transfer coefficients and fluid diffusivities at low flow rate in packed beds*. Chemical Engineering Science, 1976. **31**(12): p. 1115-1122.
23. Perry, R.H. and D.W. Green, *Perry's Chemical Engineers' Handbook (7th Edition)*. 1997, McGraw-Hill.
24. Kittilsen, P., et al., *The interaction between mass transfer effects and morphology in heterogeneous olefin polymerization*. Chemical Engineering Science, 2001. **56**(13): p. 4015-4028.
25. Reid, R.C., J.M. Prausnitz, and B.E. Poling, *The properties of gases and liquids*. 1987. Medium: X; Size: Pages: 741.
26. Pater, J.T.M., G. Weickert, and v.W.P.M. Swaaij, *Optical and infrared imaging of growing polyolefin particles*. AIChE Journal, 2003. **49**: p. 450 - 464.
27. Ferrari, D. and G. Fink, *Video Microscopy for the Investigation of Gas Phase Copolymerization*. Macromolecular Materials and Engineering, 2005. **290**(11): p. 1125-1136.
28. Hamilton, P., D.R. Hill, and D. Luss, *Optical and infrared study of individual reacting metallocene catalyst particles*. AIChE Journal, 2008. **54**(4): p. 1054-1063.
29. Andrigo, P., R. Bagatin, and G. Pagani, *Fixed bed reactors*. Catalysis Today, 1999. **52**(2-3): p. 197-221.

30. Martinez, O.M., S.I. Pereira Duarte, and N.O. Lemcoff, *Modeling of fixed bed catalytic reactors*. Computers & Chemical Engineering, 1985. **9**(5): p. 535-545.
31. Vortmeyer, D. and R.J. Schaefer, *Equivalence of one- and two-phase models for heat transfer processes in packed beds: one dimensional theory*. Chemical Engineering Science, 1974. **29**(2): p. 485-491.
32. Berger, R.J., et al., *Catalyst performance testing: bed dilution revisited*. Chemical Engineering Science. **57**(22-23): p. 4921-4932.
33. Berger, R.J., et al., *Catalyst performance testing: the influence of catalyst bed dilution on the conversion observed*. Chemical Engineering Journal, 2002. **90**(1-2): p. 173-183.
34. Karim, A., J. Bravo, and A. Datye, *Nonisothermality in packed bed reactors for steam reforming of methanol*. Applied Catalysis A: General, 2005. **282**(1-2): p. 101-109.
35. Taniewski, M., et al., *The effect of dilution of the catalyst bed on its heat-transfer characteristics in oxidative coupling of methane*. Chemical Engineering Science, 1996. **51**(18): p. 4271-4278.
36. Eriksson, E.J.G. and T.F. McKenna, *Heat-Transfer Phenomena in Gas-Phase Olefin Polymerization Using Computational Fluid Dynamics*. Industrial & Engineering Chemistry Research, 2004. **43**(23): p. 7251-7260.



# Chapter 3

*Start-up behavior of  
supported  
metallocenes in gas  
phase reactions*



<b>1. Introduction .....</b>	<b>166</b>
<b>2. Influence of reaction conditions .....</b>	<b>168</b>
2.1. Catalyst characterization .....	168
2.2. Start-up behavior under optimized conditions: homo- and co-polymerization.....	170
2.2.1. Activity and thermal profile.....	170
2.2.2. Evolution of the MWD.....	175
2.3. Start-up behavior under badly controlled regime: influence of gas velocity and catalyst amount.....	179
2.3.1. Activity and thermal profile.....	180
2.3.2. MWD evolution .....	182
2.3.3. Influence of the amount of heat generated (catalyst mass).....	183
2.4. Influence of reaction temperature .....	183
2.4.1. Activity and temperature profile .....	183
2.4.2. MWD evolution .....	184
<b>3. Influence of catalyst preparation .....</b>	<b>186</b>
3.1. Introduction .....	186
3.2. Different precatalyst.....	187
3.2.1. Introduction.....	187
3.2.2. Activity and temperature profile .....	188
3.2.3. MWD evolution .....	190
3.3. Influence of the nature and quantity of the Al .....	192
3.3.1. Influence of Aluminium content.....	192
3.3.1.1. Activity and temperature profile at start-up.....	194
3.3.1.2. MWD evolution.....	198
3.3.2. Cocatalyst impregnation time .....	199
3.3.3. Conclusions .....	203
3.4. Influence of Zr content.....	203
3.4.1. Activity and MWD profile .....	205
3.5. Conclusions .....	207
<b>4. Influence of support properties.....</b>	<b>209</b>
4.1. Introduction .....	209
4.2. Influence of support size .....	210
4.2.1. Activity and temperature profile at reaction start-up.....	212
4.2.2. MWD evolution .....	214
4.3. Influence of support pore size .....	217
4.3.1. Activity and temperature evolution at reaction start-up .....	218
4.3.2. MWD evolution .....	219
<b>5. Conclusions .....</b>	<b>220</b>
<b>6. References .....</b>	<b>224</b>

## 1. Introduction

In this chapter we investigate the influence of the reaction conditions, catalyst preparation and support properties on the yield and heat transfer from particles of supported metallocene catalysts. In particular we will present the activity profiles and the evolution of the molecular weight distribution (MWD) with reaction time; the influence of different parameters will be systematically analyzed. The thermal properties of the final polymers (melting temperature and crystallinity) will be presented in a separate chapter, as a deeper discussion is needed to explain the obtained results.

Two different metallocenes have been supported on MAO-treated silica in this work:  $\text{EtInd}_2\text{ZrCl}_2$  and  $(\text{nBuCp})_2\text{ZrCl}_2$ . The main reason for this choice is to have a more general description of the behavior of supported metallocenes at the start-up as it is known from the literature that these two complexes have different behaviors in ethylene (co)polymerization [1].  $(\text{nBuCp})_2\text{ZrCl}_2$  is known to be more active in ethylene homopolymerization, to give a polymer with higher molecular weight respect to  $\text{EtInd}_2\text{ZrCl}_2$  but to be able to insert less comonomer during copolymerization reactions. The same results have been found in this study for long time reactions (i.e. in a 2-litre gas phase polymerization reactor under similar bulk conditions for reaction times on the order of 60 minutes). The behavior of the two complexes during reaction start-up will be characterized more in detail in the following paragraphs. In addition being one of the objectives of this work to understand and optimize a tool to perform short gas phase olefin polymerizations, we decided to use these two metallocene complexes as they are very well known in literature and have been used for many years now in our lab.

First of all we will present the catalyst behavior at reaction start-up under conditions allowing optimal heat removal, which are the reference conditions of this work. Reactions performed in this section are “stopped flow” polymerizations as we will present results on polymers obtained with reaction times as low as 0.3s. They are much shorter than the reactions presented in the previous chapter, where the objective was to understand what influences the evolution of temperature in the reactor and longer times were needed. Subsequently we will investigate the impact of temperature, feed composition and gas velocity on the catalyst behavior and will study in more detail what happens if extreme care in controlling the reaction temperature overshoot is not taken. In this part a supported

$\text{Et(Ind)}_2\text{ZrCl}_2$  complex will be used as catalyst in order to ensure some continuity with the results presented in Chapter 2.

In the following part we will analyze the influence of the catalyst preparation and properties on the start-up behavior. The effect of the type of active Zr on polymerization start-up has been investigated by performing stopped flow reactions using a second metallocene ( $(\text{nBuCp})_2\text{ZrCl}_2$ ) which has a different structure than  $\text{Et(Ind)}_2\text{ZrCl}_2$ . Different supported  $(\text{nBuCp})_2\text{ZrCl}_2$  bearing different Zr content have been synthesized and tested in short time reactions. In a similar way the impregnation method has been modified in order to fix a different amount of Al on the final catalyst particle and to study its role on the active site formation and during early reaction stages. Alkylaluminium impregnation time has also been varied to check if MAO diffusion limitations influence the active site behavior during the reaction early stages.

In the last part of the chapter we will support  $(\text{nBuCp})_2\text{ZrCl}_2$  on silicas having different particle sizes and pore diameters. This will allow us to study in particular if mass or heat transfer limitation and fragmentation behavior have a strong impact during the reaction start-up or during the catalyst preparation. The higher activity of  $(\text{nBuCp})_2\text{ZrCl}_2$  complex will be responsible for bigger heat transfer constraints thus allowing to push the reactor optimization even further than what has been seen in Chapter 2. In addition, as it will be seen through Chapter 3, its higher sensitivity to thermal excursions will be the reason for some variations during the reaction course of the MWD of the polymers synthesized. This will be useful for determining the temperature evolution of the active particles during the reaction start-up. These facts, together with the objective to generalize the use of our reactor to different catalysts, motivate the use of this complex to study accurately the influence of catalyst preparation and support properties on early reaction stages.

All these reactions will be conducted under conditions that are responsible for an optimum heat transfer from the particle to the gas. These have been discussed in the previous chapter and are:

- Gas velocity of 15-20 cm/s
- 9 bar of total pressure with 33 mol % of helium in the feed
- Use of fine NaCl (10-30 $\mu\text{m}$  of single object size) as inert catalyst diluent



- Use of catalyst mass between 30 and 80 mg according to reaction time and activity to optimize the ratio between low heat and enough polymer production.

Different reaction conditions corresponding to poor heat transfer conditions will be used to study the effects of an insufficient heat removal on the activity and polymer properties.

To conclude we will present a general description of the behavior of supported metallocenes during the early reaction stages obtained from a summary of the experimental results.

## 2. Influence of reaction conditions

### *2.1. Catalyst characterization*

The metallocene used in this section is based on the  $\text{Et(Ind)}_2\text{ZrCl}_2$  complex supported on commercial silica Grace 948 treated with a MAO solution at 10 wt% in toluene following the procedure described in Chapter 2 and in the experimental part. Different catalyst batches have been used all along this study. The number of reactions needed to cover all the aspects of the work required in fact numerous batches of catalyst, so it is important to be confident that the results are reproducible from batch to batch. Reproducibility of the supporting procedure is presented in the following table, where the metal amounts in the final catalysts (measured by Inductively Coupled Plasma, ICP) and their activities are presented. The activity values presented here refer to conventional reactions lasting 1 h and performed at 80°C and 6 bars of ethylene in a 2L spherical gas phase reactor. These values will be compared with the ones related to the behavior of the catalyst at the start-up. Let us remind that in this kind of reactor the addition of an alkylaluminium (TEA in our case) is compulsory for the catalyst to be active. Without scavenger no activity is measured.

Table 1 : Metal content and activity of different catalyst batches (Et(Ind)<sub>2</sub>ZrCl<sub>2</sub> on Grace948/MAO).

<i>Exp</i>	<i>Catalyst</i>	<i>Zr content</i> (wt %)	<i>Al content</i> (wt %)	<i>Activity</i> (g/g/h)	<i>Activity</i> (g/mol Zr/h)
ETPE33	ETmet09	0.42	8.36	96	2.1 E+06
ETPE44	ETmet18	0.36	7.52	80	2.0 E+06
ETPE53	ETmet22	0.23	7.62	64	2.5 E+06
ETPE55	ETmet23	0.22	N.D.	58	2.3 E+06
ETPE56	ETmet24	0.31	7.29	66	2.0 E+06
ETPE72	ETmet40	0.27	6.89	50	1.7 E+06

It can be seen that a certain variation in the metal content is measured for different batches. We can quantify a total experimental error of our supporting procedure and of the method of measurement leading to an uncertainty in the Zr content of around 0.1wt% and of 1 wt% in the Al content. This leads to slightly different measured values of activity if they are expressed in g/g/h. Nevertheless by correcting the values for the real Zr a very good reproducibility in terms of activity can be found. In order to neglect the variations in the active metal content when comparing different sets of reactions we will express the catalyst activity in terms of g PE/ mol Zr/ h. Reaction rates in terms of g/g/h seem to be quite low but, if the very low Zr concentration is considered, acceptable values are obtained (on the order of 350 KgPE/ mol Zr/ bar/ h). Results from literature on gas phase ethylene homopolymerization using metallocenes supported on MAO treated silica are difficult to compare because of the differences in the used complex, in the supporting procedures, in the metal content of the final catalyst and in the type of silica used as support among different works. Nevertheless some indications on the expected activity of this catalytic system can come by cross-checking different studies. For example Harrison used a SMAO supported Et(Ind)<sub>2</sub>ZrCl<sub>2</sub> in gas phase ethylene polymerization [2] and obtained an average activity of 1000 KgPE/ mol Zr/ h/ bar. His catalyst nevertheless showed a very high Al content (around 30 wt%). Quijada [3] used the same metallocene complex not supported to perform ethylene homopolymerization with MAO at an Al/Zr ratio of 1750 and obtained an average activity of 6000 KgPE/ mol Zr/ bar/ h. Knowing that metallocene heterogeneization leads usually to activities 1 order of magnitude lower, this values is consistent with our results. Gas phase ethylene homopolymerizations performed with different metallocene complexes at reaction conditions similar to our work show results consistent to what we have measured: 200 KgPE/ mol Zr/ h/

bar for  $\text{Cp}_2\text{ZrCl}_2$  on SMAO bearing 24 wt% of Al [4] and 380 KgPE/ mol Zr/ h/ bar for  $(\text{nBuCp})_2\text{ZrCl}_2$  supported on polymeric particles [5] with Zr and Al content very similar to our case (0.31 and 17 wt% respectively).

MWD and thermal properties of the polymers produced during these reactions were analyzed by SEC and DSC. The polyethylenes produced in conventional reactions have an average  $M_n$  of 30 +/- 8 Kg/mol and the polydispersity index varies from 4 to 5.5 according to the measured sample. It can easily be seen how heterogeneization of the metallocene complex corresponds to a broadening of the MWD since the theoretical PDI of a single site catalyst is 2. Average melting temperature is 131°C and crystallinity is around 50%.

## *2.2. Start-up behavior under optimized conditions: homo- and co-polymerization*

### *2.2.1. Activity and thermal profile*

Different reactions have been performed at the conditions described above to determine the behavior of the supported  $\text{Et}(\text{Ind})_2\text{ZrCl}_2$  complex at reaction start-up. Each reaction was stopped at a different predetermined time and the polymer production measured by reactor weight difference for each time in order to obtain a reaction rate profile. Ethylene homopolymerization and ethylene-butene copolymerization have been studied for reaction times ranging from 0.3s to 75s. Reaction rate is defined as the time derivative of the yield centered on the calculation interval.

In Figure 1 the activity and yield values are plotted against the reaction time for ethylene homopolymerization at 80°C and 6 bars.

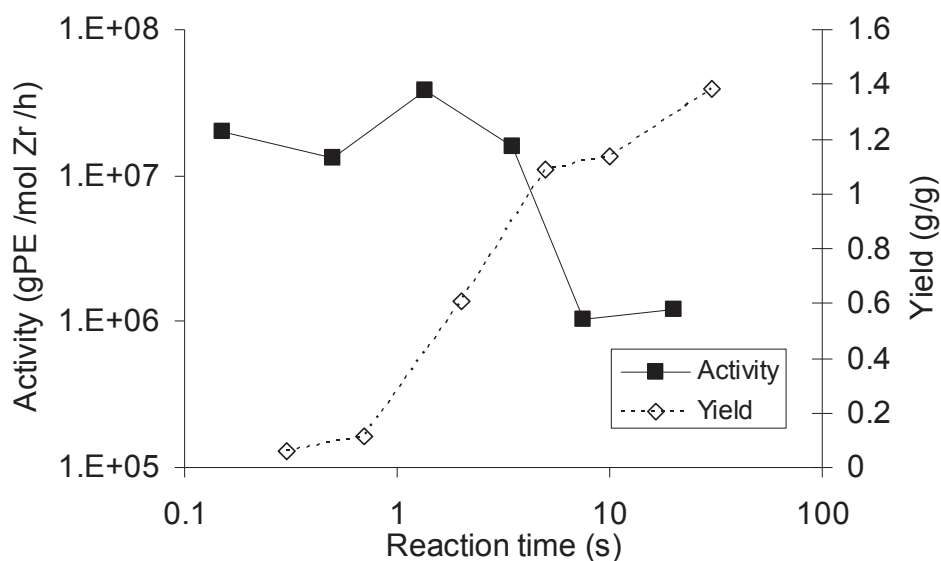
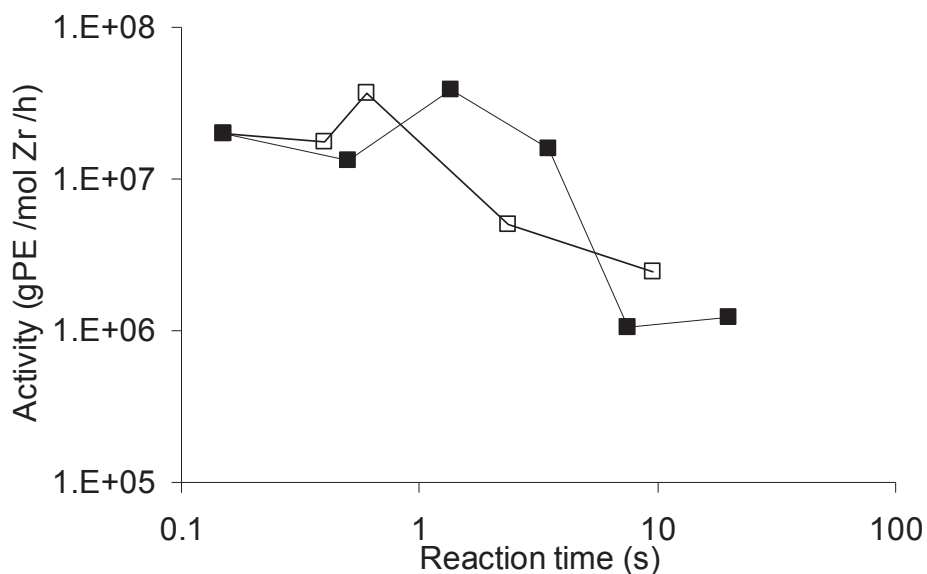


Figure 1: Yield and reaction rate evolution for short time ethylene homopolymerization

Reproducibility studies have been carried on also for stopped flow reactions. In addition to the variations in metal content between different batches of catalyst some fluctuations may also come from the reaction procedure. Dead volumes in the lines, or response time of the equipment (electro valves, thermocouples) can be a source of error when performing very short reactions. The very small amounts of catalyst used and of polymer recovered with respect to the total mass of the reactor (around 40g) can lead to measurement errors during weighing. From Figure 2 it can be seen that effectively some fluctuations may be present from a batch to another especially at very short reaction times. Dynamics of the activity evolution can be shifted of +/-0.5 second (c.f. the maximum activity for both curves) and time for decay has an uncertainty of +/-1.5 seconds. Nevertheless the measured profiles are very similar in shape, the overall evolution of the curves and the peak and steady state activities are similar enough for the two sets of data that we can conclude that the experiments are reasonably reproducible.



**Figure 2: Reproducibility study for short reaction times between two different batches of catalyst**

It can be seen that activity of the fresh catalyst can be very high for reaction times lower than 3-4s. This should not be a surprise as the same kind of behavior was found by Di Martino [6, 7] for ZN catalysts in slurry phase, and Machado [8] for ZN catalysts in gas phase polymerizations. It is then confirmed here that the high initial activity does not depend on the reaction phase or on the catalyst used. Risks of reaction runaway or poor morphology due to uncontrolled fragmentation are then confirmed. The activity at the beginning is 10-20 times higher than the steady state value. After few seconds the activity starts to decrease then reaches a plateau after approximately 10s. It seems that then the activity stabilizes around this value (see the yield increasing constantly in Figure 1) which is very close to the one found for “classic” long term reactions. The initial activity values are in the order of  $2-5 \times 10^7$  gPE/ mol Zr/ h which is ten or twenty times more than what is found in long term reactions. This kind of initial activity peak is not visible in the large turbosphere reactor as the time scale is too small to be detected.

We doubt that this decrease in activity is due to diffusion limitation induced by the presence of a polymer film around the active sites after few reaction seconds. It should be recalled that the activities expressed in terms of g/g/h are not excessive here in the second part of the reaction (around 100 g/g/h) so that existence of monomer diffusion limitations is not expected [9]. It is possible nevertheless that the presence of a polymer layer, especially if highly crystalline, could have an impact on the reaction rate (monomer can diffuse only through the amorphous phase of the polymer), but for certain it will not be responsible for an order of magnitude decrease in activity as is the case here. In addition the similarity between the

values of activity after 50s and the ones measured after 60 minutes suggests that no considerable diffusion limitation is present.

It should also be pointed out that even if a maximum effort has been made to find the optimum reaction conditions with our equipment, it might be possible that the heat removal at the particle level is insufficient and that particle heats up so much that reaction rate shuts down either because the polymer melts and imposes significant mass transfer resistance, or because the catalyst is thermally deactivated. Calculated temperature profile inside the reactor was shown in Figure 37 of the previous chapter for similar experiments and it was seen that the maximum temperature reached in the hottest point of the reactor during the reaction course for these conditions is about 110°C. In addition the control reached over the temperature during the reaction is clearly represented by the following graph (the dashed vertical line represents the reaction end). Given that the melting point of the polymer is 131°C, it is very unlikely that it melts. Furthermore, the curve in Figure 3 shows that there is no runaway of the reactor temperature.

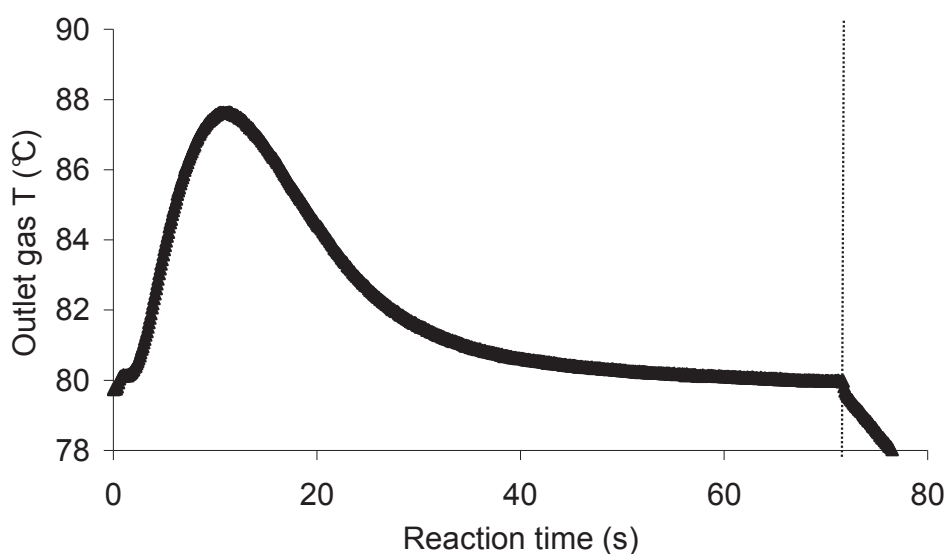


**Figure 3: Outlet gas temperature profile for 75s ethylene homopolymerization using supported  $\text{Et}(\text{Ind})_2\text{ZrCl}_2$  at 80°C and 6 bars of ethylene.**

The very high activity at the beginning followed by a rapid decay to steady state values can be explained with a natural evolution of the active site behavior with reaction time. Some sites can present a “one-off” behavior and work only at the beginning while others are more stable and responsible for the activity at long term.

The behavior of the same catalyst in ethylene copolymerization was tested by addition of 4 mol % of 1-butene to the flowing feed. Tests performed in a “classic” long term reaction show that the addition of butene does not change the activity of this catalyst. A polymer

having a melting temperature of 113°C and a crystallinity of 32% (homopolymer shows 131°C and 50% respectively) has been recovered, meaning that 3.5 mol% of butene has been effectively introduced into the polymer backbone. This is what one expects based on literature correlations [10]. Detailed discussion of results coming from DSC analysis will be presented in the following chapter.

The activity profile for stopped flow reactions is shown in the following picture and compared with the homopolymerization case. It's clear that even in presence of a comonomer the same profile starting from a high activity values and fast decaying to steady state is present.

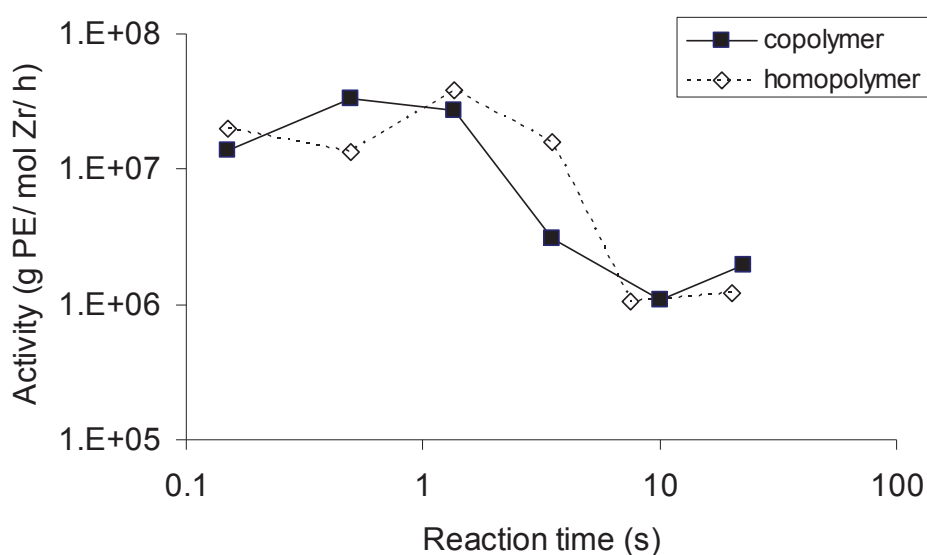


Figure 4: Comparison between activities in homo and copolymerization

Figure 5 shows that the temperature profiles of the two reactions are similar each other. The same temperature in the bed (around 110°C in the hottest points for one second according to Figure 37 of Chapter 2) can than be reached. The lower activity (or faster decay) of the copolymerization in the first 5-10 seconds is reflected by a slightly lower outlet temperature.

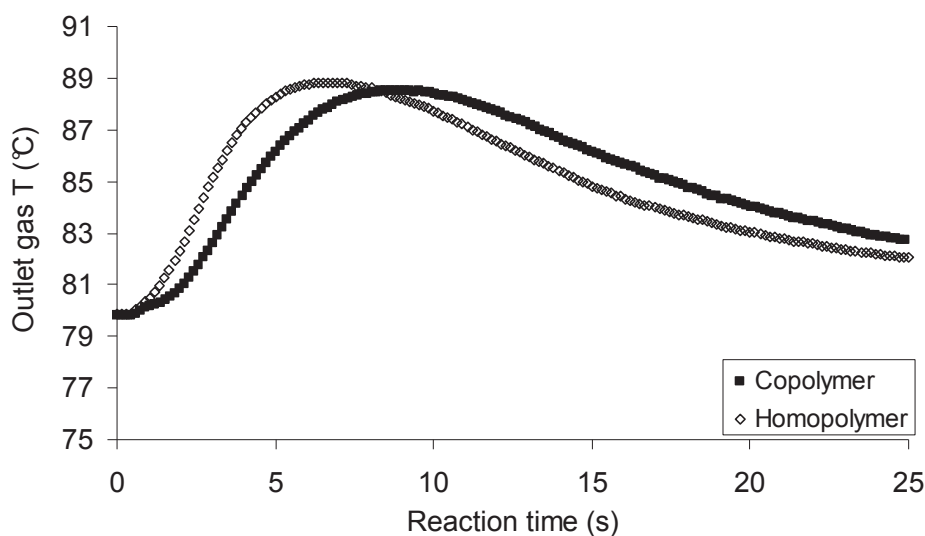


Figure 5: Outlet gas phase temperature profiles for homo and copolymerization

### 2.2.2. Evolution of the MWD

The polymers produced in the previous reactions have been analyzed by Size Exclusion Chromatography (SEC) in order to determine the molecular weight distribution (MWD). The MWD gives an indication of the functioning of the active sites. In particular, given that the MWD is determined by the ratio between  $k_p$ , the effective propagation rate constant, and  $k_t$ , the effective transfer rate constant, variations in the number average molecular weight ( $M_n$ ) or the polydispersity index (PDI) are symptoms of a change in the active site behavior. This will be clearly visible when, as is the case, a metallocene catalyst is used. These types of complexes, even if supported, are known to give polymers with narrow molecular weight distribution because of the homogeneity of the steric and electronic environment surrounding the active metals. A change in the catalytic behavior will be immediately detected in the broadening of the MWD. Let us recall here that the PDI of the polyethylene samples made in conventional polymerizations using silica supported  $\text{Et}(\text{Ind})_2\text{ZrCl}_2$  is around 4.5 while ZN catalysts typically produce polymers with a PDI between 4 and 10. Broadening of the MWD will be less easy to detect when using a catalyst which intrinsically produces an highly heterogeneous polymer.

The average molecular weights of homopolymers produced at short reaction times and their distribution are presented in Figure 6 and top of Figure 7. It can be seen that the values of  $M_n$ ,  $M_w$ , and PDI are quite constant all along the reaction start-up and close to the values found after 1h of reaction time. Only a slight decrease is seen during the first reaction second. This



means that once the very short period of very high reaction rate is passed, the active sites do not seem to change after a few seconds under the tested conditions. It has to be pointed out that there will always be some temperature gradients into the fixed bed. The result of this is that active sites will likely behave slightly differently according to the position that they occupy inside the reactor. The kinetic constant  $k_p$  and  $k_t$  are in fact dependent upon reaction temperature following an Arrhenius law with the activation energy of the transfer reaction being higher than the one of the propagation reaction [11-13]. Nevertheless, as we mentioned above, the reaction conditions used here are such that relevant temperature gradients are very limited in time and space. The average properties of the polymer chains produced inside the bed are then homogeneous and do not depend on the time or the position. Only in the first one or two seconds do we observe slight variations in the values of the average molecular weights and this is exactly the time range in which maximum temperature excursions appear.

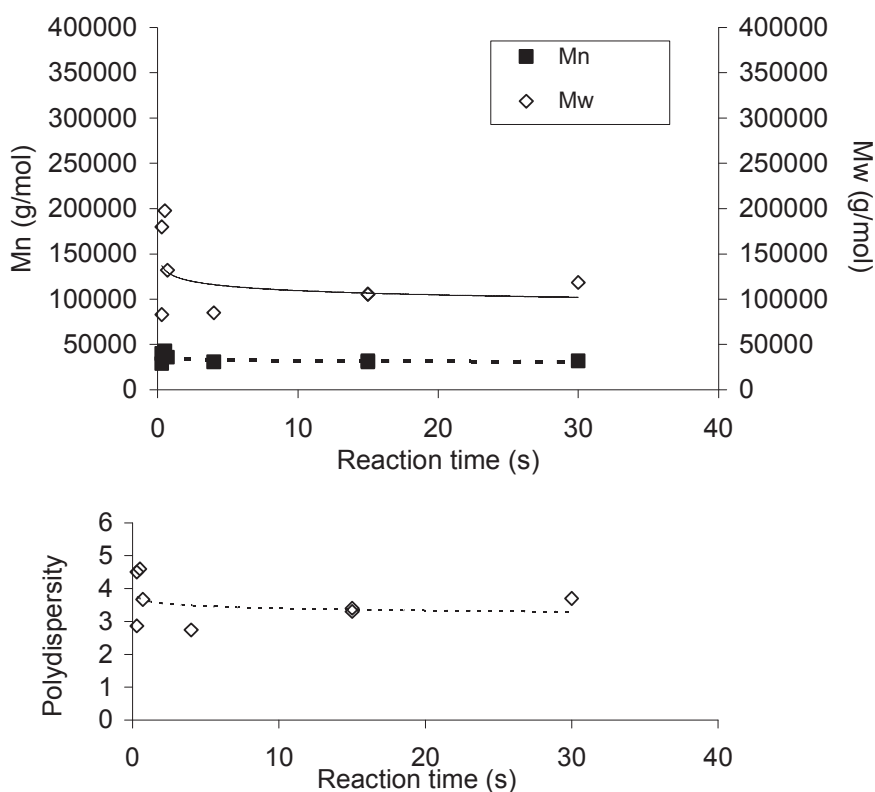


**Figure 6: MWD of ethylene homopolymers produced by supported  $\text{Et}(\text{Ind})_2\text{ZrCl}_2$  at short reaction times**

MWD of copolymers shows a slightly different behavior (bottom of Figure 7). First of all it can be seen that the MWD of the copolymers are slightly shifted towards lower values.  $\beta$ -H transfer reaction can be amplified by the comonomer insertion. The number average molecular weight decreases consistently (down to 10000 g/mol) between 1 and 5s (as it is shown by the MWD tails towards low values of the corresponding curves of Figure 7) and

then goes back progressively to the original value after 15s. As a consequence the PDI reaches surprisingly high values (around 6) in this time range but this “deviation” from expected behavior seems to be only temporary and PDI around 4 is measured again from 15s of reaction.

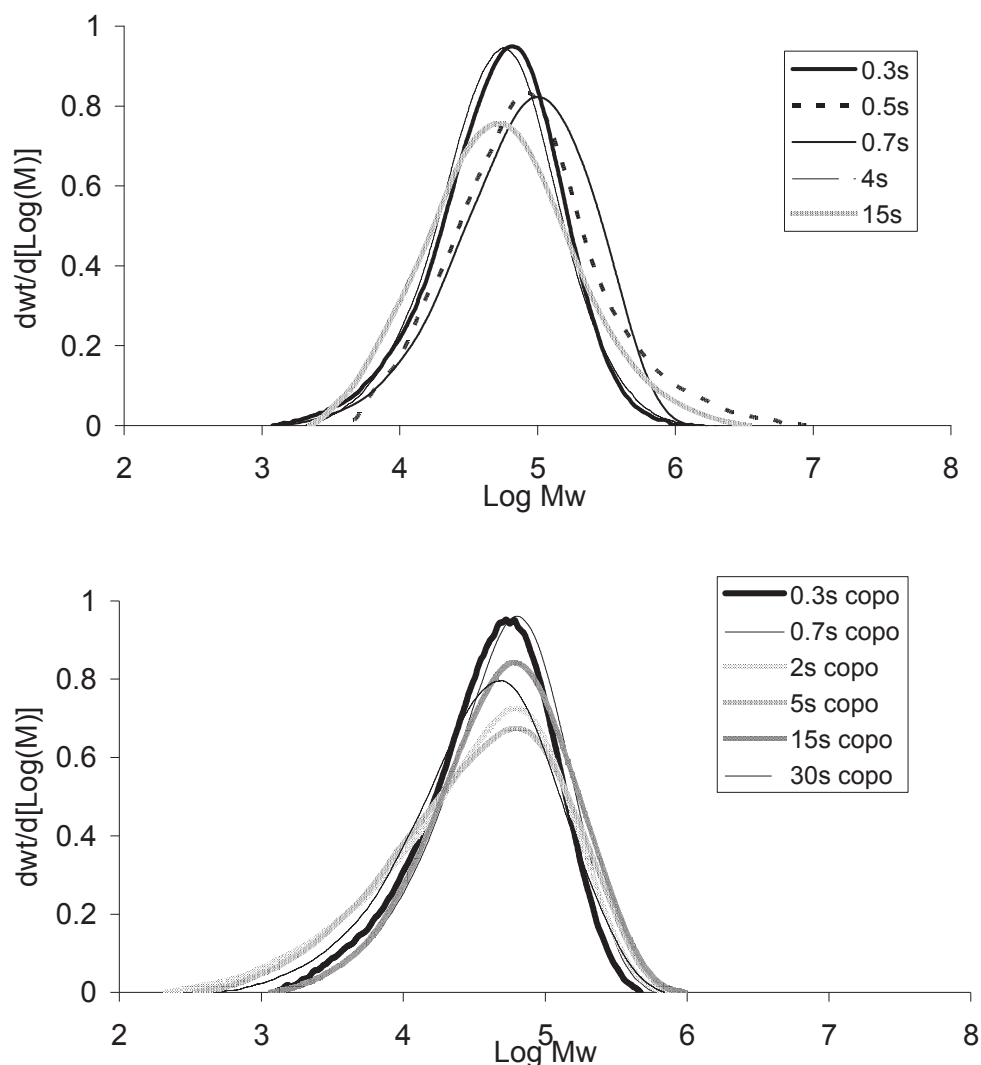


**Figure 7: MWD of polymers produced by supported  $\text{Et}(\text{Ind})_2\text{ZrCl}_2$  at short reaction times: homopolymerization (top) and copolymerization (bottom).**

The polymer MWD is surprisingly broad during the start-up of the reaction (i.e. between 2 and 10s). Once again, this particular time range is where the measured gas temperature reaches its maximum, and so too should do the particles. In addition in this period the catalyst is still much more active than at its steady state. It can be that in the first reaction seconds, i.e. from 1 to 10s, there are some active sites responsible for the high activity and, since they are working at quite high temperatures, producing short chains. These sites work together with the ones giving the polymer that we recover at longer reaction times (higher  $M_n$ , narrower MWD, lower activity). This situation lasts for few seconds, then this “special” sites

deactivate, the activity decays, and the MWD starts to narrow. After 30s we have (more or less) the properties found with long lasting reactions. This is particularly true for copolymerization.

Figure 8 shows the calculated solid average temperature for the homo- and copolymerizations. The average solid temperature has been calculated with the method explained in Chapter 2, which is based on using the inlet and outlet gas temperatures together with the yield values to calculate the heat accumulated into the bed for each reaction time supposing the reactor to be adiabatic. This allows to calculate a reasonable bed average temperature if all the specific heats are taken into consideration (silica, polymer, NaCl, outlet frit). The assumptions of the reactor being adiabatic and the solids being under thermal equilibrium are clearly not fully true but justified as they allow a tremendous simplification of the calculations without affecting the trends of the results.

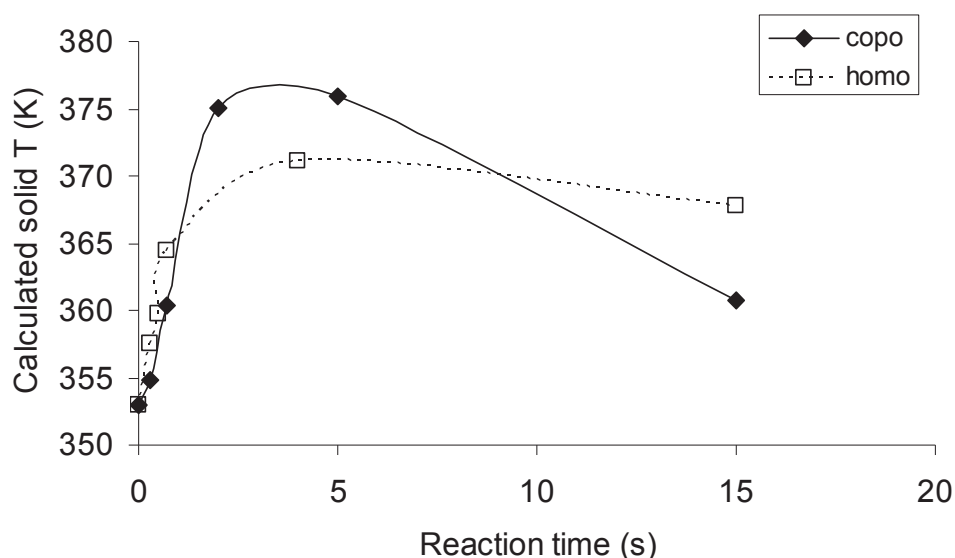


Figure 8: Calculated solid temperature evolution for (co)polymerization reactions with  $\text{Et}(\text{Ind})_2\text{ZrCl}_2$ .

It is visible that the solid particles undergo higher temperature excursions in the copolymerization case respect to the homopolymerizations conducted under the same reaction conditions. This can partly explain why between 2 and 5 seconds (that is when the solid temperature is at the highest values) the MWDs of the produced copolymers are broader.

### 2.3. Start-up behavior under badly controlled regime: influence of gas velocity and catalyst amount.

We have seen in the previous chapter how it's possible, by appropriately tuning the reaction conditions, to work under controlled regime and to avoid polymer melting. While avoiding a melt down of the particles is important, it is equally important to avoid the particles from significant overheating, especially if we want to study with confidence the behavior of the catalyst during the time frame where heat transfer is the most difficult. Insufficient heat removal from the particle can lead to temperature increase that, even if not enough to melt the polymer, is responsible for uncontrolled behavior during the reaction start-up. Only slight variations of the gas velocity, the most important parameter for heat transfer, are responsible for these effects. From Figure 9 (reproduction of Figure 30 of Chapter 2) it can be seen that a velocity of 2.8 cm/s is sufficient to avoid reaction thermal runaway and to control the measured outlet gas phase temperature if fine NaCl and He are used. Nevertheless this is not enough to have a control on polymer properties, since it is possible to have non-negligible temperature excursions in the particles upwards of 10-30°C under such conditions.

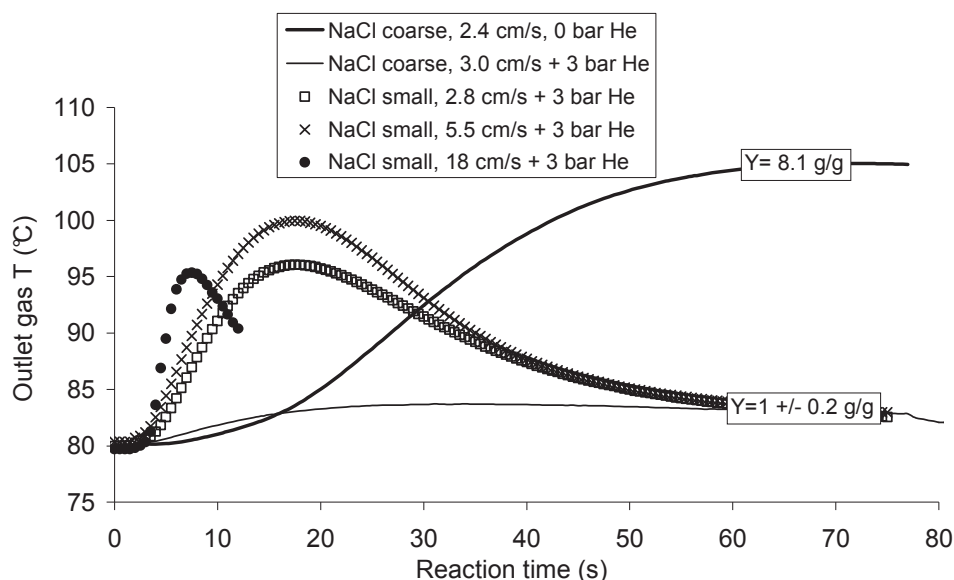


Figure 9: Outlet gas temperature and yield for different reaction conditions (80°C, 30 mg catalyst, 75s)

### 2.3.1. Activity and thermal profile

The relative gas-particle velocity is one of the most important parameters when working with gas-solid reactions whether they are conducted in packed, stirred or fluidized beds. The set of reactions discussed above have been conducted with a gas velocity of 20cm/s and a mass of catalyst of 30 mg for reactions longer than 2s, 40 mg for reactions lasting 2s and 80 mg for shorter reactions. In order to simulate slightly worse heat removal and to check what could be the drawbacks at the reaction start-up, we decreased the velocity to 5.5cm/s and increased the catalyst mass to 50 mg for reactions longer than 1s.

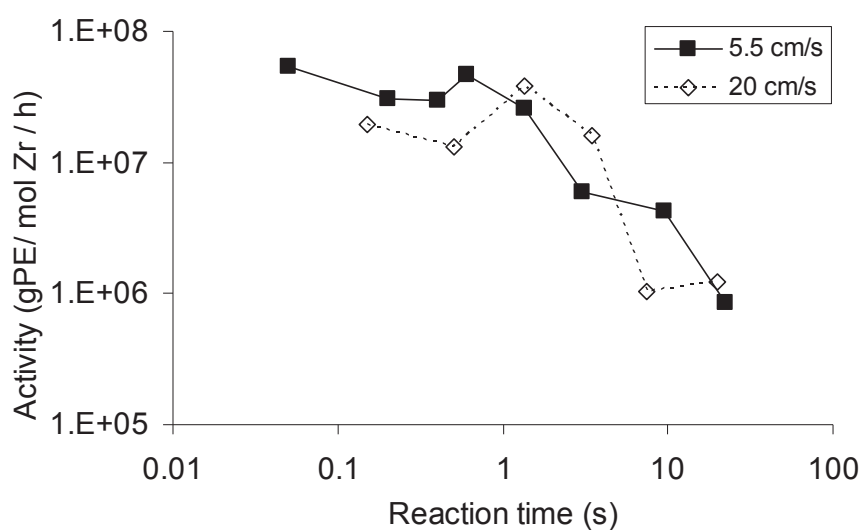


Figure 10: Influence of gas velocity on activity profile at reaction start-up

Figure 10 and Figure 11 show that a poorer heat removal gives a higher activity for very low reaction times (up to 2s). The higher activity at the beginning can be due to higher temperature in the bed.

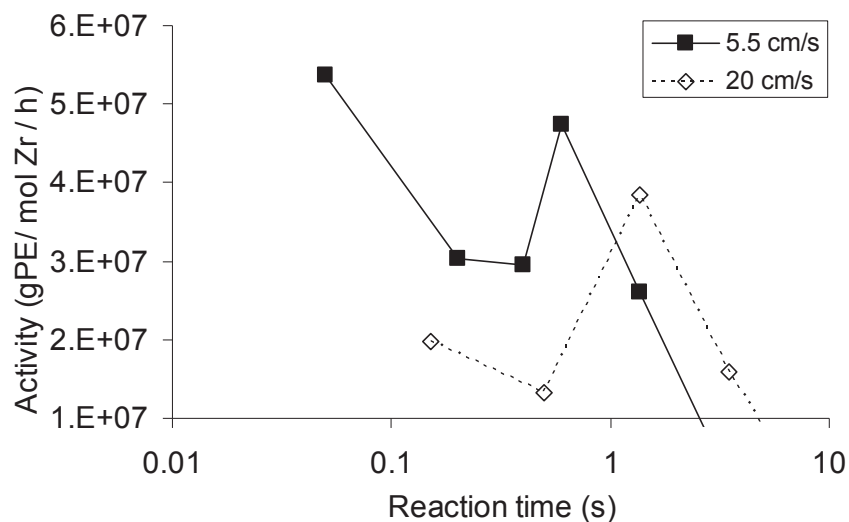


Figure 11: Zoom of first 5s of Figure 10

For the same reason thermal deactivation of the catalyst seems to be more pronounced with lower gas velocity. This is proven in Figure 12, where the evolution of the calculated average bed temperature is shown for the two different gas velocities (squares) together with the measured outlet gas temperature (lines). It can then be seen that for lower gas velocities the catalyst particles remain at high temperatures for much longer time. This can easily be the reason for an increased catalyst deactivation. Nevertheless the differences in the activity profile for the two sets of reaction are not dramatic and runaway is avoided for both reaction conditions (even if it takes a longer time for the bed temperature to decrease with low gas velocity). Figure 12 shows also that a considerable difference is present between the measured outlet gas and the calculated solid phase temperatures when a low gas velocity is used.

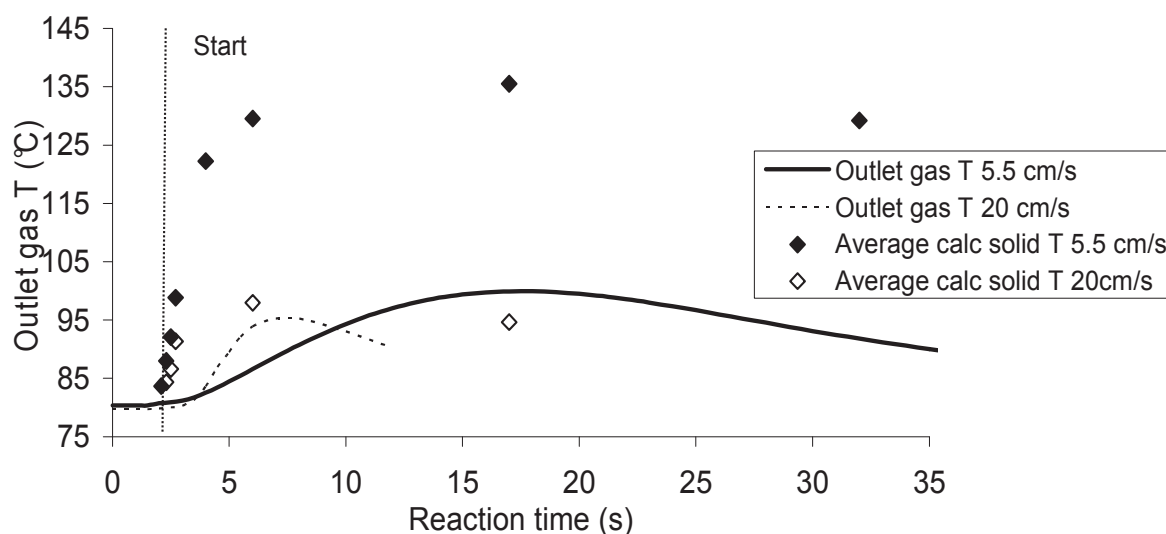


Figure 12: Outlet gas temperature for different gas velocities.

## 2.3.2. MWD evolution

But even if in both cases the outlet gas temperatures decrease sooner or later to the isothermal value, the differences between the two thermal profiles are not negligible. The polymer properties and in particular the MWD can be strongly influenced by the particle temperature during the polymerization. Figure 13 clearly tells us that if the particle heats up too much (as shown in Figure 12) the average molecular weight drops and the MWD broadens. The measured MWD is in fact an average of the MWDs of all the chains produced at different reaction times and reactor locations under different temperatures. The higher the temperature excursions in time and space, the more heterogeneous will be the catalyst behavior and the broader the MWD. In particular in our case the activation energy of the transfer reaction is bigger than the one of the propagation so that at higher temperatures shorter chains are produced. Values of PDI increase with a higher temperature and values of  $M_n$  decrease as shorter chains are added to longer chains produced previously.

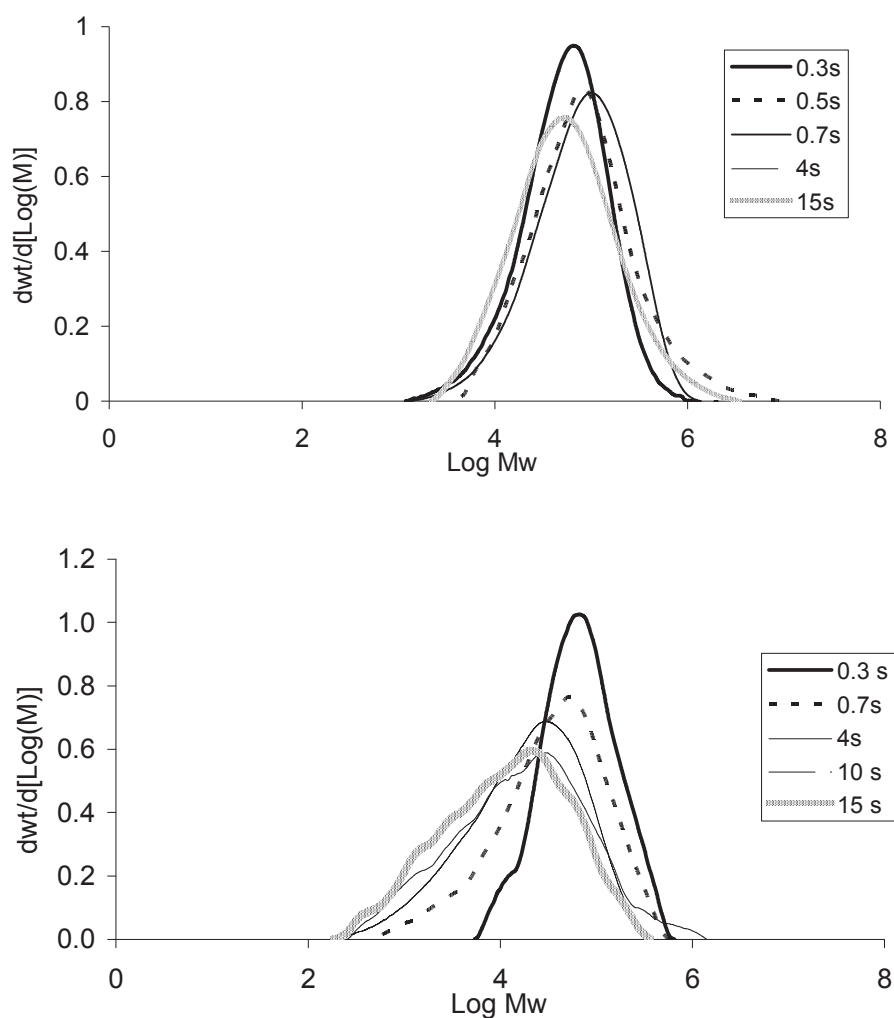


Figure 13: MWD evolution for different gas velocities: 20 cm/s (top) and 5.5 cm/s (bottom).

### 2.3.3. Influence of the amount of heat generated (catalyst mass)

These conclusions are also confirmed if we act the other way around: working with optimum heat removal (gas velocity of 20 cm/s) and increasing the quantity of energy to be evacuated by increasing the amount of catalyst in the bed. Table 2 shows the results of catalyst activity and SEC analysis performed on polymers produced at a feed temperature of 80°C, 6 bars of monomer, 3 bars of helium, gas velocity of 20cm/s in reactions lasting 30s. It is clear that even if doubling the quantity of catalyst (SFG328 with respect to SFG327) does not provoke a reaction runaway (see Yield column), Mn decreases significantly and the PDI increases with higher catalyst loading. Calculations of the average bed temperature confirm these results as the bed of SFG328 is found to be at 80°C after 30s of reaction while the one of SFG327 is still around 95°C.

**Table 2: Influence of heat generation on polymer MWD, 30s reaction.**

<i>Exp</i>	<i>Catalyst</i>	<i>Catalyst mass (mg)</i>	<i>Yield (g/g)</i>	<i>Mn (g/mol)</i>	<i>Mw (g/mol)</i>	<i>PDI</i>
SFG327	ETmet26	47	1.1	13000	99000	7.6
SFG328	ETmet26	25	1.1	32000	118000	3.7
SFG329	ETmet26	14	0.8	45000	135000	3.0
SFG330	ETmet26	4.5	0	x	x	x

## 2.4. Influence of reaction temperature

### 2.4.1. Activity and temperature profile

Reactions performed at 60°C have been compared with the results previously presented and obtained at 80°C. The remaining reaction parameters are the ones giving optimum heat transfer. From Figure 14 it can be seen that decay type behavior of the activity and its values are not influenced by reaction temperature.



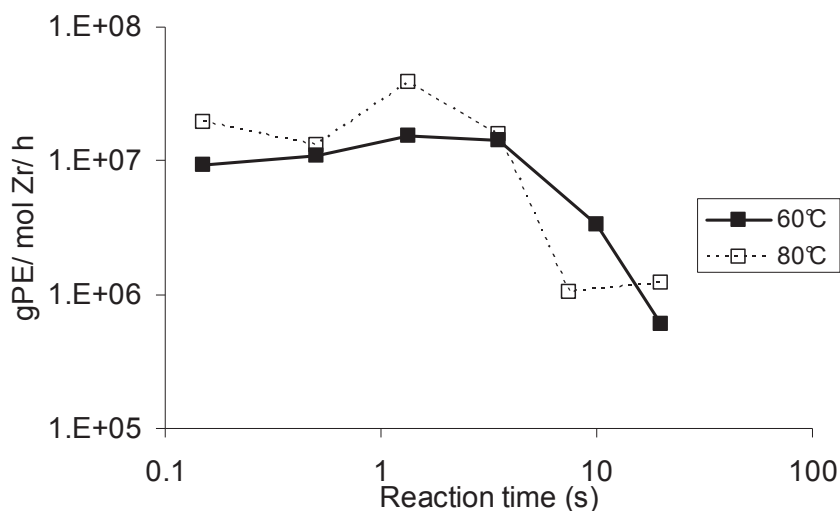


**Figure 14: Influence of reaction temperature on start-up activity profile**

Even if not shown here, the outlet gas temperature profile is very similar for the two sets of reactions both in terms of dynamics (maximum reached after 6-7 seconds) and of temperature excursions (8°C at 80°C, 10°C at 60°C).

Comparison of different gas velocities has been performed at 60°C too. The conclusions in terms of activity are the same: the lower the gas velocity is and the higher is the activity in the first reaction seconds and the more rapid the decay. In this case for a velocity of 5.5 cm/s an outlet gas temperature increase of 30°C after 13-14 s is measured, which is three times the value measured with a gas flowing at 20 cm/s.

#### 2.4.2. MWD evolution

MWD evolution of polymers produced at 60°C are shown in Figure 15 and compared with the results obtained at 80°C. First of all it can be seen that average molecular weight values and the width of the distribution do not differ consistently from the ones measured at 80°C except for the 5s and 15s reactions performed at 60°C. As already found for the copolymerization case, also here we can notice that in this time range an amount of shorter chains high enough to modify the MWD shape is produced. Mn is then lowered and PDI shows the opposite behavior. The distribution then rapidly goes back to the initial shape (Mn around 30000 g/mol and PDI around 4). This is probably due the temperature excursions into the bed. This fact shows that the important factor responsible for a MWD broadening is the temperature excursion and not its absolute value (the maximum measured in this reaction set

for the outlet gas temperature is 70°C). Finally, a light shift of the right part of the MWD towards higher values is seen as the reaction time increases.

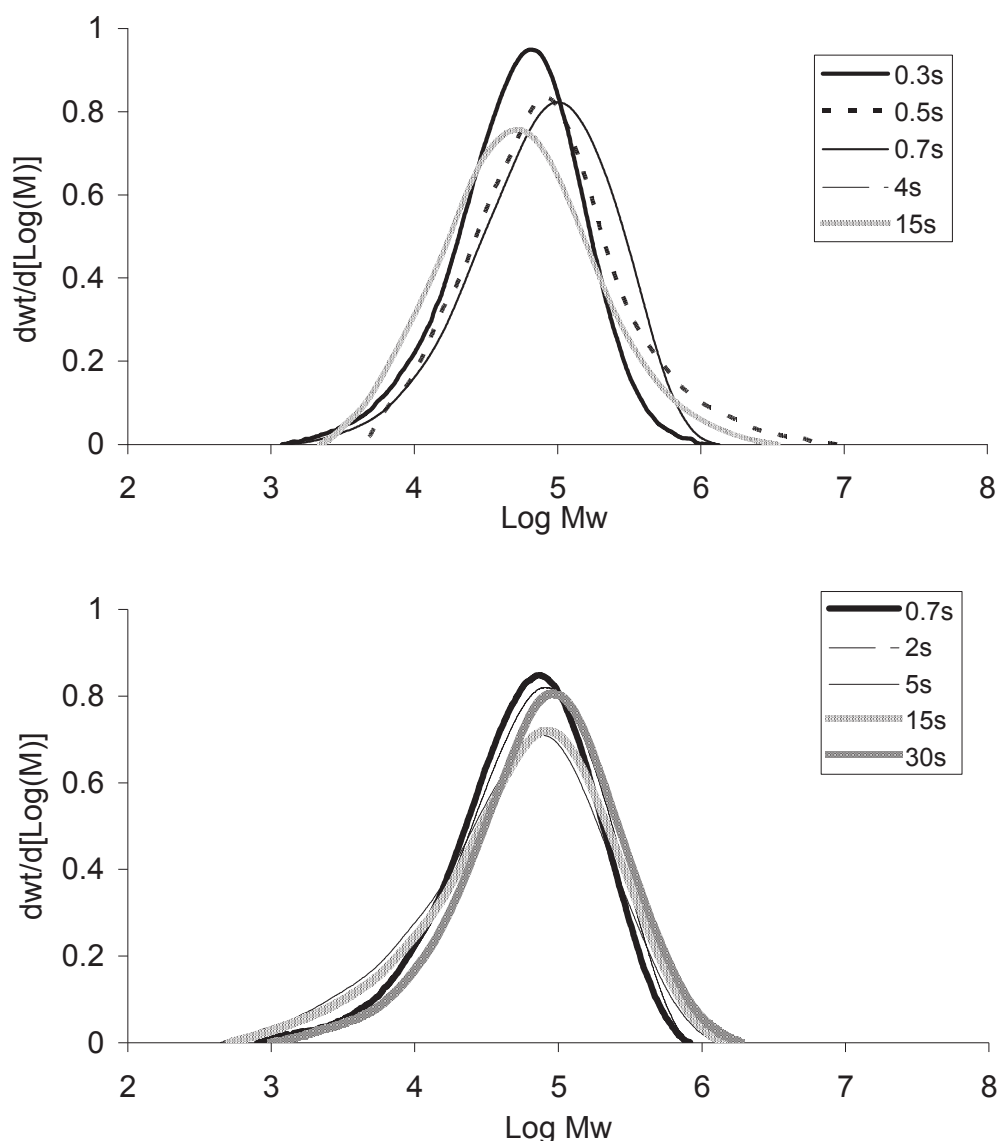


**Figure 15: Influence of reaction temperature on MWD evolution: 80°C (top) and 60°C (bottom).**

In the following graph a comparison between the Mn evolution of the polymers produced at 60°C using two different gas velocities is shown. It is remarkable that at the very beginning of the reaction, when temperature excursions just appeared, the two curves are very similar. As the reaction goes on the quantity of polymer produced at high temperature (low Mn) is much more important if a low gas velocity is used (the temperature remains to high values longer in this case). The curve of the average measured Mn remains then to low values for longer times.

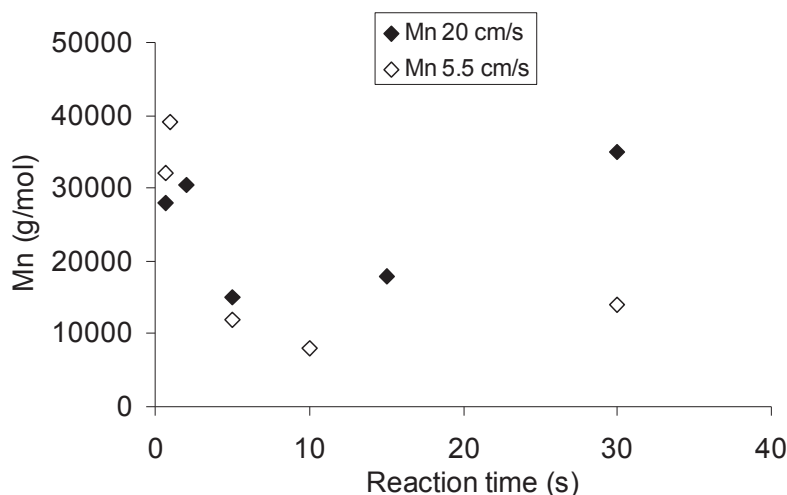


Figure 16: Influence of gas velocity on Mn of polymers produced at 60°C

### 3. Influence of catalyst preparation

#### 3.1. Introduction

As already discussed in the literature review, the method of preparing the supported metallocene is obviously going to have a strong influence over the way the active sites are created. The electronic and steric environments of the metal centers are responsible for the active site behavior in terms of activity and molecular weight distribution of the polymer produced (mainly depending on the propagation and transfer kinetic constants). These variables are controlled by the impregnation parameters like temperature and time, by the type of metallocene used and by the quantity of active metal and cocatalyst present on the support. Related works can be easily found in literature, where a number of teams have published studies on the influence of the catalyst preparation on the polymerization reaction. A good review on this subject is the one of Severn et al. [14]. Nevertheless it is hard to find any result about the influence of these parameters on the evolution of the active site at the reaction start-up even if it is in this time range that the metal center undergoes the bigger transformations. In the following paragraphs we will try to gain some understanding of this aspect by studying systematically the parameters influencing the environment around the active center: the nature of the Zr center (metallocene type), the quantity and the distribution of the Al (cocatalyst amount and impregnation time) and the concentration of Zr (precatalyst quantity).

## 3.2. Different precatalyst

### 3.2.1. Introduction

It is known that the structure of a metallocene complex (that is the ligands bonded to the metal) influences the active site behavior. Activity and kinetic constants depend in particular on the type and number of cyclopentadienyl ligands and on the presence of a bridge between them. In order to study this effect and to generalize the use of our gas phase stopped flow reactor we decided to impregnate the same MAO treated silica with a different metallocene complex. The chosen precatalyst is  $(n\text{BuCp})_2\text{ZrCl}_2$ . As the molar masses of the two metallocenes are close each other and as we used the same amount of catalyst during the supporting procedure, the Al and Zr contents of the final catalysts are similar for both complexes. More in detail the average metal loading of the  $(n\text{BuCp})_2\text{ZrCl}_2$  based catalyst is of 0.31 wt% Zr and 7.16 wt% Al while the  $\text{EtInd}_2\text{ZrCl}_2$  based catalyst showed average values of 0.32 wt% and 7.63 wt% respectively. The structure of the two molecules is slightly different. The bridge present in  $\text{EtInd}_2\text{ZrCl}_2$  between the two indenyl groups is responsible for a more open structure respect to the other complex and for an easier coordination of the monomer. This is responsible for different activities and different kinetic constants [1].  $(n\text{BuCp})_2\text{ZrCl}_2$  has then been chosen because it has a different behavior respect to  $\text{EtInd}_2\text{ZrCl}_2$ . One of the main reasons that has pushed us to work with this specific non-bridged complex is its higher activity and its capacity to produce polymers with narrower MWD. 1 hour reactions with the new catalyst gave an average activity of  $2.6\text{E}+06$  gPE/ mol Zr/ h, which is 30% higher than the one obtained using  $\text{EtInd}_2\text{ZrCl}_2$ .  $M_n$  of the produced polymer is around 59000 g/mol, which is almost twice that obtained with the  $\text{EtInd}_2\text{ZrCl}_2$ . PDI is around 2.8 while  $\text{EtInd}_2\text{ZrCl}_2$  gave broader MWD distributions with PDIs of around 4. Thermal properties of the polymers are similar for both metallocene complexes. With  $(n\text{BuCp})_2\text{ZrCl}_2$  supported on MAO-treated Grace 948 we have measured a melting temperature of  $131.8^\circ\text{C}$  and a cristallinity of 54% (with  $\text{EtInd}_2\text{ZrCl}_2$  we have  $131^\circ\text{C}$  and 50% respectively). In the same type of long term reaction we have seen that addition of 4 mol % butene to the feed increases the activity of this catalyst of about 30%. A polymer having a melting temperature of  $120^\circ\text{C}$  and a cristallinity of 35% has been recovered meaning that butene has been effectively introduced into the polymer backbone at the height of 2 mol% [10]. In other words, as expected the  $(n\text{BuCp})_2\text{ZrCl}_2$  sites do not incorporate comonomer as well as the first catalyst [1]. This is due to the fact that the more open structure of  $\text{EtInd}_2\text{ZrCl}_2$ , due to the bridge between the two

indenyl groups, is responsible for less sterical hindrance at the active site, making it less difficult to insert the bulkier comonomer. A detailed discussion of the DSC analyses will be presented in the following chapter. The  $M_n$  of the copolymer is of about 36000 g/mol with an  $M_w$  of about 103000 g/mol and a PDI of 2.8. The presence of comonomer results in a slight decrease of  $M_n$  and  $M_w$  and increase in PDI. This is also well known and it is due to the increased transfer rate due to the comonomer.

### 3.2.2. Activity and temperature profile

Two sets of reaction using two different catalyst batches were performed at the usual reaction conditions (80°C, 6 bar ethylene, 3 bar helium, 20cm/s gas velocity, NaCl fine as seedbed, catalyst mass from 30 to 80 mg) to study the reproducibility of the experiments performed with this second metallocene complex. Figure 17 shows that the measured activities are highly reproducible in terms of evolution with reaction time and very similar to what found for the  $\text{EtInd}_2\text{ZrCl}_2$ .

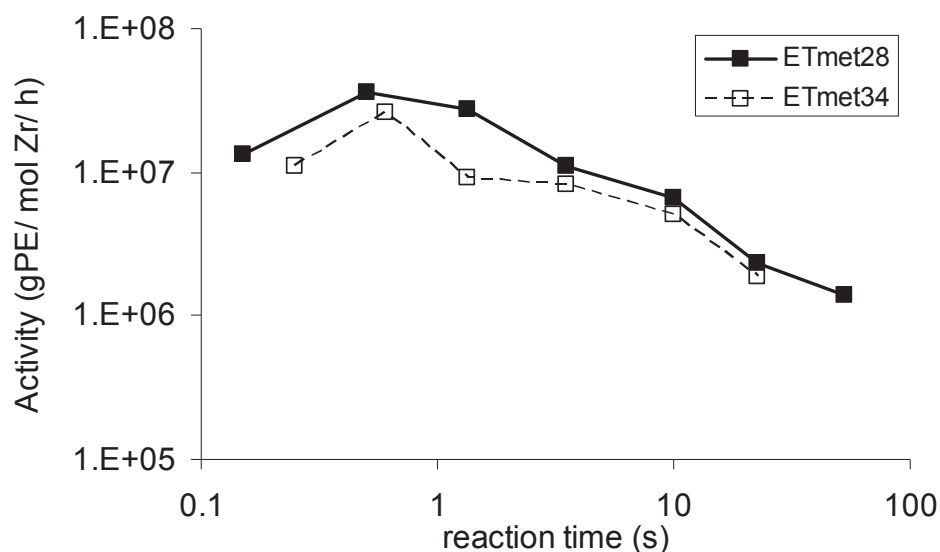


Figure 17: Repetability study of short time reactions with supported  $(\text{nBuCp})_2\text{ZrCl}_2$

A high activity is present at the reaction start-up, with a maximum happening between 0.5 and 1s. The activity then rapidly decays to a plateau. Activity values between the two catalyst batches differ of 20% for reactions longer than 5s and of 30% for shorter reactions.

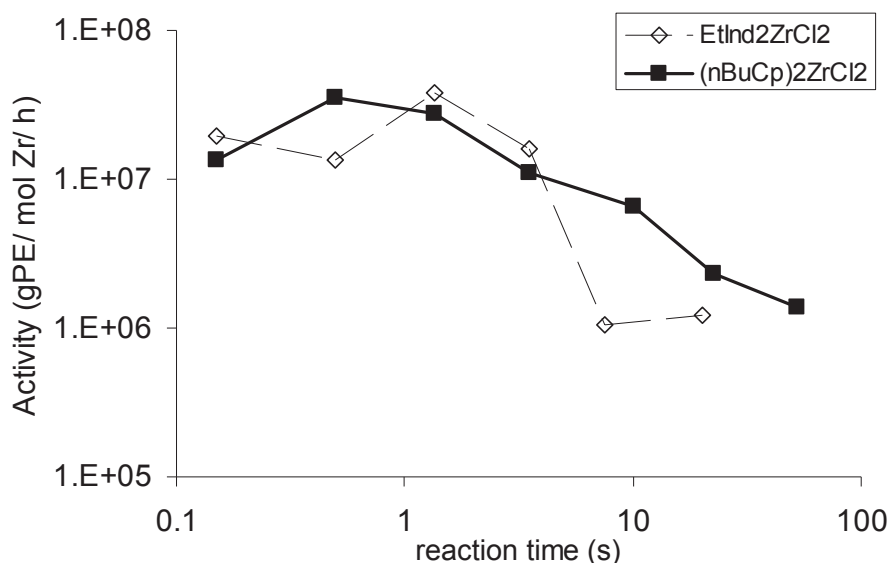


Figure 18: Activity profile of two different metallocene complexes.

Figure 18 shows a comparison between the activity evolution with reaction time of the two metallocene complexes previously cited. It can be seen that activities in the first 2 seconds are similar. For reactions longer than 5s it seems that (nBuCp)<sub>2</sub>ZrCl<sub>2</sub> deactivates more slowly. This fact is also visible in the outlet gas temperature profile. If supported EtInd<sub>2</sub>ZrCl<sub>2</sub> is used the outlet gas temperature decreases to the initial temperature after 40 seconds. As shown in Figure 19, at a reaction time of 30s the outlet gas temperature in case of (nBuCp)<sub>2</sub>ZrCl<sub>2</sub> is 2°C higher. The evolution of these curves is what one would expect based on the activity profiles.

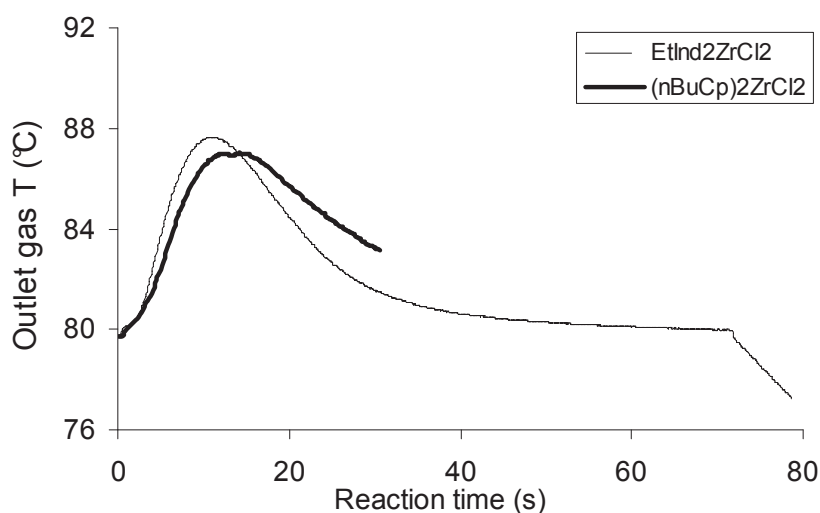
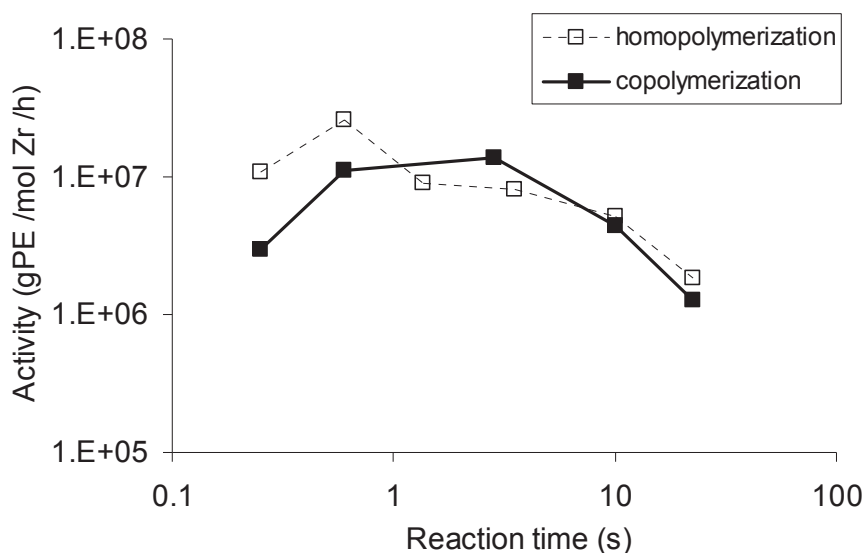


Figure 19: Differences in outlet gas phase temperature between the two metallocene complexes.

The behavior of the same catalyst in the start up of ethylene copolymerization was tested by addition of 4 mol % of 1-butene to the flowing feed. The activity profile for stopped flow

reactions is shown in Figure 20 and compared with the homopolymerization case. It's clear that even in presence of a comonomer the same profile starting from a high activity values and fast decaying to steady state is present. Nevertheless it seems that in case of copolymerization the reaction rate at the very beginning (0.25s) is lower. The decay is very similar in both cases.



**Figure 20: Comparison between activity profiles of homo- and co-polymerization using supported  $(nBuCp)_2ZrCl_2$ .**

As seen when using  $EtInd_2ZrCl_2$  and shown in Figure 5, the maximum outlet gas phase temperature for  $(nBuCp)_2ZrCl_2$  is reached few seconds later in case of copolymerization.

### 3.2.3. MWD evolution

The MWD evolution of polyethylenes produced at a feed temperature of  $80^\circ C$  and 6 bars at reaction start-up are shown in Figure 21 for the two metallocenes used up to this point. It can be seen that the polymer average molecular weights are similar for the two catalysts. Mn values of the polymers produced with  $(nBuCp)_2ZrCl_2$  have values around 25000 g/mol which are much lower than the values measured after a polymerization in a classic reactor. In a similar but more clear manner than what was measured using a  $EtInd_2ZrCl_2$  heterogeneous catalyst it can be seen that with an increasing reaction time there is a clear tendency to produce bigger chains (MWDs tending to shift to the right). At the same time increased production of short chains is seen for the reactions lasting 5s and 30s. As a consequence the Mw of the produced polymers increase from 90000 g/mol after 0.5s to 140000 g/mol after 30s of reaction. The PDI also increases going from values around 3 at very low times to values

around 5 after 30s of reaction. The PDI values measured in the first 2 reaction seconds are comparable to what is found after long term reactions (around 3). Nevertheless they become quite high for stopped flow reactions longer than 5s. This difference was not seen in the EtInd<sub>2</sub>ZrCl<sub>2</sub> series.

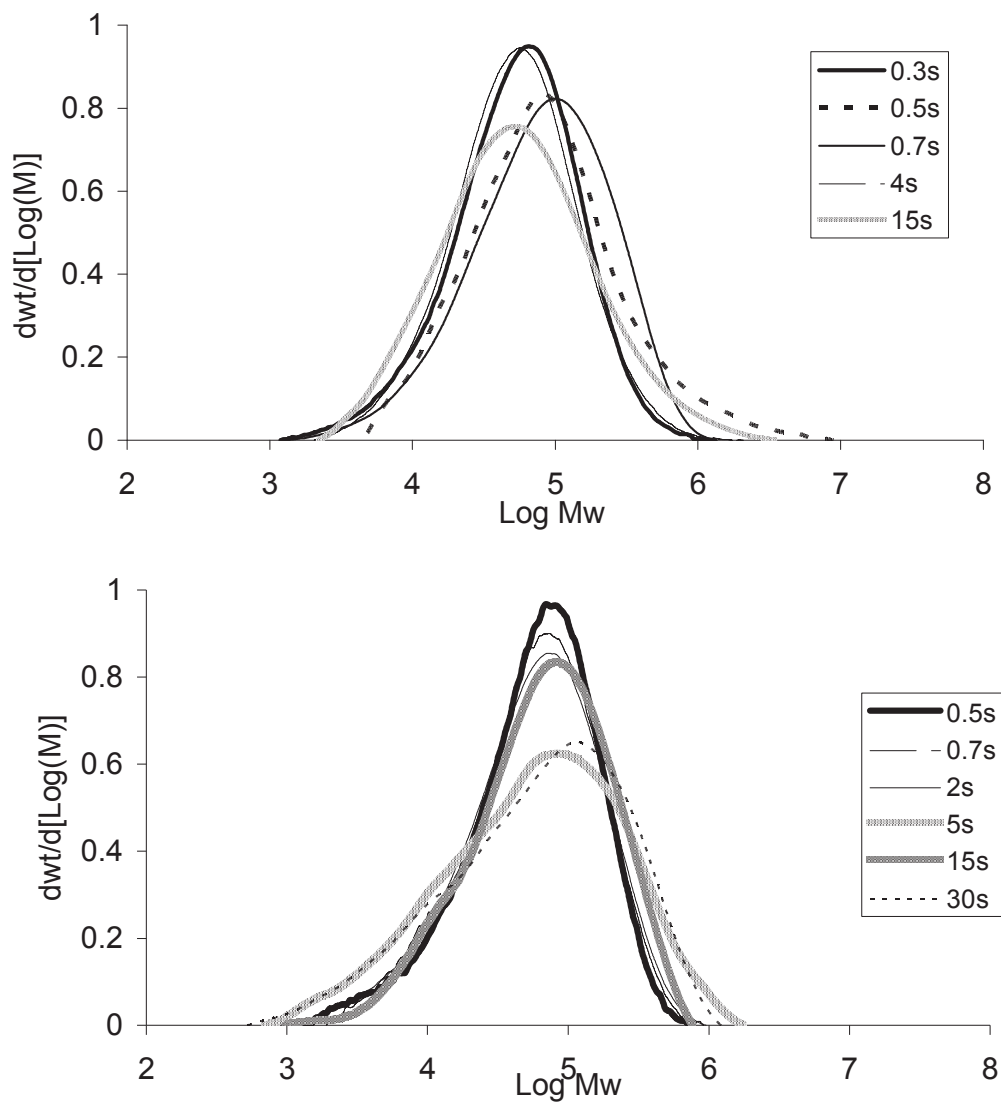


**Figure 21: MWD evolution of ethylene homopolymers produced with EtInd<sub>2</sub>ZrCl<sub>2</sub> (top) and (nBuCp)<sub>2</sub>ZrCl<sub>2</sub> (bottom) at 80°C.**

It is possible that the kinetic constants of propagation and transfer of the second metallocene complex are more sensitive to temperature variations. For a similar temperature evolution we obtain then a more heterogeneous mixture of chains. It is also possible that, due to the fact that, even if only for very short time, temperature gradients are present in our reactor, a very narrow molecular weight distribution is difficult to obtain over the whole reacting bed. This can be an intrinsic limitation of our stopped flow reactor due to its packed bed configuration. Nevertheless performing the polymerizations with a metallocene complex that is highly



sensitive to temperature values can be an advantage as the variations of the Mn and PDI of the polymers can be used as “sensors” to record the thermal history of the catalyst particles inside our reactor.

In Figure 22 the MWD evolution in case of co-polymerization is shown. Comparing it with bottom of Figure 21 it is easy to see that a higher transfer rate in case of copolymerization gives a distribution that is shifting clearly towards lower values with increasing reaction times. An important decrease in both Mn and Mw is seen as the reaction proceeds (from 30000 g/mol to 10000 g/mol and from 110000 g/mol to 50000 g/mol respectively in 30s of reaction). The active sites are gradually changing their behavior during the reaction course. This could be due to the reactor temperature variation or to an evolution of the active site in presence of the comonomer. It has to be reminded that this is the only case in this work where Mw decreases with reaction time. PDI of copolymers follows exactly the same trend of the homopolymers.

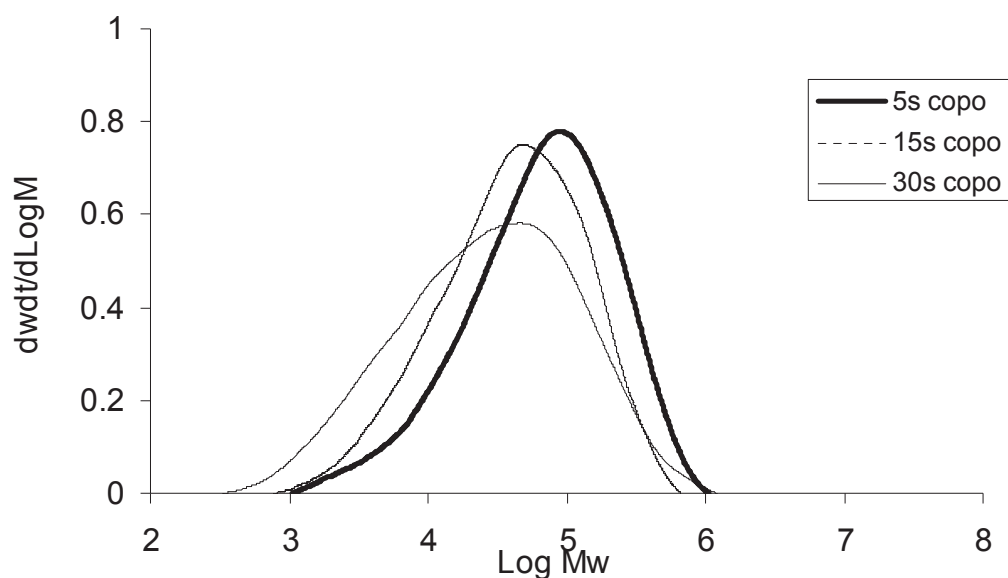


Figure 22: MWD evolution during co-polymerization with  $(nBuCp)_2ZrCl_2$ .

### 3.3. Influence of the nature and quantity of the Al

#### 3.3.1. Influence of Aluminium content

Apart from changing the nature of the Zr by switching to another metallocene complex, the active site behavior can be modified during the catalyst preparation by playing on the amount of Zr adsorbed on the inorganic support. It would then have been logical to study the effect of

the quantity of Zr just after have studied the effect of the nature of Zr. Unluckily, as we will explain more in detail in the related section, increasing the quantity of Zr in the final catalyst cannot be done without increasing the quantity of Al supported on silica. This is logical as the active center is formed by the ion pair  $Al^- Zr^+$  at the silica surface and an increase in Zr content should be counterbalanced by an increase in the Al content in order to maintain the catalyst activity. Each Zr atom needs in fact in average a high number of Al atoms to generate an active site with acceptable activity. Just putting more Zr during the synthesis leads to inactive catalysts (see paragraph 3.4 for more details). Decreasing the quantity of Zr would have been possible but, due to the very low metal concentration already present in the reference catalyst we preferred to avoid this option. These are the reasons why the discussion on the influence of the Al supporting procedure on the catalyst behavior at the reaction start-up will precede the one referring to the influence of the amount of Zr .

The active site in olefin polymerization is formed upon reaction between the metallocene precatalyst and the cocatalyst (MAO in our case). This creates the vacant site and the metal carbon bond needed for olefin coordination and insertion. It is known from various publications that the ratio between Al and Zr has an influence on the activity of the final catalyst and on the MWD of the polymers produced [15-18]. An investigation on the influence of the aluminium content on the reaction start-up will be presented in the following paragraphs.

The catalysts synthesized up to now in this work showed an aluminium content of about 7 +/- 1 wt % and were prepared by adding a fixed amount of a 10 wt % MAO solution on a suspension of silica in toluene. The amount was calculated in order to add 15 wt% Al to the support. It is clear that it was possible to fix only half of the added MAO on the silica surface. Increasing the quantity of alkylaluminium solution added to the suspension, no improvement in the amount of fixed Al was measured. This comes from the adsorption isotherm of MAO on silica. In order to react more alkylaluminium with the hydroxyl groups of the silica, a more concentrated initial solution is needed. For this study a 30 wt % MAO solution from Albemarle was then used and the same supporting procedure as described in Chapter 2 and in the experimental part was used. The  $(nBuCp)_2ZrCl_2$  complex was used for this study as we have seen that its higher activity and its sensitivity to temperature variations could help us in determining the thermal history of the catalyst particle during the reaction start-up and its dependence on the factors varied in this section.

The final catalyst has an Al content of 12.4 wt% and a Zr content of 0.66 wt% and it was tested in a 2L gas phase reactor at 80°C and 6 bar of ethylene pressure. Results are presented in the following table. It has to be remembered that the catalyst bearing a lower Al content had also a Zr content of 0.31 wt%, which is half of what it is found here.

Table 3: Activity and polymer properties of catalyst with higher Al content.

<i>Exp</i>	<i>Catalyst</i>	<i>Activity</i> (gPE/ mol Zr/ h)	<i>Mn</i> (g/mol)	<i>Mw</i> (g/mol)	<i>PDI</i>	<i>Crystallinity</i> (%)	<i>Tm</i> (°C)
ETPE77	ETmet46	4.5E+06	49000	130500	2.67	62.5	131.6

The MWD and the thermal properties of the polyethylene are not dependent on the Al content of the catalyst while the activity per mole Zr is doubled if a higher amount of Al is fixed onto the silica (as might be expected).

### 3.3.1.1. Activity and temperature profile at start-up.

The catalyst was tested in the stopped flow reaction under the same conditions used in the previous paragraphs. It is quite noticeable from Figure 23 that the evolution of the temperature of the outlet gas stream is quite different from what has been seen up to now.

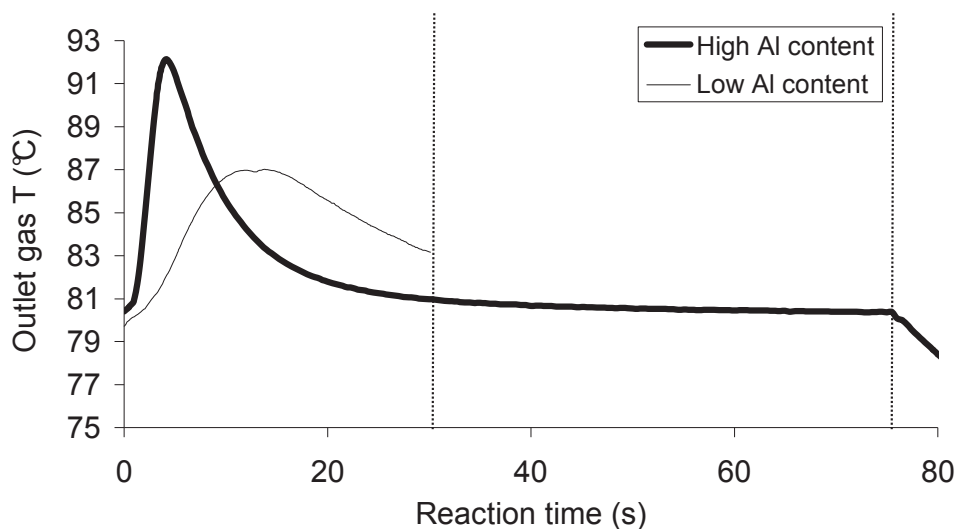


Figure 23: Outlet gas temperature evolution using catalyst with low Al content (30s) and high Al content (75s), 30 mg catalyst.

Figure 23 shows how, for the same amount of catalyst, the temperature increases more rapidly and to higher values if a support with high Al content is used. It seems that this catalyst is highly active at the beginning and that deactivates faster than what seen up to now. In order to optimize the quantity of heat generated with the new catalyst a sensitivity study on the catalyst mass needed to be performed before proceeding.

Different experiments lasting 75s were performed with varying catalyst mass and the yield and the maximum gas phase temperature excursions were measured (Figure 24). Yield reaches stable values for catalyst amount at least equal to 25 mg while outlet gas temperature excursion is increasing linearly with the catalyst mass. In order to minimize the temperature increase and maximize yield, a catalyst mass of 25 mg will be used for reactions longer than 2s. This gives a measured outlet gas  $\Delta T$  of about 12°C, which is close to what has been measured for the other catalysts and thus low enough to avoid polymer melting.

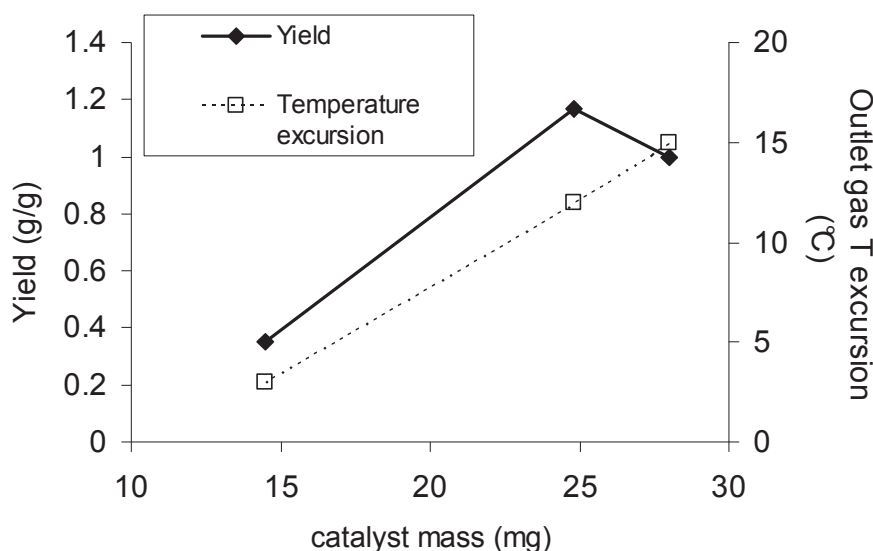
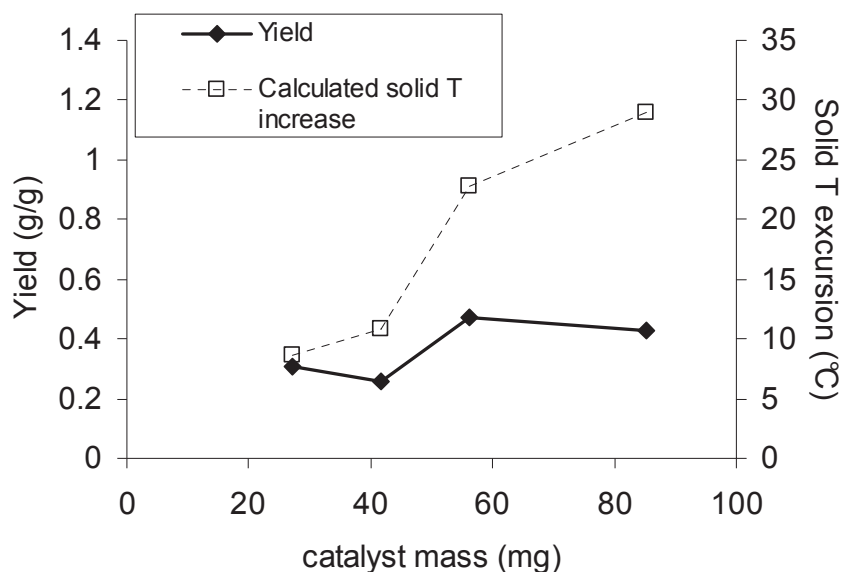


Figure 24: Influence of catalyst amount on yield and outlet gas temperature; 75s reaction time

But since this catalyst seems to be very active at the beginning and due to the fact that, according to simulations of temperature profiles inside the bed (c.f. chapter 2), the temperature peak at the particle level should appear between 1 and 2s, the same kind of analysis must be conducted for short reaction times. In addition we noticed that for a reaction lasting 0.3s performed with 80mg of catalyst (as was done for the other catalysts) the outlet gas phase temperature reached a value of 95°C during the CO<sub>2</sub> flow, which is clearly too high. Different experiments lasting 0.7s were performed with varying catalyst mass and the yield and the calculated average solid temperature excursions were compared.



**Figure 25: Influence of catalyst amount on yield and outlet gas temperature; 0.7s reaction time**

Figure 25 shows that the yield is constant around 0.3 +/-0.1 g/g with varying catalyst amount. On the other hand the calculated average solid temperature increases with the catalyst mass and excursions can be higher than 20°C if more than 40mg are used. In order to minimize the temperature increase and maximize yield, a catalyst mass of 30 mg will be used for reactions shorter than 2s. In synthesis a constant catalyst amount around 25-30mg will be used independently on the reaction time.

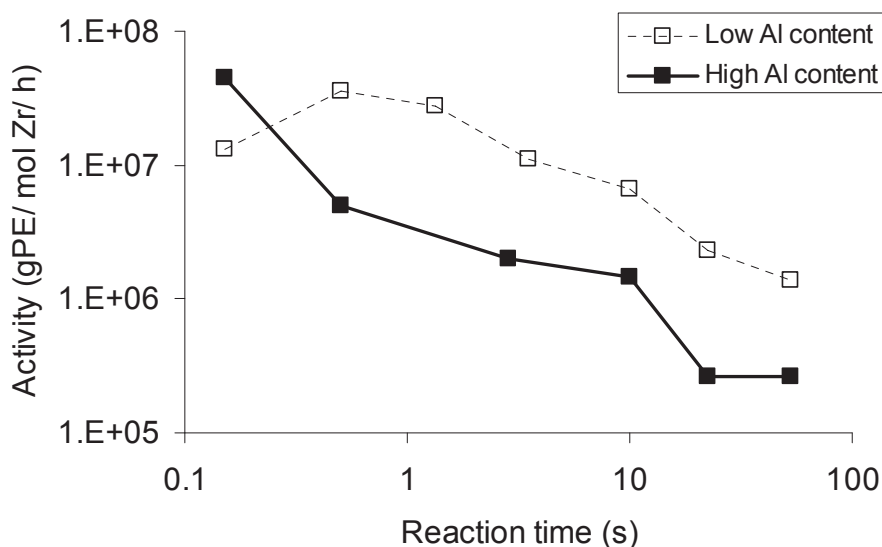


**Figure 26: Influence of Al content on activity at the start-up**

Figure 26 shows that an increased Al content is responsible for a very active catalyst at the start-up of the reaction (as suggested from the measured temperature profile). The increased

initial activity respect to the reference catalyst is even more visible by looking at Table 4, where the activities expressed in g/g/h are presented.

**Table 4: Influence of Al content on activity expressed in g/g/h.**

<i>Reaction time (s)</i>	<i>Yield reference(g/g)</i>	<i>Yield high Al (g/g)</i>	<i>Activity reference (g/ g/ h)</i>	<i>Activity high Al (g/ g/ h)</i>
0.3	0.023	0.27	276	3240
0.7	0.1	0.31	738	360
5	0.5	0.48	228	142
15	0.88	0.77	137	105
30	1.08	0.85	48	19
75	1.44	1.09	29	19

The activity peak appears suddenly after 0.15s of reaction. It is possible that the higher Al content is responsible for a better site activation or for the production of a higher number of active sites having a “one-off” way of functioning. The activity then decreases rapidly and stabilizes after 20s to values 1 order of magnitude lower than the ones obtained from the catalyst with lower Al content. The result is unexpected as the same catalyst tested in a 1h long reaction showed an activity twice higher than the reference. The difference between the two reactors, as already said, is the presence of scavenger (TEA) in the big reactor while it is absent in the stopped flow reactor. It is possible that the high concentration of Al onto the support results in a high surface density of Al centers. This could be responsible of a very short distance between some active Zr atoms that can mutually deactivate each other. Note, in fact, that the Zr quantity is almost doubled when the Al quantity is increased. Independently of the reason for which some active centers can deactivate, if additional alkylaluminium is present during the reaction, it can activate some inactive or dormant sites and increase the catalyst activity [19]. If no scavenger is present the deactivation process is unstoppable. It is also possible that a thermal deactivation is happening here. It is true that here the temperature excursions in the first reaction seconds are similar to the ones measured with the reference catalyst but it has to be remembered that the catalyst amount for each reaction is greatly reduced. If a comparable quantity of heat is produced, the temperature at the particle level is higher.

3.3.1.2. MWD evolution

A comparison between the MWD evolution of the polymers produced using catalyst bearing different Al content is shown in Figure 27. It has to be noticed how increasing the quantity of Al is responsible for the production of an higher quantity of shorter chains and of polymers having lower average molecular weights for a given reaction time. Also in this case supported  $(n\text{BuCp})_2\text{ZrCl}_2$  produces bigger and bigger chains with increasing reaction times. Mw in fact increases constantly in the studied reaction time from 70000 g/mol to 140000 g/mol. In general, but especially from 15s of reaction, the MWDs are broader if more Al is present on the support. The PDI in fact increases steadily in 15s to quite high values (7-8) and remains high even after 75s of reaction. The catalyst with lower amount of Al produces polymers with PDIs increasing gradually up to 5 after 30s of reaction. These observations support the idea that a thermal deactivation can be the reason for the strong decaying activity profile measured in the stopped flow reactor.

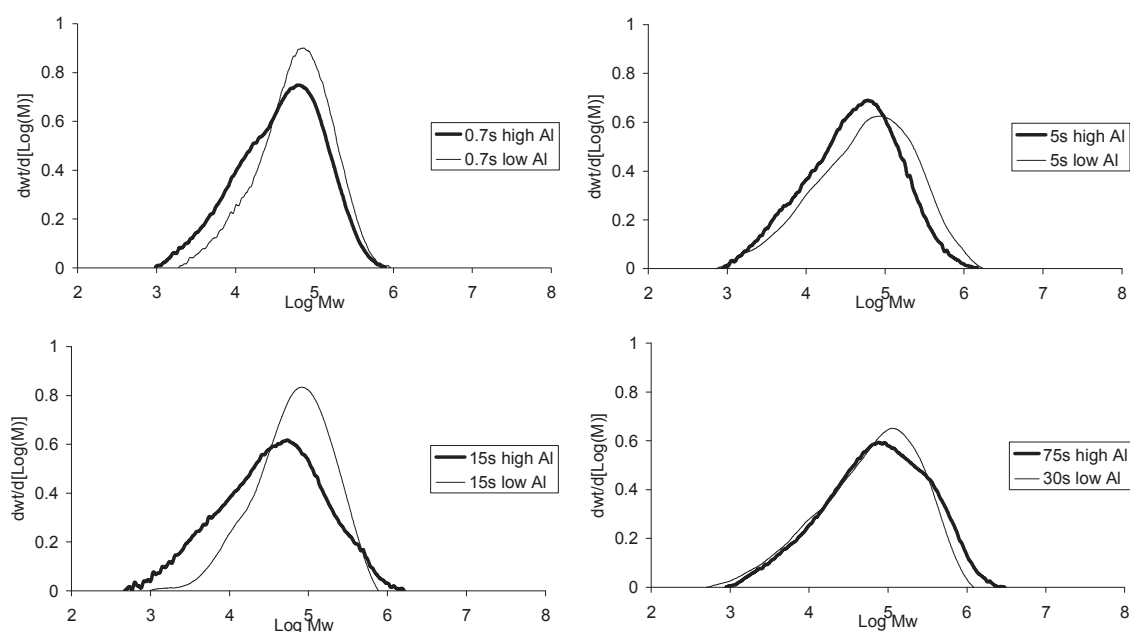


**Figure 27: Influence of Al content on MWD evolution.**

This idea is partly confirmed by Figure 28, where the calculated average solid temperature dependence on reaction time for the catalyst bearing an high amount of Al is plotted. These values are compared to the ones obtained performing the same reactions with the supported  $(n\text{BuCp})_2\text{ZrCl}_2$  bearing a lower Al amount.

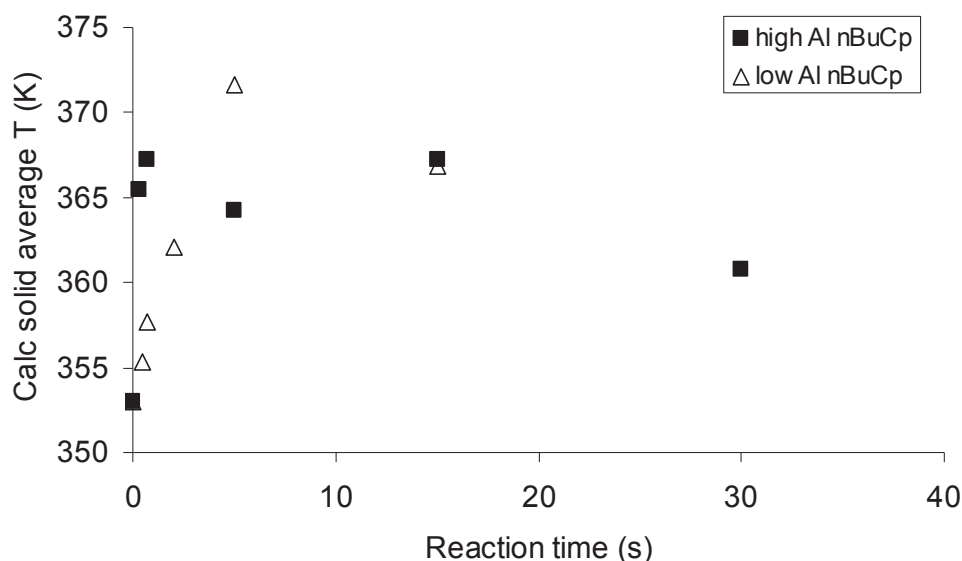


**Figure 28:** Calculated average solid T using supported  $(nBuCp)_2ZrCl_2$ ; dependence on Al content.

It can easily be seen that during the reactions performed with the catalyst containing a high quantity of Al the growing particles are exposed to high temperatures from the very beginning of the reaction. In other words they work at high temperatures for longer times than during the reactions performed with the catalyst having a lower Al content. This comes from the activity of the catalyst, which is very high at very short times for the first catalyst (c.f. Figure 26). The rate of transfer reactions is then important and production of shorter chains is favored. In addition such activity profile is responsible for the fact that the quantity of polymer produced after 15s is negligible respect to the one produced earlier. The impact of the polymer produced in the second part of the reaction on the average Mn and PDI is then negligible even if it has been synthesized under controlled conditions (lower temperatures) and the MWD cannot become as narrow as it was at very short times.

### 3.3.2. Cocatalyst impregnation time

The role of the Al in the active site behavior at reaction start-up can not only be studied by changing the quantity of Al present on the final catalyst, but also the homogeneity of its distribution. This can be done by varying the conditions of the reaction between MAO and silica during catalyst preparation. One of the main concerns while supporting MAO on mesoporous silica is to have a homogeneous distribution of the bulky alkylaluminium into the particle pores. Due to the size of the MAO molecule, some mass transfer limitations might be present, potentially leading higher concentration of Al in the outer part of the particle and to the production of hollow polymer particles. The works presented in literature investigate the



influence of impregnation temperature and time on the distribution of Al into the particle pores [20-22] (see related section of the literature review chapter). Due to the fact that the impregnation temperature of our supporting method is a result of an optimization work, here we will focus on the influence of cocatalyst impregnation time on the catalyst behavior at the polymerization start-up. A further motivation for this decision comes from the results of a similar work conducted by Tisse in her PhD study [23]. She showed that for “classic” long reactions, activity of the bigger metallocene catalyst particles is improved if the MAO impregnation time is raised from 1h to 4h. This might possibly be symptom of the existence of diffusion limitation during the MAO impregnation step.

To see if MAO diffusion limitations are present and if they have a strong influence on catalyst behavior, we prepared a supported  $\text{EtInd}_2\text{ZrCl}_2$  catalyst on silica treated with MAO for 4h instead of 1h. As we are focusing here on the role of Al impregnation time, the type of metallocene used is less relevant. The impregnation temperature has been kept constant at 85°C. The two catalysts have similar Al content (6.5 +/- 0.3 wt %) and Zr content (0.27 +/- 0.06 wt %).

The catalyst produced with longer alkylaluminium impregnation time has been first of all tested in the 2L gas phase reactor at 80°C and 6 bars of ethylene pressure. The measured activity is of  $1.7\text{E}+06$  gPE/ mol Zr/ h, very close to the one measured for the catalyst produced using an impregnation time of 1h. The polymer produced has a Mn of 36000 g/mol and a Mw of 114000 g/mol, values very close to the ones measured usually. The PDI is around 3, and it is 1 point lower than what is usually measured using a catalyst prepared with the normal procedure. In this case PDIs around 4 are normally found. It can be that a longer MAO impregnation time is responsible for a better distribution of the alkylaluminium in the inorganic support and for a more efficient formation of the  $\text{Zr}^+-\text{Al}^-$  ion pair thus determining a more similar behavior of the different active sites.

A set of short time experiments has been performed using the “long impregnation time” catalyst and results have been compared to what obtained for the reference catalyst. Reaction conditions are as previously: 80°C, 6 bars of ethylene, 3 bars of helium, gas velocity of 20 cm/s, fine NaCl as seedbed and catalyst mass varying from 30 to 80mg according to reaction time. As visible from Figure 29, multiplying the cocatalyst impregnation time by 4 has only a small effect on catalyst activity.

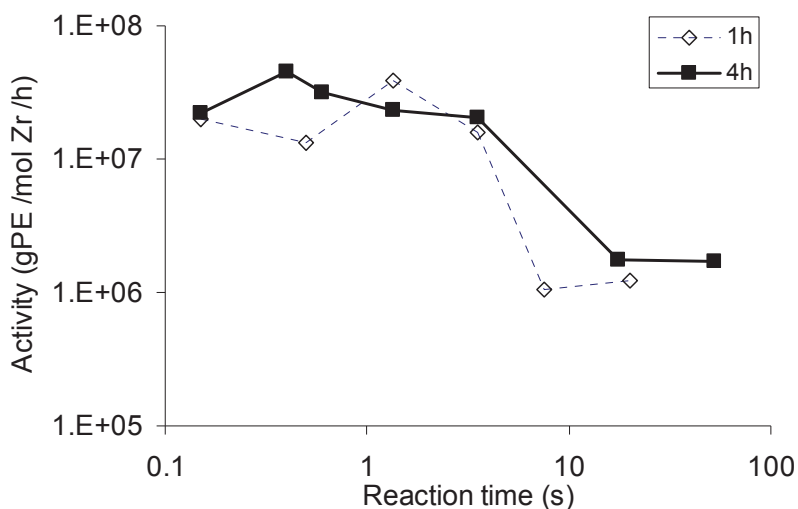


Figure 29: Influence of MAO impregnation time on catalyst activity profile.

For reaction times higher than 5s a rapid decay to a plateau corresponding to the final activity values is measured (as usual). For this time range the activity of the catalyst produced with long impregnation time is 40 % higher. Similar findings for 1h reaction time in slurry phase have been described in the work of Tisse with the same catalyst/support system (although she studied the influence of MAO impregnation time only on large particles with dimensions between 80 and 100  $\mu\text{m}$ ).

Figure 30 shows the outlet gas temperature profile for reactions conducted at 75s using these two catalysts. It can be seen that a longer MAO impregnation time gives a higher temperature peak and a faster increase. Even after some tens of seconds the outlet gas temperature is higher if longer impregnation times are used. This reflects what has been explained in the paragraph just above.

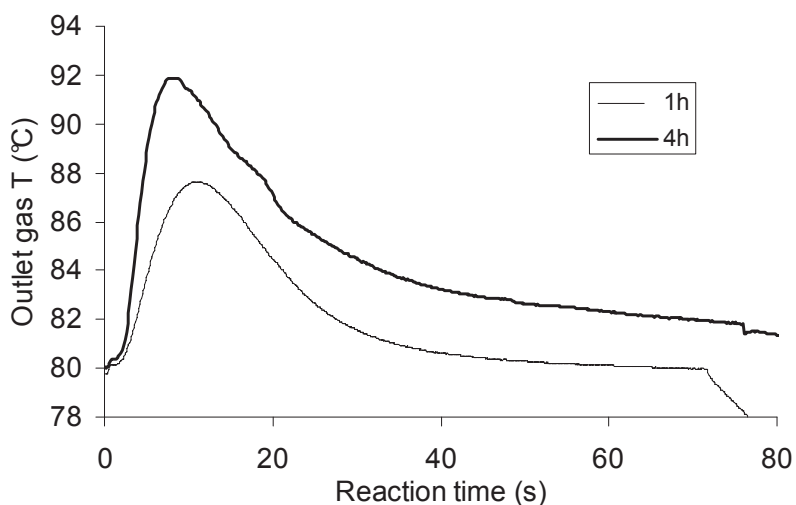


Figure 30: Outlet gas temperature profile for 75s reaction: MAO impregnation time comparison

The MWD evolution of the polymers with reaction time is represented in Figure 31 (bottom) and compared with the results obtained with the “short impregnation time” catalyst (top). The molecular weights of the polymers remain constant during the studied reaction time (only for the reaction lasting 0.5s a slight decrease is seen). These values are similar to the ones found after 1h reaction in a classic reactor. The PDI is constant all along the studied reaction times around a value of 3 and the MWD of the polymers is narrower if MAO is impregnated for longer times during the catalyst preparation. The reference catalyst under the same reaction conditions produced polymers having a PDI around 4.

In conclusion increasing the impregnation time of MAO on silica seems to lead to a better activation of the metallocene and to an active site which, even for short reaction times, is capable to produce polyethylene with a sound control over the transfer reactions.

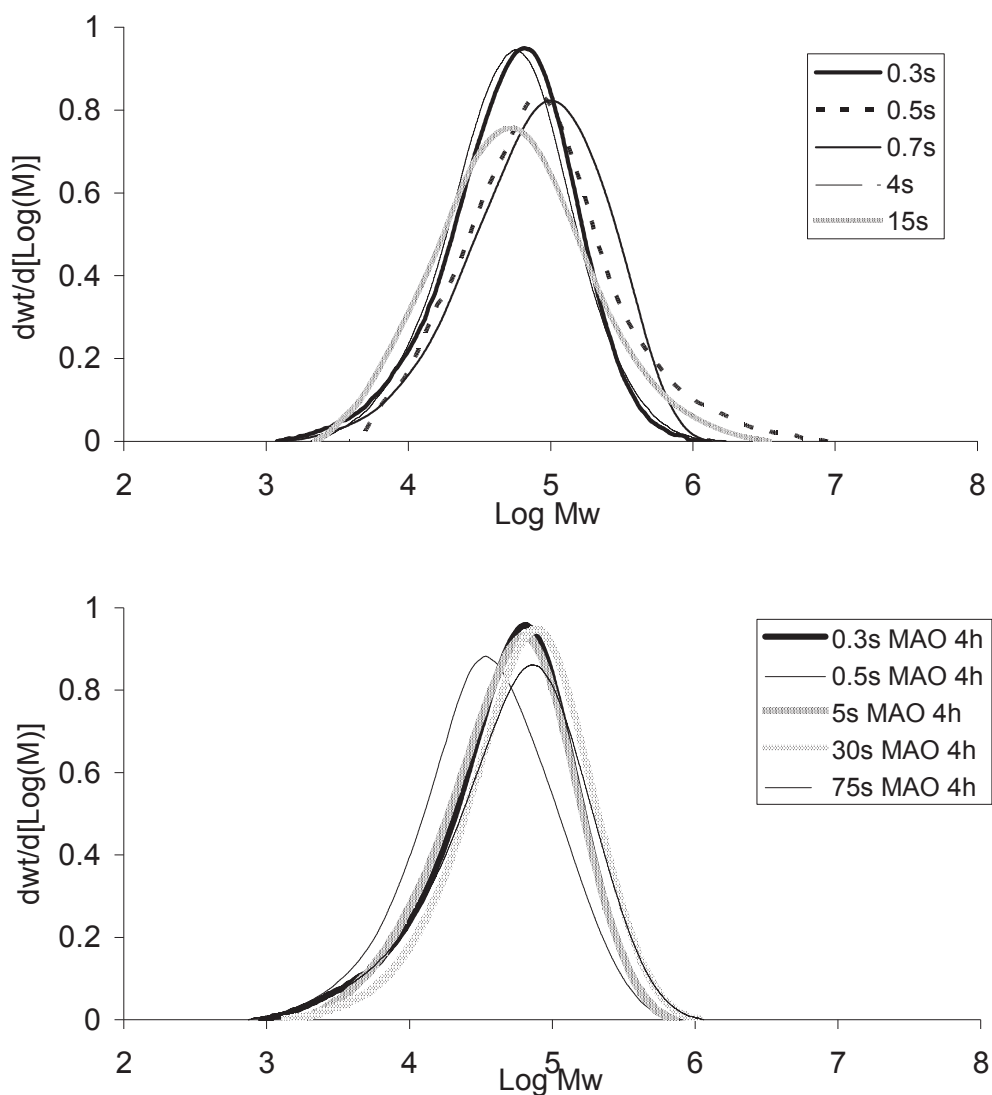


Figure 31: Influence of MAO impregnation time on MWD evolution of polymers: 1h (top) and 4h (bottom).

### 3.3.3. Conclusions

The role of the Al atom on the behavior of the active site during the reaction start-up seems to be complex and important at the same time. It has been seen that an increase of the quantity of Al supported onto the silica particle can be obtained by working with more concentrated MAO solutions. A simple Al content increase in the final catalyst modifies consistently the active site behavior. Much higher activities at the very early reaction stages are measured together with MWD that are generally broader because of the increased tendency to produce small chains. The formation of “one-off” extremely active sites seems to be favored when a lot of Al is present in the catalyst. This leads to the development of high temperature gradients in the reactor from the very beginning of the reaction and can explain the broad MWD and the production of small chains.

It is also interesting to note that the catalyst having a higher density of active sites (more Al and more Zr) deactivates very quickly in stop flow reactions. Active sites that are too close each other can easily combine to form inactive species. These can be reactivated if an excess of alkylaluminum is present in the reactor, as in the case of 1h reactions, where the activity is higher if more Al is present in the catalyst. In stopped flow reactions, where no additional alkylaluminium is added, deactivation continues unperturbed and the activity of the catalyst having a lower amount of Al is one order of magnitude higher for the studied time range.

The distribution of the Al atom inside the support particle has been varied, keeping its amount constant, by varying the time of contact between MAO and silica. It has been seen that this leads to a more homogeneous activation of the Zr species, as slightly higher activities at long reaction times and narrower MWDs at short and long reaction times are measured. This could be used as an additional method (together with a research on the best reaction conditions) to ensure the production of polymers under a fully controlled regime from the very first reaction instants.

## 3.4. *Influence of Zr content*

It is known from the literature that the amount of Zr supported on a heterogeneous metallocene has a great influence on the catalyst performance. There is a non linear relation between the quantity of fixed Zr and the activity: if an insufficient amount of precatalyst is adsorbed on the MAO-treated support, then there are not enough active centers to ensure

fragmentation of the support and a good polymer production. On the other hand if too much precatalyst is used, the high density of Zr centers is responsible for the formation of inactive species and the specific catalyst activity decreases. There is thus an optimum concentration of Zr in order to obtain the highest possible activity. The interested reader is referred to the works of Dos Santos et al. [15, 16, 24-26] for a more detailed discussion.

In this paragraph results obtained using a catalyst containing a high amount of Zr will be exposed and compared with the reference (nBuCp)<sub>2</sub>ZrCl<sub>2</sub> supported on MAO treated silica. We first tried to increase the Zr content of the final catalyst just by adding more precatalyst during the reference supporting procedure (that is onto the suspension of the silica treated with a 10 wt % MAO solution). As can be seen from the first two rows of Table 5 no big increase in the amount of Zr fixed is measured after this simple modification. In addition the higher the quantity of Zr added to the preparation is, the lower is the efficiency of the impregnation. It is also remarkable to notice that activity, both in the stopped flow reactor and in the 2L reactor drops when a higher amount of Zr is used during the supporting procedure. The two last rows of Table 5 refer to catalysts prepared from a support having an high Al content. First of all it can be seen that using this support is the only effective way to increase the amount of Zr in the final catalyst (column 5). Activity of the catalyst ETmet47 in the stopped flow reactor is the highest among the catalysts prepared with high amount of Zr, even if this value is lower than the reference. This is probably coming, as said previously, from a combination of some zirconocene molecules to form inactive species. In fact catalysts showing the lower Al/Zr show the lower activity in stopped flow reactions.

**Table 5: Comparison of different ways to increase Zr content in the finished catalyst and activity of them.**

<i>Catalyst</i>	<i>Wt % Al added</i>	<i>Wt % Al fixed</i>	<i>Wt % Zr added</i>	<i>Wt % Zr fixed</i>	<i>Al/Zr (mol)</i>	<i>Activity stopped flow (gPe/ mol Zr/ h)*</i>	<i>Activity in 2L reactor (gPe/ mol Zr/ h)</i>
Ref.	15	9.0	0.5	0.38	80	1.5 E+06	2.6 E+06
ETmet30	15	8.53	4.0	0.47	62	1.5 E+05	0
ETmet46	15**	12.4	0.5	0.66	65	2.7 E+05	4.5 E+06
ETmet47	15**	13.3	1.0	1.0	45	4.5 E+05	traces

\* Activity calculated for a 75s reaction under optimized conditions

\*\* Prepared from 30 wt% MAO solution.

It can be concluded that increasing the Zr content on our support using the standard procedure is a critical step if one wants to maintain the long term activity because of the too low values of the Al/Zr. Nevertheless being our objective to study the influence of the amount of Zr on the final catalyst at the reaction start-up we decided to choose catalyst ETmet47 to perform the study and to compare the results with the ones obtained with the catalyst having a comparable Al amount (ETmet46).

### 3.4.1. Activity and MWD profile

In Figure 32 a comparison of the activity evolution of the reaction start-up for different contents of Al and Zr is presented. It has to be said that the initial activity of the catalyst containing a high quantity of Zr is not as high as the one of the catalyst containing a lot of Al and studied in paragraph 3.3.1 so that temperature excursions are limited and the usual amount of catalyst is used in these reactions (that is 80 mg for reactions shorter than 2s, 40mg for 2s reactions and 30mg for longer reactions).

The initial profile of the reaction rate curve follows the one of the reference catalyst. The initial temperature excursion seems to be limited enough to avoid a massive active site deactivation differently from what is happening when a catalyst with a high Al content is used. This situation is similar to the one of the reference catalyst. The second part of the activity curve follows the one corresponding to the catalyst with a high amount of Al. In this case a high density of both Al and Zr and a low Al/Zr ratio can be responsible for formation of inactive species as discussed above. This deactivation is strong enough that even in a 2L reactor, where additional alkylaluminium is present, the reaction rate is low. This is confirmed by the fact that the activity values measured for a catalyst containing a high amount of Zr are almost always lower than the ones of the other catalysts.

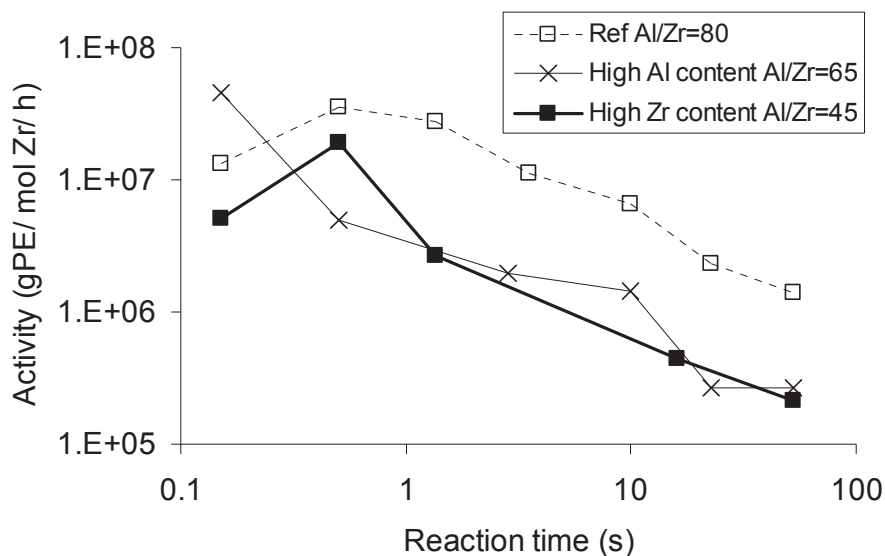
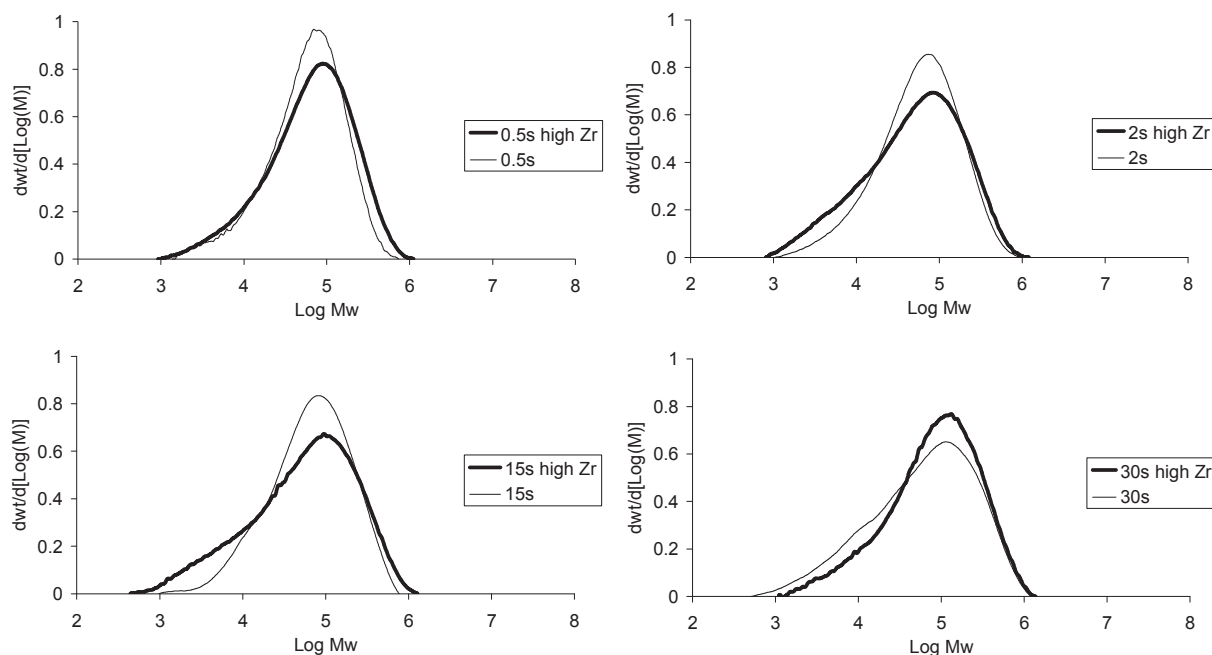


Figure 32: Influence of Al and Zr content on activity at the reaction start-up.

Figure 33 shows the MWD evolution of the polymers produced using this catalyst. There is generally no big differences between the MWD of the polymers produced at a certain reaction time using two catalysts bearing different Zr content. Only between 2s and 15s the catalyst with more Zr shows an increased tendency to produce smaller chains. This difference is only temporary as after 30s of reaction the two catalysts produce polymers having more similar MWD. The  $M_n$  decreases from values of 30000 g/mol to 15000 g/mol in 15s then goes back to the initial values.  $M_w$  increases from 90000 g/mol to 170000 g/mol and PDI shows a sudden increase up to 7 in the first reaction seconds while it decreases to values around 5 (close to what is measured for the polymers produced with the catalyst having a low Zr content) for longer reactions.



**Figure 33: MWD evolution of polymers produced with catalyst having high and low Zr content**

In general the  $M_n$  and the PDI values follow the same trend than the ones related to the catalyst having high Al content for the first 15 reaction seconds and then evolve in a manner similar to the reference catalyst (c.f. Figure 27).

In conclusion it seems that the Al content in the final catalyst is responsible for the MWD evolution in the first reaction seconds: the higher it is, the lower the  $M_n$  and the higher the PDI. It is possible that enhanced transfer to the alkylaluminium is the reason for this behavior. For longer reaction times the behavior is less dependent on the metal content.

In any case the sensitivity of  $(n\text{BuCp})_2\text{ZrCl}_2$  to temperature excursions is confirmed in this section: no matter how the catalyst is prepared, MWD broader than expected (PDI around 5 instead of 3) are always measured after a certain reaction time.

### 3.5. Conclusions

The results presented in the previous paragraphs show that describing the behavior of the supported metallocenes at the reaction start up is a quite difficult task. The particular reaction phase under study is still a kind of unexplored land and the formation and the functioning of the active site of ethylene polymerization is known to be a complicated subject. Nevertheless some general conclusions on the effect of the catalyst preparation on the reaction start-up can be given.



First of all we have seen that changing the environment around the Zr atom by changing the metallocene complex is responsible for a strong modification of the catalyst behavior during reaction start-up. Even more important to say, these differences can be in conflict with what is found for long term reactions. For example a  $(n\text{BuCp})_2\text{ZrCl}_2$  based catalyst produces a narrower polymer respect to a  $\text{EtInd}_2\text{ZrCl}_2$  based catalyst in long term reactions (PDI of 2.8 and of 4 respectively). On the contrary in stopped flow reactions a PDI increasing with reaction time from 3 to 6 is usually measured using the non bridged complex. Higher sensitivity to temperature variations for the  $(n\text{BuCp})_2\text{ZrCl}_2$  complex is thought to be responsible for these results. It is in fact inevitable to have, at least for few seconds, a temperature gradient in our stopped flow reactor. This sensitivity can be used advantageously as it is an indication of the thermal history undergone by the catalyst particle.

Increasing the quantity of Zr on the final catalyst seems to favor the production of inactive species (lower specific activity in stopped flow reactions and negligible activity in long term reactions) without decreasing the sensitivity of the catalyst to temperature variations (gradual MWD broadening with reaction time).

The role of the Al atom on the active site formation and on its behavior at reaction start-up seems to be more complicated. Increasing the quantity of Al present on the support (keeping the Al/Zr ratio almost constant) gives a catalyst much more active in long term reactions. The same is true also in stopped flow reaction but only for a very short time ( $< 1\text{ s}$ ). For longer times the opposite trend is measured. It seems then that a high quantity of Al is responsible for the formation of a high number of sites initially very active which probably deactivate because they generate too much heat to remain stable. The increased density of active sites of this catalyst (both Al and Zr content are increased) can also be responsible for a more easy combination of neighboring active sites into inactive species. In long term reactions the presence of external alkylaluminium can be responsible for a re-activation of part of them, which is not possible in our stopped flow reactor as no additional alkylaluminium can be easily added in this system. The strong initial evolution of the active sites of a catalyst containing a big amount of Al together with the high amount of heat generated locally by the “super-active” sites can be responsible for the broad MWD and the increased tendency to produce small chains measured in this case after few reaction seconds. Increasing the contact time between the alkylaluminium and the hydroxyl groups of the inorganic support during MAO impregnation on silica is responsible for a more efficient formation of the active ion pair throughout the entire particle. This is proven by the production of polymers having

slightly narrower MWD respect to the reference case both for long term and for stopped flow reactions. This is probably due to an increased homogeneity of the alkylaluminium complex inside the particle causing a more homogeneous formation of the different  $Al^-Zr^+$  ion pairs.

## 4. Influence of support properties

### 4.1. Introduction

When a polymerization is performed using an heterogeneous catalyst, its method of preparation and the molecule used as precatalyst are not the only factors influencing the performances of the finished product. The properties of the carrier are also very important. Support size and porosity are fundamental in determining the rate of mass and energy transport, the active site and cocatalyst distribution and the fragmentation path.

It is known from the literature that the size of the particles of the carrier is influencing the heat transfer rate and thus the activity of the polymerization [21, 27, 28]. Bigger particles exhibit a poorer heat transfer capability and a lower activity than small particles due to the increased heat and mass transfer resistances respectively. Porosity, pore volume and pore size of the carrier are known to influence the mass transport of the active species and thus the activity of the catalyst [21, 26, 29, 30]. Pores that are too small lead to non-active catalyst because of the diffusion limitations of the bulky MAO into the pores, because of pore blockage by the growing polymer or because of overly strong interactions between the carrier surface and the active species. The fragmentation path of the support is also influenced by the pore size distribution and by the location of the pores inside the particle volume [31]. If not enough large pores are accessible to the monomer then fragmentation might be very slow. A deeper discussion on the subject can be found in the literature review chapter.

The literature on this subject deals with classic reactions at steady state. Nevertheless these effects might be different at the reaction start-up when activity is at least 1 order of magnitude higher than at steady state and temperature excursions can be large and sudden.

In the following paragraphs we will study the effect of support properties including particle and pore size on the activity profile and MWD evolution at the reaction start-up. In order to

have comparable results to build a general picture of the influence of catalyst preparation and support properties on reaction start-up we used also here  $(n\text{BuCp})_2\text{ZrCl}_2$  as precatalyst.

## **4.2. Influence of support size**

In order to study the influence of support particle size different catalysts were synthesized having different carrier sizes. The reference support used in this work (Grace 948) was sieved in order to obtain different cuts and each fraction was treated at 200°C for 4h, as was done previously for the basic catalyst preparation. Catalysts were prepared from selected cuts with the usual procedure (1h treatment of the silica with MAO followed by 1h impregnation of metallocene) using  $(n\text{BuCp})_2\text{ZrCl}_2$  as precatalyst and a solution of MAO at 10 wt % in toluene. Zr and Al content of the different catalysts were measured to be sure that there was no influence of the particle size on the impregnation procedure. Ideally the catalyst should have been sieved after the supporting step in order to have imposed the same treatment to all the fractions. However, given the sensitivity of the catalyst to air, it would have been necessary to sieve the catalyst in the glove box and this is highly impractical. Nevertheless the supporting procedure is repeatable enough and the activity values will be related to the moles of Zr so that any differences in Zr concentration between the different fractions will be insignificant.

Two measurements of the weight percentage of each fraction of Grace 948 are represented in Figure 34. Such silica has an average particle size of 58  $\mu\text{m}$ , pore volume of 1.6 mL/g (corresponding to 75-80% of void fraction), surface area of 280  $\text{m}^2/\text{g}$  and average pore size of 24nm as measured by BET absorption technique (c.f. the experimental part Chapter). It can be seen from Table 6 how the particle size does not influence the support physico-chemical properties.

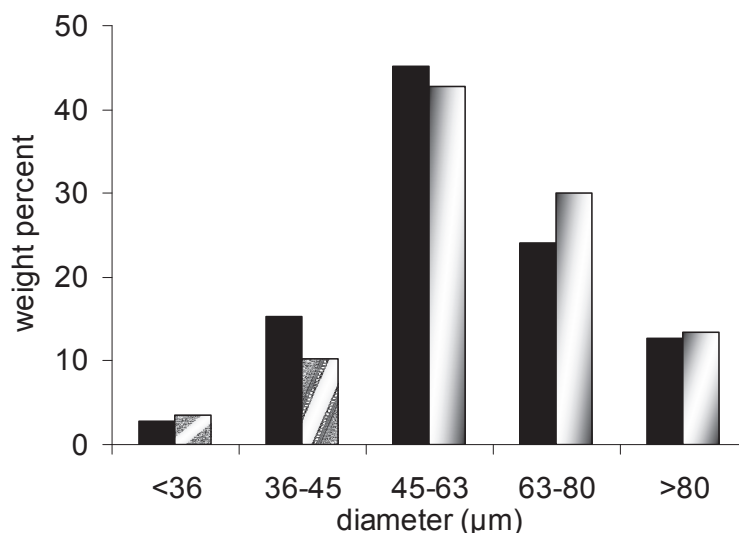


Figure 34: Relative weight of each fraction after sieving.

The support surface area, porosity and pore size have been measured by BET analysis. The concentration of OH groups has been measured by a methodology developed in our laboratory consisting of reacting TEA with the surface hydroxyl groups of the support and measuring the pressure increase caused by the production of ethane (c.f. the experimental part).

Table 6: Physicochemical properties of different silica fractions.

<i>Particle size (μm)</i>	<i>Specific area (m<sup>2</sup>/g)</i>	<i>Pore size (nm)</i>	<i>Pore volume (mL/g)</i>	<i>OH conc. (OH/nm<sup>2</sup>)</i>	<i>Zr content (wt %)</i>	<i>Al content (wt %)</i>
All	271	24.5	1.66	5.4	0.31	7.16
36-45	267	24.4	1.63	5.2	0.27	7.44
45-63	270	24.6	1.66	5.7	0.27	7.34
63-80	270	24.6	1.66	5.8	N.A.	N.A.
>80	269	24.6	1.65	5.6	0.23	7.12

For this study the cuts 36-45, 45-63 and >80 have been used as supports for catalyst heterogeneization. Each catalyst has been tested in a 2L gas phase reactor for 1h before performing short reaction times. The metal content of each catalyst has also been measured by ICP. Results are summarized in Table 7.

**Table 7: Influence of support size on activity and polymer properties in long term gas phase reactions.**

<i>Particle size (<math>\mu\text{m}</math>)</i>	<i>Zr content (wt %)</i>	<i>Al content (wt %)</i>	<i>Activity (gPE/mol Zr/h)</i>	<i>Mn (g/mol)</i>	<i>Mw (g/mol)</i>	<i>PDI</i>
All	0.31	7.16	2.4E+06	59000	165200	2.8
36-45	0.27	7.44	3.3 E+06	67000	192400	2.7
45-63	0.27	7.34	1.5 E+06	39200	128900	3.2
>80	0.23	7.12	0.8 E+06	N.A.	N.A.	N.A.

It is clear that, as already found in literature, bigger particle show a reduced activity. It seems also that Zr content decreases with particle size. Nevertheless it is difficult to say if this really an effect of the support diameter or the difference in the measured values is simply due to the experimental error.

#### 4.2.1. Activity and temperature profile at reaction start-up.

In order to study the influence of the support size on the behavior of supported metallocenes at the reaction start-up a series of reaction stopped at different times were performed for each catalyst.

Just by looking at the outlet gas temperature profile of 75s reactions it is possible to see that, while the first part of the profile is more or less similar for all the catalysts, from 30 s a clear tendency appears: the smaller the support size the higher is the temperature of the outlet gas phase. Two reasons for this immediately spring to mind: first, smaller particles have a better capability to transfer the reaction heat to the flowing gas, and second, smaller particles might give higher activities.

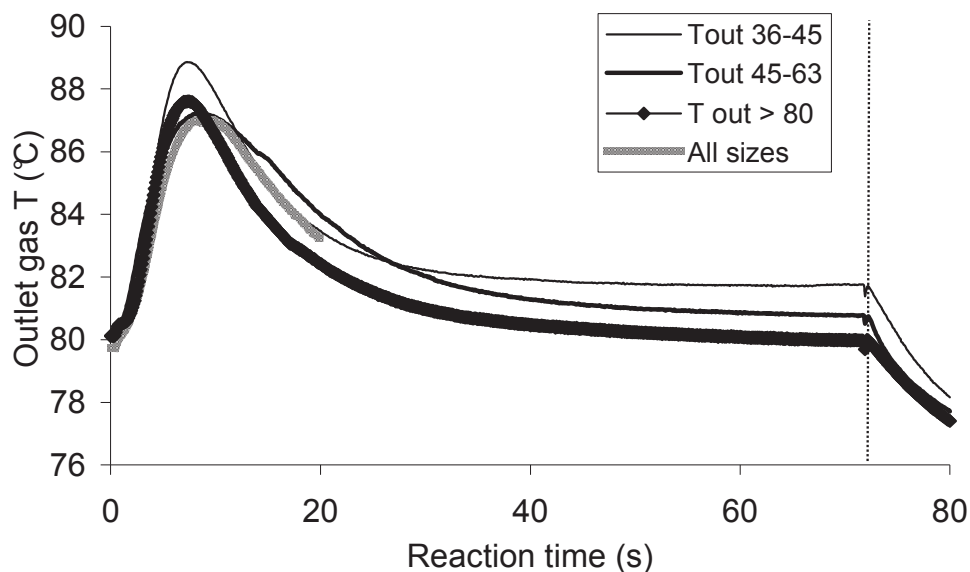


Figure 35: Influence of support size on outlet gas phase temperature

The second hypothesis is confirmed by plotting the measured value of activity for all the catalysts (Figure 36). The activity curve can be separated in two parts. The trend observed for 1h reactions starts to appear at reaction times of 20s and at 50s it is clear that the smaller particles have a steady state activity higher than the bigger ones.

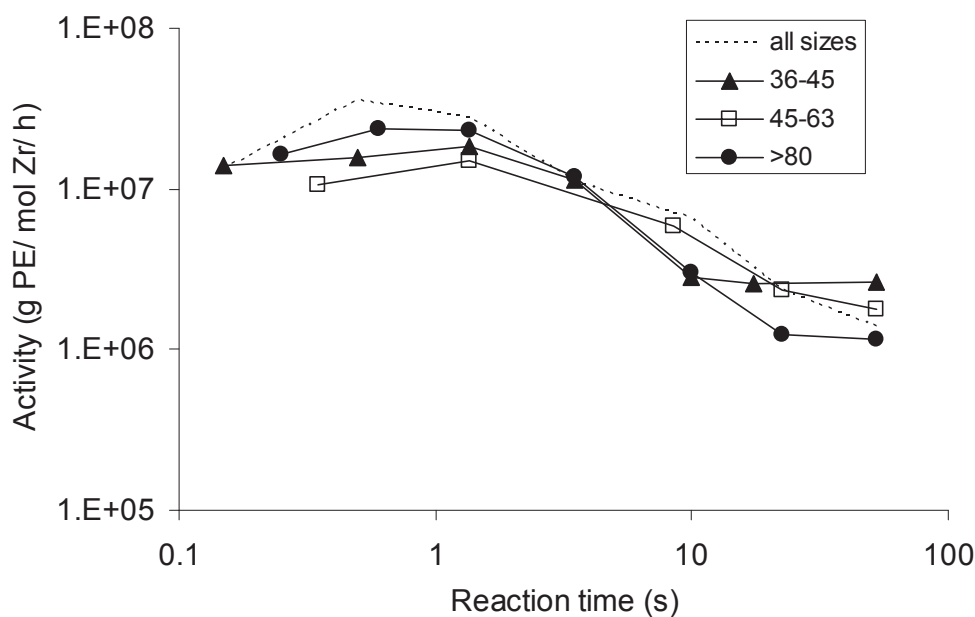


Figure 36: Influence of support size on activity profile using supported  $(n\text{BuCp})_2\text{ZrCl}_2$  at  $80^\circ\text{C}$ , 6 bar of ethylene.

For very short reaction times (up to 5s) there is no clear relation between support size and activity. It seems even than the bigger particles are more active than some other fractions. This can come from the fact that big particles may be hotter than the small ones at the reaction start-up (they have lower surface to volume ratio) It is remarkable to notice that the dynamics

of the activity profile is very similar for all the catalysts for reaction times lower than 5s with a maximum attained around 1s. This means that this behavior is not due to mass or heat transfer at the particle scale but it is more likely dependent on the intrinsic catalytic behavior (active site evolution) or on the pore filling and support fragmentation path. The transition between the two situations described happens between 5 and 20s when the bigger is the particle, the higher is the decay in activity.

#### 4.2.2. MWD evolution

The MWD of the polyethylene produced with these catalysts does not show a clear dependence on the support size. There are some tendencies that can be observed and common trends that are found using supported  $(n\text{BuCp})_2\text{ZrCl}_2$  under these conditions independently on the size of the support. The slight influence of the support size on the MWD of the polymers is visible especially for reactions longer than 30s, which is the same time range for which clear differences in activity can be seen:

- Mn starts from values around 25000g/mol then decreases to 15000g/mol in 2 to 5 seconds, after which it increases more slowly and reaches steady values of 30000 g/mol after 30s.
- Mw remains constant around values of 90000 g/mol for the first 2 to 5 seconds and then increases to reach values of 160000 g/mol after 75s. A more or less clear dependence on support size can be seen for the weight average molecular weight only for reactions longer than 30s. It seems that the bigger is the support particle the more the MWD is shifted towards lower values (Figure 37). For reaction times lower than 30s no clear difference is visible between the MWDs measured for a same reaction time.
- In general PDI starts from values around 3.5 and increases gradually to values around 5 or 6 after 75 s.

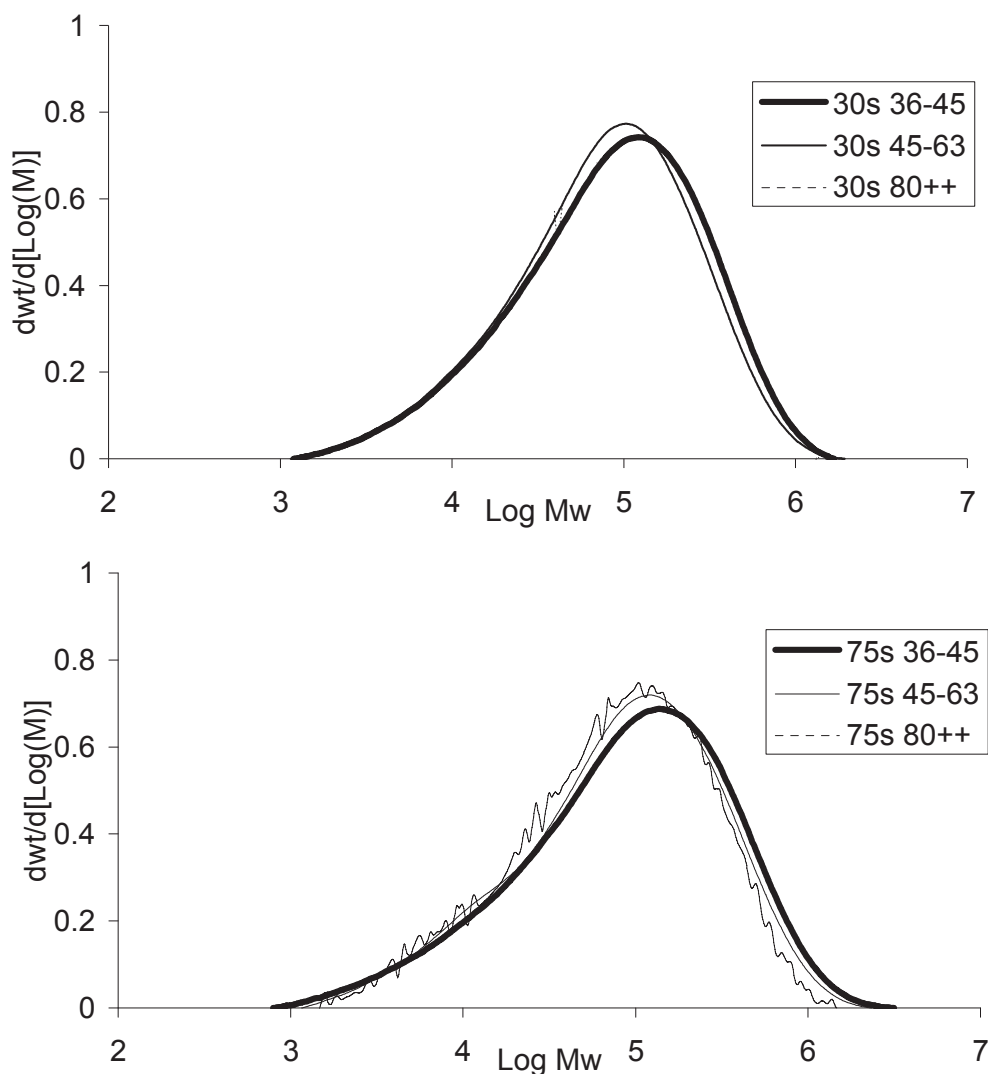


Figure 37: Influence of support size on Mw evolution.

The conclusions for the Mw explained above together with the results obtained measuring the activity profile suggest that some mass transfer limitation could be present in the bigger particles for reaction times higher than 5s. The PDIs of the polymers should then be higher if bigger catalyst particles are used. However this dependence is not seen here. It is probably difficult to separate the effects of the temperature and of the particle size (heat and mass transport together) on the PDI evolution. The following table summarizes the data obtained for the different catalysts by SEC.



Table 8: SEC results on polyethylene produced using different support sizes.

<i>Particle size (<math>\mu\text{m}</math>)</i>	<i>Reaction time (s)</i>	<i>Mn (g/mol)</i>	<i>Mw (g/mol)</i>	<i>PDI</i>
All	0.5	28700	87900	3.1
All	0.7	29700	91000	3.1
All	2	26900	94300	3.5
All	5	18000	129600	7.2
All	15	25900	106190	4.1
All	30	24400	131760	5.4
<hr/>				
36-45	0.3	26800	97600	3.6
36-45	0.7	22800	77200	3.4
36-45	2	16900	89400	5.3
36-45	5	16100	86800	5.4
36-45	15	18800	101410	5.4
36-45	30	33600	156000	4.6
36-45	75	28100	185200	6.6
<hr/>				
45-63	0.7	29700	109500	3.7
45-63	2	20500	100000	4.9
45-63	15	28700	125800	4.4
45-63	30	31300	139000	4.4
45-63	75	29800	164000	5.5
<hr/>				
> 80	0.5	24300	79900	3.3
> 80	0.7	15700	59400	3.8
> 80	2	11900	58500	4.9
> 80	5	23400	99000	4.2
> 80	15	20000	91900	4.6
> 80	30	23200	120000	5.2
> 80	75	29400	140200	4.8

### 4.3. Influence of support pore size

Support pore size can have a strong influence on monomer transport to the active site and on particle fragmentation. In addition it can be an important factor also in the catalyst preparation step as support porosity determines the way the active species (cocatalyst and precatalyst) are fixed onto the inorganic support and the homogeneity of the Al/Zr inside the particle.

In order to study its influence we selected a silica with different pore size but having surface area as close as possible to the reference Grace 948 silica used in this work as this variable determines the concentration of active sites per gram of support if a similar concentration of hydroxyl groups is present. Our objective is to work under equal active site concentration in order to detect only the influence of the support material. The choice was then to use the commercial silica PQMS 3030. It has to be said that this support gave a catalyst with low activity in long polymerization runs as it was seen after a 1h polymerization in a 2L gas phase reactor. Nevertheless it was the only one available having the desired characteristics and it proved to be active for short reactions.

Table 9 shows a comparison between the properties of the two supports and of the two finished catalysts. It should be noted that, due to the fact that we have larger pores with a similar surface area, the particle size and the pore volume are greater in case of the PQMS 3030 support. In order to take into consideration the difference between the average particle size of the two supports, the results using PQMS 3030 will be compared to the ones obtained using Grace 948 and to the ones obtained using particles of Grace 948 bigger than 80  $\mu\text{m}$ . The hydroxyl concentration, measured with the method described in the experimental part, is similar for both supports, confirming that this property depends only on the conditions of the thermal treatment.

**Table 9: Properties of the two different silicas and of the finished catalysts supported on them**

<i>Silica</i>	<i>Particle size</i> ( $\mu\text{m}$ )	<i>Specific area</i> ( $\text{m}^2/\text{g}$ )	<i>Pore size</i> ( $\text{nm}$ )	<i>Pore volume</i> ( $\text{mL/g}$ )	<i>OH conc.</i> ( $\text{OH}/\text{nm}^2$ )	<i>Zr content</i> ( $\text{wt } \%$ )	<i>Al content</i> ( $\text{wt } \%$ )
Grace 948	58	280	24	1.7	5.4	0.31	7.16
PQMS 3030	85	290	38	2.8	5.5	0.22	7.14

## 4.3.1. Activity and temperature evolution at reaction start-up

The usual reaction conditions have been used to compare the effect of pore size on the catalyst behavior at the reaction start-up. Even if  $n\text{BuCp}_2\text{ZrCl}_2$  supported on PQMS 3030 does not show considerable activity in long term reactions, it can be seen from the temperature profiles of Figure 38 that this catalyst is active during the early stages of the reaction. For similar catalyst quantities in the reactor we obtain similar temperature excursions.

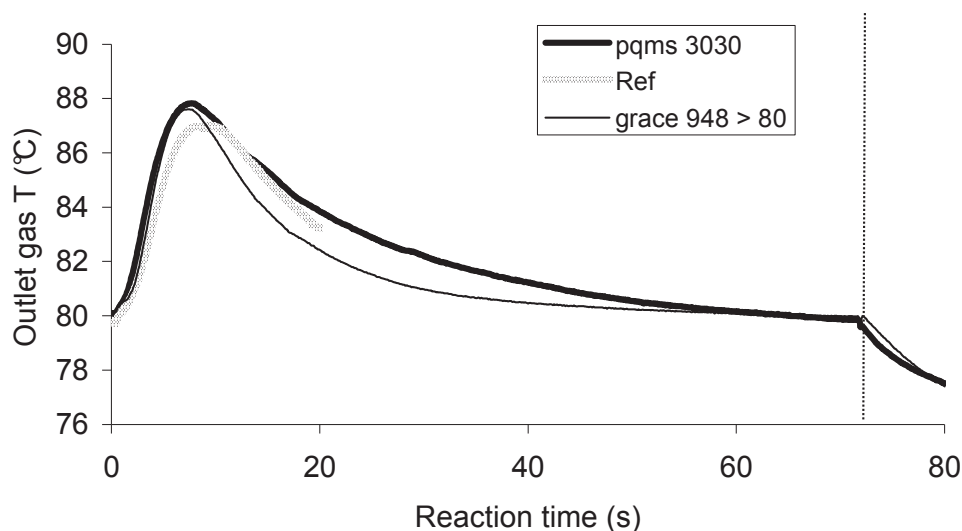


Figure 38: Outlet gas phase temperature profile of supports with different pore size and particle size.

From the same graph it can be noticed how the outlet gas phase temperature of the reaction conducted with this catalyst seems to decrease continuously even after 75s of reaction without reaching a steady value. This suggests that activity follows the same behavior. Such hypothesis is confirmed from Figure 39, where the activity profile obtained using the support with bigger pores is compared to the reference support and to the fraction of the bigger particles of the same silica. It can also be seen that activity profile of the new support is quite close to that of the reference one: a high activity is present at very short reaction times with a maximum around 1 second followed by a rapid decay.

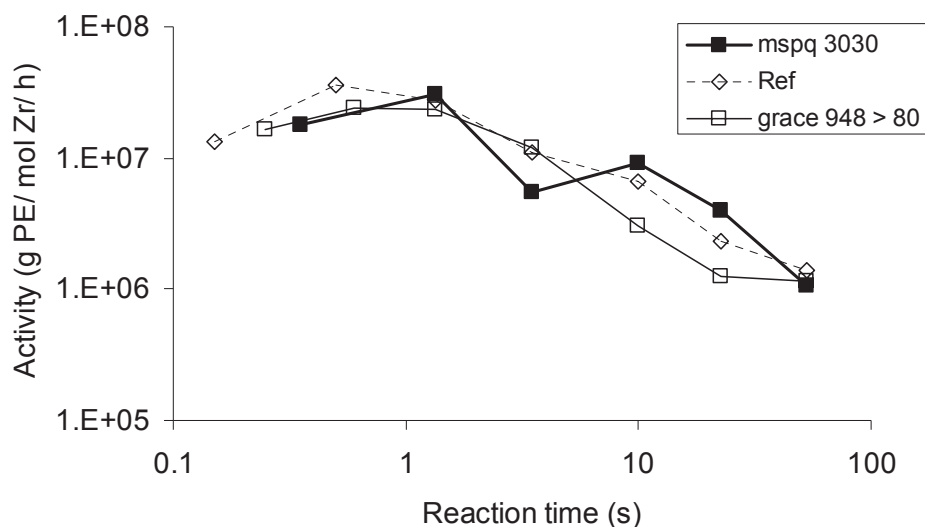


Figure 39: Activity profile at reaction start-up for supports having different pore and particle sizes.

#### 4.3.2. MWD evolution

There is not an evident dependence of the polymer MWD evolution on the pore size of the support. Mn and Mw evolve, for the three catalysts compared here, in the same manner as described in paragraph 4.2.2. From Figure 40 it seems that MWD is more affected by particle size than by pore size. PDI, Mn and Mw of the polymers produced using  $n\text{BuCp}_2\text{ZrCl}_2$  supported on PQMS 3030 are closer to the ones related to the bigger fraction of Grace 948 than to the ones corresponding to the reference catalyst. This is true especially for shorter reaction times, when the activity is at its maximum values. Mass diffusion limitations inside the particle can be the reason for this behavior.

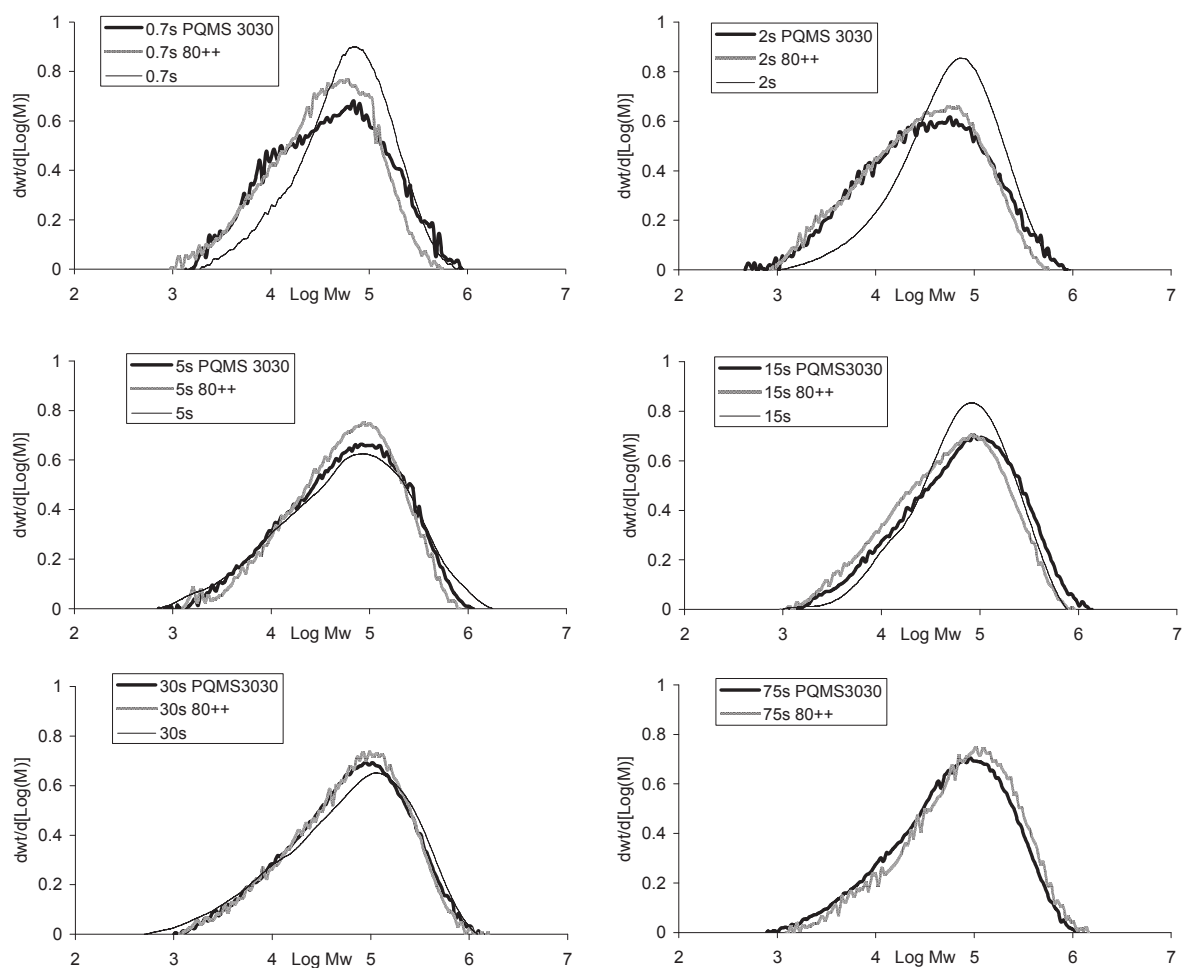


Figure 40: Influence of pore size and support size on MWD evolution.

In summary the pore size seems not to have an important influence on the start-up activity profile or MWD evolution (at least for the times studied here). The pore size has however a bigger influence on the way the polymer crystallizes and on its melting temperature. We will just anticipate here that if a PE chain can arrange freely in bulk to form crystals, where it has no space constraints, this is not true when the chains are confined into the support pore, that is the location where the first polymer chains grow. This introduces the concept of crystallization in confined space during reaction start-up which will be developed in the following chapter.

## 5. Conclusions

In this chapter we have seen how a supported metallocene behaves during the start up of the gas phase ethylene polymerization.

In general a very high activity is measured for the first 5 seconds with values that can be 20 times higher than what is measured at longer times. The reaction rate passes through a maximum around 1s and then decays to reach a plateau around 10s. The steady state value is comparable to the average activity measured after 1h of reaction. This behavior is common for almost all the conditions studied here and it cannot be explained only with mass transfer limitations arising because of the polymer layer formed around the active site or with a partial reaction runaway during the first seconds. The magnitude of the decay suggests that there exist some active sites that are working for only a short period of time. Their deactivation can be partially due to the temperature excursions measured in the first seconds but it seems that this behavior is inherent to the chemistry of the reaction and is due to the natural evolution of the active sites. From the first results it seems that this type of sites is more important if a higher quantity of Al is present in the final catalyst. The MWD of the produced polymers is constant throughout the reaction times if optimum conditions for heat transfer are used.

Varying the reaction conditions or the catalyst preparation has also an influence on the polymerization.  $(n\text{BuCp})_2\text{ZrCl}_2$  shows a slower activity decay than  $\text{Et}(\text{Ind})_2\text{ZrCl}_2$  if supported on the same carrier and reaches steady state activity values a bit higher for both short and long time reactions. However this metallocene seems to be more sensitive to temperature variations during the early reaction stages as the MWD broadens up for reaction times between 5 and 75 seconds and it is broader than what is found after 1h of reaction. Mn decreases temporary between 5 and 30s while increase again later reaching the starting values. Increased rate of the transfer reactions during this time interval is thought to be the reason. Mw of the polymers produced using both metallocenes increases with reaction time (to a lower extent if  $\text{Et}(\text{Ind})_2\text{ZrCl}_2$  is used).

A more extreme situation has been simulated by reducing the gas velocity or increasing the catalyst mass. By doing this we created important temperature gradients in the reactor. A reaction rate that decreases faster together with a very low Mn and high PDIs have been measured for reaction times between 5 and 75s. This shows how an insufficient heat removal at the reaction start-up can lead to uncontrolled transfer reactions and poor polymer properties even if polymer melting is avoided.

In case of copolymerization the known effect of decreased polymer molecular weight has been measured also for short times. The activity profile showed the usual shape (high starting values + decay) but no reaction rate increase in presence of comonomer was measured.

A broadening of the MWD can be measured also if the heat transfer is at its optimum. In some cases in fact we have seen the Mn decrease to half of its initial values for few seconds and then increase again to steady state values after 30s. The PDI followed the opposite path. This temporary deviation from the controlled conditions comes from the fact that the reactor, especially during the first reaction seconds, operates under a thermal gradient. This leads to a heterogeneous behavior of the active sites according to their position in the reactor. Being the chromatography performed on an average sample it is possible to measure broad MWD especially at reaction times for which the temperature gradient is maximum (1 to 5s). The MWD evolution of the produced polymer can then be used as a “sensor” to measure the thermal history of the catalyst particle during reaction start-up.

An opposite behavior has been measured if the MAO impregnation time during the catalyst preparation was raised from 1h to 4h. In this case more homogeneous MWD through the reaction time was measured and the reaction rate was 40% higher for reactions longer than 5s. It is possible that lengthening the MAO impregnation step leads to a more homogeneous distribution of the cocatalyst into the particle pores so that more sites are activated. This allows to synthesize polymers under a highly controlled regime (giving narrow MWD) from the very first reaction instants if appropriate reaction conditions are accurately chosen.

Increasing the quantity of Al fixed on the support leads to a very active catalyst for long reaction times while in stopped flow conditions a very high reaction rate at the beginning is followed by a quick activity decay to values one order of magnitude lower to what measured at steady state. Increasing the quantity of active metal (Zr) leads to an activity start-up similar to the reference catalyst while after few seconds the reaction rate profile follows the deactivation of the catalyst containing a lot of Al. This behavior is assigned to the combination of the active sites into inactive species which is favored by an increased concentration of active sites onto the support (higher Al and/or Zr contents). Thermal deactivation, especially for the catalyst containing a high Al amount, is also responsible for this decay. A too high temperature overshoot at the reaction start up is also the reason for a broadened MWD. This is seen in particular for the catalyst with a high Al content, that is the one having the highest activity for reaction times shorter than 1s. The same effect on MWD is seen if the Zr content is increased but the difference with the behavior of the reference catalyst lasts only for 15s. For longer reaction times the MWD of the polymers produced using the two catalysts (high and low Zr content) are similar.

In the last part of the chapter we have studied the influence of the support properties on the reaction start-up.

Smaller particles show higher activity for reaction times higher than 30s while for shorter polymerizations there is no clear dependence between activity and support size. The decay type profile of the reaction rate is not dependent on the particle size. Bigger pores do not have an important influence on reaction rate. For the specific support with bigger pores chosen in this work (PQMS 3030) the activity seems to drop even after 75s and no relevant activity is measured in a 1h reaction. This can be caused by support fragmentation problems as the activity in stopped flow reactions is reasonable. MWD does not clearly depend on the support properties. Only a slight dependence of the Mw on the support size has been seen for reactions longer than 30s. The bigger the particle size, the lower the Mw value. In general MWD seems to be more affected by the support size than by the pore diameter.



## 6. References

1. Kaminsky, W. and A. Laban, *Metallocene catalysis*. Applied Catalysis A: General, 2001. **222**(1-2): p. 47-61.
2. Harrison, D., et al., *Olefin polymerization using supported metallocene catalysts: development of high activity catalysts for use in slurry and gas phase ethylene polymerizations*. Journal of Molecular Catalysis A: Chemical, 1998. **128**(1-3): p. 65-77.
3. Quijada, R., et al., *Study of the effect of the monomer pressure on the copolymerization of ethylene with 1-hexene*. Journal of Applied Polymer Science, 1997. **64**(13): p. 2567-2574.
4. Tannous, K. and J.B.P. Soares, *Gas-phase polymerization of ethylene using supported metallocene catalysts: Study of polymerization conditions*. Macromolecular Chemistry and Physics, 2002. **203**(13): p. 1895-1905.
5. Zhou, J.-M., et al., *Gas-phase ethylene polymerization over polymer-supported metallocene catalysts*. Journal of Applied Polymer Science, 2003. **90**(5): p. 1319-1330.
6. Di Martino, A., G. Weickert, and T.F.L. McKenna, *Contributions to the Experimental Investigation of the Nascent Polymerisation of Ethylene on Supported Catalysts, 2*. Macromolecular Reaction Engineering, 2007. **1**(2): p. 229-242.
7. Di Martino, A., G. Weickert, and T.F.L. McKenna, *Contributions to the Experimental Investigation of the Nascent Polymerisation of Ethylene on Supported Catalysts, 1*. Macromolecular Reaction Engineering, 2007. **1**(1): p. 165-184.
8. Machado, F., et al., *Evaluation of the Initial Stages of Gas-Phase Ethylene Polymerizations with a SiO<sub>2</sub>-Supported Ziegler-Natta Catalyst*. Macromolecular Reaction Engineering, 2009. **3**(1): p. 47-57.
9. Floyd, S., et al., *Polymerization of olefins through heterogeneous catalysis. III. Polymer particle modelling with an analysis of intraparticle heat and mass transfer effects*. Journal of Applied Polymer Science, 1986. **32**(1): p. 2935-2960.
10. Crist, B. and P.R. Howard, *Crystallization and Melting of Model Ethylene-Butene Copolymers*. Macromolecules, 1999. **32**(9): p. 3057-3067.
11. Soares, J.B.P. and A.E. Hamielec, *Kinetics of propylene polymerization with a non-supported heterogeneous Ziegler-Natta catalyst: effect of hydrogen on rate of polymerization, stereoregularity, and molecular weight distribution*. Polymer, 1996. **37**(20): p. 4607-4614.

12. Yuan, H.G., et al., *Polymerization of olefins through heterogeneous catalysis, I. Low pressure propylene polymerization in slurry with Ziegler–Natta catalyst*. Journal of Applied Polymer Science, 1982. **27**(5): p. 1691-1706.
13. Huang, J. and G.L. Rempel, *Kinetic Study of Propylene Polymerization Using Et(H4Ind)2ZrCl2/Methylalumoxane Catalysts*. Industrial & Engineering Chemistry Research, 1997. **36**(4): p. 1151-1157.
14. Severn, J.R., et al., *"Bound but Not Gagged" - Immobilizing Single-Site  $\alpha$ -Olefin Polymerization Catalysts*. Chemical Reviews, 2005. **105**(11): p. 4073-4147.
15. Bianchini, D., F.C. Stedile, and J.H.Z. dos Santos, *Effect of MAO silica surface loading on (nBuCp)2ZrCl2 anchoring, on catalyst activity and on polymer properties*. Applied Catalysis A: General, 2004. **261**(1): p. 57-67.
16. dos Santos, J.H.Z., et al., *Silica supported zirconocenes and Al-based cocatalysts: surface metal loading and catalytic activity*. Macromolecular Chemistry and Physics, 1997. **198**(11): p. 3529-3537.
17. Ferreira, M.L. and D.E. Damiani, *Catalysts Based on Supported Metallocenes for  $\alpha$ -Olefin Polymerization*. Macromolecular Chemistry and Physics, 2001. **202**(5): p. 694-700.
18. Moroz, B.L., et al., *Silica-supported zirconocene catalysts: Preparation, characterization and activity in ethylene polymerization*. Journal of Molecular Catalysis A: Chemical, 1998. **130**(1-2): p. 121-129.
19. Kaminsky, W., *The discovery of metallocene catalysts and their present state of the art*. Journal of Polymer Science Part A: Polymer Chemistry, 2004. **42**(16): p. 3911-3921.
20. Smit, M., et al., *Effects of methylaluminoxane immobilization on silica on the performance of zirconocene catalysts in propylene polymerization*. Journal of Polymer Science Part A: Polymer Chemistry, 2005. **43**(13): p. 2734-2748.
21. Tisse, V.F., R.M. Briquel, and T.F.L. McKenna, *Influence of Silica Support Size on the Polymerisation of Ethylene Using a Supported Metallocene Catalyst*. Macromolecular Symposia, 2009. **285**(1): p. 45-51.
22. Zheng, X., et al., *Fragmentation Behavior of Silica-Supported Metallocene/MAO Catalyst in the Early Stages of Olefin Polymerization*. Macromolecules, 2005. **38**(11): p. 4673-4678.
23. Tisse, V.F., *Kinetics and morphology of metallocene catalysts used in ethylene polymerization*, 2006, PhD Thesis, Université Claude Bernard Lyon 1.
24. dos Santos, J.H.Z., et al., *The effect of silica dehydroxylation temperature on the activity of SiO2-supported zirconocene catalysts*. Journal of Molecular Catalysis A: Chemical, 1999. **139**(2-3): p. 199-207.

25. dos Santos, J.H.Z., et al., *Optimization of a silica supported bis(butylcyclopentadienyl)-zirconium dichloride catalyst for ethylene polymerization*. *Macromolecular Chemistry and Physics*, 1999. **200**(4): p. 751-757.
26. Silveira, F., et al., *Effect of the silica texture on the structure of supported metallocene catalysts*. *Journal of Molecular Catalysis A: Chemical*, 2009. **298**(1-2): p. 40-50.
27. Hamilton, P., D.R. Hill, and D. Luss, *Optical and infrared study of individual reacting metallocene catalyst particles*. *AIChE Journal*, 2008. **54**(4): p. 1054-1063.
28. Pater, J.T.M., G. Weickert, and v.W.P.M. Swaaij, *Optical and infrared imaging of growing polyolefin particles*. *AIChE Journal*, 2003. **49**: p. 450 - 464.
29. Kumkaew, P., et al., *Gas-phase ethylene polymerization using zirconocene supported on mesoporous molecular sieves*. *Journal of Applied Polymer Science*, 2003. **87**(7): p. 1161-1177.
30. Kumkaew, P., et al., *Rates and product properties of polyethylene produced by copolymerization of 1-hexene and ethylene in the gas phase with (n-BuCp)<sub>2</sub>ZrCl<sub>2</sub> on supports with different pore sizes*. *Polymer*, 2003. **44**(17): p. 4791-4803.
31. McDaniel, M.P., *Fracturing silica-based catalysts during ethylene polymerization*. *Journal of Polymer Science: Polymer Chemistry Edition*, 1981. **19**(8): p. 1967-1976.





# Chapter 4

*Morphological  
interpretation of the  
thermal properties  
of polyethylene at  
reaction start-up*



<b>1. Introduction .....</b>	<b>232</b>
<b>2. Overview of polymer crystallization at reaction start-up .....</b>	<b>236</b>
2.1. Ethylene (co)polymerization by EtInd <sub>2</sub> ZrCl <sub>2</sub> .....	236
2.2. Ethylene (co)polymerization by (nBuCp) <sub>2</sub> ZrCl <sub>2</sub> .....	239
2.3. Conclusions .....	242
<b>3. Morphological interpretation of the crystallization behavior.....</b>	<b>243</b>
3.1. Introduction .....	243
3.2. Fragmentation and crystallization in confined space .....	246
3.3. Morphological (re)interpretation of DSC results .....	249
3.3.1. <i>DSC study on homopolymers</i> .....	249
3.3.2. <i>X-ray microtomography study on homopolymer particles</i> .....	252
3.3.3. <i>Copolymerization</i> .....	260
3.3.4. <i>Influence of support size</i> .....	261
3.3.5. <i>Influence of support pore size</i> .....	264
3.3.6. <i>Influence of catalyst preparation</i> .....	268
<b>4. Conclusions .....</b>	<b>274</b>
<b>5. References .....</b>	<b>277</b>



# 1. Introduction

Solid polyethylene is a semicrystalline material which can be considered as a composite of crystalline and noncrystalline regions. The noncrystalline phase (also called amorphous phase) forms a continuous matrix in which the crystalline regions are dispersed. Amorphous phase consists of segments of polyethylene chains in a disordered conformation. Crystallites consist of chain segments that are packed in regular arrays. The same polymer chain will be partly arranged in crystallites and partly in the amorphous phase so that the crystallites are, in some extent, limiting the degrees of freedom of the amorphous phase. It is known that the thickness of the crystallites lies between 80 and 200 Å and that the extended length of a polyethylene chain can be as high as 10000 Å. A single chain can then cross many times the crystallite thickness [1]. The specific morphology of the semicrystalline structure is governed by the molecular characteristics of the chains: short branches, for examples, are excluded from the crystalline domains and thus are responsible for a decrease of the degree of crystallinity of the material. It's for this reason that HDPE, which is mainly formed by linear chains with a very low number of branches, has a melting temperature between 120°C and 135°C and a crystallinity up to 80% while LLDPE, in which the degree of branching is more important, shows melting temperatures normally comprised between 105°C and 115°C and crystallinities from 30 to 60%. The decrease in the melting temperature of the polymer with an increasing number of ethyl branches can be seen in Figure 1.

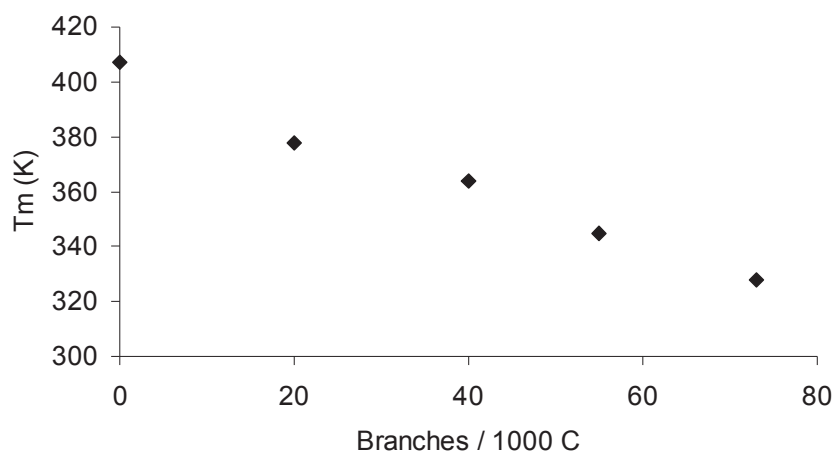


Figure 1: Influence of ethyl branching degree on melting temperature (adapted from [2]).

It has to be pointed out that the molecular weight has not an influence on the melting temperature for the polymers analyzed in this study. An increase of melting temperature with

the polymer molecular weight is seen only for molecular weights up to 5000 g/mol. At this value a plateau is attained and no variations are measured for higher molecular weights [3].

Polyethylene chains crystallize from the molten state or from solution if the crystalline state is more stable than the disordered one. This phenomenon is then driven by the minimization of the free energy. Nevertheless the overall mechanism of crystallization is determined by a balance between thermodynamic and kinetic factors. Kinetic factors include molecular properties like viscosity, degree of branching, and chain mobility and reaction conditions like temperature, pressure, reaction medium and the presence of nucleating compounds.

The formation of a crystallite is a two step phenomena consisting in crystallite initiation (nucleation) and crystal growth. Nucleation takes place when a number of neighboring chain segments adopts a regular parallel conformation and pack together to form a structure large enough that exceeds a critical size for stability. This can happen spontaneously if the melt is cooled below the equilibrium melting temperature of the crystals. This process is called homogeneous nucleation. The high energy barrier for crystal stability is responsible for the 50°C of supercooling (lowering the temperature of a liquid below its crystallization point without it becoming a solid) needed to have homogeneous nucleation [1]. It is for this reason that this mechanism is rarely predominant. Nucleation can also be favored by the presence of impurities of any type into the molten phase. In this case the process is called heterogeneous nucleation, which is the dominant mechanism of crystal formation. If impurities are polyethylene crystallites that did not melt in the previous heating, the process is called self-nucleation. More frequently impurities are catalyst fragments, cracks, discontinuities and cavities. In this case a group of chain segments deposit on the surface of the impurity which acts as a pattern for the crystallite formation. The deposition of a chain on a surface lowers its free energy and the critical size of the polyethylene nuclei so that a much lower degree of supercooling is needed to have stable crystals in this case. Besides the effect of impurities, nucleation can also be initiated by stresses accumulated into the polymer and by local variation of temperature and pressure. Once a nucleus is formed the crystallite can grow by addition of successive lamellae to a size which is dependent on the chain molecular properties and on the external conditions.

Semicrystallinity is a fundamental property of polyolefins (and many other polymers). Many of the interesting mechanical properties that are the key for the success of polyethylene come from its semicrystalline structure. A pure crystalline polymer would be a brittle and

friable material while a pure amorphous polymer would result in a viscous fluid with poor mechanical properties or a glass.

Crystallinity of the polymer is also an important parameter determining the evolution of the start-up of the catalytic polymerization of olefins. In Chapter 1 we have presented a review on single particle models where we have seen that the polymer properties are responsible for the way the tensions produced by the polymer accumulation into the pores are stored and released to provoke the polymer deformation or to initiate the fragmentation of the particles. Such properties are strictly linked to the degree of crystallization of the polyolefin. In addition we have also explained how the diffusion coefficient of the monomer into the polymer/support particle is fundamental in determining the monomer concentration at the active site and thus the reaction rate and the fragmentation path. To reach the active site the monomer has to diffuse through the pores of the support and through the polymer layer surrounding the active site itself. This second mechanism is strictly connected to the crystallinity of the material since diffusion is possible only in the amorphous domains. The newest single particle models available in literature are capable to calculate the temperature and concentration profiles and the morphology of the particle and their evolution with time, but they use the properties of the polymer produced in long term reactions as input values. This is of course not reliable but comes from the lack of data regarding the properties of the polymers produced at very short reaction times. One of the objectives of the work presented in this Chapter is to fill this void.

When studying the early stages of olefin polymerization it has to be kept in mind that crystallization of polymer chains is happening together with the polymerization itself. Monomers arriving at the active sites react to form chains that show an amorphous part near the metal center and a crystalline domain which forms after some ethylene units are inserted (the number of these depending on the ratio between polymerization rate and crystallization rate). Properties like local temperature and active site concentration can influence the relative ratio between crystallization and polymerization. This is responsible for different morphologies of the nascent polymers. Loos et al. [4] studied deeply this aspect and came to the conclusion that if high temperature or active site concentration or polymerization rate is present, a morphology consisting of highly entangled molecules and disordered folded chain crystals may result. The rate of molecule production is high enough that the chains do not have the time to organize in ordered structures. If the number of catalytically active sites is very low and/or the polymerization temperature is far below the melting and/or dissolution temperature, the formed polymer chains can be considered as separated from each other.

Therefore, the molecules may crystallize as folded chain lamellae without entanglements in the amorphous phase. If the crystallization and the polymerization rates are similar, nascent morphology with low entanglement density and extended chain crystals should be favorable. This shows how the chain morphology is dependent on the reaction parameters. We have seen in the previous Chapter that during the reaction start-up both particle temperature and polymerization rate rapidly change. The effect on the chain crystallization behavior should then not be negligible. In addition in the early stages of olefin polymerization the catalyst and the support are still representing an important fraction of the whole particles (yields lower than 1 g/g are measured for reactions shorter than 5s) and their influence on the crystallization can be quite important.

The interest of studying the melting and crystallization behavior of polyethylene at the reaction start-up is confirmed in literature by the works of Di Martino [5, 6] and Machado [7] who studied the behavior of ZN catalysts in slurry phase and in gas phase respectively. Di Martino found that for very short reactions highly amorphous polymers with a low melting temperature are produced ( $T_m$  around 118°C, crystallinity of 20%). She explained this behavior with the high reaction rate in the early stages producing disordered chains with entanglements limiting the formation of crystallites. In addition she found bimodal peaks in the DSC thermograms for low reaction times and attributed them to the active site evolution during the first reaction instant which can be responsible for the production of different types of polymer (namely branched chains coming from insertion errors). Nevertheless no spectroscopic evidence was given to support this theory. It's interesting to notice that this type of behavior is not influenced by reaction temperature, catalyst activation or presence of hydrogen (which is not compatible with the proposed explanation) and that the low values of crystallinity and melting temperature correspond to reaction times for which fragmentation is just started. Machado found the same results working in gas phase with silica supported ZN catalysts. He attributed this behavior to the formation of longer chains as the reaction time increases but no additional proof was given to support this theory.

This short introduction on polyethylene crystallization and its behavior during the early stages of the polymerization shows how the phenomena happening at short reaction time can be quite different from what is measured in long term reactions. In our case the presence of the support into the final particle cannot be neglected neither we can forget the high activity values and the temperature excursions measured during the first seconds of reaction. These phenomena can greatly influence the way the polymer chains organize themselves.

In what follows we will briefly present some interesting results about the evolution of the melting temperature and the crystallinity during the reaction start-up and we will show the effect of the reaction conditions on it. In order to explain the measured behavior we will recall the concept of crystallization in confined space (i.e. the support pores). Finally we will use this concept to explain the results found about the influence of the support properties on the evolution of the crystallization behavior of the polymer. The results presented here have been performed with the analysis method presented in the experimental part. Values corresponding to the second heating step are presented in order to get rid of the thermal history of the sample. Nevertheless, unless specified in the text, the two heating steps show very similar profiles.

It has to be said that the values of  $T_m$  and crystallinity measured at the reaction start-up are not a criterion to determine the quality of the produced polymer in terms of thermal properties (which are dependent on the feed composition, the catalyst used and the reaction conditions). In other words measuring a low melting temperature at short reaction times does not mean that we are producing a polymer with poor thermal properties. Such values are instead a mean to describe the evolution of polymer chains from the reaction start towards the final product and the evolution of the particle morphology from a pure support particle to a pure polymer particle.

## 2. Overview of polymer crystallization at reaction start-up

### 2.1. Ethylene (co)polymerization by $EtInd_2ZrCl_2$

Polymers produced at different reaction times using  $EtInd_2ZrCl_2$  supported on MAO-treated silica under the optimized conditions presented in the previous Chapter have been recovered and analyzed in DSC. The catalyst used in this section is the reference one, prepared according to the classical procedure exposed in chapter 2 (1h impregnation of 10 wt % solution of MAO onto silica and 1h impregnation of 2 wt % metallocene). The catalyst/polymer particles have been separated from NaCl before analysis by washing with cold demineralized water but we did not proceed to the extraction of the polymer from the

support. Our intention is in fact to measure the properties of the polymers as they are during the early reaction stages. A correction based on yield values for the real mass of polymer introduced into the calorimeter is necessary to calculate the exact value of crystallinity. We used a value of enthalpy of fusion of 288 J/g for a 100% crystalline polymer. Crystallinity of the sample is calculated from the ratio between the measured value of enthalpy and the previous value.

Figure 2 shows the evolution of the melting temperature and of the crystallinity of the produced polymers for reaction times between 0.3 and 30s. The melting temperature is quite low at the reaction start-up, as it was found in the previously cited works of Di Martino and Machado. Note how even after 30s the melting temperature is around 127°C while the same catalyst used under the same temperature (80°C) and ethylene pressure (6 bar) in long term reactions gives a polymer that melts around 131°C. Crystallinity is around 50% at the very beginning of the reaction, passes through a maximum (65%) after 2 seconds and goes back to 50% later. This value is similar to what is measured on a polymer produced after long term reactions. It has to be said how the experimental error for the crystallinity value, which takes into account the error of the calorimeter and the error in the sample weighing step, is around 10%. In addition there can be some inhomogeneities in our samples as we are taking an average quantity of material representing all the bed and we have seen at the end of Chapter 2 that there can be a 20% difference in yield between the most and the less active zone of the reactor. Crystallinity values and trends have then to be considered with the due precautions. Melting temperature, being not related to the exact mass of polymer inserted into the calorimeter, can be measured more precisely.

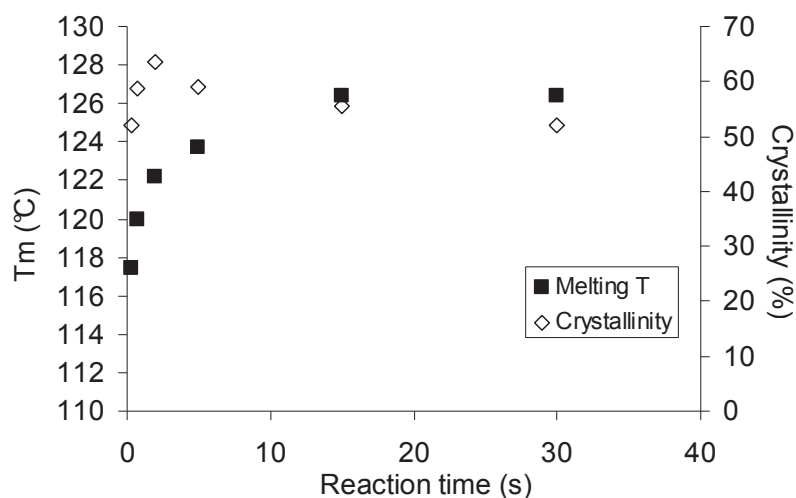


Figure 2: Evolution of melting temperature and crystallinity with reaction time for reference catalyst  $\text{Et}(\text{Ind})_2\text{ZrCl}_2$  under optimum conditions

We can exclude that this behavior is due to variation in the chain length of the produced polymers as the MWD of the samples is not changing during the studied reaction time (see paragraph 2.2.2 of chapter 3).

Let's store these informations in a corner for the moment as we will come back later on these results.

The same catalyst used at the same reaction conditions to copolymerize ethylene with 1-butene (4 mol % in the feed) produced copolymers which melting temperature and crystallinity are shown in Figure 3 and 4 and compared to the results obtained in homopolymerization.

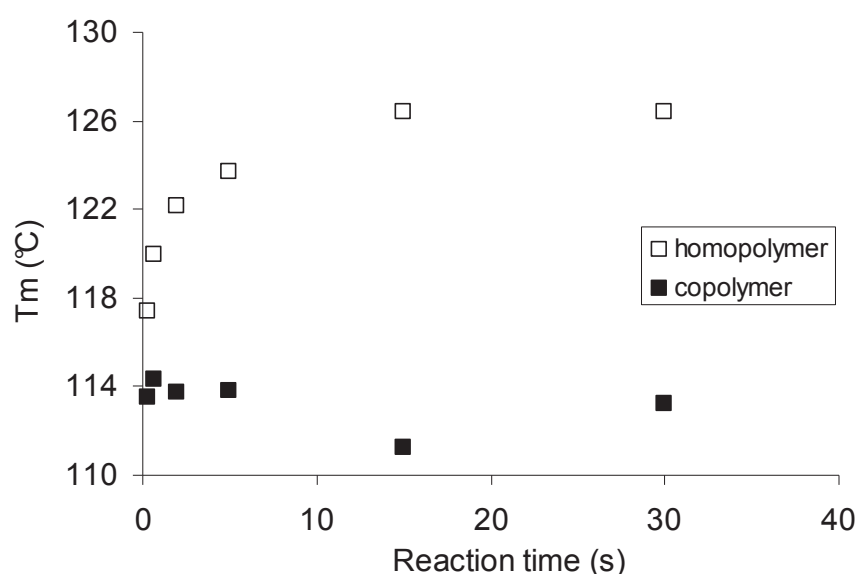


Figure 3: Evolution of melting T at reaction start-up in homo and copolymerization.

In case of copolymerization the melting temperature evolution with reaction time is different. The measured values remain constant through the studied reaction times around 114°C. The same value is measured for polymers produced in long term reactions and corresponds to an insertion of about 3.2 mol % of butene if compared with Figure 1. The reactivity of the two monomers seems to remain constant during the reaction start-up and this let us exclude the presence of mass transfer limitations for this series of experiments.

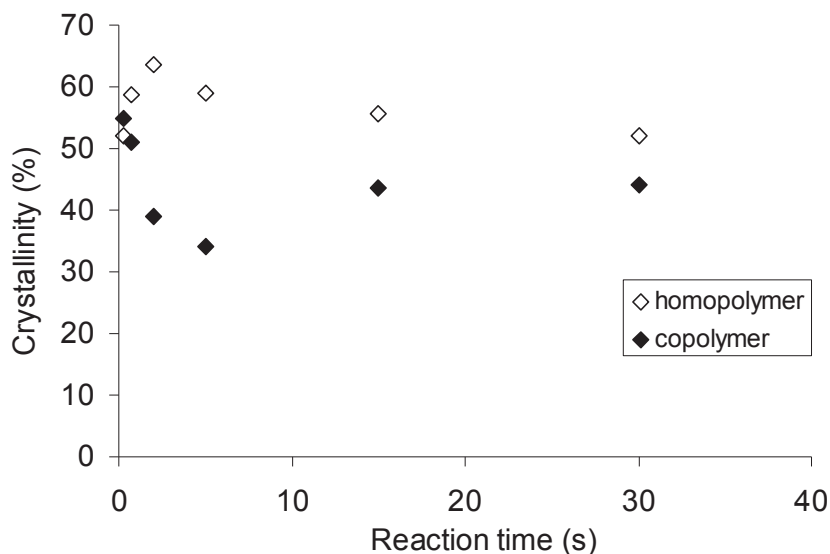


Figure 4: Evolution of crystallization at reaction start-up in homo and copolymerization.

Crystallinity is also evolving differently in the copolymerization case. The starting value is similar to the one of the homopolymer but then the crystallinity decreases rather than pass through a maximum and reaches final value which are more or less 15% lower than the ones of the homopolymer. This is consistent with the fact that the ethyl branches of the chains are an additional obstacle for the formation of regular crystals and have the effect to decrease the total polymer crystallinity. The different behavior measured in the first 10 reaction seconds can be explained with the fact that during this reaction time MWD of the copolymers showed a small tail towards lower masses as shown in paragraph 2.2.2 of chapter 3. If a lot of small branched chains are formed during some time they can have the effect to temporarily decrease the crystallinity of the material.

From these first results it is clear that the crystallization of the polymer at the reaction start-up is a complicated phenomenon and that properties of polymers produced in long term reactions are not suitable to describe the situation at low reaction times.

## 2.2. Ethylene (co)polymerization by $(n\text{BuCp})_2\text{ZrCl}_2$

The same kind of analysis can be applied to polymers produced using the second metallocene complex of this work. This will help in determining if there is some influence on the crystallization behavior of the type of metallocene used. Figures 5 and 6 show the melting temperature and crystallinity evolution of the polymers produced using this catalyst and compare them with the values obtained using  $\text{EtInd}_2\text{ZrCl}_2$ .



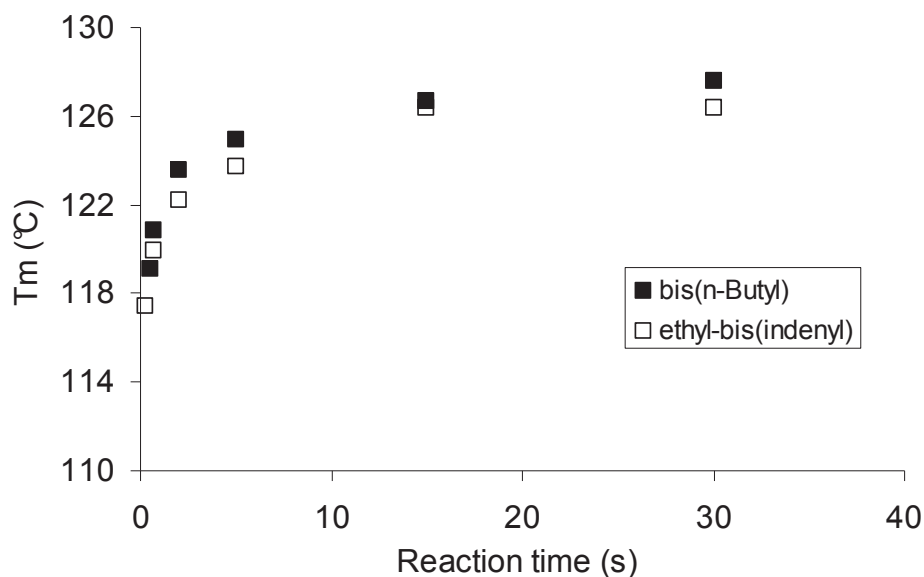


Figure 5: Melting temperature evolution with reaction time for different metallocene complexes.

Only slight differences can be found in the melting temperature evolution: using  $(n\text{BuCp})_2\text{ZrCl}_2$  gives a polymer which has a melting temperature  $1^\circ\text{C}$  higher, which is also maintained in case of long term reactions. However the evolution of the two melting temperatures are very close each other.

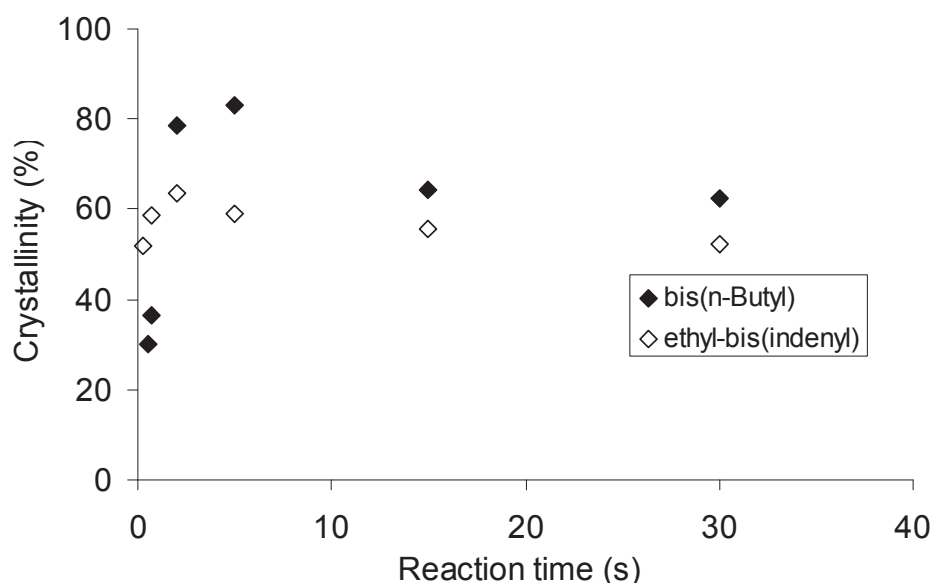
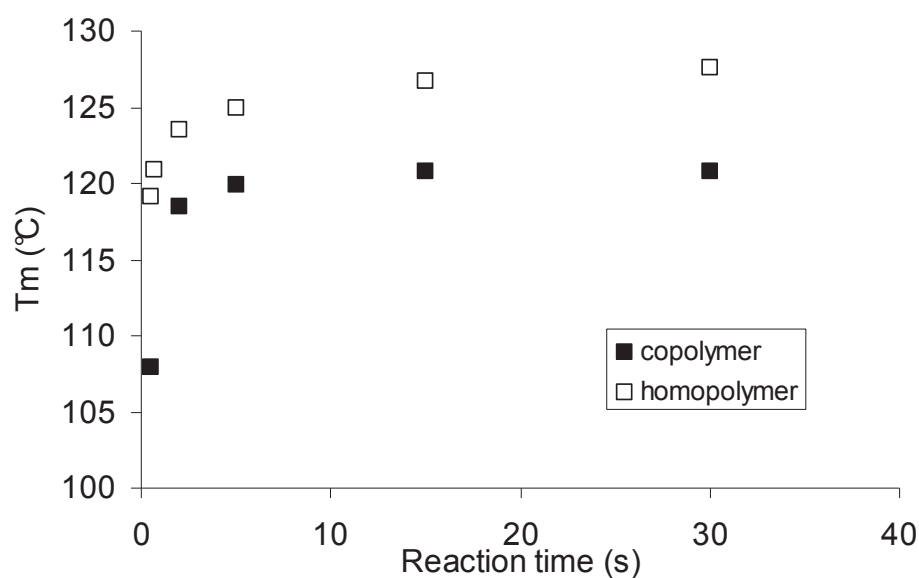


Figure 6: Crystallinity evolution with reaction time for different metallocene complexes.

The crystallinity of the polymers produced using the two different metallocenes also evolve in a similar manner, passing through a maximum around 2 to 5 seconds and then decreasing. However in case of polymers produced by  $(n\text{BuCp})_2\text{ZrCl}_2$  a very low crystallinity is measured at very short reaction time. The maximum, on the contrary, is much higher when this second metallocene is used. The final values are 10% higher if  $(n\text{BuCp})_2\text{ZrCl}_2$  is used and this difference is maintained in long term reactions.

Copolymerizations have also been performed using the second metallocene complex under the same conditions as above. DSC analysis shows that melting temperature of the copolymer in this case evolves in way similar to the case of homopolymerization: low values are found at the very short times and higher values later (Figure 7). Final values are around 121°C which is 8°C higher than what found with  $\text{EtInd}_2\text{ZrCl}_2$  but still 10°C less than the homopolymer and corresponds, according to Figure 1, to a butene insertion of 2 mol % into the chain (the feed contained 4 mol % of comonomer). It seems that the less the monomer is inserted, the closer to the homopolymerization case is the temperature evolution. It can also be that the comonomer insertion is evolving for short reaction times because of an evolution of the active site behavior (caused by temperature excursion?).



**Figure 7: Evolution of melting T at reaction start-up in homo and copolymerization with  $(\text{nBuCp})_2\text{ZrCl}_2$ .**

Crystallinities of the copolymer and of the homopolymer show a similar evolution (Figure 8). Homopolymer shows nevertheless a higher maximum and lower initial values. Final values are not very different each other, as the butene incorporation is quite low in this case.

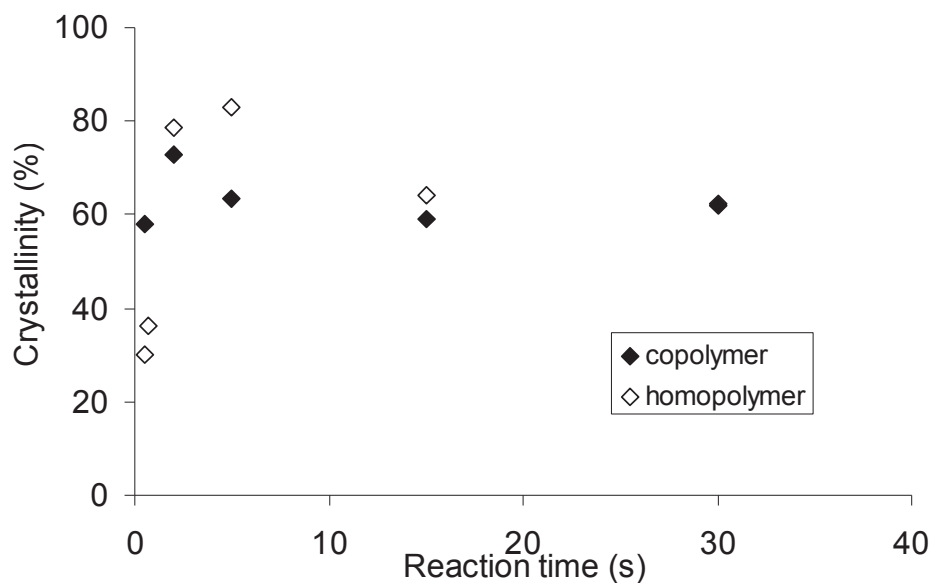


Figure 8: Evolution of crystallinity at reaction start-up in homo and copolymerization with  $(nBuCp)_2ZrCl_2$ .

### 2.3. Conclusions

To summarize, melting temperature and crystallinity show an unusual behavior at reaction start-up:

- Melting temperature is very low for very short reaction times (less than 120°C for the homopolymers) and then increases gradually to more classic values.
- It seems also that the higher the comonomer insertion, the more constant is the melting temperature during the studied time range
- Crystallinity passes through a maximum (70-80 %) around 2-5 s before decreasing to classic values (50-60 %). In some cases very low crystallinity values can be measured at very low reaction times (30% at 0.3s). It has to be said that experimental errors can have a strong impact on crystallinity measurements so that these values have to be considered with the due precautions

Even if not presented here, we have to inform the reader that the behavior measured for the melting temperature and the crystallinity in case of homopolymerization is independent on the reaction temperature, the time of MAO impregnation, the support size and the quantity of Zr present in the final catalyst. Only the crystallinity evolution presents some differences if big particles are used and the melting temperature evolves slightly differently with a catalyst having a bigger amount of Al. A deeper discussion is presented in the following paragraphs.

This unusual behavior is then confirmed by many experiments and the explanations for it must be found somewhere else than in the chain microstructure or in the competition between polymerization and crystallization. Very similar behavior has in fact been measured in previous works on short time reactions even if the reaction rates and the MWD of the produced polymers are very different for the different studies.

### 3. Morphological interpretation of the crystallization behavior

#### 3.1. *Introduction*

The unusual crystallization behavior measured in our experiments can be due to the presence of a high quantity of support into the polymer particle. Remember that the reactions corresponding to the polymers analyzed in the previous paragraph show a maximum yield around 1.5 gPE / g catalyst. This means that in the samples analyzed by DSC there is 40% or more inorganic support. The same is true at the single particle level. A confirmation of the effect of the presence of the support on the polymer crystallization comes from the following figure. In the picture we compare the DSC spectrum of a classic sample with two other samples in which polymer has been extracted and separated from the support before the analysis. It has to be said that the three samples come from the same reaction performed using  $(n\text{BuCp})_2\text{ZrCl}_2$  supported on MAO/silica at low gas velocity (5.5 cm/s), 80°C, 6 bars of ethylene and 3 bars of helium for 5s. The yield of the reaction is of 0.5 g/g.

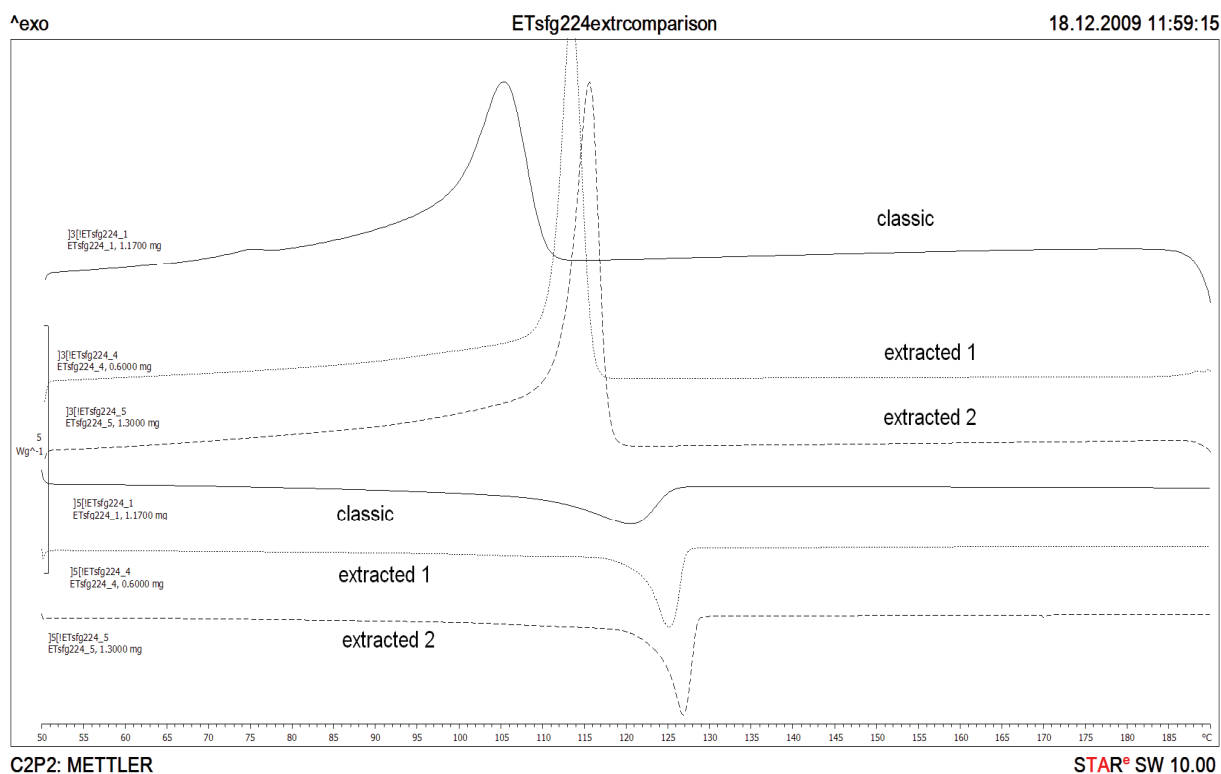


**Figure 9: DSC thermograms of the cooling and the 2nd melting of three samples, one non extracted (classic) and two where the support has been separated from the polymer.**

The extractions have been performed with boiling xylene (140°C) for 4 hours in a Soxhlet. The polymer in the extraction 1 has been recovered after xylene evaporation while in extraction 2 it has been precipitated by methanol addition and filtered. The three upper curves are the crystallization step while the other three curves represent the second melting of the polymer.

The non extracted sample shows a melting temperature of 121°C which is coherent with what showed previously. The two other samples (without support) show a melting temperature increased by 5-6°C. This is still somewhat lower than the classic value measured for PE but it clearly shows that unusual melting temperatures and crystallization values are (at least partially) due to the presence of the support.

We can then exclude that the low melting temperature is due to the particular MWD of the polymer produced in the first reaction instants. As already said, when working with the optimized reaction conditions, the MWD does not change enough during the reaction course to justify this behavior. RMN study of polymers produced at different reaction times confirms that chain branches due to insertion errors during start-up of homopolymerization reactions are not the reason for the low melting temperatures.

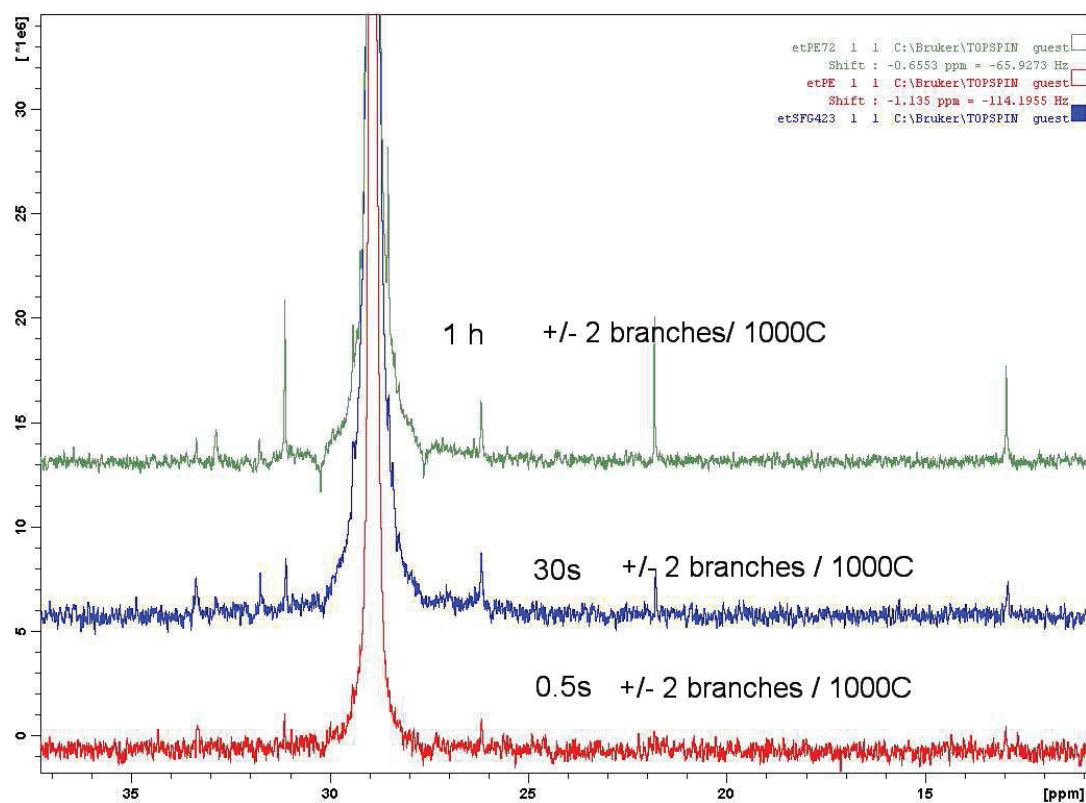


Figure 10: Comparison of  $^{13}\text{C}$  NMR spectra of polymers produced at different reaction times.

In Figure 10 the NMR spectra of three polymers produced using supported  $\text{Et}(\text{Ind})_2\text{ZrCl}_2$  under optimized conditions are compared. The number of branches in the polymer chains is very low independently on the reaction time and no chain ends are detected. The high noise in the spectrum related to the 0.5s reaction is due to the fact that a low quantity of polymer was present in the sample even if the reaction had to be repeated 8 times to supply enough polymer for the analysis.

The following table shows the melting temperature and crystallinity values of the polymers produced with different catalysts in reactions lasting 180s. The longer reaction time gives particles with higher yield (and then less support). Independently on the support size, the catalyst treatment or the particle pores, the melting temperatures are higher in this case than what shown in Figure 5. It is then clear that the responsible for the unusual crystallization of the polymers at reaction start-up is the support. The lower is the quantity of inorganic carrier in the particle, the closer is the melting temperature to the values classically measured after long term reactions. It seems then that the crystallization behavior at reaction start-up is strictly connected to the ratio of the quantity of polymer and inorganic phase in the particle. The next step is to find in which way and for which reasons the support can influence the polymer behavior to give the melting temperature and crystallinity values that have been shown above.

**Table 1: Melting temperature of polymers produced using different catalysts after 180s; comparison with long term values.**

<i>Exp</i>	<i>Catalyst</i>	<i>Catalyst features</i>	<i>Yield</i> (g/g)	<i>T<sub>m</sub></i> (°C)	<i>T<sub>m</sub> long</i> <i>term</i> (°C)
ETSFG499	ETmet41	4h MAO treatment	2.35	127.7	130.8
ETSFG532	ETmet42	Support 36-45 μm	3.67	131.5	130.9
ETSFG533	ETmet43	Support 45-63 μm	2.19	130.3	130.7
ETSFG534	ETmet44	Bigger pores (PQMS3030)	1.98	127.2	128.0
ETSFG535	ETmet45	Support > 80 μm	1.49	128.6	129.2
ETSFG536	ETmet46	High Al	1.67	129.2	131.6
ETSFG537	ETmet47	High Al High Zr	1.76	130.0	129.5

### 3.2. Fragmentation and crystallization in confined space

During the early reaction stages the polymer is growing from the active sites which are located inside the support pores throughout all the particle volume. As already exposed in the literature review Chapter, the polymer grows layer by layer from the pore wall and proceeds until the pore is filled. At this point the deposited polymer can deform a little and let new fresh polymer accumulate into the pore volume but, sooner or later, the pressure exerted on the support walls will be high enough that the carrier will start to fragment locally. This leads to an increase or to the destruction of the pore volume and makes new pores easily accessible to the monomer. The process is gradual, with the most accessible pores being filled and destroyed before the less accessible ones. Accessibility of the pores depends on their position within the particle volume and on their size. The size of the pores of a mesoporous silica is distributed over an interval which spans typically from few nanometers to few tens of nanometers (typically 3 to 60 nm). In general, until the fragmentation can be considered completed, the growing particle will be constituted of empty pores, partially or completely filled pores, pure polymer volumes (corresponding to destroyed pores) and pure support volumes coexisting together. The point at which fragmentation of a silica carrier can be considered completed depends on a number of factors like particle size, particle pore volume, pore size, reaction rate profile. In general it is accepted that fragmentation can be completed at

yields on the order of few g/g at least. Yields reached in this work are fairly lower, meaning that we are studying the particle during the early stages of its fragmentation process. The samples that we are analyzing by DSC consist then of support particles having polymer distributed onto the external support surface and into the pores that can be empty, filled or broken. The environment into which the polymer chains are crystallizing can then be very heterogeneous and this is the reason why, at this low yields, the presence of the support has a strong influence on the crystallization behavior of the polyethylene chains.

It is known in the literature that polymer chains which crystallize in a confined space show different behavior respect to chains which are free to move in a bulk. Polymer present in the pores of our support can be considered in a confined space. Remind that in this paragraphs any situation for which the chains are free to crystallize independently on what is surrounding them will be called bulk. This can be a much smaller volume than what is normally thought (i.e. a pore big enough to not perturb the crystallization is considered as bulk for us).

The works of Woo et al [8, 9] are in particular well suited to explain the phenomena that are measured in our samples. The authors deposited by an annealing method linear polyethylene with narrow MWD into the pores of different alumina membranes. Such pores have a controlled diameter which can vary from 15 to 220 nm. The crystalline structures and the melting temperature of the polymers confined into the pores were then measured by X-ray diffraction and DSC. First of all it was found that the melting temperature of the polymers measured during the second heating step at 10°C/min is decreasing with decreasing pore size. Values of 122°C were found for pores of 15nm while the same polymer in bulk melted at 133°C. The reason for this depression is the confinement created by the pore which has the consequence to reduce the crystal thickness of the polymer once cooled. According to the Gibbs-Thompson equation (1), smaller crystals melt at lower temperature. This is exactly what we are seeing in our case. The equation is

$$T_m = T_m^0 \left[ 1 - \left( \frac{\sigma_1}{L_1} + \frac{\sigma_2}{L_2} + \frac{\sigma_3}{L_3} \right) \frac{2}{\rho_c \Delta H_m^0} \right] \quad (1)$$

where  $\sigma_1$ ,  $\sigma_2$ , and  $\sigma_3$  denote the specific surface free energy of a crystallites, and  $L_1$ ,  $L_2$ , and  $L_3$  are the dimensions of the crystallite. The subscripts represent the three orthogonal directions in a chain-folded lamella.  $T_m^0$  is the equilibrium melting temperature of the crystal with infinite thickness (146°C),  $\rho_c$  is the crystal density (1 g/cm<sup>3</sup>), and  $\Delta H_m^0$  is the heat of fusion per unit mass (288 J/g). In general the lateral dimensions of a crystal in bulk are much



higher than the thickness so that only the terms with the subscript 1 remains in equation 1.  $\sigma_1$  has the value of 94 mJ/m<sup>2</sup>. Applying this equation to the homopolymers produced with our catalysts, which melt at 131°C in bulk, we obtain a crystal thickness of 17 nm. This value is very close to the average pore size of our support which is 24 nm for Grace 948 and 38 nm for PQMS 3030. In addition one of the two lateral dimensions will be greatly reduced if the polymer crystal is formed into a pore. According to equation 1 smaller crystallites show a lower melting temperature. It is then clear that melting temperature depression at low reaction time (low yield) can be attributed to the presence of polymer into the pores of the yet-non-fragmented support. A deeper analysis will be conducted in the following paragraph.

The same authors performed isothermal crystallization analysis on their polymers and used the Avrami equation to find that when the polymer is confined in pores, nucleation is favored respect to crystal growth. The interested reader is referred to ref. [8] for more details. Let us just tell here that a limited crystal growth by nanospace confinement leads to a decreased crystallization temperature and crystallinity. In their work the authors measured a crystallinity of 70% for the polymer in bulk and of 30% for the polymer in 15nm pores.

By performing nonisothermal crystallization studies at a cooling rate of -10 K/min the authors were also able to see different nucleation mechanisms according to pore size. It is known that PE in bulk crystallizes around 115°C with a heterogeneous mechanism. Crystallization peaks of polymers confined in pores having diameters from 62 to 110nm are appearing around 80°C and present a sharp aspect. As explained earlier, homogeneous nucleation requires high supercooling because of the high critical nucleus size needed for crystal stability. In addition the authors found that in this kind of pores the crystallization rates are highly dependent on temperature, which is typical of homogeneous nucleation. It is then believed that homogeneous nucleation is the dominant mechanism for polymer confined in this type of pores. For smaller pores (15 to 48 nm) a broad crystallization peak spanning from 80 to 110°C has been measured together with a small dependence of the crystallization rate on the temperature. This is a clear sign that heterogeneous nucleation is the dominant mechanism in very small pores. This is evident if we think about the high surface-to-volume ratio of small pores, which increases the chances for the polymer chain to form a nucleus on the pore wall. For more details the reader is referred to [9].

A detailed discussion of the crystallization of the polymer in our samples will be given in the next paragraph together with the related DSC thermograms.

Before concluding, it has to be said that this type of behavior it is not only typical of polymer in pores, but it is general for macromolecules that evolve in any type of confined space. Melting temperature depression is known for thin films on substrates [10, 11] while homogeneous nucleation and decrease of the crystallization temperature of tens of degrees is known for crystalline mesophases in block copolymers [12] and for polymer in droplets [13-16].

### 3.3. Morphological (re)interpretation of DSC results

In this section we will interpret (and re-interpret) the DSC thermograms of our samples in light of the theory explained above and giving special attention to the particle morphology. It will be interesting to see how it is possible to infer about the particle morphology (or the degree of fragmentation) just by carefully analyzing the DSC spectra.

#### 3.3.1. DSC study on homopolymers

We have already seen how the melting temperature and crystallinity of the homopolymers produced using supported metallocenes in short reactions evolve. Such behavior is independent on the type of metallocene used, the supporting procedure and the type of support selected. In Figure 11 the DSC thermograms corresponding to polymers produced at different reaction times using  $(n\text{BuCp})_2\text{ZrCl}_2$  at reference conditions are shown. In the lower part of the figure the 2<sup>nd</sup> heating steps are represented. It is easy to see how the melting temperature increases with reaction time. In the upper part of the figure the curves corresponding to the cooling step are shown. In general three crystallization peaks are visible: one appearing for very low reaction times at 75°C, one appearing for reaction times higher than 2s and spanning from 90 to 110°C and one appearing for reactions longer than 5s at 115°C. The first crystallization peak disappears quickly and is no more visible for reactions longer than 2s. The second one is predominant in the time range between 2 and 15s and becomes less and less visible as the reaction time increases. The third peak is visible from 5s and becomes more and more important. This peak is the one (and the only one) that can be seen for polymers produced in long term reactions. It is very interesting to notice that the temperatures at which the three peaks are appearing are very close to the values reported by Woo et al. [8, 9] as previously explained. If the different peaks represent the crystallization of

PE chains in different space confinements, we can then explain this evolution by recalling the process of morphogenesis of a polyolefin particle.

In the very first reaction instants the pores that are more accessible are gradually filled with polymer. This kind of pores should be on the particle external volume or can be big pores located anywhere in the particle. The polymer confined in such big pores, as shown in the previous paragraph, crystallizes according to a homogeneous nucleation mechanism that requires high supercooling. That's why at very short reaction times we measure a crystallization peak at 75°C. This crystallization peak is really representative of chains evolving in confined space and it is not an artifact due to the specific used method of analysis. This is confirmed by the fact that the melting and crystallization peaks measured during a third heating step and a second heating step on the sample produced by reaction lasting 0.7s are also appearing around 119°C and 75°C respectively. Increasing the heating rate from 5 to 50 K/min is responsible for a shift of the melting temperature peak to 123°C, which is simply due to a delay of the real sample temperature respect to the programmed temperature (50K/min is a really high heating rate for DSC). Crystallization peaks remain unchanged also in this case. An annealing imposed for 2 hours at 90°C during the cooling step (that is just before the apparition of the crystallization peak at 75°C) does not change either the crystallization exotherm. These findings confirm that the unusual crystallization peak found at very short reaction times is really due to homogeneous polymer crystallization into the support bigger pores.

Successively, as the reaction goes on, also the smaller pores start to be filled. In this pores heterogeneous nucleation is dominant but, as the chains are confined in a small space, the crystal cannot growth freely and this reduces the crystallization temperature. That's why a crystallization peak at 105°C is measurable. As this kind of pores (smaller than 40 nm) contributes to the majority of the pore volume of our supports, the second crystallization peak becomes rapidly dominant and the first one becomes rapidly negligible. The quantity of polymer which can be accommodated in this type of pores is in fact much bigger than the one that can be present in the larger pores. In addition it is possible that the disappearance of the first crystallization peak is also partly due to the fragmentation of the pores firstly filled.

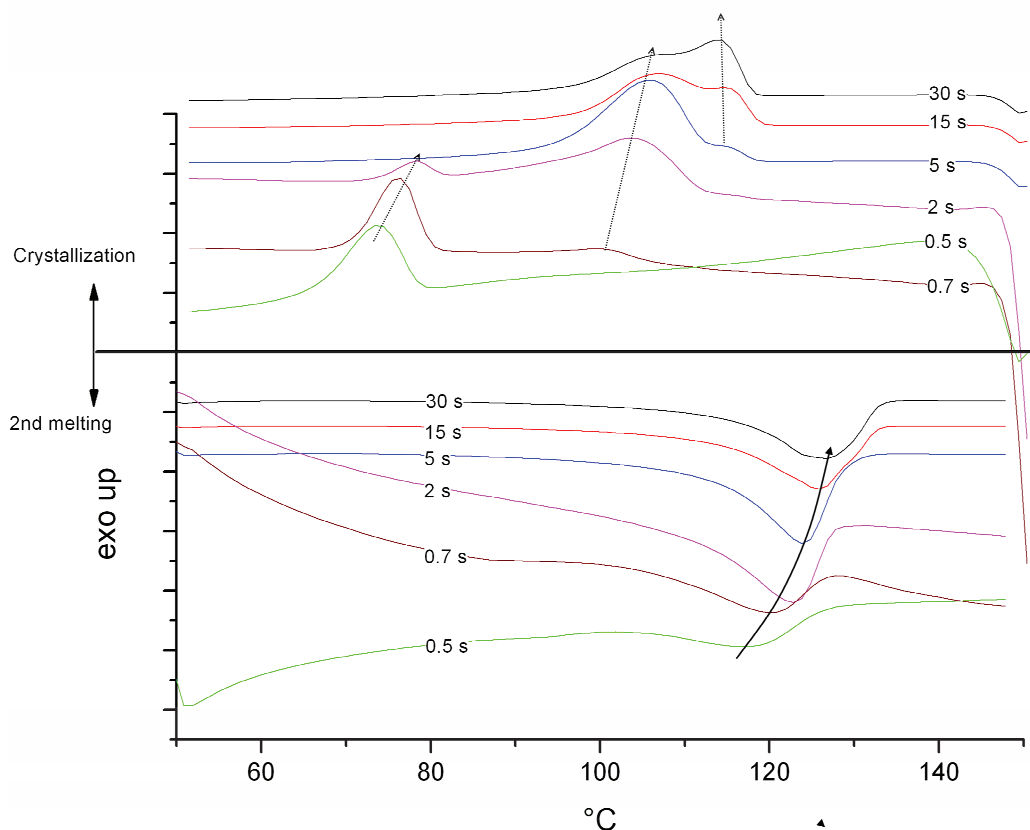


**Figure 11: DSC thermograms of polymers produced at different reaction times using supported  $(nBuCp)_2ZrCl_2$  under reference conditions.**

During this time range (that is when the polymer is confined in pores), the crystal growth is limited and the melting temperature is depressed. The depression is however less and less important because of the gradual pore fragmentation which decreases the average space confinement of the chains present in our support. The presence of chains that are confined in different environments together with chains that are not confined is visible in the quite broad shape of the melting temperature peaks.

For longer times, as the reaction goes on, the first pores are gradually fragmented (5s). There is then a certain amount of polymer chains that goes from a confined environment to a bulk environment. In this case the crystals can nucleate and grow freely to minimize the surface energy, giving a classical crystallization peak at  $115^\circ C$ . This peak becomes more and more predominant as the reaction continues because more and more pores are fragmenting. However, due to the decrease in the reaction rate for this time range ( $> 5s$ ) the increase of the third peak is slow and at 30s we can still observe a coexistence of the second and the third crystallization peaks. For the same reasons the melting temperature grows to values closer to the classical values. The reactions presented in Table 1 (180s reaction time) show melting temperatures very close to the bulk values and, not shown here, third crystallization peaks

much bigger than the second ones. The amount of chains in bulk environment is now predominant (a big part of the pores is already broken) and the situation is closer and closer to what is found after long term reactions.

### 3.3.2. X-ray microtomography study on homopolymer particles.

The analysis of the evolution of the internal morphology of the polymer particles with reaction time at start-up can give a confirmation of the conclusions exposes in the previous lines. Internal morphology can be followed by analyzing the samples by Synchrotron X-ray tomography. This technique allows to visualize the internal structure of the object of interest in a non-destructive way and, due to the difference in the absorption of X-rays between the void and the different solid phases, allows to visualize the spatial distribution of the pores, the polymer and the inorganic phase. More details on the analysis technique are given in the Experimental Part. NaCl was not removed from the samples for analysis as the contact with water can alter the particle morphology. NaCl has a big attenuation coefficient towards X-rays and is very bright in tomography images. The darker phase will be the void space while the polymer and the silica will be light grey, with silica a bit lighter than polymer. It has to be said that the presence of NaCl lowers the phase contrast between silica and polymer. Each pixel on the image has a size of 0.35  $\mu\text{m}$  so that only bigger pores and domains can be visible.

Nevertheless some general conclusions can be drawn from the following images which refer to reactions performed under reference conditions.

From Figure 12 it is possible to see that the original support (Grace 948) is formed of pseudospherical particles highly heterogeneous in terms of internal structure. Some of them are compact, other very porous, other show small fragments around a big central fragment with porosity only on the exterior of the particle. This will of course be responsible for some heterogeneity in particle morphogenesis.

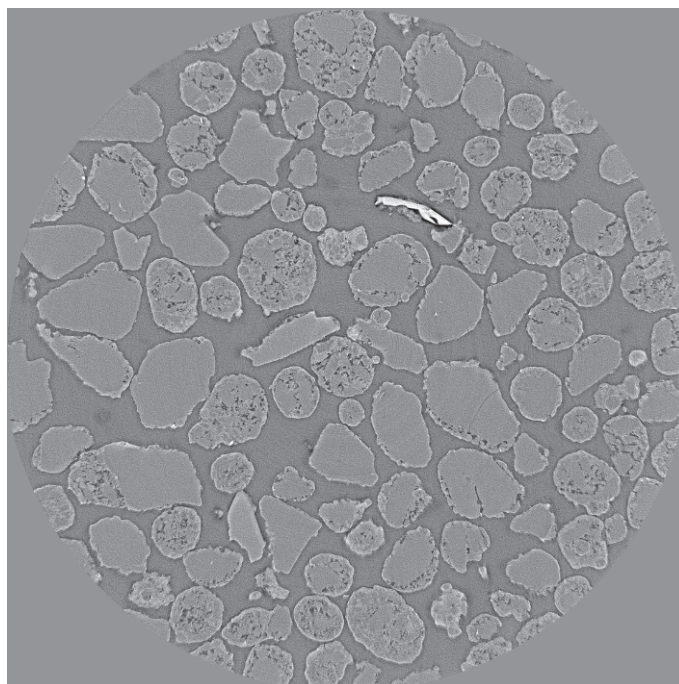


**Figure 12: Tomography image of Grace 948**

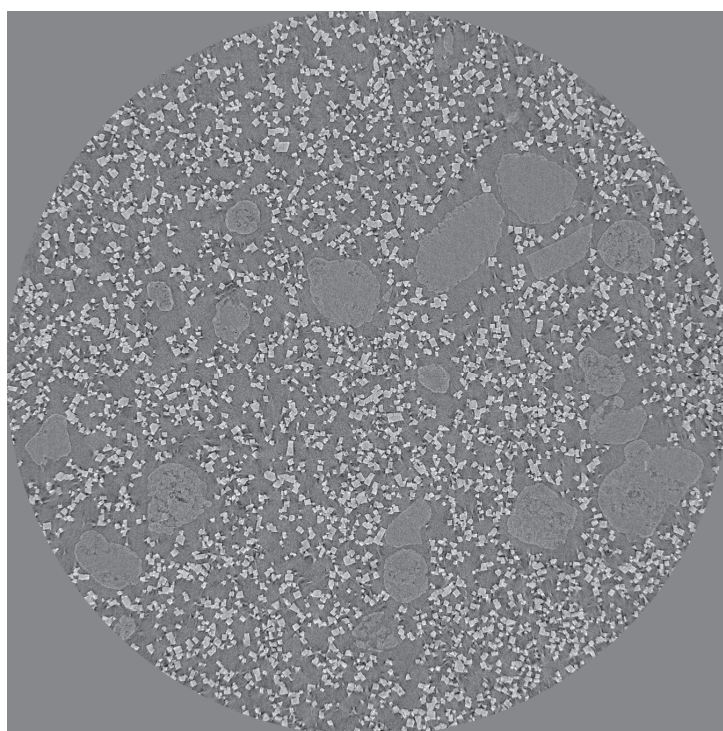


**Figure 13: 0.3 s reaction.**

After 0.3 seconds of reaction no PE is visible onto the catalyst particles with our resolution and the internal pores seem to be still empty. After 0.7s (Figure 14) some polymer forming a thin film around the particles is visible. Starting of pore filling is also visible together with the first concentric structures recalling on onion-like fragmentation (Figure 15).

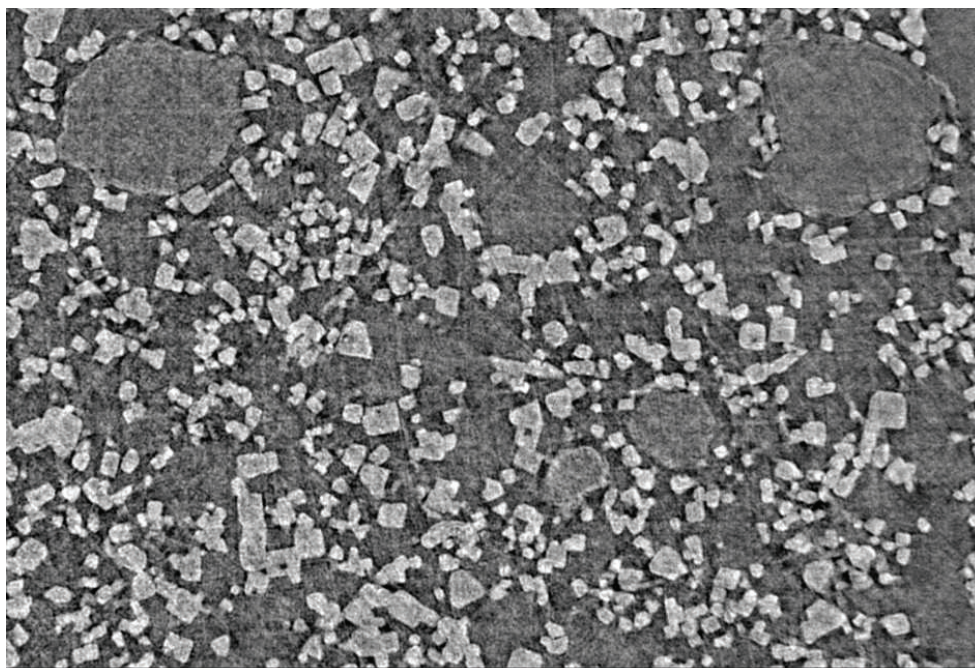


Figure 14: 0.7s pore filling (left particle) and thin PE film (right)

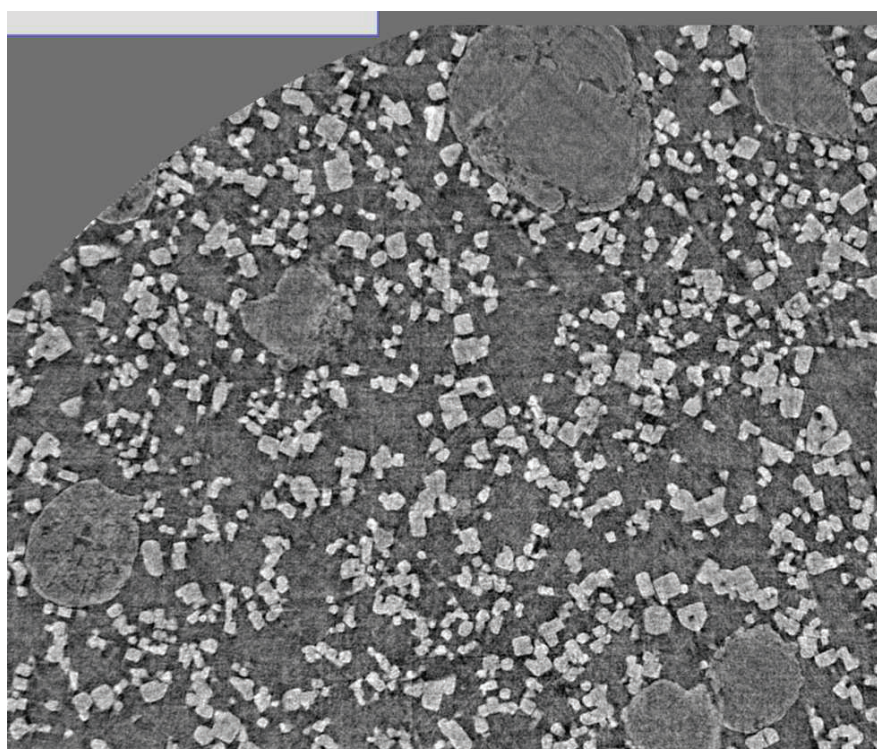
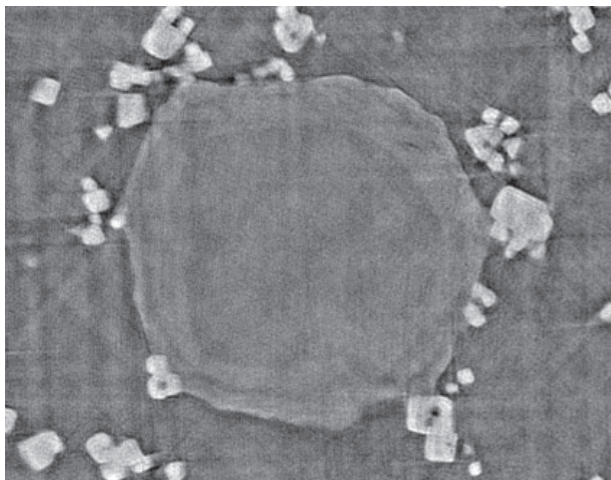


Figure 15: 0.7s first concentric structures (upper big particle)

After 5s the evolution is clearer: concentric structures are more and more frequent; the outer particle shell seems to be an alternance of polymer and silica layers while the core seems to be formed by silica fragments dispersed in a more or less continuous PE matrix (Figures 16 and 17). Note that some polymer is visible on the outer particle surface in Figure 17. The chains

located on the external surface are not confined in space and behave like if they were in bulk. Nevertheless some particles show still some internal pores not filled (Figure 18) (not communicating with the outer surface?). Particles that are not easily fragmented seem to prefer the formation of a thick polymer film on the outlet surface (Figure 17).



**Figure 16: 5s; particle showing outern concentrical structure and internal silica fragments in a PE matrix**

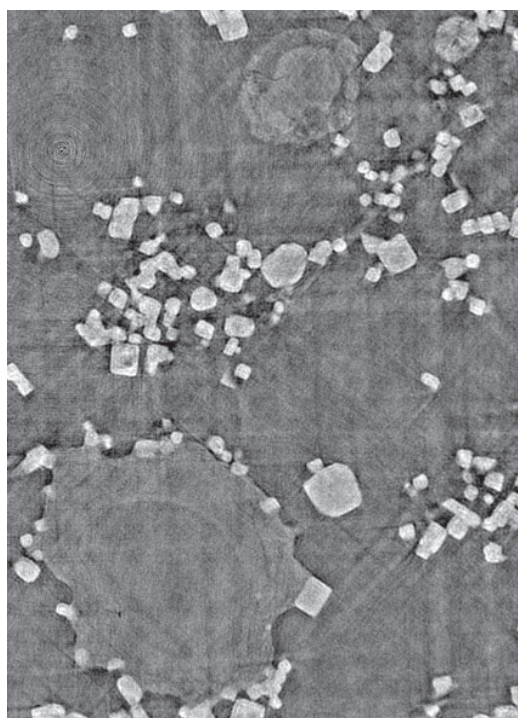


**Figure 17: 5s; particle showing concentrical structures in the outer shell (down) and particle showing preference to external PE film formation (up)**



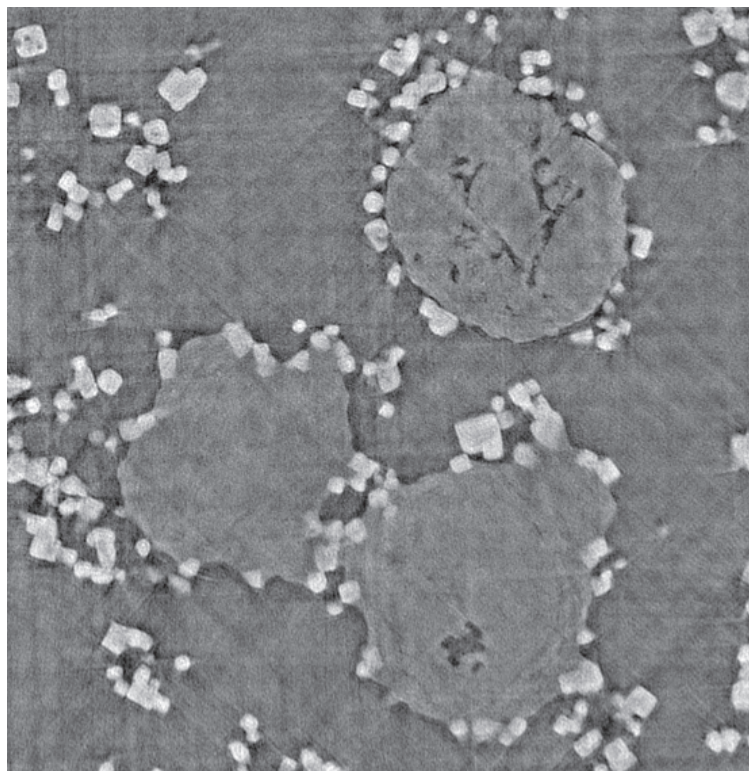


**Figure 18: 5s, particles showing inner empty pores**

After 30s of reaction the polymer layer around the particle starts to become more consistent and frequent (Figures 20 and 21). NaCl crystals stuck around the particles are a sign of the presence (and maybe the softening) of the PE external layer. Internal empty pores are less and less frequent (Figure 19).

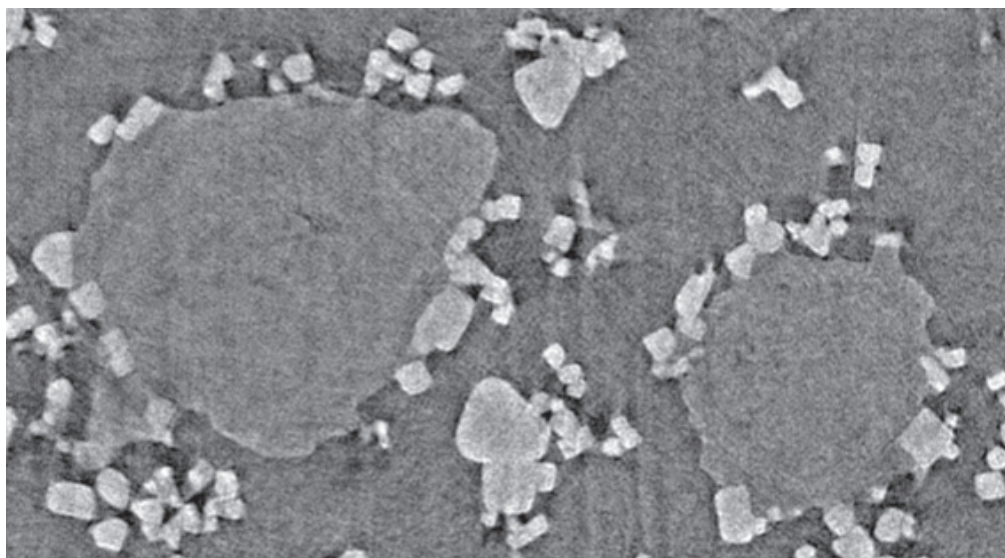


**Figure 19: 30s, PE external layer and complete internal pore filling**

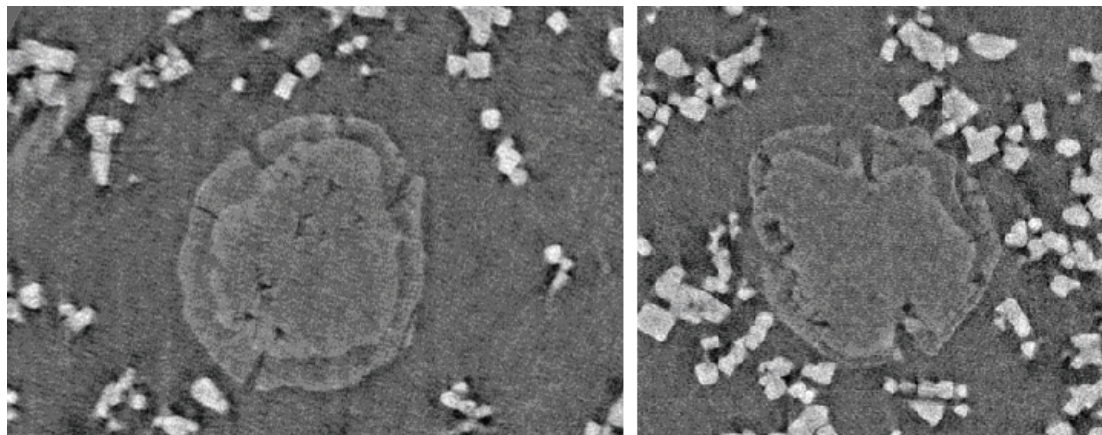


Figure 20: 30s; example of two particles with a consistent PE external layer.

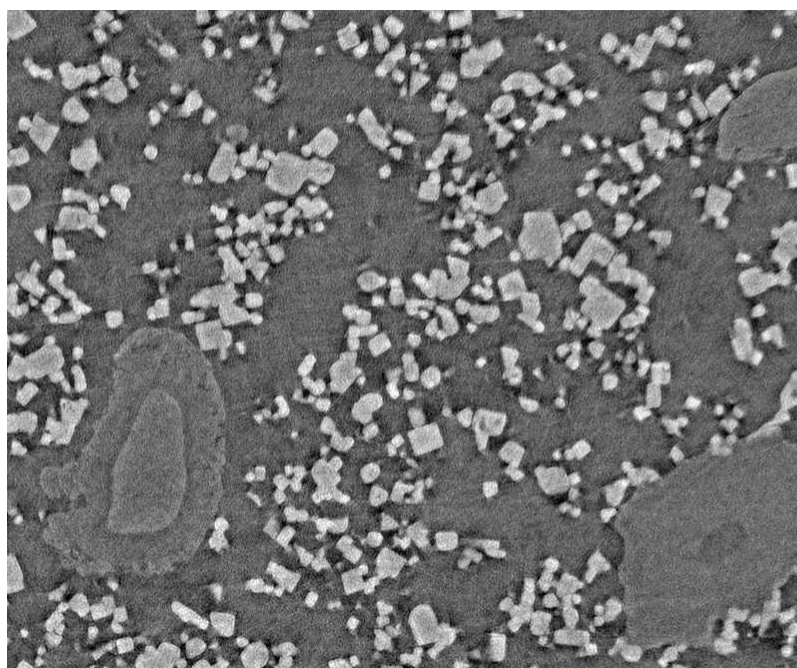


Figure 21: 30s, thick PE layer around unfragmented core (right) and thinner PE layer around hollow core with PE filled center (left).

After 75s of reaction almost all particles have a PE layer on the outlet surface and core is formed by a matrix of PE in which more or less big and numerous silica fragments are present (Figures 22-25). The images presented here cover a yield range from 0 to 1.87 g/g that corresponds to support pore filling, start of gradual layer by layer fragmentation from the outlet and start of the deposition of the PE layer on the outer surface. More spectacular fragmentation effects can be visible for higher reaction yields (some g/g).

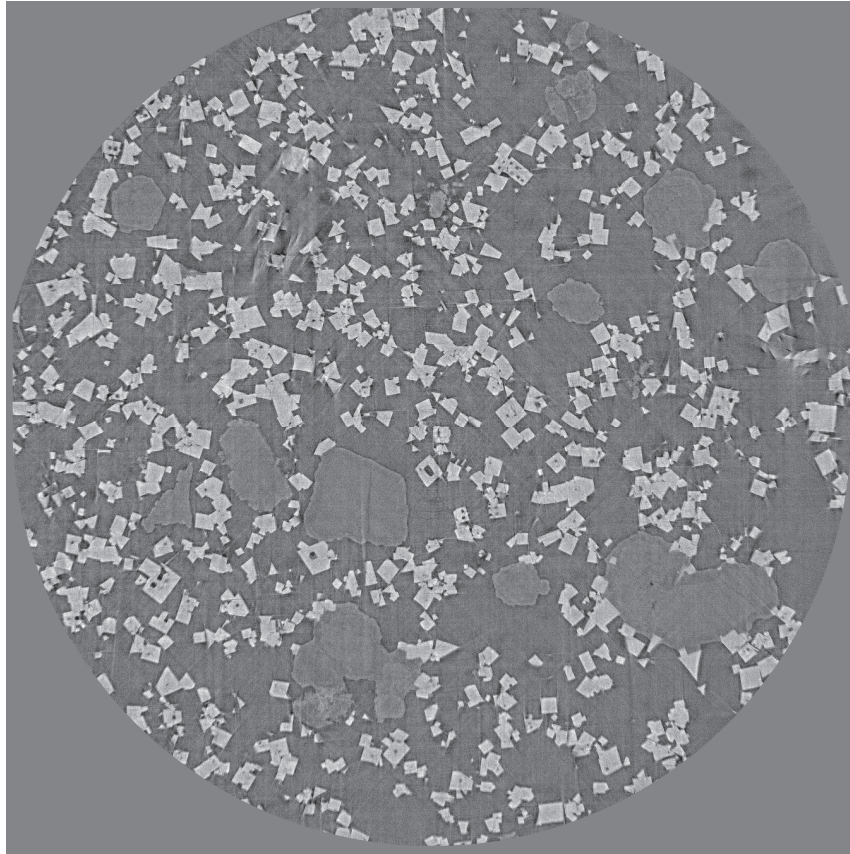


Figure 22: 75s, general overview; almost all particles show external PE layer and internal core formed by bright areas (silica) more or less fragmented in a dark matrix (PE)

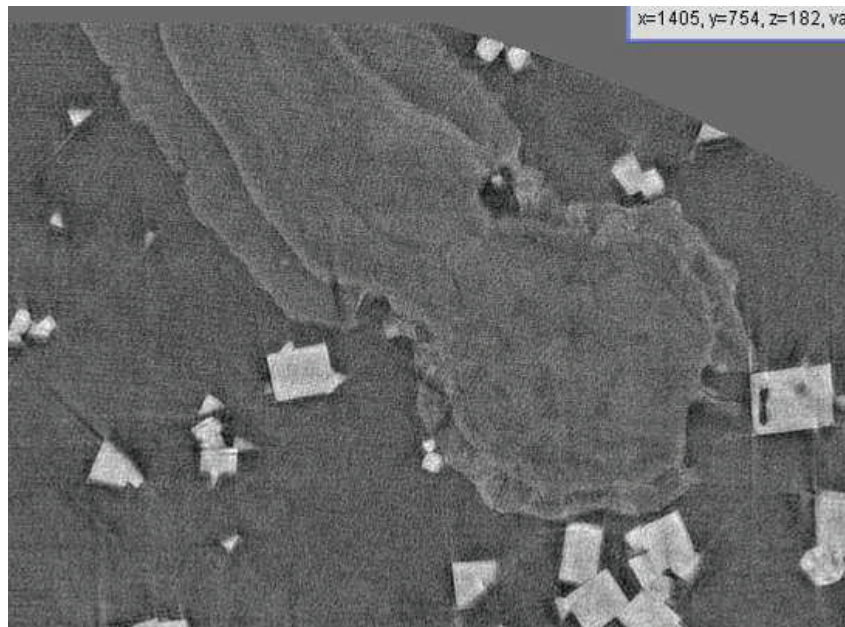


Figure 23: 75s, zoom on particle, note the pore filling and beginning of fragments separation

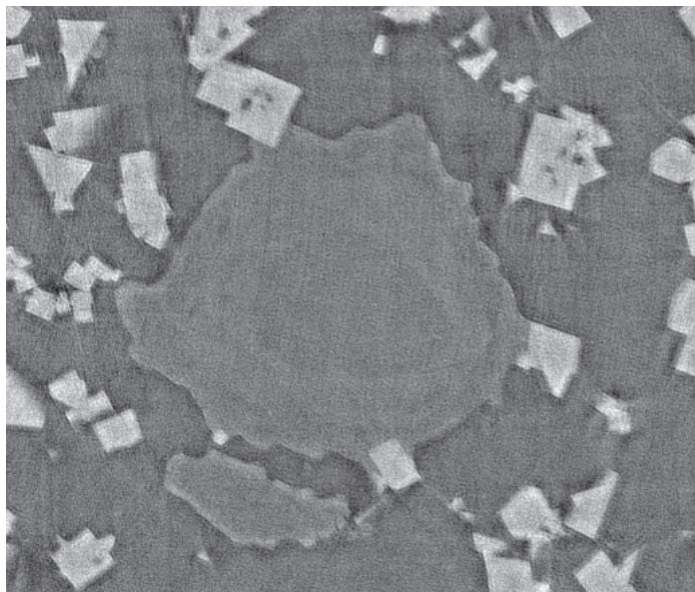


Figure 24: 75s, zoom on particle, note the concentric structures

The observations on morphology evolution just explained match the hypotheses on crystallization introduced in the previous paragraph. External polymer film formation and advanced pore filling and fragment separation is seen clearly only from 5s reaction ( $Y = 0.8-1$  g/g). This yield value is a kind of borderline after which crystallization exotherm corresponding to bulk PE crystallization starts to appear. For lower yields and reaction times the small amount of visible polymer seems to be confined into the particle pores and even not all of them are filled. In parallel the corresponding DSC thermogram shows crystallization exotherms that we can assign to PE crystallization in confined space. For yields lower than 0.2 g/g only the first crystallization peak at 75°C is visible and the melting temperature is highly depressed (around 120°C). This probably corresponds to filling of the bigger or most accessible pores. In this time range only gradual pore filling can be seen from the tomography images.

In the previous paragraph we have also seen that the crystallinity of the homopolymers at reaction start-up is around 40-50% for times lower than 2s and passes through a maximum at 70-80% between 2 and 5s to stabilize lately on classical values of 50-60%. It is difficult to explain this behavior with the crystallization in confined space. However it has to be noticed that the maximum in crystallinity is reached in the time range when the second crystallization peak is dominant. The reasons for which the crystallinity of the polymer confined in small pores should be so high are not clear. In addition it has to be said that the beginning of the reaction rate decay corresponds to the time in which maximum crystallinity is measured so that it is possible that part of the reasons for the decaying activity profile is the limited monomer diffusion to the active sites due to low amount of amorphous domains.

### 3.3.3. Copolymerization

We have seen in the previous paragraphs that copolymers produced with supported  $(n\text{BuCp})_2\text{ZrCl}_2$  have a melting temperature and crystallinity evolution very similar to the one of the homopolymers. The melting temperature is however 7 to 10°C lower for the copolymer for each reaction time due to the incorporation of butene into the polymer backbone. The DSC thermograms (not shown here) are also very close to the ones of the homopolymer with crystallization temperatures few degrees lower for the homopolymer for the same reason. A more interesting result come from the DSC analysis of copolymers made with supported  $\text{Et}(\text{Ind})_2\text{ZrCl}_2$  which has an increased capability to incorporate the comonomer into the backbone giving a copolymer that melts at 113°C for long term reactions. Using the Gibbs-Thompson equation for this copolymer gives a crystal thickness of about 8nm. The crystallites in this case should then be less perturbed by the space confinement. This is reflected in Figure 3, which shows that the copolymer melting temperature is constant in the reaction time range from 0.5s to 30s (and also after 1h reaction the same melting temperature is measured). Figure 25 shows a comparison between the thermograms of the copolymer and the respective homopolymer for three relevant reaction times. The yields of two samples collected at the same reaction times are similar. It is clear that the same trend for the crystallization peaks is seen no matter if the comonomer is present or not. This means that also for the copolymers, despite what can be thought by calculating the copolymer crystal thickness, the space confinement due to the pores in the first reaction seconds is present. However, due to the fact that the crystallites are smaller for the copolymer, the space confinement does not provoke a melting temperature depression. In addition one have to notice that, for the same reason, crystallization peaks of the copolymers are shifted of 10°C towards lower temperatures.

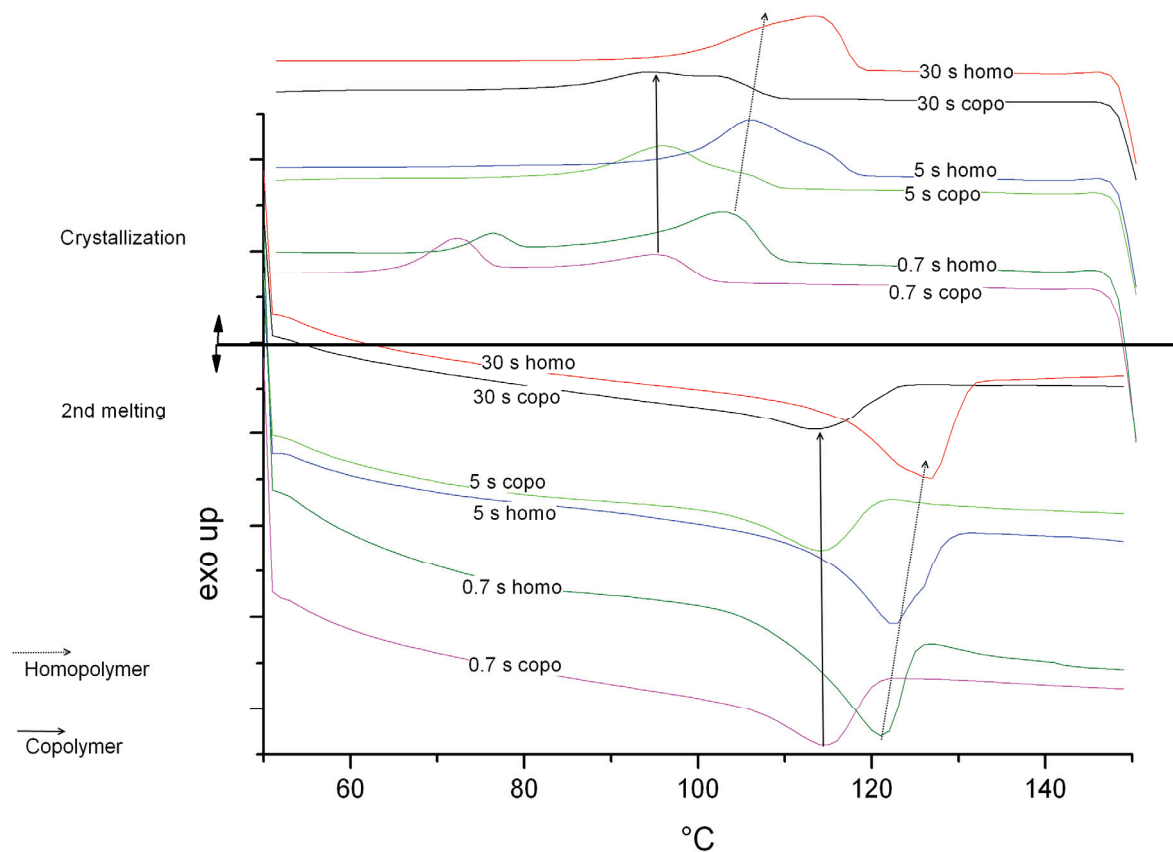


**Figure 25:** DSC thermograms of homo- and co-polymers produced at different reaction times using supported  $\text{Et}(\text{Ind})_2\text{ZrCl}_2$  under reference conditions.

### 3.3.4. Influence of support size

The size of the support should not influence the crystallization of the polymer if carriers with similar pore volume and pore size distribution are used. This is exactly our case as we have prepared catalysts supported on particles having different sizes but similar pore volume and pore size as shown in the previous chapter. That's why a certain surprise can come from looking at Figure 26, where the melting temperature of polymers produced using different catalyst sizes are compared at various reaction times.

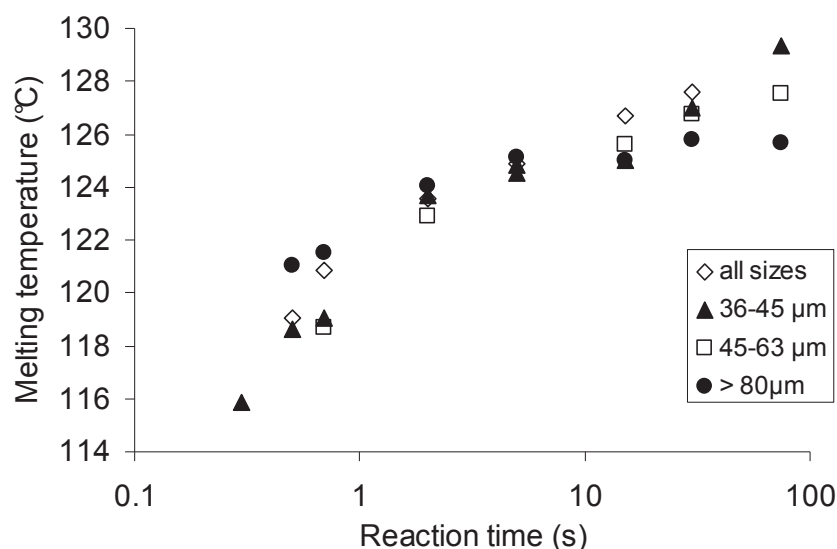


Figure 26: Melting temperature evolution for polymers produced using different catalyst sizes.

First of all the same evolution can be seen independently on the particle size: low  $T_m$  at the beginning increasing with reaction time. However it seems that the smaller the particles are, the higher the difference between the final (75s) and the initial values (0.3 or 0.5s) of the melting temperature is. This has two reasons: as we have previously seen the support size has an influence on the activity for reaction times higher than 15s, with the bigger particles being less active than the small ones. In addition one has to consider the yield as independent variable rather than the reaction time. If we go back to the idea that the low  $T_m$  at the beginning is due to the fact that at low yields the polymer is formed and crystallizes in the pores more than in the bulk we see that the important parameter giving the final overall melting temperature is the ratio between the polymer quantity in the pores and the one in the bulk. At low yields the majority of the polymer is in the pores. With increasing yield the proportion of PE in the bulk becomes bigger and bigger and the  $T_m$  higher and higher. Depending on catalyst activity a certain value of yield can be reached at different reaction times. The concept is demonstrated clearly in Figure 27 where all the measurements, independently on the support size, are put into the same graph and are nicely fitted by a logarithmic function.

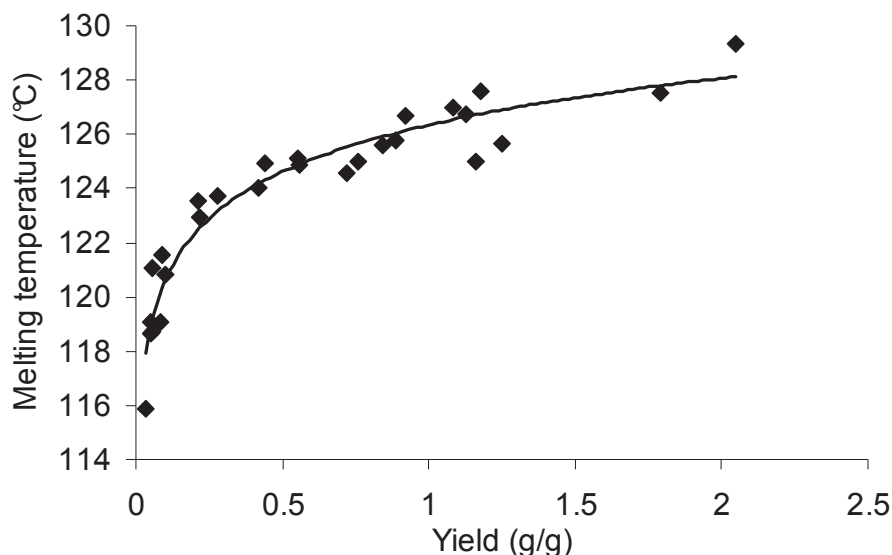


Figure 27: Melting temperature dependence on reaction Yield.

The differences in the activity of particles having different sizes has as consequence to give DSC spectra (especially the cooling step) that are slightly different for the same reaction time. This can be very important during the modelling step: not only the activity at a certain time is a function of the support size, but also the polymer properties, which in turn influence the monomer diffusivity and the fragmentation path.

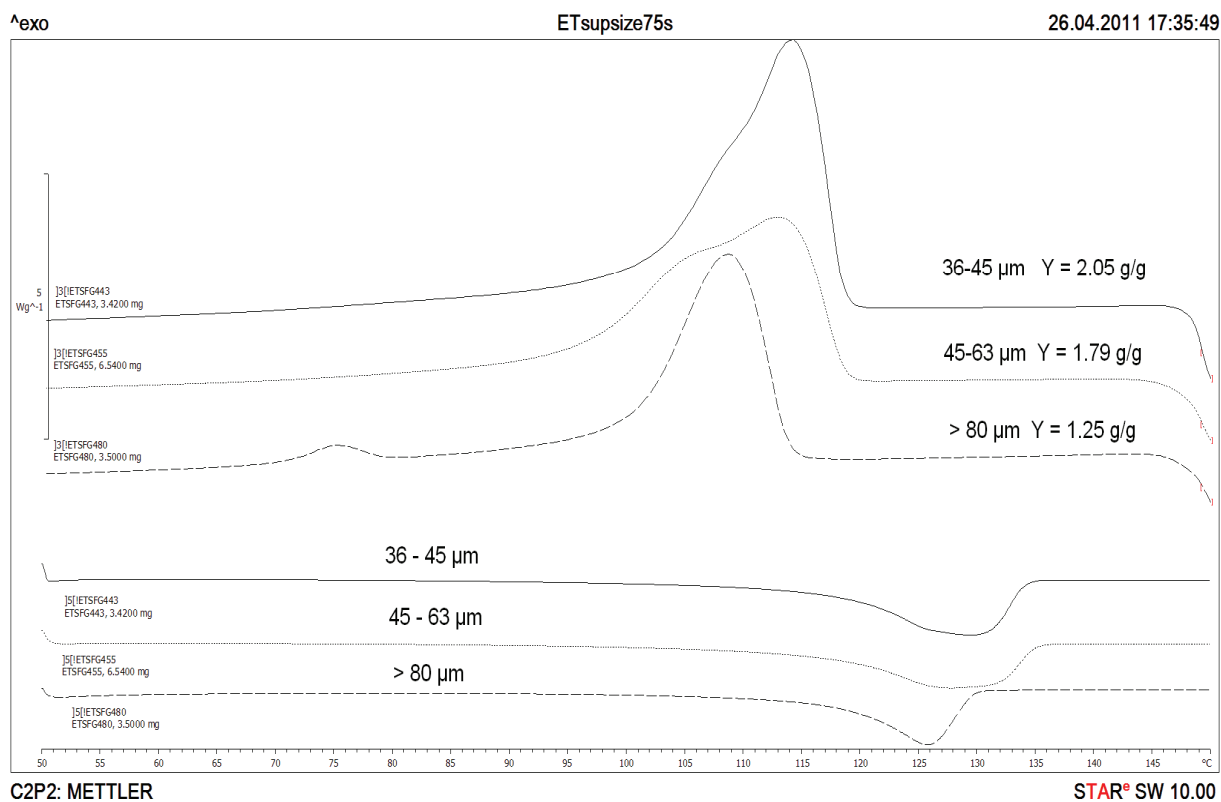


Figure 28: DSC thermogram of polymers produced by catalyst of different sizes in a 75s reaction: upper curves = cooling step, lower curves = 2<sup>nd</sup> heating step.



Figure 28 clearly shows that the higher is the yield, the higher is the melting temperature and the more dominant is the third crystallization peak (corresponding to the bulk crystallization).

The evolution of the crystallinity of the produced polymers with reaction time shows less straightforward dependence on particle size (Figure 29). In addition there is no clear relation with the reaction yield as is the case for the melting temperature. It has to be said that the experimental error for crystallinity measurement is higher than for melting temperature but this does not justify the scattering of the data. In addition it is easy to see that the classical behavior (low values at the beginning, peak around 2-5 s, and then decrease to steady state value) is not always verified in this case. For big particles the crystallinity seems to have high values even after very short reactions. The reasons for this behavior are difficult to understand.

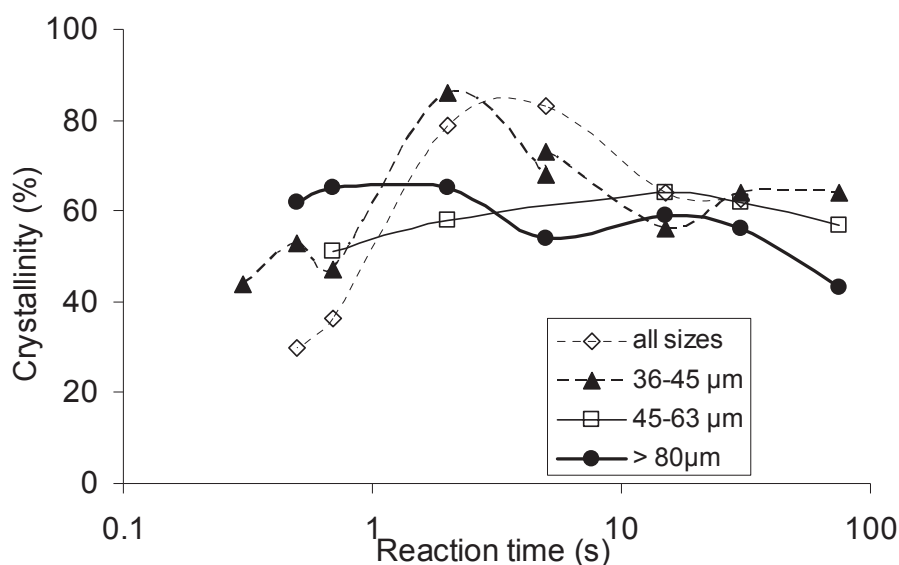


Figure 29: Crystallinity evolution for polymers produced using different catalyst sizes.

### 3.3.5. Influence of support pore size

Pore size can of course affect the crystallization of polyethylene in confined space and modify the values of the melting temperature and crystallinity of the polymers produced under similar yields and reaction times.

To study this phenomena we replaced the Grace 948 support having an average pore size of 24 nm with the commercial silica PQMS 3030 which has an average pore size of 38 nm. The difference in pore size might not impress the reader but it has to be said that the choice of the second support was limited by the fact that commercial silica had to be selected having the

same specific surface of Grace 948. A different specific surface will in fact lead to a different concentration of active sites per gram of catalyst and then to a superposition of chemical and physical effects with blurred results. The same metallocene used above ( $(n\text{BuCp})_2\text{ZrCl}_2$ ) was supported using the standard procedure and the polymers produced at different reaction times were analyzed by DSC. According to the concepts exposed above, the increased pore size should decrease the degree of confinement of the crystallites and then give slightly higher melting temperature for the same yield. However the pore size lies still in the range where important space confinement is present, and as a consequence the increase in the melting temperature should not be spectacular.

In Figure 30 one can see the evolution of the melting temperature (lower part) and of the crystallization peaks (upper part) of the polymers produced using the support with bigger pore size. The main features like melting temperature increasing with reaction time and evolution of three different crystallization peaks are clearly visible in this case too. The melting temperatures of the polymers produced using this catalyst are, as predicted, few degrees higher at the reaction start-up if compared to the ones of the polymers produced using the support with smaller pores. A bigger pore allows the growth of bigger confined crystallites which have a melting temperature slightly higher (but still quite depressed respect to bulk). This phenomenon is shown on Figure 31, where the melting temperature evolution of the polymers produced using the two different supports with the reaction yield is compared. It is interesting to notice that for yield higher than 1g/g the opposite behavior is found: melting temperatures of polymers produced with the support having bigger pores are lower. A possible reason for this behavior can reside in the pore volume. The support PQMS3030 has a pore volume of 2.8 mL/g while Grace 948 has a pore volume of 1.7 mL/g. This means that the PQMS 3030 support can accommodate more polymer into the particle pores than the other support. If two particles with the same yield (high enough) are produced, the Grace 948 one will be more fragmented than the PQMS 3030 one because of this. The consequence is a longer lasting depression of the  $T_m$  for polymers produced using PQMS 3030.

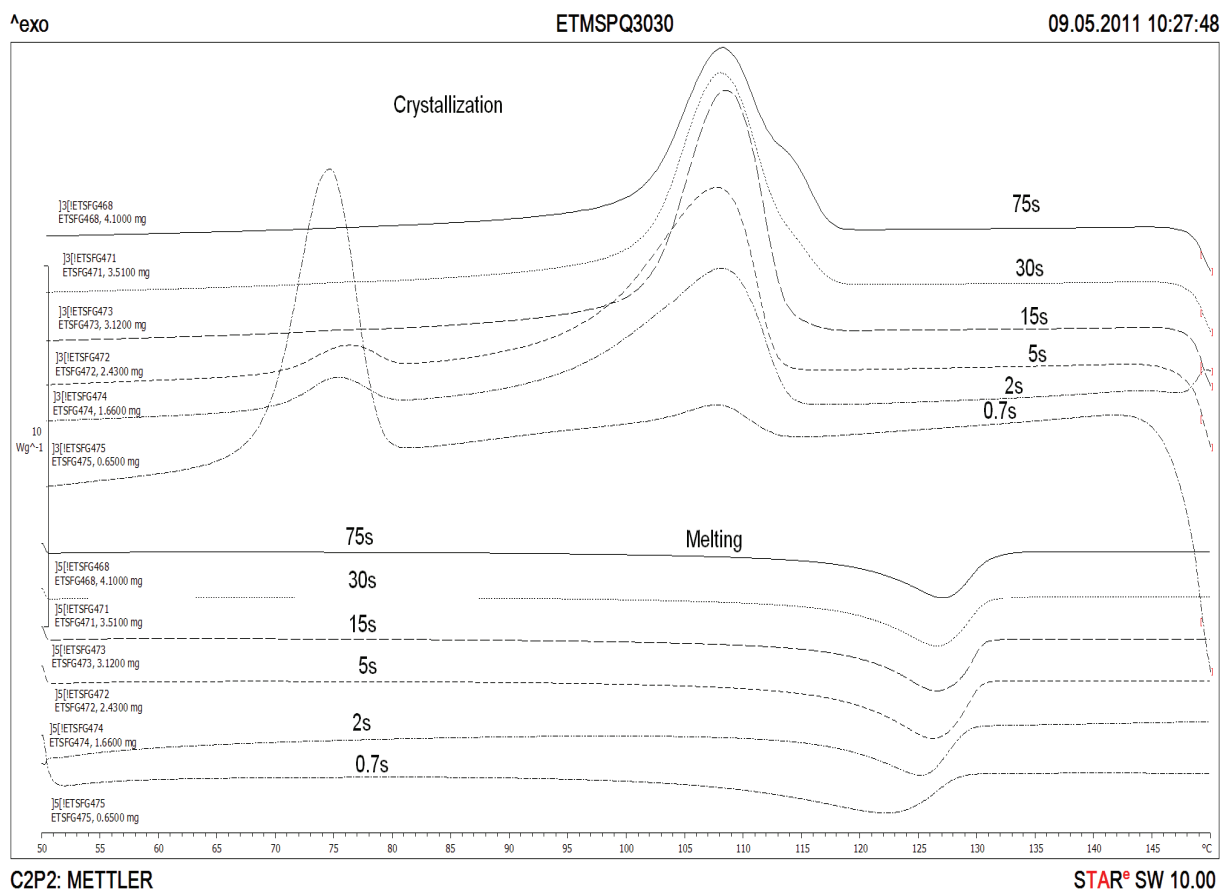


Figure 30: DSC thermograms of polymers produced at different reaction times using  $(n\text{BuCp})_2\text{ZrCl}_2$  on MAO treated PQMS3030.

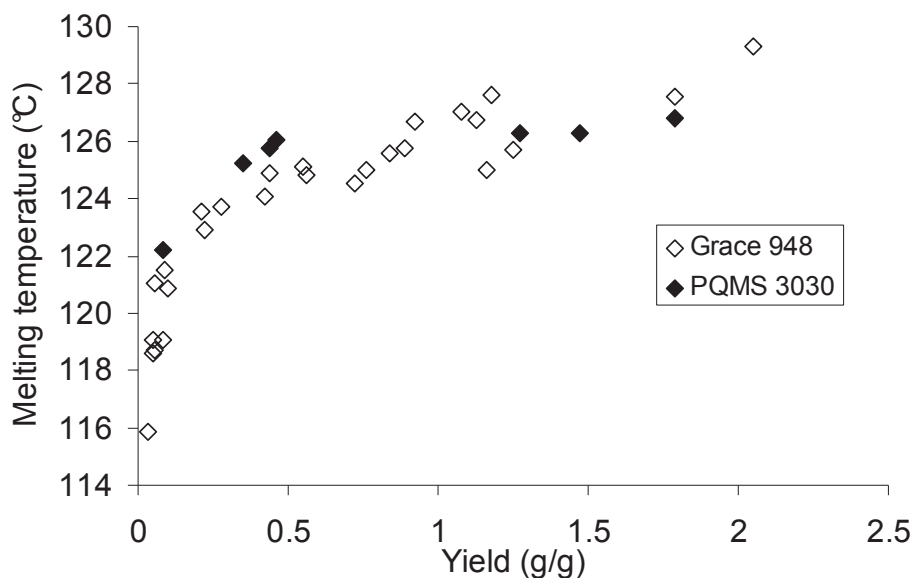


Figure 31: Influence of pore size on melting temperature evolution.

These differences are also seen in the evolution of the crystallization peaks. The ones corresponding to PQMS 3030 seem to be always delayed (late) in time respect to the ones corresponding to Grace 948, even if the yields are similar. Figure 32 compares the

crystallization peaks of the two supports. In case of PQMS 3030 the peak corresponding to bulk crystallization of PE (115°C) is very weak even for yields higher than 1.5, when it should be preponderant. Check out the 30s reactions in Figure 32. For PQMS 3030 support the yield is 1.47 g/g while for Grace 948 > 80µm is lower, 0.89 g/g. Nevertheless the crystallization peak at 115°C is more important in the thermogram corresponding to the Grace 948 support and this difference is even more evident at 75s.

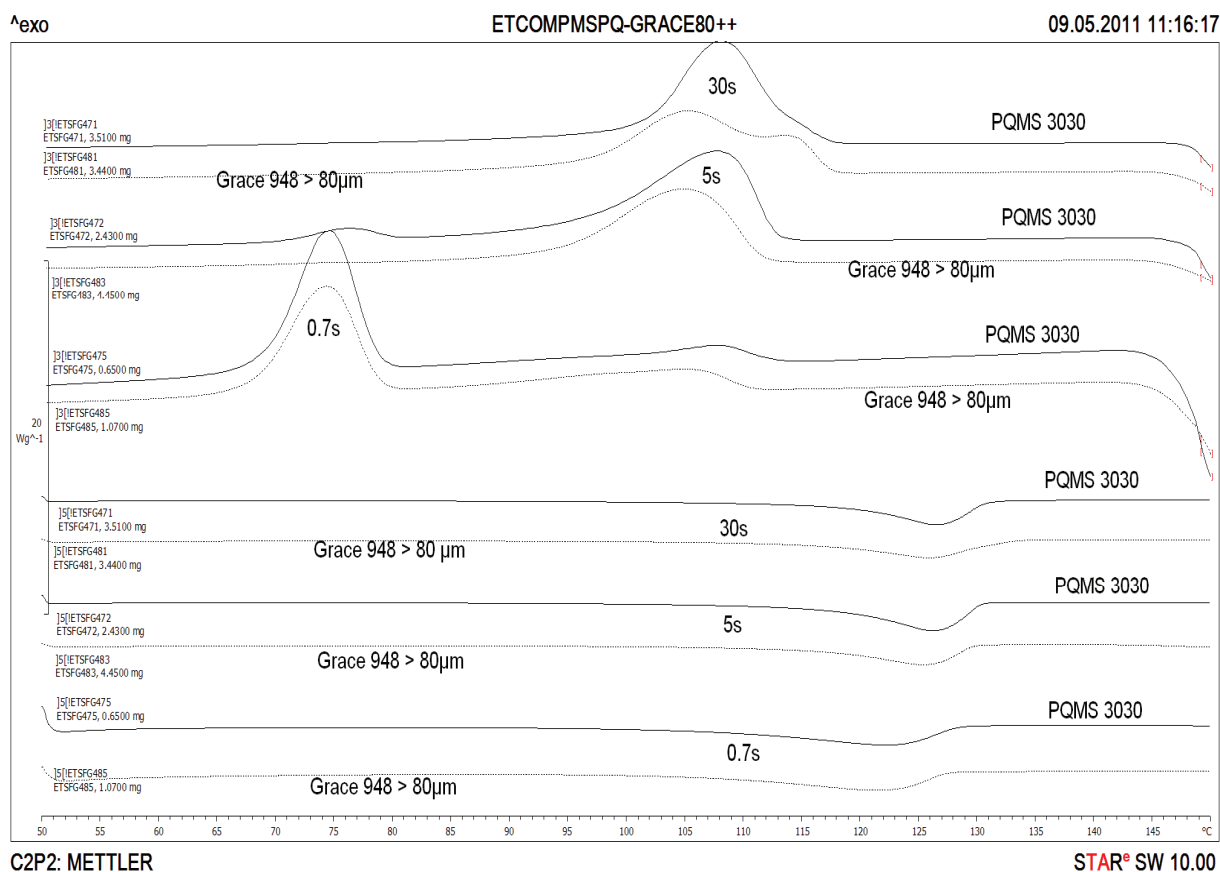


Figure 32: Effect of pore size on evolution of crystallization peaks.

As usual the crystallinity evolves in a less straightforward manner as shown in Figure 33. The support having bigger pores (PQMS 3030) has also an average particle size of 85µm, while the average particle size of the other carrier is 58µm. That's why we compare the results of PQMS 3030 also with the bigger cut (> 80µm) of Grace 948. In fact it seems that the evolution of the crystallinity depends more on the particle size than on the pore size, even if no logical explanation can be given to justify this behavior. Big particles do not show low crystallinity values at the beginning and maximum around 2s but have slightly decreasing values from 60-70 % for less than 1s to 45-60% for 75s reaction.

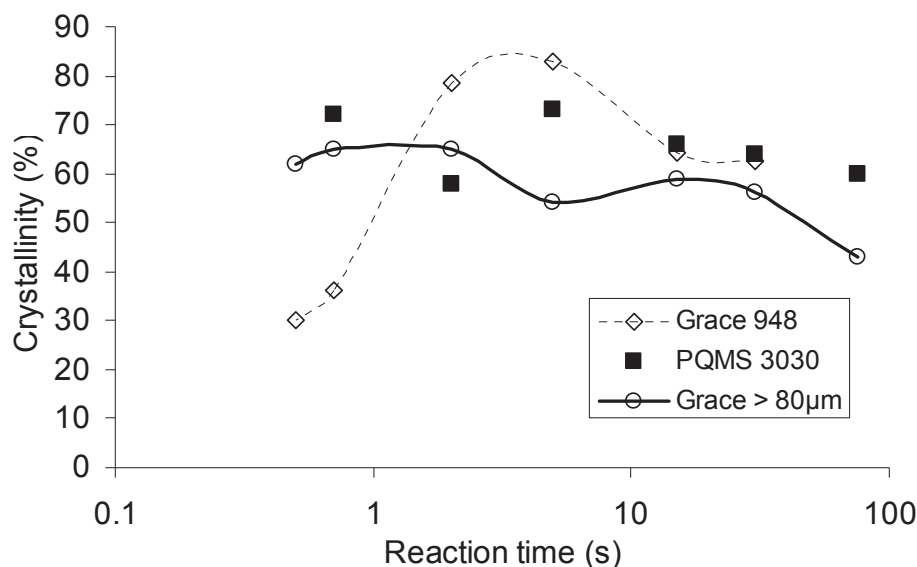


Figure 33: Influence of pore size and particle size on crystallinity at the reaction start-up.

### 3.3.6. Influence of catalyst preparation

We have seen in the previous paragraph that different contents of Al and Zr can be the reason for a different reaction rate profile at the start-up. This influences the rate at which the pores are filled and the way they fragment. In light of the confined crystallization behavior explained above it can be that a different reaction rate profile gives different crystallization behaviors.

First of all let's consider the  $(n\text{BuCp})_2\text{ZrCl}_2/\text{MAO}/\text{Grace948}$  catalyst (ETmet47) bearing a high Zr content (remember that in order to fix a high quantity of Zr we had to increase the Al content too). We have seen in the previous paragraph that the intrinsic activity of this catalyst has the same profile than the reference catalyst but with values one order of magnitude lower and a stronger deactivation. However if one converts the activity in  $\text{gPE/g cat/h}$ , which are the interesting units when dealing with crystallization in pores, he can see that this catalyst reaches a very high activity after 0.7s of reaction which decreases suddenly to values lower than the reference catalyst (Table 2). This means that a much bigger quantity of polymer is produced in the first reaction seconds respect to the reference series and much less in the following time, as it can be seen from the yield values.

Table 2 : Influence of Zr content on reaction rate and yield.

<i>Reaction time (s)</i>	<i>Yield reference(g/g)</i>	<i>Yield high Zr (g/g)</i>	<i>Activity reference (g/ g/ h)</i>	<i>Activity high Zr (g/ g/ h)</i>
0.7	0.1	0.2	738	2160
2	0.31	0.31	568	304
30	1.08	0.7	48	50
75	1.44	1.0	29	24

This also means that at the very beginning of the reaction the particle having more Zr has a higher degree of fragmentation respect to the reference one. Due to the faster deactivation, the opposite is true for longer reaction times. As a consequence higher melting temperatures respect to the reference series due to less confinement are measured for short reaction times if the catalyst having more Zr is used and the opposite is measured for long reaction times (Figure 34).

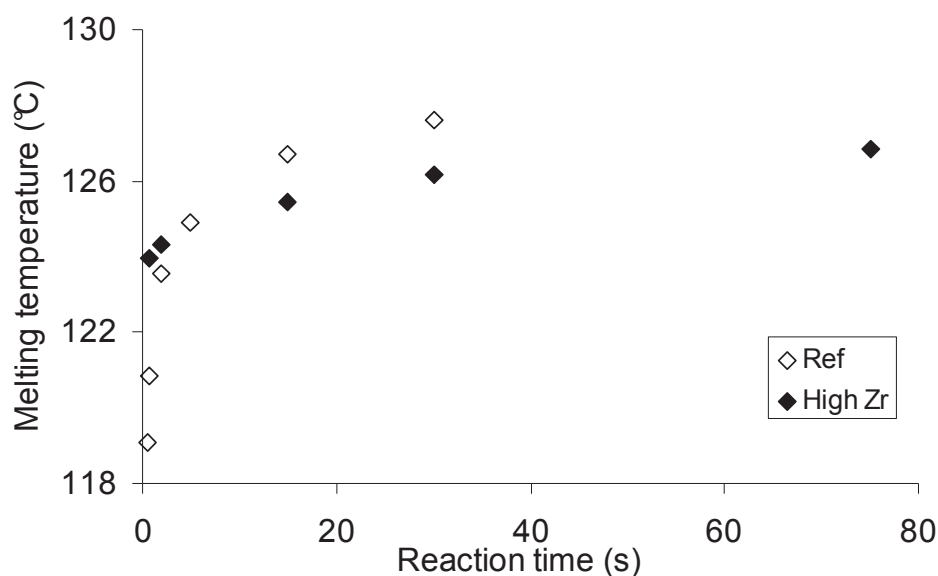


Figure 34: Evolution of melting temperature with reaction time for different Zr content.

It is nice to see from Figure 35 that if the melting temperature values are plotted against the yield, no differences are seen between the two series. The same is true for crystallinity.

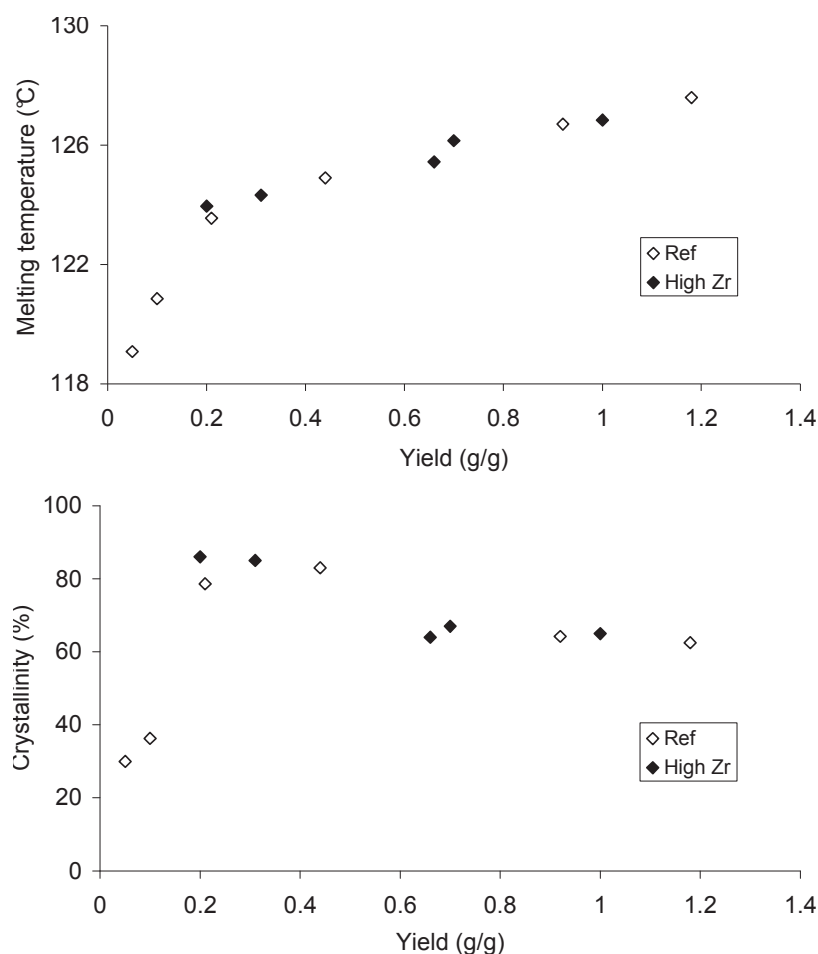


Figure 35: Evolution of melting temperature and crystallinity with yield for different Zr content.

In summary the change in activity at reaction start-up due to a change in the catalyst Zr content induces a different melting temperature evolution which is just an effect of the different speeds at which a certain yield value is reached.

Let us now consider the  $n\text{BuCp}_2\text{ZrCl}_2$  based catalyst prepared with a Zr content closer to the reference one but bearing a much higher Al content (ETmet46). If we perform the same analysis on activity as done previously, we see that the reaction rate, both in terms of g/g/h or in terms of g/ mol Zr/ h and the yield are much more higher from the very beginning of the reaction when a catalyst with high Al content is used (Table 3).

Table 3: Influence of Al content on reaction rate and yield.

<i>Reaction time (s)</i>	<i>Yield reference(g/g)</i>	<i>Yield high Al (g/g)</i>	<i>Activity reference (g/ g/ h)</i>	<i>Activity high Al (g/ g/ h)</i>
0.3	0.023	0.27	276	3240
0.7	0.1	0.31	738	360
5	0.5	0.44	228	142
15	0.88	0.75	137	104
30	1.08	0.85	48	19
75	1.44	1.1	29	19

The main consequences of this fact can be seen in the thermograms of the polymers produced with the catalyst having an high Al content, shown in Figure 36.

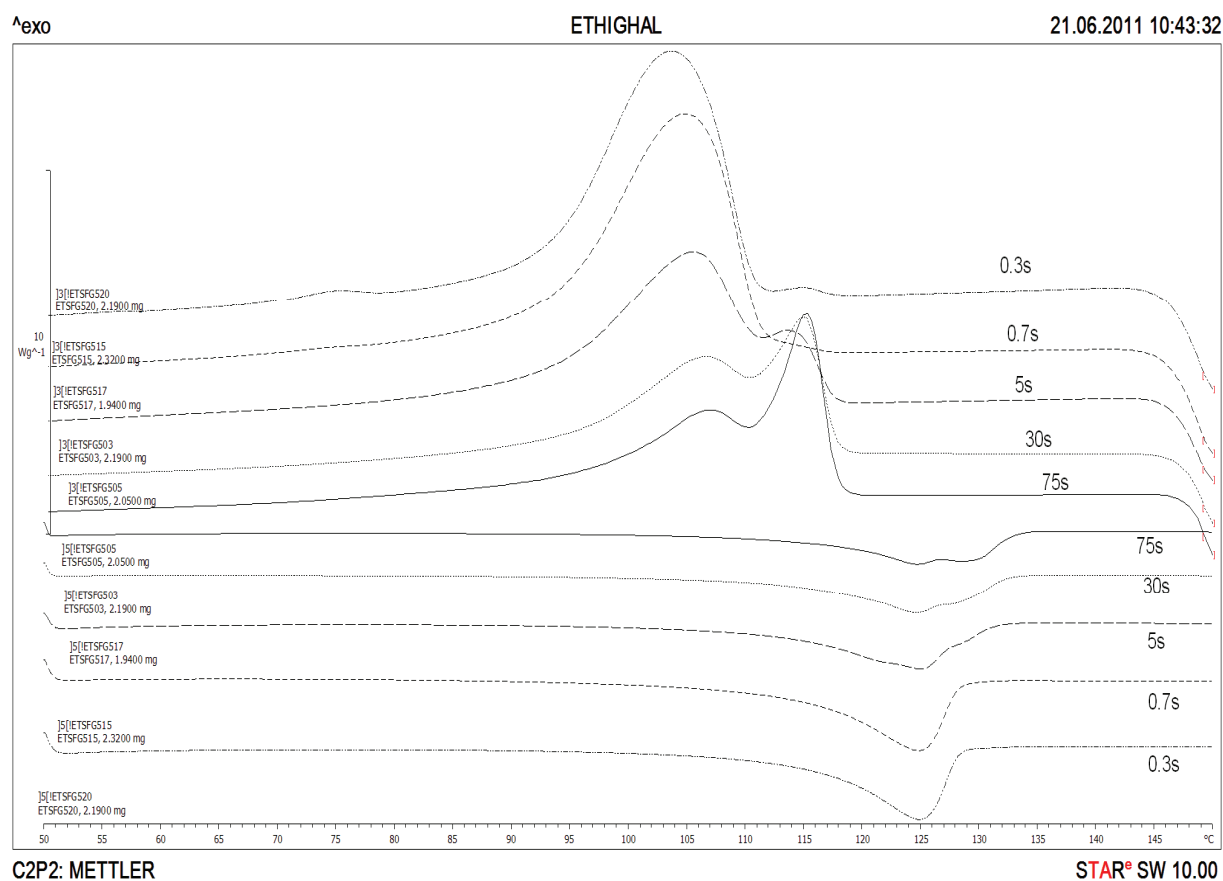


Figure 36: DSC thermograms of polymers produced using the high Al content catalyst.

First of all, due to the rapid pore filling and fragmentation, in this case no important crystallization peak at 75°C (corresponding to homogeneous crystallization in pores) is visible. In addition the main difference with the previously shown results is that the melting endotherm shows shoulders or even double peaks in this case for reaction times higher than



5s. For yields lower than 0.4 g/g the melting temperature of the polymers is around 125°C, which is in accordance with the values presented above. For higher yields a development of a shoulder becoming an independent peak at even higher yields is visible around 129°C. In this case we do not see a peak shifting toward higher temperature but a co-existence of the two melting peaks at 125 °C and 129 °C for yields higher than 0.4g/g. The situation is clearly shown in Figure 37. Crystallinity (not shown here) follows the trend presented in Figure 35.

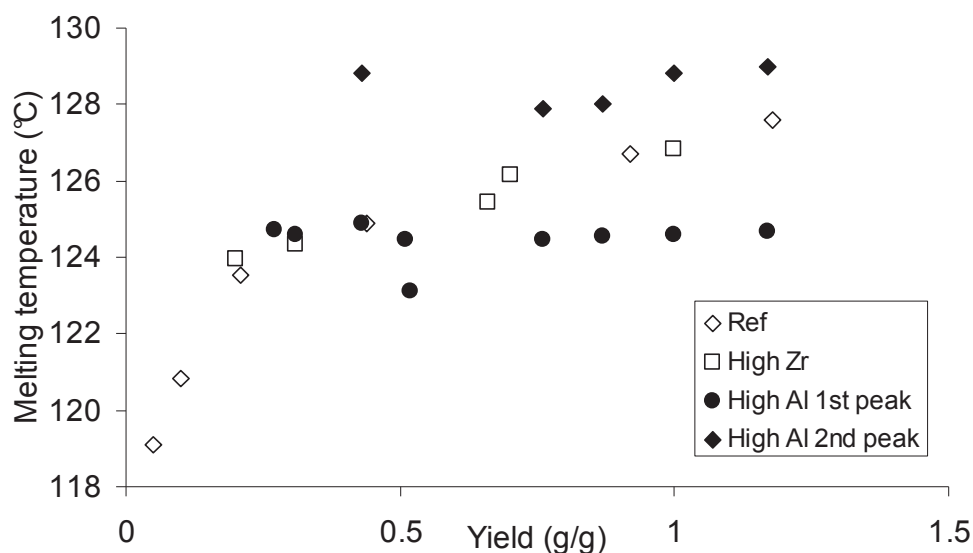
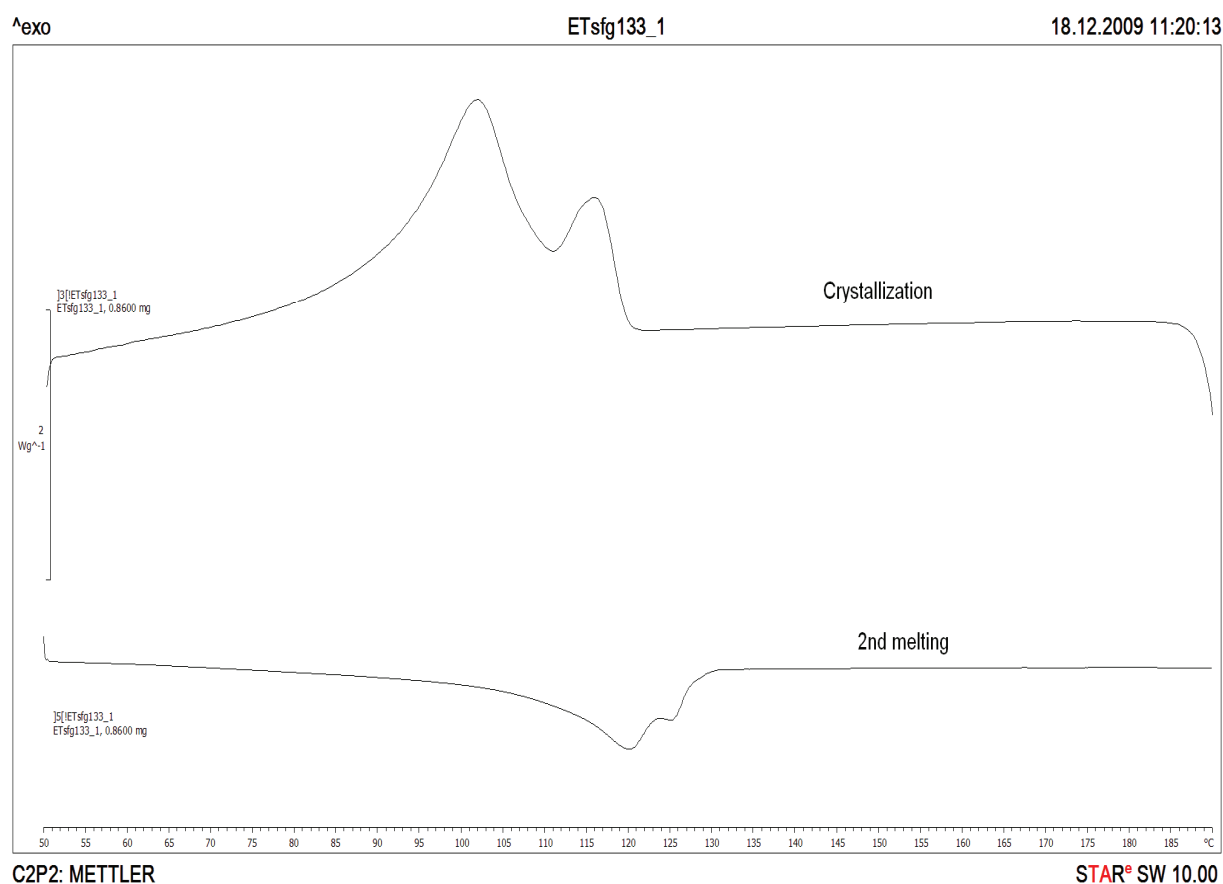


Figure 37: Influence of Al content on melting temperature evolution with yield.

The melting peak at 125°C can be assigned to the polymer produced in the first reaction seconds, which is when only one melting peak is visible. This situation is true up to a yield of about 0.5 g/g. The polymer formed in this time range is located into the particle pores and crystallization is perturbed by space confinement, as proved by the low  $T_m$  values. The peak at 129°C can be assigned to the polymer produced from 5s of reaction and is typical of a polymer which is almost in a bulk situation. For some reason it seems that the polymer produced early in the reaction is not able to fragment the pore into which is located, so that its melting peak at 125°C is visible throughout all the studied time range. For longer reaction times new polymer is added which is capable of fragmenting the pores or which is growing in an environment that is not perturbing the chain crystallization. After a reaction of 75s the quantity of polymer produced before 5s is equal to the one produced between 5 and 75 seconds, so that the two melting peaks have a similar intensity.

The reason for this heterogeneity in the behavior of the polymer produced before and after 5s can come from the temperature profile. We have seen in the previous chapter that the catalyst having a high Al content is very active at the beginning and deactivates extremely

fast. It is believed that one of the possible reasons for this behavior is the high temperature reached by the particles in the early stages. We have in fact seen that an outlet gas temperature profile similar to the one obtained for the reference series can be measured in this case even if the catalyst amount is divided by three. This means that the single particle will be hotter than the reference case. In addition in the reaction series performed using an  $\text{EtInd}_2\text{ZrCl}_2$  based catalyst at low gas velocities and higher catalyst mass (conditions giving high particle temperature excursions too) the same behavior showing two melting peaks has been seen (example in figure 37).



**Figure 38: DSC thermogram of PE produced after 4 s of reaction at 5.5cm/s gas velocity and with 50 mg of  $\text{EtInd}_2\text{ZrCl}_2$  / MAO / Grace 948 catalyst ( $Y=0.9$  g/g).**

Being the common factor between the two reaction series a high temperature excursion, it can be that the doubled melting peak can come from a fraction of polymer which has softened into the pores and has too poor mechanical properties to provoke the fragmentation of the pore walls. However, being the catalyst and the reaction conditions different, this hypothesis has to be considered with the due precautions.

## 4. Conclusions

In this chapter we have seen how the crystallization behavior of the PE chains at the reaction start-up can be very different from what is measured after long term reactions.

In general, a melting temperature increasing with reaction time is measured. Crystallinity starts from low values and passes through a maximum before reaching the classical steady state values. Crystallization exotherms show three distinct peaks: one appearing for very low reaction times at 75°C, one appearing for reaction times higher than 2s and spanning from 90 to 110°C and one appearing for reactions longer than 5s at 115°C. The first crystallization peak disappears quickly and is no more visible for reactions longer than 2s. The second one is predominant in the time range between 2 and 15s and becomes less and less visible as the reaction time increases. The third peak is visible from 5s and becomes more and more important. This peak is the one (and the only one) that can be seen for polymers produced in long term reactions. The reason for this behavior is to be found into the presence of a high amount of support in the final particle due to the low yields reached in our stopped flow reactions (max 2 g/g). The support/polymer particle is then just at the beginning of the fragmentation process and a relevant quantity of polymer is still located into unfragmented pores. This space confinement has the effect to perturb the chain crystallization by limiting the crystal growth. The low melting temperatures and the three crystallization peaks measured during DSC studies can be then explained. These effects are less important (or even disappear) for copolymers containing a high quantity of comonomer. The presence of branches reduces in fact the crystallite size to a value low enough that crystal growth is much less perturbed by the confinement in pores.

The morphology evolution of the particle, which can be followed by Synchrotron X-ray tomography, allows to explain the evolution of the crystallization peaks with the gradual filling of the most accessible pores first, the smaller pores later and the beginning of fragmentation even later, which creates bulk-like environments for the chain crystallization.

By analyzing polymers produced using catalysts supported on different support sizes and bearing different Zr contents we have seen that the yield has to be considered as the independent variable rather than the reaction time when studying the evolution of the melting temperature. The important parameter determining the degree of melting temperature depression is the ratio between the quantity of polymer confined in pores and the one

evolving in a bulk-like environment. This fact has to be taken into account when modeling the behavior of the single polymerizing particle: for example particles of different size will have not only a different activity at a certain time, but also will produce polymer that crystallize in different ways according to the yield reached. Crystallinity seems to evolve less clearly: for bigger particle the values of crystallinity are more or less constant throughout the studied time range rather than being low at the beginning and passing through a maximum.

An increased pore size allows to reduce the effects of space confinements and is responsible for the production of polymer that melts at slightly higher temperatures (but still quite far from the bulk values). If a support with a higher pore volume is used, the melting temperature depression due to the confined space is lasting for longer reaction times (and higher yields). There is in fact more space to accommodate more polymer in the pores before reaching an extensive fragmentation degree.

Catalysts that are too active at the beginning and that can be source of high temperature excursions (i.e. catalyst bearing high Al content) can lead to double melting temperature peak rather than a peak shifting towards higher temperature with yield. It is possible that the polymer formed in the pores in the first reaction instants can reach a temperature high enough to degrade its properties and impede the pore rupture. The depressed melting temperature of this polymer caused by space confinement will be visible throughout all the reaction time also because of the high quantity of polymer produced during the first instants.

More in general the broad melting temperature peak and the complex evolution of the crystallization peaks come from the fact that a commercial, heterogeneous support has been used. It would be interesting to see if such behavior is common for other type of heterogeneous catalysts showing different start-up activity profiles (Phillips) or different supports and fragmentation behaviors ( $\text{TiCl}_4/\text{MgCl}_2$ ). In addition, study of supports with a well defined pore size distribution like mesoporous silica (i.e. MCM-41) or Sirius type could give more precise indications on the relation between melting and crystallization peaks evolution and support geometrical features. In a second time, if a clear relation between polymer properties (melting temperature and crystallinity) and stress-strain relations influencing fragmentation is determined, a predictive use of these informations could be done. For example one could determine the best support pore size which fixes the right polymer properties to have the desired particle morphology evolution.

To conclude, in this chapter we have described the general behavior of the crystallization and melting of PE at reaction start-up and we have proven that using values coming from long term reactions to model the particle behavior for short times is a too rough approximation. We have also seen how the melting temperature and the crystallization behavior of the polymers produced at very short reaction times can be used as a kind of sensor to measure the particle morphology evolution.

## 5. References

1. Peacock, A.J., *Handbook of Polyethylene: Structures, Properties and Applications*. 2000, New York: Marcel Dekker.
2. Crist, B. and P.R. Howard, *Crystallization and Melting of Model Ethylene-Butene Copolymers*. *Macromolecules*, 1999. **32**(9): p. 3057-3067.
3. Brandrup, J., E. Immergut, and E. Grulke, *Polymer Handbook*. Vol. II. 1999, New York: John Wiley & Sons.
4. Loos, J., et al., *Melting behavior of nascent polyolefins synthesized at various polymerization conditions*. *Polymer Bulletin*, 2002. **48**(2): p. 191-198.
5. Di Martino, A., G. Weickert, and T.F.L. McKenna, *Contributions to the Experimental Investigation of the Nascent Polymerisation of Ethylene on Supported Catalysts, 2*. *Macromolecular Reaction Engineering*, 2007. **1**(2): p. 229-242.
6. Di Martino, A., G. Weickert, and T.F.L. McKenna, *Contributions to the Experimental Investigation of the Nascent Polymerisation of Ethylene on Supported Catalysts, 1*. *Macromolecular Reaction Engineering*, 2007. **1**(1): p. 165-184.
7. Machado, F., et al., *Evaluation of the Initial Stages of Gas-Phase Ethylene Polymerizations with a SiO<sub>2</sub>-Supported Ziegler–Natta Catalyst*. *Macromolecular Reaction Engineering*, 2009. **3**(1): p. 47-57.
8. Shin, K., et al., *Crystalline Structures, Melting, and Crystallization of Linear Polyethylene in Cylindrical Nanopores*. *Macromolecules*, 2007. **40**(18): p. 6617-6623.
9. Woo, E., et al., *From Homogeneous to Heterogeneous Nucleation of Chain Molecules under Nanoscopic Cylindrical Confinement*. *Physical Review Letters*, 2007. **98**(13): p. 136103.
10. Wang, Y., et al., *Crystallization in the Thin and Ultrathin Films of Poly(ethylene-vinyl acetate) and Linear Low-Density Polyethylene*. *Macromolecules*, 2004. **37**(9): p. 3319-3327.
11. Wang, Y., et al., *Substrate Effect on the Melting Temperature of Thin Polyethylene Films*. *Physical Review Letters*, 2006. **96**(2): p. 028303.
12. Loo, Y.-L., R.A. Register, and A.J. Ryan, *Polymer Crystallization in 25-nm Spheres*. *Physical Review Letters*, 2000. **84**(18): p. 4120.
13. Massa, M.V., J.L. Carvalho, and K. Dalnoki-Veress, *Confinement Effects in Polymer Crystal Nucleation from the Bulk to Few-Chain Systems*. *Physical Review Letters*, 2006. **97**(24): p. 247802.
14. Massa, M.V. and K. Dalnoki-Veress, *Homogeneous Crystallization of Poly(Ethylene Oxide) Confined to Droplets: The Dependence of the Crystal Nucleation Rate on Length Scale and Temperature*. *Physical Review Letters*, 2004. **92**(25): p. 255509.

15. Weber, C.H.M., et al., *Single Lamella Nanoparticles of Polyethylene*. Nano Letters, 2007. 7(7): p. 2024-2029.
16. Bauers, F.M., R. Thomann, and S. Mecking, *Submicron Polyethylene Particles from Catalytic Emulsion Polymerization*. Journal of the American Chemical Society, 2003. **125**(29): p. 8838-8840.







# Conclusions and perspectives

During this PhD work we have studied, developed and validated a tool to investigate the start-up of gas phase olefin polymerizations, and demonstrated its use by studying the behavior of heterogeneous metallocene catalysts during the initial moments of the catalytic gas phase polymerization of ethylene. We have tried to give the most complete experimental picture of the behavior of the catalyst particle during the first instants of the reaction, focusing on catalyst activity, particle temperature profile and morphology and polymer properties. The evolution of these properties has been followed by means of a specially conceived gas phase packed bed reactor and their dependence on process conditions and catalyst and support parameters has been described.

The motivation that has pushed us to accomplish this work is mainly the lack of experimental data related to early stages of olefin polymerization despite the fact that it is widely recognized by industry and academia that this stage of the reaction is fundamental for the performance of the entire polymerization process, especially in terms of particle morphology and optimization of catalyst activity. This lack of data is especially severe for gas phase reactions. The reason for this fact resides mainly in the difficulty of building a suitable experimental gas phase apparatus that can simultaneously allow us to evaluate catalyst kinetics, polymer properties, particle morphology and temperature on the one hand, while varying a number of process-related parameters over an industrially pertinent range. It is these difficulties that are at the origin of the need to make a large number of assumptions, especially about the particle structure and the transfer coefficients, when modeling the early evolution of the growing polymer particle. Plugging this gap can be considered as a second main motivation for this work which in fact aims to provide reliable experimental data to be used as input for modern single particle models.

We began by performing an in-depth analysis and optimization of this tool by performing gas phase polymerizations using metallocene complexes supported on MAO-treated silica particles for times on the order of seconds to several tens of seconds. The basic part of the reactor tool is a 3 mL packed bed reactor into which pulses of gases of different composition can be sent. An accurate control of the effective reaction time, the possibility of measuring rapid variations of gas temperature, and the ability to recover the polymer particles under inert atmosphere make this reactor very well suited to study catalytic polymerization start-up. As it is known that gas phase polymerizations present a high risk of thermal runaway, the optimization has been conducted through a systematic analysis of the equation representing the heat transfer between the reacting particles and the gas phase to maximize the quantity of heat transferred to the flowing fluid. This has led us to find a set of process conditions (gas composition, gas velocity, size of the solid inert diluent and mass of catalyst) that limit the catalyst overheating. It has been found that addition of 33 mol % of helium to the monomer feed, use of a gas velocity of 20 cm/s, use of NaCl crystals (as inert solid to dilute the catalyst into the reacting bed) having size comparable to the one of the catalyst particles and limiting the catalyst mass to 30 mg are the most suited process conditions in order to avoid thermal runaway and polymer melting while ensuring the production of enough polymer to perform all the analysis needed. More in particular the thermal runaway leading to an outlet gas phase temperature increase of 30°C in 75s found using the original conditions responsible for a bad heat transfer has been greatly reduced. The best process conditions lead in fact to a temperature increase of only 10°C reaching its maximum after 5s of reaction and rapidly returning to isothermal conditions after 10 s. Polymer melting and thermal runaway are then avoided and particles with good spherical morphology can be recovered.

Direct measurement of the catalyst particle temperature is very hard to perform and reliable knowledge of its value by means of experimental work is still missing in the literature. The results achieved in this part of the work can partly fill this void as they allow to have measurable outlet gas phase temperature as close as possible to the actual particle temperature, or at least to know the relation between them by simple calculations. This is an important information for validation of single particle models, and to the best of our knowledge, the first time such an experimental procedure has been proposed in a flow-through system (until now temperature measurements have been done using infrared cameras in a quiescent gases).

A preliminary version of an accurate model capable of giving the temperature distribution along the two reactor dimensions and its time dependence is available thanks to the collaboration between LCPP and LGPC. It has to be said that, due to the high catalyst concentration in the reacting bed and its high activity, temperature gradients along the reactor length in the order of 20°C are calculated in the first reaction seconds which can be responsible for some space dependent catalyst behavior introducing heterogeneities in the properties of the recovered polymer. Nevertheless these gradients become rapidly negligible after 10s of reaction. Decreasing the catalyst mass will of course reduce these gradients but not enough polymer will be produced. This is one of the main limitations of this type of reactor. Highly active catalysts must in fact be extremely diluted in a packed bed in order to avoid excessive temperature gradients. It can be interesting for future works to modify the system in order to be able to work at higher gas velocities (i.e. 50 cm/s, which is close to the velocity used industrial fluidized beds) or to change the temperature control method (i.e. condensed mode cooling). A sensitivity study on the influence of the bed geometry on the heat transfer could also be carried on using the model developed in collaboration with LGPC. It would be also very interesting to modify the model in order to have an “inline” continuous measurement of the catalyst activity by using the outlet gas phase temperature profile.

The optimum process conditions established in the first part of this work have been used to characterize the behavior of metallocene complexes (supported on commercial silica Grace 948 pretreated with MAO) at the reaction start-up. Preliminary results obtained by some works in this field and suggesting that the catalyst can behave unusually at the reaction start-up have been confirmed here and studied in detail. In particular the relation between heat transfer from the particle and catalyst behavior at the transient state has been elucidated showing that thermal runaway at the start-up can not only generate problems on a macroscopic level (i.e. polymer melting) but it can influence the reaction performance in a more subtle way by provoking local perturbations in the active site behavior which translates in an alteration of the MWD of the produced polymers. As an example, decreasing the gas velocity from 20 cm/s to 5.5 cm/s led to small changes in the activity profile, did not cause polymer melting, but was responsible for a reactor and particle temperature reaching higher values and decreasing more slowly. This led to the production of polymer having Mn rapidly decreasing with reaction time (from 35000 to 5000 g/mol) and PDI having the opposite behavior and reaching extremely high values (up to 10 after 10 s of reaction). The MWD (Mn and PDI) of the produced polymers is instead constant throughout the reaction times if

optimum conditions for heat transfer are used. This shows how an insufficient heat removal from the catalyst particle at the reaction start-up can lead to uncontrolled transfer reactions and poor polymer properties even if polymer melting is avoided. A similar unusual behavior (MWD presenting a tail in the low Mw region) can be temporarily measured for a short interval also if the heat transfer is at its optimum. This short lasting deviation from the controlled conditions comes from the fact that the reactor, especially during the first reaction seconds, operates under a thermal gradient. This leads to a heterogeneous behavior of the active sites according to their position in the reactor. Given that the chromatographic measurements are performed on an average sample it is possible to measure broad MWD especially at reaction times for which the temperature gradient is maximum (1 to 5s). For longer reaction times, when the temperature excursion has been absorbed, narrower MWD are measured if optimum reaction conditions are used. It should be noted that without the combination of measuring the temperature of the catalysts particles (or a close approximation thereof) and of the yield of the reaction, one could draw very inaccurate conclusions with respect to the kinetics of this type of reaction. For instance if one assumed that temperature effects were negligible, it could be tempting to say that the catalyst is insensitive to the temperature if all we have are yields that are similar at different temperatures (as we did in Chapter 3).

More in general the tested heterogeneous metallocene catalysts show a very high activity for the first 2 to 5 seconds with values that can be 20 times higher than what is measured at longer times independently on the reaction conditions (temperature, presence of comonomer, type of metallocene). The values measured after 75s of reaction are comparable to the average activity measured after 1h. The magnitude of the decay suggests that there exist some active sites that are working for only a short period of time. Their deactivation can be partially due to the temperature excursions measured in the first seconds but it seems that this behavior is inherent to the chemistry of the reaction. It has to be said that in this type of reactor, the external alkylaluminium, which can act as scavenger or site re-activator, is very difficult to introduce in an effective way and it was not used for short time reactions. In addition it was found that the presence of TEA in the packed bed is responsible for an activity increase of 2 to 5 times only for reactions longer than 15s. For shorter reactions no important activity increase upon addition of scavenger to the bed was measured. Nevertheless it would be interesting for the future works to find a viable method to introduce alkylaluminium into the reacting bed to operate as closely as possible to the industrial conditions.

A study of the effect of the preparation of the metallocene catalyst supported on MAO-treated silica on reaction start-up was also performed. The results show that increasing the quantity of Al fixed on the support leads to a very active catalyst for long reaction times while in stopped flow conditions a very high reaction rate at the beginning is followed by a quick activity decay to values one order of magnitude lower to what measured at steady state. Increasing the quantity of active metal (Zr) leads to an activity start-up similar to that of the reference catalyst, while after few seconds the reaction rate profile follows the deactivation of the catalyst containing a lot of Al. This behavior is assumed to originate from the combination of the active sites into inactive bimetallic species which is favored by an increased concentration of active sites onto the support (higher Al and/or Zr contents). Thermal deactivation and polymer softening, especially for the catalyst containing a high Al amount, is also responsible for this decay. A excessive temperature overshoot at the reaction start up is also the reason for a broadened MWD. This is seen in particular for the catalyst with a high Al content, which is the one having the highest activity for reaction times shorter than 1s. The same effect on MWD is seen if the Zr content is increased but the difference with the behavior of the reference catalyst lasts only for 15s. For longer reaction times the MWD of the polymers produced using the two catalysts (high and low Zr content) are similar.

In the last part of Chapter 3 we studied the influence of the support properties on the reaction start-up. We have shown that smaller particles have higher activity for reaction times higher than 30s while for shorter polymerizations there is no clear dependence between activity and support size. The decay type profile of the reaction rate is not dependent on the particle size. In addition bigger pores do not have an important influence on reaction rate. A commercial silica under the name of PQMS 3030 having a pore size of 38 nm (Grace 948 has an average pore size of 24 nm) was chosen to study the effect of pore size on reaction start-up. For this support the activity seems to drop even after 75s and no relevant activity is measured in a 1h reaction. Only a slight dependence of the Mw on the support size has been seen for reactions longer than 30s. The bigger the particle size, the lower the Mw value. In general MWD seems to be more affected by the support size than by the pore diameter.

In the last part of this work we focused on the thermal properties of polyethylene at the reaction start-up. For the first time in literature the unusual behavior which was also found by other authors has been explained thanks to the phenomenon of the chain crystallization in confined space.

In general, a rapid increase in the melting temperature of PE with reaction time is measured. For very short reaction times (less than 1s) melting temperature can be as low as 117°C, while the same catalyst usually produces polymers that melt around 131°C. The reason for this behavior is to be found in the presence of a high amount of support in the final particle due to the low yields reached in our stopped flow reactions (max 2 g/g). The support/polymer particle is then just at the beginning of the fragmentation process and a relevant quantity of polymer is still located into unfragmented pores. This space confinement has the effect of perturbing the chain crystallization by limiting the crystal growth, and it is known that smaller crystals melt at a lower temperature. These effects are less important (or even disappear) for copolymers containing a high quantity of comonomer. The presence of branches reduces in fact the crystallite size to a value low enough that crystal growth is no more perturbed by the confinement in pores. As the reaction proceeds and the support pores starts to break, the quantity of polymer confined in pores decreases respect to the one evolving in a bulk-like environment. As a consequence the average melting temperature of the sample increases and becomes closer and closer to the “classic” values. Melting temperatures around 130°C have been measured for yields around 2-3 g/g. The yield is then the independent parameter determining the degree of melting temperature depression. In a similar but more precise way the crystallization behavior of polyethylene at reaction start-up is highly dependent on the yield. For very low yields a crystallization peak around 75°C is measured, which is typical of homogeneous crystallization of PE. For higher yields a peak around 105°C is seen, which represent the heterogeneous crystallization of PE in confined space. Only for yields higher than 1 g/g the crystallization peak at 115°C, typical of linear PE, starts to become predominant. This behavior can be explained with the typical morphology evolution of the polymerizing particle which can be followed by Synchrotron X-ray tomography: gradual filling of the most accessible pores first, the smaller pores later and the beginning of fragmentation even later, which creates bulk-like environments for the chain crystallization. The melting and crystallization temperatures of the polymers produced at very short reaction times can then be used as kind of sensors to measure the particle morphology evolution.

The broad melting temperature peak and the complex evolution of the crystallization peaks come from the fact that a commercial, heterogeneous support has been used. It would be interesting to see if such behavior is common for other type of heterogeneous catalysts showing different start-up activity profiles (Phillips) or different supports and fragmentation behaviors (TiCl<sub>4</sub>/MgCl<sub>2</sub>). In addition, study of supports with a well defined pore size

distribution like mesoporous silica (i.e. MCM-41) or Sirius type could give more precise indications on the relation between melting and crystallization peaks evolution and support geometrical features. In a second time, if a clear relation between polymer properties (melting temperature and crystallinity) and stress-strain relations influencing fragmentation is determined, a predictive use of these informations could be done. For example one could determine the best support pore size which fixes the right polymer properties (Young modulus, shear modulus and relaxation time) to have the desired particle morphology evolution.

In this work we have developed a tool to study the start-up of gas phase olefin polymerization under conditions close to the ones used in industry. The main strength of such tool is the possibility to give a complete picture of the catalyst behavior during the early reaction stages by measuring catalyst activity, polymer properties, particle morphology and temperature. Future research can be dedicated to modifying the existing set-up or building a new one in order to get even closer to the industrial situation. First of all a method to introduce a scavenger in the system needs to be developed. It would be possible to absorb the alkylaluminium on the NaCl particles, but then a way to trap the scavenger entrained by the flowing gas has to be found (i.e. a silica bed capable to react with the alkylaluminium could be added at the gas outlet). It will also be interesting in this sense to perform a study with the objective of finding a new inert solid having a specific surface high enough to absorb a sufficient quantity of scavenger or having suitable moieties (i.e. -OH groups) capable of reacting with the alkylaluminium. The inert solid should be easily separable from the catalyst/polymer particles (i.e. by dissolution in solvent, by sedimentation, by sieving...).

We have already said that one of the main limitations of the packed bed stopped flow reactor is the development of temperature gradients along the reactor axis when using highly active catalysts. Even if these gradients are only temporary, they can be high enough to modify the catalyst behavior for a certain time. Modifications of the system in order to reach higher gas velocities or implement different cooling methods (i.e. condensed mode cooling) to reduce such gradients have already been proposed at the beginning of this section. The packed bed configuration can also be entirely replaced by a (semi-) fluidized bed configuration. This will not only allow a better heat removal from the catalyst particles, but also to simulate a real industrial configuration (and to use higher gas velocities and condensed mode cooling). Very short reactions can be a hard task to perform in such kind of reactor. A solution could be to



initiate the particle fluidization with an inert gas and then rapidly switch to a monomer stream followed by a quenching gas stream. The same system used for the packed bed configuration (electrovalves controlled by a Programmable Logical Controller) could be capable to perform this task. It would also be interesting in the same sense, and avoiding a complete re-design of the reactor, to perform a study in order to define the maximum monomer pulse duration to limit the temperature excursion to a predetermined value. Reactions longer than the pulse length could be performed by operating multiple pulses separated by inert gas flow to decrease the temperature to the initial conditions. Catalyst deactivation by contaminants present in the monomer and inert gas will be increased but this will not be a problem if a scavenger will be present in the reacting bed.

Future works could also be focused on the reactor modeling that is being actually developed at the LGPC. It has already been said that it would be interesting to develop a model allowing to have an “inline” measurement of the activity profile (i.e. calorimetric model). The same model could be also modified in order to calculate the local MWD of polymers produced in different reactor locations (i.e. population balance) and its dependence on the local temperature. This could help in determining if the temporary variations of the average MWD found in this work are due only to the temperature profile variations in the bed during the reaction course. MAO-silica supported metallocenes giving narrow MWD could be good candidates to start the study.

The reactions performed in this work have been stopped to yield values lower than 3g/g. The recovered polymer particles are then at the beginning of their fragmentation process. A future work dedicated to the study of particles having a yield comprised between 2 and 20 g/g would be interesting to perform. This will allow to describe the complete particle morphology evolution during the fragmentation process and to follow the catalyst activity profile towards higher reaction times. Catalysts with higher productivity or longer reactions could be used in this sense. The evolution of internal particle morphology can also be followed with an intensive EDX work to determine the distribution of Al and Si atoms inside the particle and their evolution with reaction time. X-ray synchrotron nano-tomography could also be used in this sense with the advantages to keep the particle integrity and have a resolution of few nanometers. Nevertheless an accurate choice of the samples to analyze has to be done because of the high analysis cost.

In Chapter 4 it has been seen how the PE thermal properties ( $T_m$  and crystallinity) at the reaction early stages can be linked to the particle fragmentation degree. It has already been

proposed as future work to use catalyst showing different activation profiles (i.e. Phillips) or narrow pore size distribution (i.e. Sirius and MCM-41) to perform a similar DSC study. ZN catalyst having higher activities and showing a much more rapid fragmentation process could also be used for a similar study. It would be interesting to see if, for a given yield, the same PE thermal properties are measured with a completely different support. In the same sense different catalyst could be prepared on supports selected over a wide pore size range and the related polymer thermal properties evolution could be measured. The DSC studies suggested here could be completed by X-ray diffraction analysis with the aim to determine the evolution of the polymer crystal structure and size with the particle fragmentation degree. The knowledge of the dependence of the polymer mechanical properties (Young modulus, shear modulus and relaxation time) over the chain architecture, the crystallinity and the crystal size could be useful to link the properties of the produced polymers with the support fragmentation path.



# Experimental part

<b>1. Synthesis of solid materials.....</b>	<b>293</b>
1.1. Supported metallocene catalysts .....	293
1.2. Silica/TEA .....	294
1.3. Fine NaCl .....	294
<b>2. Polymerization technique .....</b>	<b>295</b>
2.1. “Classic” gas phase reactor .....	296
<b>3. Analytical techniques .....</b>	<b>297</b>
3.1. Size Exclusion Chromatography (SEC).....	297
3.2. Differential Scanning Calorimetry (DSC).....	297
3.3. Porosimetry .....	298
3.4. [OH] measurement .....	298
3.5. Synchrotron X-ray microtomography .....	299
3.6. SEM.....	299
<b>4. References .....</b>	<b>301</b>

All chemicals are handled using standard Schlenk procedures under argon atmosphere. Synthesis of catalysts are performed under inert atmosphere. Solid products (catalyst and seedbeds) are stored in a glove box under argon atmosphere.

Organic solvents used during the synthesis are dried over molecular sieves before use.

Ethylene (purity 99.95%) is purchased from Air Liquide. The gas is passed through three different purification columns before use: a first one filled with reduced BASF R3-16 catalyst (CuO on alumina), a second one filled with molecular sieves (13X, 3A, Sigma-Aldrich) and a last one filled with Selexsorb® COS (Alcoa). Butene (purity > 99%), Helium (purity > 99.999%), Nitrogen (purity > 99.99%) and Carbon dioxide (purity > 99.995%) are purchased from Air Liquide and used without further purification.

# 1. Synthesis of solid materials

## 1.1. Supported metallocene catalysts

The preparation of this type of catalyst is largely discussed on the literature and we followed the synthesis developed by Welborn [1] and Takahashi [2]. The whole procedure consists in three different steps:

### 1. Dehydroxylation of silica

Two types of commercial silica have been used in this work: Grace 948 from Grace Davidson and PQ MS 3030 from PQ Corporation. Around 5g of silica are introduced in a Schlenk tube and put under primary vacuum at room temperature for 30 minutes. The Schlenk is successively connected to secondary dynamic vacuum ( $\sim 10^{-5}$  mbar) and silica is calcinated using the temperature program represented in Figure 1.

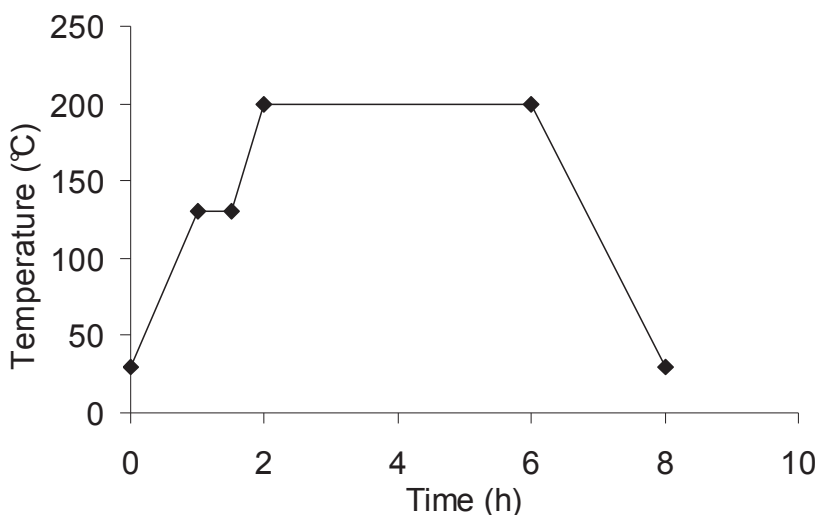


**Figure 1: Temperature program for silica calcination.**

After this treatment the concentration of the hydroxyl groups on the surface of silica is around 5 OH/nm<sup>2</sup> (measured following the method presented in paragraph 3.4).

### 2. Impregnation of MAO

Around 2g of dehydroxilated silica are introduced in a three-neck round bottom flask equipped with a mechanical agitation system under argon atmosphere. The silica is covered with around 50 mL of dry toluene. A commercial solution of MAO at 10 wt % (Aldrich) or 30 wt % (Albemarle) in toluene is added to the suspension in order to have 15 wt% aluminium on silica. The average weight fraction of aluminium in MAO is 46% while the relative

densities of the MAO solutions are of 0.92 and of 0.875 for the 30 wt% and the 10 wt% solution respectively. The flask is then heated by an oil bath and equipped with reflux condenser. The mixture is stirred at 250 rpm at 85 °C for 1h. The suspension is finally washed three times with toluene at 85°C. After each washing step the supernatant is removed. The residual solid is then dried under vacuum. The solid SMAO obtained is a white free-flowing powder

### 3. Impregnation of the metallocene complex

The SMAO is suspended in toluene in a three-neck round bottom flask equipped with a mechanical agitation system under argon atmosphere. A known quantity of metallocene complex is then added to the suspension after it has been dissolved in a minimum amount of hot toluene. The reference catalyst is synthesized by adding 2 wt% of metallocene complex. The catalyst bearing higher Zr content is synthesized by adding 5 wt% of metallocene complex. The mixture is stirred at 250 rpm and 30°C for 1h. After the reaction the solid is washed in a way similar to what described above using heptane at room temperature instead of hot toluene and dried under static vacuum. The final catalyst is a yellow-orange free flowing powder.

#### *1.2. Silica/TEA*

Around 2g of calcined silica are added to a three-neck round bottom flask equipped with a mechanical agitation system under argon atmosphere and suspended in 50 mL of dry heptane. A molar solution of TEA in heptane is slowly added to the suspension under gentle stirring by means of an addition funnel over 20 minutes. The quantity of TEA added is calculated to have 2 equivalents of Al respect to the number of hydroxyl groups of the silica. The mixture is then stirred at room temperature during 1 hour. After the reaction the mixture is washed three times with toluene as previously described and dried under vacuum.

#### *1.3. Fine NaCl*

In order to obtain small NaCl crystals to use as seedbed an antisolvent method for salt crystallization has been used. The original salt (Laurylab, France) was dissolved and crystallized in a controlled way to obtain single crystals of 5 µm [3]. According to this

method, 450 mL of NaCl saturated water solution was added in one shot to 900 mL of 0.06 M solution of citric acid (Sigma Aldrich) in ethanol. Citric acid avoids excessive agglomeration of the crystals. NaCl precipitates immediately at the contact with the antisolvent and the solution becomes milky. The resulting suspension was stirred for 45 min at 370 rpm and the NaCl was recovered and washed with ethanol to eliminate the remaining water. The solid was dried for 2 h at 100°C and finally sieved. The fraction smaller than 45  $\mu\text{m}$  was retained and dried for 4 h at 200°C to remove any trace of adsorbed water before use. All the inert seedbeds were dried under vacuum at 200°C for 4 h (same temperature program used for silica calcinations) to remove the adsorbed water molecules before mixing with active catalyst.

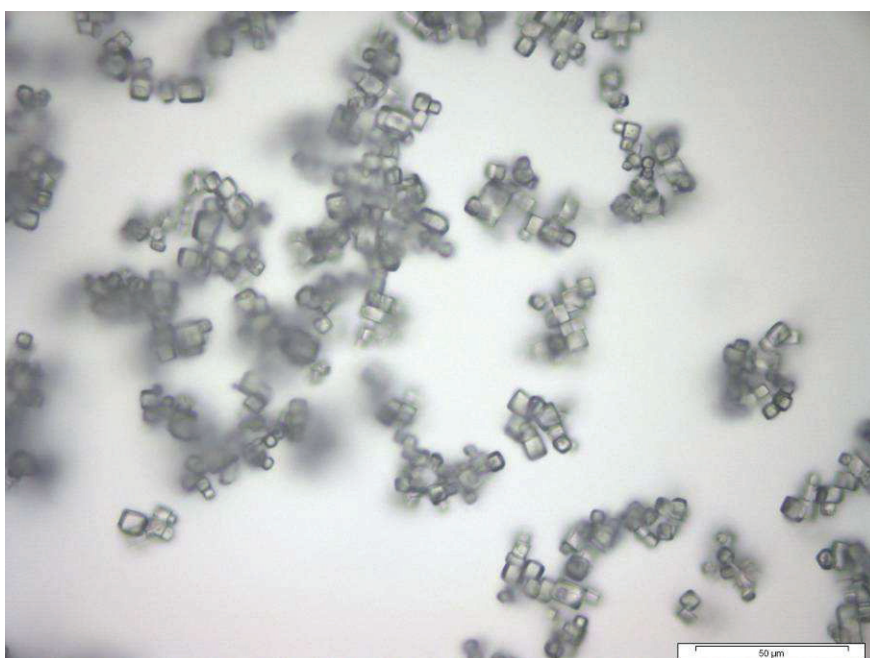


**Figure2: Optical microscopy image of fine NaCl.**

## 2. Polymerization technique

Polymerization procedure for the gas phase stopped flow reactor is deeply described in Chapter 2. In this section the procedure used for the classic reactor to perform long term reactions is described.



## 2.1. “Classic” gas phase reactor

The reactor used to perform long term reactions in this study is a steel spherical reactor called “Turbosphere” and equipped with a three blade stirrer specially designed to improve the powder homogeneity into the reactor volume. The temperature is regulated by water circulating in a double jacket. The reacting gases are premixed in a ballast and the catalyst activity is calculated by following the pressure decrease of the ballast necessary to keep the reactor pressure constant. Reaction conditions used in this work are 80°C, 6 bar of ethylene and eventually 0.25 bar of butene.

The reactor is heated up to 80°C before the reaction start and is filled with argon and successively kept under vacuum for 30 minutes. The cycle is repeated three times in order to minimize the quantity of impurities remaining in the reactor. In a glove box 20 mL of dried NaCl with particle size between 250 and 500  $\mu\text{m}$  are put in a 50 mL round bottom flask. About 60 mg of supported metallocene is mixed with 3 g of NaCl in a second similar flask. The inert NaCl is used to increase the heat removal from the catalyst particles and to improve the dispersion of the catalyst into the reactor. The inert solid contained into the first flask is injected into the reactor under argon atmosphere and stirring speed of 300 rpm. Successively a known quantity of scavenger (TEA) is injected in order to reach an Al/Zr ratio of 2000. The reactor filled with the inert powder and the scavenger is then kept at 80°C for 30 minutes. In a second time the reactor is cooled down to 50°C and the solid contained in the second flask (inert powder and catalyst) is injected into the system. The reactor is heated up again and pressurized with monomer in order to reach the working temperature and pressure at the same time.

Once the reaction is finished (normally 1 hour) the monomer inlet is close and the reactor is rapidly cooled down and depressurized. Polymer is recovered after washing with demineralized water to dissolve NaCl and heptane. The final powder is then dried for at least 1 hour at 80°C to remove the remaining traces of solvent.

### 3. Analytical techniques

#### 3.1. *Size Exclusion Chromatography (SEC)*

The molecular weight distributions of polymer samples were characterized by SEC (Waters, Alliance GPCV 2000). The system was equipped with two detectors (a refractometer and a viscometer) and with three columns (PL gel Olexis 7\*300 mm from Varian). Analyses were performed in trichlorobenzene (TCB) at a flow rate of 1 mL/min. The molecular weight distributions were calculated by a calibration based on polyethylenes of different weight average molecular weights and only the RI signal was used for calculations in order to erase any possible artifact coming from experimental errors during the determination of the polymer mass. The original samples were in fact support/polymer particles that had been separated from the NaCl seedbed by washing at ambient temperature with demineralized water. The exact polymer quantity (varying between 1 and 10 mg depending on yield) was calculated using the total sample weight and reaction yield value. The particles were then dissolved in trichlorobenzene at 150°C for 3 hours and filtered before injection into the chromatography columns in order to remove the inorganic support particles. Heterogeneities in the original samples or incomplete removal of the inorganic support could lead to errors in the molecular weight calculations if the viscometer signal was taken as reference.

#### 3.2. *Differential Scanning Calorimetry (DSC)*

The crystallinity and melting temperatures of the polymer samples were measured by DSC (Mettler DSC 1). The samples were placed in the holder without separation of the polymer phase from the inorganic support. The inert seedbed was previously removed by washing with demineralized water at ambient temperature. The exact polymer quantity (varying between 0.5 and 5 mg depending on yield) was calculated using the total sample weight and yield value. 40 µL holders were used except for reactions with yields lower than 0.2 g/g when 100 µL holders were preferred. Two heating steps were performed from 50 to 150°C at heating rate of 5K/min separated by a cooling from 150°C to 50°C at a rate of 20K/min. Crystallinity of the samples was calculated using a value of 288 J/g for a full crystalline polyethylene. We consider data obtained during the second heating step.

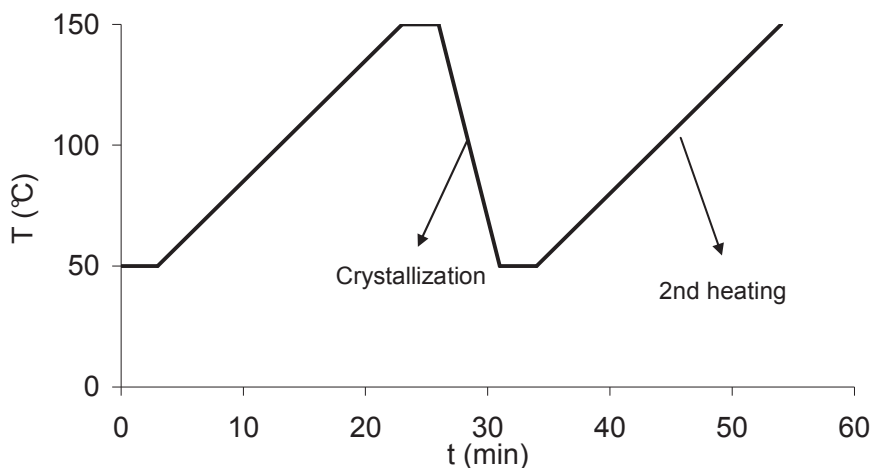


Figure 3: DSC temperature ramp.

### 3.3. Porosimetry

The pore volume, pore size distribution and specific area of silica samples have been performed by N<sub>2</sub> porosimetry using a Micromeritics ASAP 2020 porosimeter. The measurement is performed on around 300 mg of silica by absorbing nitrogen under a pressure ratio  $P/P_0$  from 0.01 to 0.99 at 77K. The desorbed nitrogen volume corresponds to the pore volume of the particles. Silica particles have been degassed at 200°C before performing the porosimetry.

### 3.4. [OH] measurement

The concentrations of hydroxyl groups on the silica surface have been measured by the method developed by V. Gachard-Pasquet in her thesis [4] which uses titration with triethylaluminium. The method consists in measuring the volume of ethane produced by the reaction between the alkylaluminium and the silica hydroxyl groups. About 1 g of calcined silica is placed in a 50 mL three-neck round bottom flask equipped with magnetic stirring. The flask is then placed under static vacuum and kept at 0°C. 4 mL of a molar solution of TEA in heptane is slowly added by means of an addition funnel over the stirred silica. The pressure increase in the flask due to ethane production is registered and the number of silanols is calculated using the following formula:

$$n_{\text{silanol}} = \frac{\Delta P \cdot (V + 3V_{\text{TEA}})}{22400 * m_{\text{silica}}} \quad (1)$$

where  $n_{\text{silanol}}$  are the moles of silanol per grams of silica,  $\Delta P$  is the measured pressure increase,  $V$  is the volume of the system,  $V_{\text{TEA}}$  is the volume of TEA solution added and  $m_{\text{silica}}$  is the mass of silica originally present in the flask.

### 3.5. *Synchrotron X-ray microtomography*

Tomographic images of samples using a Synchrotron X-ray source were performed in the ESRF facilities in Grenoble on the line ID19. Microtomography is a non-invasive and non-destructive technique which allows the visualization of the internal structure of materials (porosity, morphology, distribution of phases). A monochromatic X-ray beam is sent through the sample to produce a series of 2D images representing the spatial distribution of the attenuation coefficients along the section of the analyzed sample. In our case the sample is constituted by the reacting bed (polymer/catalyst particles and NaCl crystals). The sample is introduced under inert atmosphere (glove box) into a thin glass capillary which is mounted on a holder located between the beam and the detector. The capillary is then sealed with paraffin. The sample is allowed to rotate around the capillary axis from  $0^\circ$  to  $180^\circ$  during imaging and for each position an image is recorder by the detector. Before acquisition an alignment is performed to verify the correct position of the sample, the beam and the detection apparatus. 2000 rotation angles were imaged for 0.1s with beam energy of 17.6 keV. The image resolution (pixel size) is of  $0.35 \mu\text{m}$  and a sample slice with a radius of  $700 \mu\text{m}$  could be imaged per picture. For each sample we recovered 2000 pictures representing 2000 slices separated by  $0.35 \mu\text{m}$  each other. The resulting imaged volume is then a cylinder with height and radius of  $700\mu\text{m}$ . The attenuation coefficient is proportional to the material density and to the atomic number. More absorbing material will result lighter in the final image.

### 3.6. *SEM*

Surface morphology of polymer particles was evaluated by SEM technique at the “Centre technologique des microstructures” (CT $\mu$ ) at the Lyon 1 University. The sample for this analysis is constituted by the support/polymer particles and the inert seedbed together. The images were produced using an accelerating voltage of 10kV and carrying out the observation

under inert conditions. The particles are mounted under inert atmosphere on a standard aluminium slotted head covered with carbon adhesive tab. The samples are then sputter coated using a specific combination of gold – palladium which makes them conducting and gives a better degree of contrast to the images.

## 4. References

1. Welborn, J. and C. Howard, US 4 808 561, Exxon Chemical Patents Inc., 1989.
2. Takahashi, T., US 5 026 797, Mitsubishi Petrochemical Co., Ltd., 1991.
3. Gaillard, C., J.F. Despois, and A. Mortensen, *Processing of NaCl powders of controlled size and shape for the microstructural tailoring of aluminium foams*. Materials Science and Engineering A, 2004. **374**(1-2): p. 250-262.
4. Gaschard-Pasquet, V., 1985, PhD Thesis, Universite Claude-Bernard-LYON 1.







---

## RESUME en français

La phase initiale (de quelques fractions de seconde à quelques minutes) de la polymérisation catalytique des oléfines est encore peu comprise. Elle est pourtant reconnue comme une étape cruciale pour contrôler la morphologie de la particule de polymère et pour garantir la performance optimale du catalyseur et une certaine stabilité thermique du procédé. Ce travail présente l'étude et l'optimisation d'un mini réacteur à lit fixe pour mener des polymérisations catalytiques en phase gaz avec des durées très faibles (minimum 0.1s) dans des conditions proches à celles utilisées industriellement. La possibilité de suivre la température du gaz et de récupérer les particules de polymère pour les caractériser permet de décrire d'une façon complète le comportement du catalyseur au début de la réaction. L'étude a été limitée à la polymérisation de l'éthylène (avec un catalyseur métallocène supporté sur silice) et l'attention a été particulièrement mise sur la relation entre transfert de chaleur de la particule et performance du catalyseur. Il a été montré que des températures trop élevées peuvent être responsables localement de la modification du comportement du site active et de l'altération des propriétés des polymères. Un choix adéquat des conditions de réaction permet de suivre indirectement l'évolution de la température des particules en mesurant celle de la phase gaz. Dans un deuxième temps différents métallocènes ont été utilisés pour étudier l'influence des conditions de réaction, de la préparation du catalyseur et des propriétés du support sur l'activité, les propriétés du polymère et la morphologie des particules au temps court. Une attention particulière a été portée sur l'évolution des sites actifs et sur la cristallisation des chaînes de polymère dans un support poreux en évolution. Une activité élevée a été mesurée dans les premières cinq secondes et les températures de fusion et cristallisation des polymères ont été utilisées comme sondes pour mesurer l'avancement de la fragmentation du support. Les résultats ainsi obtenus peuvent non seulement clarifier certains aspects clé du début de la polymérisation mais aussi être utilisés comme données de départ pour modéliser la particule en croissance et contribuer à réduire l'écart qui est actuellement présent entre comportement réel du catalyseur et prédictions des modèles.

---

## TITRE en anglais

Optimization of a tool to study the start-up of the gas phase olefin polymerization

---

## RESUME en anglais

The early stages (from less than 1s to few minutes) of catalytic olefin polymerization are still fairly understood even if they are nowadays recognized to be crucial for the determination of the morphology of the polymer particle, the optimization of the whole catalyst performance and the thermal stability of the process. In this work we will present how we studied and optimized a specially conceived packed bed reactor to perform gas phase catalytic olefin polymerizations as short as 0.1s under industrially relevant conditions. The possibility to measure the reactor temperature and to recover unaltered the polymer particles allows to take a complete picture of the catalyst behavior at the reaction start-up. The study will be restrained to ethylene polymerization with silica supported metallocenes and special attention will be given to the relation between heat transfer from the growing particle and catalyst performance. It will be seen how particle temperature evolution can be followed indirectly by measuring the gas phase temperature. In the second part of this work different metallocene complexes will be used to study the influence of process conditions, catalyst preparation method and support properties on the evolution of reaction rate, and polymer MWD during the first reaction seconds. Special attention will be given to the active site evolution during the transient phase and it will be shown that temperature excursions can be responsible for a local variation in active site behavior thus altering the properties of the formed polymer. The last section will be dedicated to the study of the peculiar crystallization behavior of the polymer chains in an evolving inorganic support. It will be shown how the melting and crystallization temperatures of the polymers can be used as "sensors" to measure the degree of fragmentation of the support particle. The results obtained in this work allow to gain a deeper understanding of the key parameters for the polymerization start-up and can be used as input for single particle models thus allowing to reduce the gap actually present between real catalyst behavior and model predictions.

---

## DISCIPLINE

Chimie – Génie des procédés

---

## MOTS-CLES

Olefin polymerization, gas phase, early stages, heat transfer, active site, crystallization.

---

## INTITULE ET ADRESSE DE L'U.F.R. OU DU LABORATOIRE :

C2P2 – Equipe LCPP, Bât. F308, B.P. 2077

43 Bd du 11 Nov. 1916

69616 Villeurbanne Cedex

FRANCE